The University of Nottingham
UNITED KINGDOM · CHINA · MALAYSIA

Department of Chemical and Environmental Engineering
Efficient Fossil Energy Technologies

Moving Bed Temperature Swing Adsorption Processes for Post-Combustion CO_2 Capture

A thesis submitted to the University of Nottingham for the degree of *Doctor of Engineering*.

Bishan Meghani

November 2014

Abstract

Due to high regeneration energy demands for amine absorption processes for post-combustion CO_2 capture, alternative technologies such as adsorption processes using solid adsorbents have been considered. Other practical issues such as corrosion of equipment and loss of solvent can be avoided with adsorption processes. Fixed bed adsorption processes, in which CO_2 adsorption and adsorbent regeneration are performed successively in a vessel packed with adsorbent, are the most common adsorption processes. However, in fixed bed temperature swing adsorption (TSA) processes, large columns and long heating and cooling times would be needed. Fixed bed pressure swing adsorption (PSA) processes use electrical energy, which is more expensive than thermal energy in a power plant. Therefore, the feasibility of moving bed adsorption processes including fluidised-bed, co-current and counter-current systems is investigated. In these systems, the adsorbent continuously circulates from a CO_2 adsorber to a regenerator. The adsorbents considered are a supported amine adsorbent, activated carbon and zeolite 13X.

Numerical simulations of moving bed TSA cycles for CO_2 capture have been carried out. The effects of influential parameters in the process have been assessed via sensitivity analyses. It was found that counter-current beds with supported amine adsorbent give the best overall performance. Compared to an amine absorption process, it was found that a moving bed TSA process without heat integration requires the same heat consumption per unit mass of CO_2 captured. There is a potential for a lower heat consumption in moving bed TSA processes if, similarly to amine absorption processes, heat integration is carried out or if the CO_2 working capacity of the adsorbent can be increased.

Acknowledgements

I would like to take the opportunity to thank everyone who has supported me through this challenging but fulfilling experience.

First of all, I wish to express my gratitude to my industrial supervisor, Andrew Wright and my academic supervisors Trevor Drage, Sean Rigby and Begum Tokay. I am very grateful to them for having let me work on this research project. I am particularly thankful to Andrew for all his help and advice. He took the time to assist me when when I had specific difficulties and he allowed me to develop my understanding and knowledge in adsorption. I am also thankful to my other supervisors for their guidance.

I want to thank all members of R&D at Air Products in the UK and US including Vince White, Paul Higginbotham, Andrew Shaw, Geoff Achilles and Kevin Fogash for their friendliness and their advice but also for having taken me into their group during my three years at Air Products in Hersham (UK).

I thank members of the Centre of Efficient Fossil Energy Technologies at University of Nottingham including Colin Snape, Anup Patel and Diane Vincent for the running of the Engineering Doctorate (EngD) course. I also thank all other staff at the University of Nottingham. I have appreciated the friendship and support of my fellow EngD colleagues. I wish them well for their future and career.

Last but not least, I will never be able to express enough gratitude to my parents and sister for their strong support and understanding throughout the duration of my studies.

Contents

Abstract i

Acknowledgements ii

Contents iii

List of Figures viii

List of Tables xx

Nomenclature xxii

1 General Introduction 1

1.1 Motivations 2

1.2 Thesis Structure 3

2 Literature Review 5

2.1 Context for CO_2 Capture and Storage 5

2.1.1 Climate Change 5

2.1.2 Sources of CO_2 Emissions 6

2.1.3 Methods for Reducing CO_2 Emissions 7

2.1.4 Pathways for CO_2 Capture and Technologies 8

2.1.5 Post-combustion CO_2 Capture Technologies 9

2.2 Adsorption Separation 16

2.3 Adsorption Equilibrium and Loading 17

2.3.1 Equilibrium Loading and Isotherms 17

2.3.2 Types of Isotherms 18

2.3.3 Isotherm Models 19

2.4 Kinetics 21

2.5 Methods of Desorption for Adsorption Processes 24

2.6 Review of Adsorbents for Post-Combustion CO_2 Capture 26

2.6.1 Physisorbents and Chemisorbents 27

2.6.2 Desirable Adsorbent Properties 27
2.6.3 Carbon Based Adsorbents 29
2.6.4 Zeolite 31
2.6.5 Amine Functionalised Adsorbents 32
2.6.6 Alkali-Carbonate Adsorbents 34
2.7 Review of Moving bed Adsorption Processes for Post-Combustion CO_2 Capture 36
2.7.1 Moving bed Adsorption and Regeneration Process with a Supported Amine Adsorbent 36
2.7.2 Counter-current Adsorption and Regeneration Process with Activated Carbon Adsorbent 38
2.7.3 Moving bed Adsorption and Regeneration Process with Potassium Carbonate Adsorbent 40
2.7.4 Other Studies of Moving bed CO_2 Adsorption Processes 41
2.8 Considerations of Energy for Adsorbent Regeneration 44
2.9 Conclusions 45

3 Mathematical Modelling of Moving Bed Adsorption Systems 47
3.1 Introduction 47
3.2 Numerical Methods Used in the Model 49
3.2.1 Finite Difference Method 49
3.2.2 Finite Volume Method 49
3.2.3 Comparisons of the Finite Difference Method and the Finite Volume Method 51
3.2.4 Discretisation and Approximations at the Boundary of a Control Volume 51
3.2.5 Newton-Raphson Method for a Nonlinear System of Equations 52
3.2.6 Gaussian Elimination with a Banded Matrix 55
3.3 Assumptions 57
3.3.1 One-dimensional Model 58
3.3.2 Spherical and Identical Adsorbent Particles 59
3.3.3 Cylindrical Vessel 59
3.3.4 Ideal Gas 59
3.3.5 Negligible Axial Dispersion 59
3.3.6 Steady State 59
3.3.7 Local Thermal Equilibrium 59
3.3.8 Constant Mass Transfer Coefficients 60
3.3.9 Cooling and Heating Assumptions 60

3.3.10 Conservation of Adsorbent in the Overall Cycle 60
3.3.11 Constant Heats of Adsorption 61
3.4 Material Balances 61
3.4.1 Material Balance for a Gas Component 62
3.4.2 Material Balance for an Adsorbed Component 63
3.4.3 Overall Material Balance for the Gas 65
3.4.4 Material Balance for the Adsorbent 66
3.5 Energy Balance 66
3.6 Momentum Balance 70
3.6.1 Momentum Balance for Fluidised Bed Systems 70
3.6.2 Momentum Balance for Co-current Systems 70
3.6.3 Momentum Balance for Counter-current Systems 71
3.7 Mathematical Models for Isotherms 73
3.7.1 Adsorption Isotherms for a Supported Amine Adsorbent 73
3.7.2 Adsorption Isotherms for an Activated Carbon Adsorbent 77
3.7.3 Adsorption Isotherms for Zeolite 13X 80
3.8 Multicomponent Adsorption 81
3.9 Mass Transfer Rate Models 83
3.10 Overall Process Model 85
3.10.1 Mathematical Model of Adsorption or Regeneration Systems 85
3.10.2 Iterative Solving 87
3.10.3 Cycle Formation and Sequential Solving 88
3.10.4 Modelling of Heat Exchangers 88
3.10.5 Overall Cycle Convergence 89
3.11 Summary 91

4 Numerical and Analytical Solutions 92
4.1 Introduction 92
4.2 Assumptions 92
4.3 Analytical Model of a Co-current Bed 93
4.4 Analytical Model of a Counter-current Bed 95
4.5 Parameters 96
4.6 Results and Discussion 97

5 Fluidisation Limits for Moving Bed Systems 102
5.1 Introduction 102
5.2 Minimum Fluidisation Velocity 102
5.3 Terminal Settling Velocity 104

5.4 Fluidisation Limits for Moving bed Adsorbers 105
5.5 Limits on the Solid Velocity in a Counter-current Bed 107
5.6 Fluidisation Limits for the Adsorber 107
5.7 Fluidisation Limits for a Regenerator 112
5.8 Conclusions 112

6 Analysis of an Adsorber 114
6.1 Introduction 114
6.2 Adsorber Base Case 115
6.2.1 Base Case Conditions 115
6.2.2 Profiles for the Adsorber Base Case 118
6.3 Impact of Isotherm Model Errors on the Adsorber 121
6.4 Effect of the Type of Adsorber 121
6.5 Effect of the Adsorbent 125
6.6 Fluidised Bed Adsorbers 130
6.7 Effect of Adsorbent Flowrate 131
6.8 Effect of CO_2 Mass Transfer Constant 137
6.9 Effect of CO_2 Mole Fraction in the Inlet Flue Gas 138
6.10 Effect of Water in the Inlet Flue Gas 140
6.11 Effect of Pre-loaded CO_2 141
6.12 Effect of Pre-loaded Water 143
6.13 Effect of Molar Flowrate of Flue Gas 149
6.14 Effect of Inlet Flue Gas Temperature 149
6.15 Effect of Inlet Adsorbent Temperature 152
6.16 Effect of Heat Removal from the Adsorber 154
6.17 Conclusions 156

7 Analysis of a Regenerator 158
7.1 Introduction 158
7.2 Regenerator Base Case 159
7.2.1 Base Case Conditions 159
7.2.2 Profiles for the Regenerator Base Case 160
7.3 Impact of Isotherm Model Errors on the Regenerator 164
7.4 Effect of the Type of Regenerator 164
7.5 Effect of the Adsorbent 169
7.6 Fluidised Bed Regenerators 173
7.7 Effect of Adsorbent Flowrate 177
7.8 Effect of CO_2 Mass Transfer Constant 178
7.9 Effect of CO_2 in the Regeneration Gas 183

7.10 Effect of the CO_2 Loading at the Adsorbent Inlet 185
7.11 Effect of the Molar Flowrate of Steam 187
7.12 Effect of Inlet Steam Temperature 190
7.13 Effect of Inlet Adsorbent Temperature 191
7.14 Effect of Heat Addition to the Regenerator 193
7.15 Inadequacy of Zeolite 13X 196
7.16 Conclusions 197

8 Analysis of Adsorption-Desorption Cycles 199
8.1 Introduction 199
8.2 Moving Bed CO_2 Adsorption Cycle with Supported Amine Adsorbent 200
8.2.1 Base Case Cycle using the Supported Amine Adsorbent . 200
8.2.2 Effect of the Adsorbent Flowrate 219
8.2.3 Effect of the Regeneration Gas Flowrate 221
8.2.4 Effect of the Heat Removal from the CO_2 Lean Adsorbent in HEX 1 228
8.2.5 Effect of the Heat Addition to the CO_2 Rich Adsorbent in HEX 2 231
8.2.6 Effect of the Mass Transfer Coefficient 233
8.2.7 Addition of an Intermediate Heat Exchanger in the Cycle 236
8.3 Comparisons of the Performance of Absorption and Moving Bed Adsorption Processes 245
8.4 Comparisons of the Performance of Moving Bed and Fixed Bed Adsorption Processes 249
8.5 Moving Bed CO_2 Adsorption Cycle with Activated Carbon Adsorbent 251
8.6 Cost Considerations 253
8.7 Conclusions 253

9 General Conclusions and Future Work 255
9.1 Adsorbent Suitability 255
9.2 Adsorber Configuration 255
9.3 Fluidisation Considerations 256
9.4 Performance of Moving Bed TSA Cycles 256
9.5 Future Work 256

Bibliography 259

List of Figures

2.1 World CO_2 emissions by sector (2011) (International Energy Agency (2013a)) . . . 6
2.2 World electricity production from different fuel sources (2010) (International Energy Agency (2012)) . . . 7
2.3 CO_2 capture pathways (Figueroa et al. (2008)) . . . 9
2.4 Simplified diagram of post-combustion CO_2 capture using absorption (Metz et al. (2005)) . . . 10
2.5 Isotherm Types . . . 18
2.6 Concentration and temperature profiles in the adsorbent and bulk gas phases during adsorption and desorption Yang (1987) . 22
2.7 Isotherm and equilibrium loadings for pressure swing adsorption 25
2.8 Isotherms and equilibrium loadings for temperature swing adsorption . . . 25
2.9 Isotherms and equilibrium loadings for temperature swing adsorption using a pure component stream at the desorption pressure 25
2.10 Isotherms and equilibrium loadings for temperature swing adsorption using a heated inert stream . . . 26
2.11 Overview of adsorbents . . . 30
2.12 Process using activated carbon in a counter-current adsorption system (SRI International et al. (2011)) . . . 39
2.13 Process using carbonate adsorbent in moving bed adsorption system (Park et al. (2009b)) . . . 40
2.14 Moving bed process with heat integration (Kim et al. (2013a)) . 42

3.1 Fluidised bed adsorber . . . 48
3.2 Co-current bed adsorber . . . 48
3.3 Counter-current bed adsorber . . . 49
3.4 1D control volume . . . 50
3.5 Full matrix before Gaussian Elimination . . . 56
3.6 Full matrix after Gaussian Elimination . . . 56
3.7 Compact matrix before Gaussian Elimination . . . 57

3.8 Compact matrix after Gaussian Elimination 57
3.9 Control volume of the systems considered 62
3.10 CO_2 isotherms at various temperatures for the supported amine adsorbent (data points from Krutka and Sjostrom (2011)) . . . 74
3.11 H_2O isotherms at various temperatures for an supported amine adsorbent (data points from Didas et al. (2012)) 77
3.12 CO_2 and N_2 isotherm at 25°C for activated carbon (data points from SRI International et al. (2012)) 78
3.13 H_2O isotherm at various temperatures for activated carbon (data points from Xu et al. (2011)) 79
3.14 CO_2 isotherms at different temperatures for zeolite 13X 81
3.15 N_2 isotherms at different temperatures for zeolite 13X 81
3.16 Moving bed CO_2 capture process with heat integration 88
3.17 Representation of the model of the moving bed CO_2 capture process with heat integration 89

4.1 CO_2 mole fraction profiles in a co-current system for $y_i^0 = 1\times10^{-5}$ 98
4.2 CO_2 mole fraction profiles in a co-current system for $y_i^0 = 0.01$. 98
4.3 CO_2 mole fraction profiles in a co-current system for $y_i^0 = 0.15$. 99
4.4 CO_2 mole fraction profiles in a co-current system for $y_i^0 = 0.5$. 99
4.5 CO_2 mole fraction profiles in a counter-current system for $y_i^0 = 1\times10^{-5}$ 100
4.6 CO_2 mole fraction profiles in a counter-current system for $y_i^0 = 0.01$ 100
4.7 CO_2 mole fraction profiles in a counter-current system for $y_i^0 = 0.15$ 101
4.8 CO_2 mole fraction profiles in a counter-current system for $y_i^0 = 0.5$101

5.1 Diameters of the adsorber at minimum fluidisation and for the terminal settling velocity as a function of particle size of supported amine adsorbent ($\rho_p = 646$ kg.m^{-3}) 109
5.2 Diameters of the adsorber at minimum fluidisation and for the terminal settling velocity as a function of particle size of activated carbon ($\rho_p = 1100$ kg.m^{-3}) 110
5.3 Diameters of the adsorber at minimum fluidisation and for the terminal settling velocity as a function of particle size of zeolite 13X ($\rho_p = 1130$ kg.m^{-3}) 110

6.1 Single Adsorber (Counter-current) 116

6.2 Mole fraction profiles for a counter-current adsorber with amine supported adsorbent and pores saturated with water 118
6.3 Loading profiles for a counter-current adsorber with amine supported adsorbent and pores saturated with water 119
6.4 Temperature profiles for a counter-current adsorber with amine supported adsorbent and pores saturated with water 119
6.5 Profiles of molar flowrate and adsorbate flowrate of components in the flue gas for a counter-current adsorber with amine supported adsorbent and pores saturated with water 120
6.6 Pressure profile for a counter-current adsorber with amine supported adsorbent and pores saturated with water 120
6.7 Mole fraction profiles of CO_2 for counter-current, co-current and fluidised bed adsorbers with amine supported adsorbent and pores saturated with water 122
6.8 CO_2 loading profiles for counter-current, co-current and fluidised bed adsorbers with amine supported adsorbent and pores saturated with water 122
6.9 CO_2 concentration profiles in a counter-current adsorber with amine supported adsorbent and pores saturated with water . . . 123
6.10 CO_2 concentration profiles in a co-current adsorber with amine supported adsorbent and pores saturated with water 123
6.11 CO_2 loading profiles in a counter-current adsorber with amine supported adsorbent and pores saturated with water 124
6.12 CO_2 loading profiles in a co-current adsorber with amine supported adsorbent and pores saturated with water 124
6.13 Adsorbent temperature profiles for counter-current, co-current and fluidised bed adsorbers with amine supported adsorbent and pores saturated with water 125
6.14 CO_2 mole fraction profiles for a counter-current adsorber with amine supported adsorbent and activated carbon (pores saturated with water) 127
6.15 CO_2 isotherms for three adsorbents at 40°C 127
6.16 CO_2 loading profiles for a counter-current adsorber with amine supported adsorbent and activated carbon (pores saturated with water) 128
6.17 Adsorbent temperature profiles for a counter-current adsorber with amine supported adsorbent and activated carbon (pores saturated with water) 128

6.18 CO_2 mole fraction profiles for a co-current adsorber with amine supported adsorbent and activated carbon (pores saturated with water) . . . 129
6.19 Effect of number of co-current fluidised beds in the adsorption column on recovery ($\varepsilon_a = 0.4$) . . . 130
6.20 Effect of number of counter-current fluidised beds in the adsorption column on recovery ($\varepsilon_a = 0.4$) . . . 131
6.21 Effect of adsorbent flowrate on recovery for three different adsorbents . . . 132
6.22 Adsorbent temperature profiles for a counter-current adsorber with zeolite 13X . . . 133
6.23 Gas and solid outlet temperatures for a counter-current adsorber with zeolite 13X . . . 133
6.24 Gas and solid outlet temperatures for a counter-current adsorber with supported amine adsorbent (pores saturated with water) . . . 134
6.25 Effect of mass transfer constant on recovery for three different adsorbents . . . 137
6.26 Impact of the CO_2 mass transfer constant on the mass flowrate of supported amine adsorbent required to obtain 92.1% CO_2 recovery 138
6.27 Effect of the mole fraction of CO_2 in the inlet flue gas on recovery 139
6.28 Adsorbent temperature profiles for various CO_2 mole fractions in the gas inlet for a counter-current adsorber with amine supported adsorbent (pores saturated with water) . . . 139
6.29 Effect of the relative humidity of the inlet flue gas on recovery . . . 140
6.30 Water loading profiles for a counter-current adsorber with amine supported adsorbent for various inlet gas mole fractions of water 141
6.31 Adsorbent temperature profiles for a counter-current adsorber with amine supported adsorbent for various inlet gas mole fractions of water . . . 141
6.32 Effect of the inlet CO_2 concentration in adsorbent pores on CO_2 recovery for the three different adsorbents . . . 142
6.33 Difference between bulk gas and pore CO_2 concentrations for adsorbent pores with and without CO_2 preloaded . . . 143
6.34 Effect of initial water concentration in adsorbent pores on CO_2 recovery for supported amine and activated carbon adsorbents . . . 144
6.35 CO_2 mole fraction profiles for a counter-current adsorber with amine supported adsorbent, activated carbon and zeolite 13X (pores do not contain any water) . . . 144

6.36 Adsorbent temperature profiles for counter-current, co-current and fluidised bed adsorbers with amine supported adsorbent (pores do not contain any water) 145
6.37 Mole fraction profiles of CO_2 for counter-current, co-current and fluidised bed adsorbers with amine supported adsorbent (pores do not contain any water) 145
6.38 CO_2 concentration profiles in a counter-current adsorber with amine supported adsorbent (pores do not contain any water) . . 146
6.39 Mole fraction profiles of water for counter-current, co-current and fluidised bed adsorbers with amine supported adsorbent (pores do not contain any water) 147
6.40 Mole fraction profiles of water for counter-current, co-current and fluidised bed adsorbers with amine supported adsorbent and pores saturated with water 147
6.41 Water concentration profiles in a counter-current adsorber with amine supported adsorbent and pores saturated with water . . . 148
6.42 Effect of molar flowrate of gas on recovery for three different adsorbents 149
6.43 Effect of inlet gas temperature on recovery for three different adsorbents 150
6.44 Adsorbent temperature profiles for a counter-current adsorber with amine supported adsorbent (pores saturated with water) inlet flue gas temperatures of 123°C and 25°C 151
6.45 CO_2 loading profiles in a counter-current adsorber with supported amine adsorbent and pores saturated with water for flue gas entering at 25°C 151
6.46 CO_2 loading profiles in a counter-current adsorber with supported amine adsorbent and pores saturated with water for flue gas entering at 123°C 152
6.47 Effect of inlet adsorbent temperature on recovery 153
6.48 CO_2 loading profiles in a counter-current adsorber with supported amine adsorbent and pores saturated with water for adsorbent entering at 27°C 153
6.49 CO_2 loading profiles in a counter-current adsorber with supported amine adsorbent and pores saturated with water for adsorbent entering at 123°C 154
6.50 Adsorbent temperature profiles in a counter-current adsorber with supported amine adsorbent and pores saturated with water for inlet adsorbent temperatures of 27°C and 123°C 154

6.51 Effect of the product of the overall heat transfer coefficient and area on recovery 155
6.52 Adsorbent temperature profiles for a counter-current adsorber with amine supported adsorbent (pores saturated with water) for various $U_{ext}A_{ext}$ values 156

7.1 Single Regenerator (Counter-current) 160
7.2 Loading profiles for a counter-current regenerator with amine supported adsorbent 162
7.3 Temperature profiles for a counter-current regenerator with amine supported adsorbent 162
7.4 Mole fraction profiles for a counter-current regenerator with amine supported adsorbent 163
7.5 Profiles of flue gas molar flowrate for a counter-current regenerator with amine supported adsorbent 163
7.6 Pressure profile for a counter-current regenerator with amine supported adsorbent 164
7.7 Mole fraction profiles of CO_2 for counter-current, co-current and fluidised bed regenerators with amine supported adsorbent . . . 166
7.8 CO_2 loading profiles for counter-current, co-current and fluidised bed regenerators with amine supported adsorbent 166
7.9 CO_2 loading and equilibrium loadings in a co-current regenerator with supported amine adsorbent 167
7.10 CO_2 loading and equilibrium loadings in a counter-current regenerator with supported amine adsorbent 167
7.11 Adsorbent temperature profiles for counter-current, co-current and fluidised bed regenerators with supported amine adsorbent . 168
7.12 CO_2 mole fraction profiles for a counter-current regenerator with supported amine adsorbent and activated carbon 170
7.13 CO_2 isotherms for the supported amine adsorbent and activated carbon at 120°C 171
7.14 CO_2 loading profiles for a counter-current regenerator with supported amine adsorbent and activated carbon 171
7.15 Adsorbent temperature profiles for a counter-current regenerator with supported amine adsorbent and activated carbon 172
7.16 Water loading profile for a counter-current regenerator with activated carbon 172
7.17 Effect of the number of co-current fluidised beds in the regeneration column on CO_2 removal from the adsorbent ($\varepsilon_a = 0.4$) . . 173

7.18 Effect of the number of counter-current fluidised beds in the regeneration column on CO_2 removal from the adsorbent (ε_a = 0.4) . . . 173
7.19 Effect of the number of co-current fluidised beds in the regeneration column on the wet purity of CO_2 in the regeneration gas outlet ($\varepsilon_a = 0.4$) . . . 174
7.20 Effect of the number of counter-current fluidised beds in the regeneration column on the wet purity of CO_2 in the regeneration gas outlet ($\varepsilon_a = 0.4$) . . . 175
7.21 Effect of the number of co-current fluidised beds in the regeneration column on the dry purity of CO_2 in the regeneration gas outlet ($\varepsilon_a = 0.4$) . . . 175
7.22 Effect of the number of counter-current fluidised beds in the regeneration column on the dry purity of CO_2 in the regeneration gas outlet ($\varepsilon_a = 0.4$) . . . 176
7.23 Effect of the mass flowrate of adsorbent on CO_2 removal from the adsorbent . . . 177
7.24 Effect of the mass flowrate of adsorbent on the wet purity of CO_2 in the regeneration gas outlet . . . 178
7.25 Effect of the mass flowrate of adsorbent on the dry purity of CO_2 in the regeneration gas outlet . . . 178
7.26 Effect on CO_2 removal of mass transfer constant for two different adsorbents . . . 179
7.27 Adsorbent temperature profiles for various k_{CO_2} values at the adsorbent outlet from the counter-current regenerator with activated carbon . . . 180
7.28 CO_2 pore concentration profiles for various k_{CO_2} values at the adsorbent outlet from the counter-current regenerator with activated carbon . . . 180
7.29 Profiles of CO_2 concentration in bulk gas for various k_{CO_2} values at the adsorbent outlet from the counter-current regenerator with activated carbon . . . 181
7.30 Effect on wet CO_2 purity of mass transfer constant for two different adsorbents . . . 181
7.31 Effect on dry CO_2 purity of mass transfer constant for two different adsorbents . . . 182
7.32 Effect of CO_2 mole fraction in the regeneration gas on CO_2 removal from the adsorbent . . . 183

7.33 Effect of CO_2 mole fraction in the regeneration gas on the wet purity of CO_2 in the regeneration gas outlet 184
7.34 Effect of CO_2 mole fraction in the regeneration gas on the dry purity of CO_2 in the regeneration gas outlet 185
7.35 Effect on CO_2 removal of the concentration of CO_2 in the adsorbent at the inlet 186
7.36 Effect on wet CO_2 purity of the concentration of CO_2 in the adsorbent at the inlet 186
7.37 Effect on dry CO_2 purity of the concentration of CO_2 in the adsorbent at the inlet 187
7.38 Effect of the molar flowrate of steam on CO_2 removal from the adsorbent 188
7.39 Effect of the molar flowrate of steam on the wet purity of CO_2 in the regeneration gas outlet 188
7.40 Effect of the molar flowrate of steam on the dry purity of CO_2 in the regeneration gas outlet 189
7.41 Effect of the inlet steam temperature of adsorbent on CO_2 removal from the adsorbent 190
7.42 Effect of the inlet steam temperature on the wet purity of CO_2 in the regeneration gas outlet 191
7.43 Effect of the inlet steam temperature on the dry purity of CO_2 in the regeneration gas outlet 191
7.44 Effect on CO_2 removal of the inlet adsorbent temperature 192
7.45 Effect on wet CO_2 purity of the inlet adsorbent temperature . . 193
7.46 Effect on dry CO_2 purity of the inlet adsorbent temperature . . 193
7.47 Effect of the overall heat transfer coefficient and area on CO_2 removal from the adsorbent 194
7.48 Adsorbent temperature profiles for a counter-current regenerator with activated carbon for various $U_{ext}A_{ext}$ values 195
7.49 Effect of the overall heat transfer coefficient and area on the wet purity of CO_2 in the regeneration gas outlet 195
7.50 Effect of the overall heat transfer coefficient and area on the dry purity of CO_2 in the regeneration gas outlet 196
7.51 CO_2 isotherms for the supported amine adsorbent at adsorption and regeneration temperatures 197

8.1 Diagram of the base case CO_2 Adsorption Cycle using a counter-current adsorber and regenerator 200

8.2 Profiles of the component mole fractions in the adsorber in the full CO_2 capture cycle using supported amine adsorbent 205
8.3 Profiles of the component loadings in the adsorber in the full CO_2 capture cycle using supported amine adsorbent 206
8.4 Profile of the flue gas molar flowrates in the adsorber in the full CO_2 capture cycle using supported amine adsorbent 207
8.5 Gas and solid temperature profiles in the adsorber in the full CO_2 capture cycle using supported amine adsorbent 207
8.6 Pressure profile in the adsorber in the full CO_2 capture cycle using supported amine adsorbent 208
8.7 Adsorbent temperature profile in HEX 2 209
8.8 Loading profiles of components in HEX 2 209
8.9 Profiles of the component mole fractions in the regenerator in the full CO_2 capture cycle using supported amine adsorbent . . 210
8.10 Profiles of the component loadings in the regenerator in the full CO_2 capture cycle using supported amine adsorbent 210
8.11 Gas and solid temperature profiles in the regenerator in the full CO_2 capture cycle using supported amine adsorbent 211
8.12 Profile of the flue gas molar flowrate in the regenerator in the full CO_2 capture cycle using supported amine adsorbent 212
8.13 Pressure profile in the regenerator in the full CO_2 capture cycle using supported amine adsorbent 212
8.14 Adsorbent temperature profile in HEX 1 213
8.15 Loading profiles of components in HEX 1 214
8.16 Adsorbent temperature profiles for cycles with counter-current, co-current and fluidised bed adsorbers for supported amine adsorbent 215
8.17 Isotherms at adsorption and regeneration for the cycle with a counter-current adsorber for supported amine adsorbent 216
8.18 Isotherms at adsorption and regeneration for the cycle with a co-current adsorber for supported amine adsorbent 216
8.19 Heat supplied to produce steam as a function of steam molar flowrate 218
8.20 Effect of the mass flowrate of adsorbent on CO_2 recovery for the cyclic process using the supported amine adsorbent 219
8.21 Effect of the mass flowrate of adsorbent on the wet CO_2 purity for the cyclic process using the supported amine adsorbent . . . 220
8.22 Effect of the mass flowrate of adsorbent on the dry CO_2 purity for the cyclic process using the supported amine adsorbent . . . 220

8.23 Effect of the mass flowrate of adsorbent on the regeneration heat duty for the cyclic process using the supported amine adsorbent 221
8.24 Effect of the flowrate of steam used at the inlet to the regenerator on CO_2 recovery for the cyclic process using the supported amine adsorbent 222
8.25 Effect of the flowrate of steam used at the inlet to the regenerator on the regeneration heat duty for the cyclic process using the supported amine adsorbent 223
8.26 Effect of the flowrate of steam used at the inlet to the regenerator on the wet CO_2 purity for the cyclic process using the supported amine adsorbent 223
8.27 Effect of the flowrate of steam used at the inlet to the regenerator on the dry CO_2 purity for the cyclic process using the supported amine adsorbent 224
8.28 Effect of the flowrate of steam used at the inlet to the regenerator on the total energy required for adsorbent regeneration 225
8.29 Effect of the flowrate of CO_2 used at the inlet to the regenerator on CO_2 recovery for the cyclic process using the supported amine adsorbent 226
8.30 Effect of the flowrate of CO_2 used at the inlet to the regenerator on the heat duty in HEX 2 for the cyclic process using the supported amine adsorbent 227
8.31 Effect of the flowrate of CO_2 used at the inlet to the regenerator on the wet CO_2 purity for the cyclic process using the supported amine adsorbent 227
8.32 Effect of the flowrate of CO_2 used at the inlet to the regenerator on the dry CO_2 purity for the cyclic process using the supported amine adsorbent 228
8.33 Effect of the outlet adsorbent temperature from HEX 1 on CO_2 recovery for the cyclic process using the supported amine adsorbent 229
8.34 Effect of the outlet adsorbent temperature from HEX 1 on the wet CO_2 purity for the cyclic process using the supported amine adsorbent 230
8.35 Effect of the outlet adsorbent temperature from HEX 1 on the dry CO_2 purity for the cyclic process using the supported amine adsorbent 230
8.36 Effect of the outlet adsorbent temperature from HEX 1 on the regeneration heat duty for the cyclic process using the supported amine adsorbent 231

8.37 Effect of the outlet adsorbent temperature from HEX 2 on CO_2 recovery for the cyclic process using the supported amine adsorbent 232
8.38 Effect of the outlet adsorbent temperature from HEX 2 on the wet CO_2 purity for the cyclic process using the supported amine adsorbent 232
8.39 Effect of the outlet adsorbent temperature from HEX 2 on the dry CO_2 purity for the cyclic process using the supported amine adsorbent 233
8.40 Effect of the outlet adsorbent temperature from HEX 2 on the regeneration heat duty for the cyclic process using the supported amine adsorbent 233
8.41 Effect of the mass mass transfer constant on CO_2 recovery for the cyclic process using the supported amine adsorbent 234
8.42 Effect of the mass mass transfer constant on the wet CO_2 purity for the cyclic process using the supported amine adsorbent . . . 235
8.43 Effect of the mass mass transfer constant on the dry CO_2 purity for the cyclic process using the supported amine adsorbent . . . 236
8.44 Effect of the mass mass transfer constant on the regeneration heat duty for the cyclic process using the supported amine adsorbent 236
8.45 Diagram of CO_2 adsorption cycle with heat integration 237
8.46 Effect of the $U_{int}A_{int}$ value of the lean/rich adsorbent heat exchanger on CO_2 recovery for the cyclic process using the supported amine adsorbent 239
8.47 Effect of the $U_{int}A_{int}$ value of the lean/rich adsorbent heat exchanger on the wet CO_2 purity for the cyclic process using the supported amine adsorbent 239
8.48 Effect of the $U_{int}A_{int}$ value of the lean/rich adsorbent heat exchanger on the dry CO_2 purity for the cyclic process using the supported amine adsorbent 240
8.49 Effect of the $U_{int}A_{int}$ value of the lean/rich adsorbent heat exchanger on the regeneration heat duty for the cyclic process using the supported amine adsorbent 240
8.50 Variation in heat duties with increasing values of $U_{int}A_{int}$ 241
8.51 Percentage of heat recovered by the intermediate heat exchanger with increasing values of $U_{int}A_{int}$ 241
8.52 Temperatures of the adsorbent streams leaving the intermediate heat exchanger with increasing values of $U_{int}A_{int}$ 242

8.53 Plate heat exchanger for adsorbents with heat transfer by conduction 243
8.54 Diagram of CO_2 adsorption cycle with heat integration by using a fluid medium 244
8.55 Plate heat exchanger transferring heat between adsorbent and heating/cooling fluid (Solex Thermal Science Inc. (2014)) 244

List of Tables

2.1 Commercial scale CCS projects in operation (Global CCS Institute 2013 (2013)) . . . 14
2.2 Commercial scale CCS projects in construction (Global CCS Institute 2013 (2013)) . . . 15
2.3 Values of parameters of supported amine adsorbent (Krutka and Sjostrom (2011)) . . . 38
2.4 Values of parameters of activated carbon (SRI International (2010)) 40

3.1 Coefficients in Equation 3.36 and 3.37 . . . 69
3.2 Packing constants for Montz structured packing (Stichlmair et al. (1989)) . . . 72
3.3 Values of parameters for CO_2 on supported amine adsorbent . . 74
3.4 Values of parameters for H_2O on supported amine adsorbent . . 76
3.5 Values of parameters for CO_2 and N_2 activated carbon . . . 79
3.6 Values of parameters for H_2O on activated carbon . . . 80
3.7 Values of parameters for CO_2 and N_2 on zeolite 13X . . . 80

4.1 Parameters used to obtain analytical and numerical solutions . . 97

5.1 Constraints on the superficial gas velocity for different moving bed systems . . . 106
5.2 Column and gas parameters and gas velocity in the adsorber for different adsorbents . . . 108
5.3 Adsorbent parameters used for different adsorbents to match the terminal velocity . . . 108
5.4 Parameters and velocities of an adsorber (Yang and Hoffman (2009)) . . . 112

6.1 Parameters used for the base case adsorber . . . 117
6.2 CO_2 recoveries (molar basis) for supported amine adsorbents in three different beds . . . 125

6.3 Values of parameters for zeolite 13X (Cavenati et al. (2004), Chan et al. (2012)) . . . 126
6.4 Adsorbent flowrates required to attain 92.1% CO_2 capture . . . 128
6.5 Literature values for adsorbent flowrates required . . . 136
6.6 Cases with and without preloaded CO_2 on the supported amine adsorbent . . . 142

7.1 Parameters used for the base case regenerator . . . 161
7.2 CO_2 recoveries and purities (molar basis) for supported amine adsorbents in three different regenerators . . . 165
7.3 Parameters used for activated carbon in the single counter-current regenerator . . . 170
7.4 Performance of the three types of regenerators with activated carbon . . . 170

8.1 Parameters used in the columns and heat exchangers for the base case adsorption cycle . . . 202
8.2 Properties of streams shown in Figure 8.1 . . . 204
8.3 CO_2 recoveries, purities and regeneration heat duties for CO_2 capture cycles using the supported amine adsorbent . . . 214
8.4 Coefficients in for the enthalpy of liquid water (National Institute of Standards and Technology (2014)) . . . 217
8.5 Heat requirements of the adsorber, regenerator and heat exchangers . . . 218
8.6 Results of the performance of full CO_2 capture cycles for an outlet adsorbent temperature from HEX 1 at a value higher than the base case and for the base case . . . 229
8.7 Results of the performance of full CO_2 capture cycles for an outlet adsorbent temperature from HEX 2 at a value lower than the base case and for the base case . . . 231
8.8 Parameters for the base case intermediate heat exchanger for heat recovery . . . 238
8.9 Performance of amine absorption and moving bed adsorption systems with supported amine adsorbent . . . 246
8.10 Parameters used to find the power requirement using Equation 2.17 . . . 249
8.11 Performance for a hypothetical adsorbent in a cycle with a counter-current adsorber and regenerator without heat integration . . . 249
8.12 Results of the moving bed process (Figure 8.1) using activated carbon instead of the supported amine adsorbent . . . 252

Nomenclature

Abbreviations

1D	One-dimensional
Al_2O_3	Aluminium oxide
BET	Brunauer, Emmett, Teller
$CaCO_3$	Calcium carbonate
CaO	Calcium oxide
CCS	CO_2 Capture and Storage
CFCs	Chlorofluorocarbons
CH_4	Methane
CO_2	Carbon dioxide
CSTR	Continuous Stirred Tank Reactor
EOR	Enhanced Oil Recovery
ESA	Electric Swing Adsorption
H_2	Hydrogen
H_2O	Water
HCl	Hydrogen chloride
HEX	Heat Exchanger
K	Potassium
K_2CO_3	Potassium carbonate
LDF	Linear Driving Force

M	(Alkali) Metal
MEA	Monoethanolamine
MgO	Magnesium oxide
N_2	Nitrogen
Na	Sodium
Na_2CO_3	Sodium carbonate
$Na_2CO_3.3NaHCO_3$	Wegscheider's salt
NO_x	Nitrogen oxides
O_2	Oxygen
PSA	Pressure Swing Adsorption
SO_2	Sulphur dioxide
SO_x	Sulphur oxides
TSA	Temperature Swing Adsorption
UK	United Kingdom
US	United States
VSA	Vacuum Swing Adsorption
VTSA	Vacuum and Temperature Swing Adsorption

Subscripts

0	Initial guess
ads	Adsorbent
g	Gas
i	Component
in	Inlet
j	Component/stage/control volume
mf	Minimum fluidisation

N	Last component	
n	Iteration number	
out	Outlet	
p	Particle/pore	

Dimensionless Groups

Fr	Froude number	-
Re	Reynolds number	-

Functional Operator

$\nabla.$	Divergence	
∂	Partial differential	
Σ	Sum	
d	Full differential	
$\lvert\ \rvert$	Modulus	

Greek Letters

α	Weight factor	-
Δ	Increment	-
Δ^0	Discriminant in the co-current analytical solution	$mol^2.kg^2$
Δ^L	Discriminant in the counter-current analytical solution	$mol^2.kg^2$
γ	Value indicating the direction of adsorbent flow (1 for co-current and -1 for counter-current)	-
μ_g	Gas viscosity	$kg.m^{-1}.s^{-1}$
ϕ	Sphericity	-
ρ_g	Gas density	$kg.m^{-3}$
ρ_p	Adsorbent particle density	$kg.m^{-3}$
τ	Pore tortuosity	-
ε	Gas void fraction	-

ε_a	Fractional volume of adsorbent	-
ε_p	Void fraction of the adsorbent particles	-
ε_{mf}	Void fraction at minimum fluidisation	-
ε_{pk}	Volume fraction occupied by structured packing	-

Superscripts

0	Gas inlet position	-
in	Inlet	
L	Gas outlet position	-
out	Outlet	
$wall$	Wall of the control volume	

Roman Letters

$\mathbf{A}$	Square Matrix	
$\mathbf{b}$	Vector	
$\mathbf{n}$	Normal unit vector	
$\mathbf{x}$	Vector of unknowns	
$\Delta H_{ads,CO_2}$	Heat of adsorption of CO_2	J.mol^{-1}
$\Delta H_{ads,i}$	Heat of adsorption of i	J.mol^{-1}
ΔH_{ads}	Heat of adsorption	J.mol^{-1}
ΔT	Difference between regeneration and adsorption temperatures	K
Δx_n	Difference in x from previous iteration n	
$\dot{M}$	Molar flowrate of of gas	mol.s^{-1}
$\dot{m}$	Mass flowrate of adsorbent	kg.s^{-1}
$\dot{M}_i^{in}$	Molar flowrate of component i in the bulk gas at the inlet	mol.s^{-1}
$\dot{M}_i^{out}$	Molar flowrate of component i in the bulk gas at the outlet	mol.s^{-1}
$\dot{M}_{CO_2}^{cap,in}$	Molar flowrate of CO_2 at inlet of capture system	mol.s^{-1}

$\dot{M}_{CO_2}^{cap,out}$	Molar flowrate of CO_2 at outlet of capture system	$mol.s^{-1}$
$\dot{M}_{CO_2}^{reg,out}$	Molar flowrate of CO_2 at outlet of regenerator	$mol.s^{-1}$
$\dot{M}_{in}$	Molar flowrate of gas at the inlet	$mol.s^{-1}$
$\dot{m}_{in}$	Mass flowrate of adsorbent at the inlet	$kg.s^{-1}$
$\dot{M}_j$	Total molar flowrate at the outlet of j	$mol.s^{-1}$
$\dot{m}_j$	Adsorbent flowrate at the outlet of j	$kg.s^{-1}$
$\dot{M}_{out}$	Molar flowrate of gas at outlet	$mol.s^{-1}$
$\dot{m}_{out}$	Mass flowrate of adsorbent at the outlet	$kg.s^{-1}$
$\dot{M}_{reg,out}$	Total molar flowrate at outlet of regenerator	$mol.s^{-1}$
$\dot{n}_{i,j}$	Rate of adsorption of i at the outlet of j	$mol.m^{-3}.s^{-1}$
$\dot{n}_i$	Rate of adsorption/desorption of component i per unit volume of adsorbent	$mol.m^{-3}.s^{-1}$
$\dot{n}_{total,j}$	Total rate of adsorption at the outlet of j	$mol.m^{-3}.s^{-1}$
$\dot{V}_g$	Volumetric flowrate of gas	$m^3.s^{-1}$
A	Coefficient in polynomial to calculate enthalpy	-
a	Specific surface area of packing	$m^2.m^{-3}$
A_c	Cross sectional area	m^2
a_i	Amount of component i in the adsorbent per unit mass of adsorbent	$mol.kg^{-1}$
a_i^{in}	Amount of component i in the adsorbent at inlet per unit mass of adsorbent	$mol.kg^{-1}$
a_i^{out}	Amount of component i in the adsorbent at outlet per unit mass of adsorbent	$mol.kg^{-1}$
A_M	Coefficient used in isotherm for H_2O	-
A_w	Coefficient used in the Antoine equation	-
A_{ext}	Heat transfer area	m^2
A_{f_0}	Friction factor constant	-
A_{int}	Heat transfer area of the intermediate heat exchanger	m^2

A_{max}	Coefficient used in isotherm	mol.kg^{-1}
B	Coefficient in polynomial to calculate enthalpy	-
b_i	Langmuir equilibrium constant for component i	Pa^{-1}
b_j	Langmuir equilibrium constant for component j	Pa^{-1}
B_M	Coefficient used in isotherm for H_2O	-
B_w	Coefficient used in the Antoine equation	-
$b_{CO_2,0}$	Pre-exponential factor for CO_2 in Langmuir isotherm	Pa^{-1}
b_{CO_2}	Affinity constant for CO_2 in Langmuir isotherm	Pa^{-1}
b_{i0}	Pre-exponential factor for component i	Pa^{-1}
B_{max}	Coefficient used in isotherm	K^{-1}
b_{N_2}	Affinity constant for N_2 in Langmuir isotherm	Pa^{-1}
C	Coefficient in polynomial to calculate enthalpy	-
C	Total bulk gas concentration	mol.m^{-3}
c	Friction factor constant	-
$C_{p,i}^{in}$	Concentration of component i in the pores of the solid adsorbent particle at inlet	mol.m^{-3}
$C_{p,i}^{out}$	Concentration of component i in the pores of the solid adsorbent particle at outlet	mol.m^{-3}
C_1	Packing constant in friction factor	-
C_2	Packing constant in friction factor	-
C_3	Packing constant in friction factor	-
c_D	Drag coefficient	-
C_i	Concentration of component i in bulk fluid	mol.m^{-3}
C_w	Coefficient used in the Antoine equation	-
C_{CO_2}	Concentration of CO_2 in bulk gas phase	mol.m^{-3}
C_{H_2O}	Concentration of H_2O in bulk gas phase	mol.m^{-3}
C_j	Total gas bulk concentration at the outlet of j	mol.m^{-3}

$c_{p,ads}$	Specific heat capacity of adsorbent	$J.kg^{-1}.K^{-1}$
c_{p,CO_2}	Specific heat capacity of CO_2	$J.kg^{-1}.K^{-1}$
$c_{p,eq}$	Specific heat capacity of equipment	$J.kg^{-1}.K^{-1}$
$C_{p,i,j}$	Pore concentration of i at the outlet of j	$mol.m^{-3}$
$C_{p,i}$	Concentration of component i in adsorbent pores	$mol.m^{-3}$
$C_{Peleg,1}$	Coefficient used in the Peleg isotherm	$mol.kg^{-1}$
$C_{Peleg,2}$	Coefficient used in the Peleg isotherm	$mol.kg^{-1}$
$C_{Peleg,3}$	Coefficient used in the Peleg isotherm	-
$C_{Peleg,4}$	Coefficient used in the Peleg isotherm	-
$c_{pi,g}$	Specific heat capacity of component i in the gas	$J.mol^{-1}.K^{-1}$
D	Coefficient in polynomial to calculate enthalpy	-
d'_p	Equivalent packing particle diameter with adsorbent	m
D^*_p	Dimensionless particle diameter	-
D_C	Column diameter	m
$D_{e,C}$	Effective diffusivity of component i based on concentrations	$m^2.s^{-1}$
$D_{e,q}$	Effective diffusivity of component i based on loadings	$m^2.s^{-1}$
D_{mf}	Column diameter at minimum fluidisation	m
D_m	Molecular diffusion coefficient	$m^2.s^{-1}$
D_p	Particle diameter	m
d_p	Equivalent particle diameter	m
D_t	Column diameter to reach the terminal settling velocity	m
E	Coefficient in polynomial to calculate enthalpy	-
F	Coefficient in polynomial to calculate enthalpy	-
f	Function/Quantity flux	
f'	Jacobian	

f_0	Friction factor	-
f'_0	Friction factor with adsorbent	-
f'_0	Modified friction factor	-
f_1	General function	
f_2	General function	
f_3	General function	
f_j	Value of a flux function at control volume j	
g	Acceleration due to gravity	$m.s^{-2}$
H	Coefficient in polynomial to calculate enthalpy	-
h	Function	
$H^{in}_{i,ads}$	Specific molar enthalpy of component i in the pores of the solid adsorbent particle at inlet	$J.mol^{-1}$
$H^{out}_{i,ads}$	Specific molar enthalpy of i in the pores of the solid adsorbent particle at outlet	$J.mol^{-1}$
$H_{H_2O,gas}$	Gas specific enthalpy	$J.mol^{-1}$
$H_{H_2O,liq}$	Liquid specific enthalpy	$J.mol^{-1}$
$H_{i,ads}$	Specific enthalpy of component i in the gas in the adsorbent pores	$J.mol^{-1}$
$H_{i,g}$	Specific enthalpy of component i in the bulk gas	$J.mol^{-1}$
$H^{in}_{i,g}$	Specific molar enthalpy of component i in the pores of the solid adsorbent particle at inlet	$J.mol^{-1}$
$H^{out}_{i,g}$	Specific molar enthalpy of component i in the pores of the solid adsorbent particle at outlet	$J.mol^{-1}$
$H_{i,j}$	Specific enthalpy of i at the outlet of j	$J.mol^{-1}$
H_{ref}	Enthalpy of component i at the reference temperature	$J.mol^{-1}$
K	Slope of the linear isotherm	$m^3.kg^{-1}$
$k'_{i,A_c\varepsilon_a}$	Modified mass transfer constant	$m^2.s^{-1}$
k_i	LDF mass transfer constant of component i based on concentrations	s^{-1}

k_i'	LDF mass transfer constant of component i based on loadings	s^{-1}
L	Bed length	m
L_{mf}	Bed height at minimum fluidisation	m
$l_{N_2,1}$	Coefficient used in isotherm for N_2	$mol.kg^{-1}$
$l_{N_2,2}$	Coefficient used in isotherm for N_2	$mol.kg^{-1}.K^{-1}$
$l_{N_2,3}$	Coefficient used in isotherm for N_2	Pa^{-1}
$l_{N_2,4}$	Coefficient used in isotherm for N_2	K
m	Bandwidth	
m_{CO_2}	Mass of adsorbed CO_2	kg
m_{eq}	Mass of equipment	kg
N	Total number of components	-
n	Matrix size/iteration	
N_P	Final control volume/Number of control volumes	-
P	Final control volume	
P	Pressure	Pa
p_i	Partial pressure of a component i in the bulk gas	Pa
p_j	Partial pressure of a component j in the bulk gas	Pa
p_{CO_2}	Partial pressure of CO_2	Pa
p_{H_2O}	Partial pressure of H_2O	Pa
$p_{i,sat}$	Saturated vapour pressure of component i	Pa
P_j	Pressure at the outlet of j	Pa
p_{N_2}	Partial pressure of N_2	Pa
p_{sat}	Saturated vapour pressure	Pa
Q	Rate of heat added/removed	W
q	Total flux source	

q^*	Overall equilibrium loading in Ideal Adsorbed Solution Theory	mol.kg^{-1}
$q^*_{CO_2}$	Equilibrium loading of CO_2 per unit mass of adsorbent	mol.kg^{-1}
$q^*_{H_2O}$	Equilibrium loading of H_2O per unit mass of adsorbent	mol.kg^{-1}
$q^*_{N_2}$	Equilibrium loading of N_2 per unit mass of adsorbent	mol.kg^{-1}
q_i^{in}	Amount of component i adsorbed onto the adsorbent at inlet per unit mass of an adsorbent particle	mol.kg^{-1}
q_i^{out}	Amount of component i adsorbed onto the adsorbent at outlet per unit mass of an adsorbent particle	mol.kg^{-1}
q_i	Amount of component i loaded onto the adsorbent per unit mass of adsorbent	mol.kg^{-1}
q_i^*	Equilibrium loading of a component i	mol.kg^{-1}
q_{CO_2}	Mass of CO_2 loaded per unit mass of adsorbent	kg.kg^{-1}
Q_{ext}	Heat rate provided by external heating	W
Q_{heat}	Total heat rate provided to the regenerator	W
$q_{i,j}$	Loading of i at the outlet of j	mol.kg^{-1}
q_i^0	Loading of i at the adsobent inlet of a co-current adsorber	mol.kg^{-3}
q_i^L	Loading of i at the adsorbent inlet of a counter-current adsorber	mol.kg^{-3}
q_{max,CO_2}	Loading of CO_2 at saturation per unit mass of adsorbent	mol.kg^{-1}
$q_{max,i}$	Maximum/saturated loading of component i	mol.kg^{-1}
Q_{reg}	Energy required for sorbent regeneration	J
Q_{steam}	Heat supplied by steam	W
R	Ideal gas constant	J.mol^{-1}.K^{-1}
R_p	Adsorbent particle radius	m
Re_g	Reynolds number for gas	-
S	Surface	
s	Parameter in Wegstein method	

s'	Parameter in Wegstein method	
T	Temperature	K
t	Time	s
T_1	Adsorption temperature	K
T_2	Desorption temperature	K
T_r	Reduced temperature used in polynomial to calculate enthalpy	K
T_{ads}	Temperature of the adsorbent	K
T_{ads}^{in}	Temperature of the adsorbent at the inlet	K
T_{ads}^{out}	Temperature of the adsorbent at the outlet	K
T_{ext}	Ambient temperature	K
T_g	Temperature of the bulk gas	K
T_j	Temperature at the outlet of j	K
T_{ref}	Reference temperature	K
u	Quantity	
u_g	Superficial gas velocity	$\mathrm{m.s^{-1}}$
u_j	Quantity in control volume j	
U_s	Solid superficial velocity	$\mathrm{m.s^{-1}}$
u_s	Real solid particle velocity	$\mathrm{m.s^{-1}}$
u_t	Terminal settling velocity	$\mathrm{m.s^{-1}}$
u_t^*	Dimensionless terminal settling velocity	-
U_{ext}	Overall heat transfer coefficient	$\mathrm{W.m^{-2}.K^{-1}}$
U_{int}	Overall heat transfer coefficient of the intermediate heat exchanger	$\mathrm{W.m^{-2}.K^{-1}}$
u_{mf}	Minimum fluidisation velocity	$\mathrm{m.s^{-1}}$
u_{sett}	Settling velocity of the adsorbent	$\mathrm{m.s^{-1}}$
V	Volume	$\mathrm{m^3}$

V_j	Volume of control volume j	m^3
w_j	Weights	-
x	Axial position	m
x_1	Variable of unknown value	
x_2	Variable of unknown value	
x_3	Variable of unknown value	
x_i	Mole fraction of i in adsorbate	-
x_n	Solution for iteration n	
y	Variable	
y_i^{in}	Mole fraction of component i in the gas at the inlet	-
y_i^{out}	Mole fraction of component i in the gas at the outlet	-
y_i	Mole fraction of i in bulk gas	-
y_{CO_2}	Mole fraction of CO_2 in bulk gas phase	-
y_{H_2O}	Mole fraction of H_2O in bulk gas phase	-
$y_{i,j}$	Mole fraction of i at the outlet of j	-
y_i^0	Mole fraction of i at the gas inlet	-
y_i^L	Mole fraction of i at the gas outlet	-
Z	Length	m
$\Delta H_{ads,i}$	Heat of adsorption of component i	$J.mol^{-1}$
ΔP	Pressure drop	Pa
$\Delta P'$	Pressure drop with adsorbent	Pa

Chapter 1

General Introduction

Many industrial processes involve the use of adsorption and desorption for separating components. Adsorption can be defined as the transfer of one or more species contained in a fluid to the surface of a solid. Desorption involves the transfer of components in the opposite direction, back into the fluid phase. Examples of applications of adsorption technology in the chemical industry include: gas dehydration, sweetening of sour gas, hydrogen purification and air separation (Ruthven (1984)).

Another potential practical implementation for adsorption technology that has been considered in the last few decades is for carbon dioxide (CO_2) capture from flue gas resulting from large sources of fossil fuel combustion. There have been some setbacks in reaching global agreements over reduction targets for greenhouse gas emissions such as the Copenhagen Summit in 2009 (United Nations Framework Convention on Climate Change (2009)). Initially, this conference was aimed at reaching a target of halving greenhouse gas emissions by 2050 from emission levels of 1990. Despite these setbacks, the control over the amount of CO_2 emitted from fossil fuels is nevertheless a political priority. Eventually, CO_2 capture and storage (CCS) will be a likely option for meeting reduction targets if energy from fossil fuels continues to be used. In fact, it was proposed that to achieve the 50% CO_2 reduction target by 2050, the cost of decarbonising energy production would be 70% higher without CCS (International Energy Agency (2009), Department of Energy and Climate Change (2012)).

Until now, CCS has never been adopted commercially in the power generation sector. However, in the natural gas purification industry, CO_2 capture is a relatively mature technology which is used to enhance the value of the product. CO_2 capture from natural gas commonly uses gas-liquid absorption in vessels containing structured packing to maximise surface area and minimise mass transfer resistance. A chemical solvent such as an amine-water solution

is used as the CO_2 absorbent (Metz et al. (2005)).

CO_2 removal from fossil-fuel combustion sources used to generate power or for other industrial purposes accounts for the majority of total energy consumption required in the overall process of CO_2 capture, transport and storage (Metz et al. (2005)). Alternative technologies, that are capable of reducing the energy associated with CO_2 capture therefore need further consideration. These alternative technologies could bring down capital costs (e.g. for equipment and raw materials) as well as operating costs (e.g. energy and maintenance). The aim therefore is to develop technologies which are more adapted to the unfavourable conditions for post-combustion CO_2 capture and adsorption based processes are worth considering.

Adsorption processes commonly use vessels filled with randomly packed solid adsorbent particles which remain static as a fluid mixture flows through the void spaces left between particles. One or more of the components in the fluid adsorb onto the adsorbent material and the fluid exiting the adsorber vessel contains the least adsorbable components. In an alternative configuration, a moving bed system can be used where both gas and solid adsorbent continuously flow through a vessel. In fixed beds, the entire vessel is removed from service in order to regenerate the adsorbent and a secondary vessel with fresh adsorbent is used to continue to process the fluid. However, in a moving bed process, the adsorbent is sent to a secondary vessel where the adsorbed components can be removed. The regenerated adsorbent is then sent back to the adsorber.

This thesis aims to contribute to exploring the potential offered by moving bed adsorption processes for post-combustion CO_2 capture from a typical flue gas from a coal fired power plant. The goal being to determine if they are advantaged over the incumbent and more mature absorption technology. The evaluation of the performance of moving bed adsorption cycles will be studied by considering several cycle configurations and operating parameters. Although adsorption technology is used effectively for many applications such as for natural gas sweetening or the drying of gas streams, its use for post-combustion CO_2 capture remains questionable and uncertain. However, moving bed adsorption processes which integrate novel adsorbents that have recently been developed, could offer promising results for applications in post-combustion CO_2 capture.

1.1 Motivations

Within the context of post-combustion CO_2 capture, absorption systems using amine solutions have demonstrated high performance in terms of CO_2 capture and purity but at significant energy penalties and operating costs.

Recent progress in the development of adsorbent materials has potentially allowed research to be extended to adsorption systems and moving bed adsorption processes. However, the challenge is in designing an adsorption process that best utilises these materials. In theory, a moving bed process does this but there are clear operational challenges with moving adsorbents around.

The main goal of this work has been to construct models of continuous moving bed adsorption systems and to evaluate how much of an improvement may potentially be found if existing adsorbent materials are used in moving bed adsorption technology. If sufficient improvements in performance over the amine absorption process are found then this work may spark a desire to addressing the challenges of material handling associated with moving bed adsorption processes.

From available literature on the subject of CO_2 adsorption, a direct comparison between the performance of moving bed CO_2 adsorption processes and more mature CO_2 capture processes has not been found. Additionally, a study which compares the performance of moving bed CO_2 adsorption processes for different types of adsorbents has not been found in the literature either. Therefore, the work carried out in this thesis is novel in these regards.

Some questions that this thesis attempts to answer are:

Can the performance of adsorption processes for CO_2 removal be improved to match or surpass the performance of amine absorption processes?

Are there any suitable adsorbent materials that can be used in adsorption processes for post-combustion CO_2 capture at industrial scale? If more than one adsorbent exists, which would offer the highest potential in terms of performance, energy utilisation and overall cost reduction?

What is the best arrangement or cycle design for moving bed CO_2 adsorption processes?

1.2 Thesis Structure

This thesis is broken down as follows:

Chapter 2 contains a prior art review.

Chapter 3 describes the mathematical model developed as a tool to evaluate the performance of moving bed adsorption systems.

Chapter 4 focuses on specific cases considered to check the validity of the numerical model with analytical solutions.

Chapter 5 aims to determine the fluidisation limits of a moving bed process.

Chapters 6 and 7 analyse adsorbers and regenerators independently.

Finally Chapter 8 considers the performance of full moving bed cycles of the adsorber and regenerator. Their performance is compared to other CO_2 capture technologies.

Chapter 2

Literature Review

2.1 Context for CO_2 Capture and Storage

2.1.1 Climate Change

Carbon dioxide (CO_2) along with some other gases such as methane (CH_4) and chlorofluorocarbons (CFCs) are greenhouse gases responsible for global warming. CO_2 is the main greenhouse gas because it has the highest emissions of all greenhouse gases: in 2004, nearly 77% of total greenhouse gas emissions were CO_2 (Metz et al. (2005)).

Concerns over greenhouse gas emissions and their effect on climate change is a serious issue which needs to be tackled within the next few decades. The control over climate change will be attained by large-scale reductions in CO_2. However, since the Industrial Revolution, the concentration of CO_2 in the atmosphere has sharply increased from 280 ppm (Metz et al. (2005)) to 400 ppm in 2013 (International Energy Agency (2013b)). In parallel, the average global temperature has risen by 0.85°C over the period 1880-2012 (Intergovernmental Panel on Climate Change (2013)). It has therefore been suggested that anthropogenic greenhouse gas emissions have been the main cause for climate change in the last few centuries. The results being sea level rises, severe weather modification, ocean acidification and reductions in snow cover.

Currently, the majority of countries recognise the need for urgent action against climate change. Many countries have put in place greenhouse gas emissions reduction targets. For example, the European Commission has put in place legislations to reduce greenhouse gas emissions by 20% from 1990 levels by 2020. Additionally, a maximum increase in the global average temperature of 2°C has been proposed by the IEA to minimise the impact of climate change (International Energy Agency (2008)). However, countries worldwide face a challenge of reaching environmental targets without compromising economic

and social development.

2.1.2 Sources of CO_2 Emissions

The increase in the release of CO_2 is primarily due to the combustion of fossil fuels for energy production. About 85% of all CO_2 emissions are from power and heat generation, transport and industry sectors as shown in Figure 2.1. As expected, industrialised and developing countries are the largest CO_2 emitters with 80% of global emissions. China are followed by the United States of America as the world's greatest contributors to CO_2 emissions. Together, their emissions are 40% of total world CO_2 emissions (International Energy Agency (2013a)). The majority of worldwide CO_2 emissions result from electricity and heat generation. This sector is dominated by the use of coal (cf. Figure 2.2) which produces twice the level of CO_2 emissions produced by natural gas (for the same energy output). However, it is favoured for its low cost and widespread availability (International Energy Agency (2013b)).

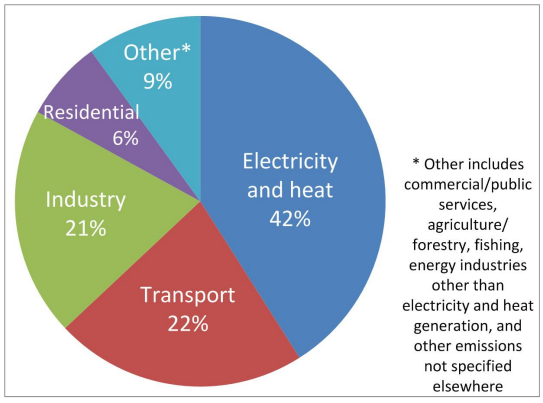

Figure 2.1: World CO_2 emissions by sector (2011) (International Energy Agency (2013a))

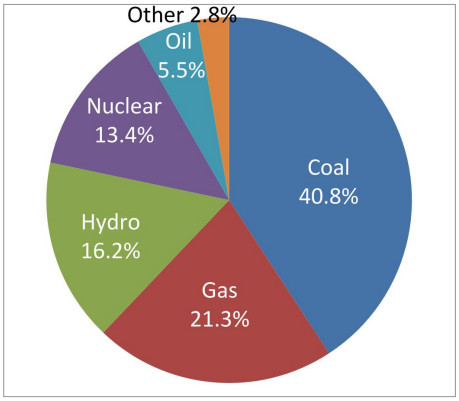

Figure 2.2: World electricity production from different fuel sources (2010) (International Energy Agency (2012))

2.1.3 Methods for Reducing CO_2 Emissions

There is a potential for significant reductions of greenhouse gas emissions if abatement measures are implemented in the power generation industry using coal, gas and oil. The three main methods are:

- **Decrease of energy consumption:** efficiencies of power plant technologies and processes consuming fossil energy could be enhanced to reduce the amount of energy needed. For example, the use of supercritical steam cycles can improve efficiency by 5-15% and the improved design of turbine blades can improve efficiency by 0.84-2.6% (Campbell (2013)).

- **Conversion to alternative fuels:** if power production is switched from fossil fuel sources to either renewable or nuclear energy, CO_2 emissions from power generation could be drastically reduced.

- **CO_2 capture and storage:** it offers the potential to reduce CO_2 emissions to a greater extent. It allows the continued use of fossil fuel and it can be implemented to various large emitters of greenhouse gases such as power stations, oil refineries or chemicals, cement and steel production plants. CO_2 capture and storage consists of chemically or physically separating CO_2 from gas produced by combustion or gasification. The gas is then purified and transported for further use or storage. CO_2 can be used for enhanced oil recovery (EOR) in the oil industry or in the chemical and food industries. It can also be permanently stored away from the atmosphere in underground rock formations, depleted oil and gas reservoirs or deep saline aquifers.

2.1.4 Pathways for CO_2 Capture and Technologies

There are three main ways to capture CO_2 produced for power generation (cf. Figure 2.3). The consideration of one pathway over another is dependent on various criteria such as the type of fuel used, retrofit capabilities, costs, size of power plant or desirable by-products needed. There are advantages and disadvantages associated with each pathway.

- **Post-combustion capture:** separation of CO_2 takes place after combustion of the fuel (e.g. coal, gas, biomass). The flue gas is composed mainly of N_2 ($\approx$ 75%) and CO_2 ($\approx$ 3-15%). Other minor components are O_2, H_2O and impurities (e.g. SO_x and NO_x). The flue gas exits the process near atmospheric pressure. Commonly stated advantages with post-combustion capture are flexibility to be retrofitted to existing power plants and the possibility to temporarily shut-down the CO_2 capture process whilst maintaining power production (Figueroa et al. (2008)).

- **Pre-combustion capture:** it involves the removal of CO_2 after gasification and the water gas shift reaction. Synthesis gas or syngas (mixture of H_2 and CO) is produced from hydrocarbons contained in fossil fuel/biomass. The fuel reacts with oxygen (pure or from air) and steam to produce CO and H_2. After the water gas shift reaction (between CO and H_2O), additional H_2 is formed along with CO_2. The syngas from the gasifier is at high pressure (2-7 MPa) and the CO_2 concentration is higher than for post-combustion capture: 15-60% (Metz et al. (2005)). Once CO_2 is removed from the syngas, the remaining H_2 can be combusted cleanly in a gas turbine to generate power.

- **Oxyfuel combustion:** Air separation is required prior to combustion to produce pure O_2 for combustion with a fuel. A stream containing CO_2 and H_2O (with impurities such as SO_x) is produced. After water is condensed, the flue gas contains a high concentration of CO_2 (>80%), requiring less treatment than for post-combustion capture (Metz et al. (2005)).

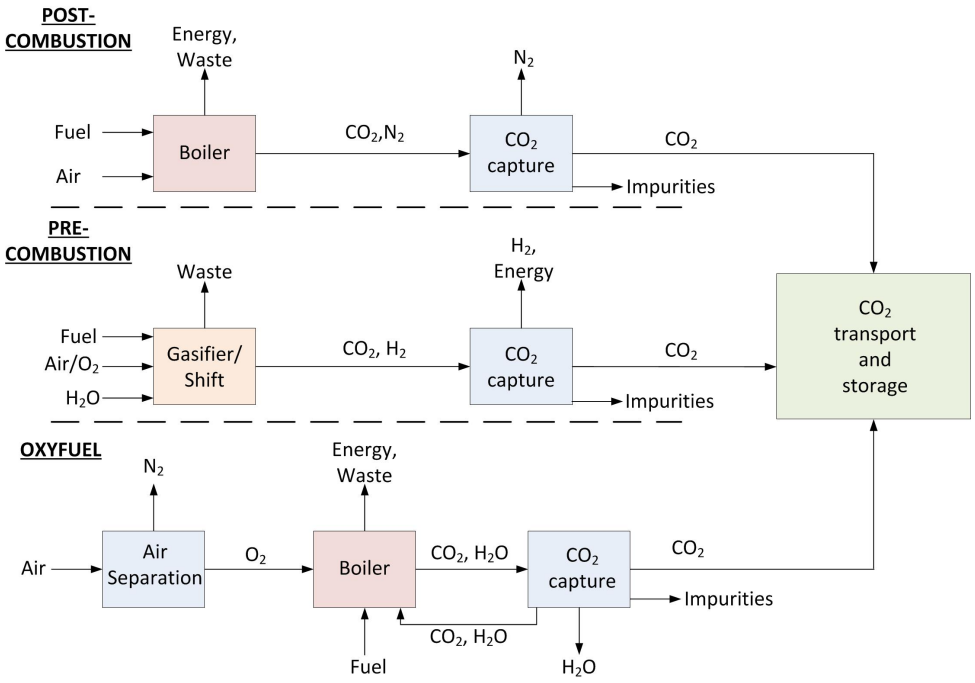

Figure 2.3: CO_2 capture pathways (Figueroa et al. (2008))

2.1.5 Post-combustion CO_2 Capture Technologies

There are a limited number of process technologies considered for removing CO_2 from flue gas. Three main ones are described here.

2.1.5.1 Absorption

Most applications of CO_2 removal are by chemical or physical absorption (cf. Table 2.1). For chemical absorption, a solvent (typically diluted amine) reacts reversibly with CO_2 (cf. Figure 2.4). The gas and solvent flow counter-currently in an absorption column. CO_2 lean gas exits at the top of the absorber whereas CO_2 rich solvent is heated and regenerated in a stripper in which a high input of energy is supplied by a reboiler to produce steam. Hot solvent from the regenerator passes heat to cooler absorbent leaving the absorber in the rich/lean solvent heat exchanger. Lean solvent also needs further cooling before entering the regenerator. For a commonly used 30wt% MEA (monoethanolamine) solution in water at 40°C and 12 kPa CO_2 partial pressure, the CO_2 loading is 0.5 mol.mol MEA^{-1} (2.5 mol.kg^{-1} of solution) (Aronu et al. (2011)). The heat of reaction with CO_2 and the heat capacity are higher than for solid adsorbents (Kim et al. (2013b)) which results in higher energy requirements for regeneration.

This technology is effective as it gives a high CO_2 recovery and purity and the solvent is thermally stable. Additionally, there is an advantage of being able

to run the regenerator at an elevated pressure to obtain a CO_2 product at high pressure requiring less power for compression. However, there are high costs associated with large flowrates of steam needed to regenerate the amine solvent. Pre-treatment steps are usually required to remove SO_x/NO_x. The solvent undergoes degradation in presence of SO_x or O_2 and it causes corrosion to equipment. The length of the columns used tend to be high for post-combustion CO_2 capture and a high reboiler heat duty is necessary. Research carried out in CO_2 absorption focuses on reducing steam consumption by process optimisation (Duan et al. (2012)), improved heat integration (Gao et al. (2014)), development of novel solvents with higher CO_2 loadings, faster kinetics (Zhicheng et al. (2013)), lower potential for degradation (Wang and Jens (2014)) or corrosion (Pearson et al. (2013), Gunasekaran et al. (2013)) and requiring less heat for regeneration (Mangalapally et al. (2012), Liebenthal et al. (2013)).

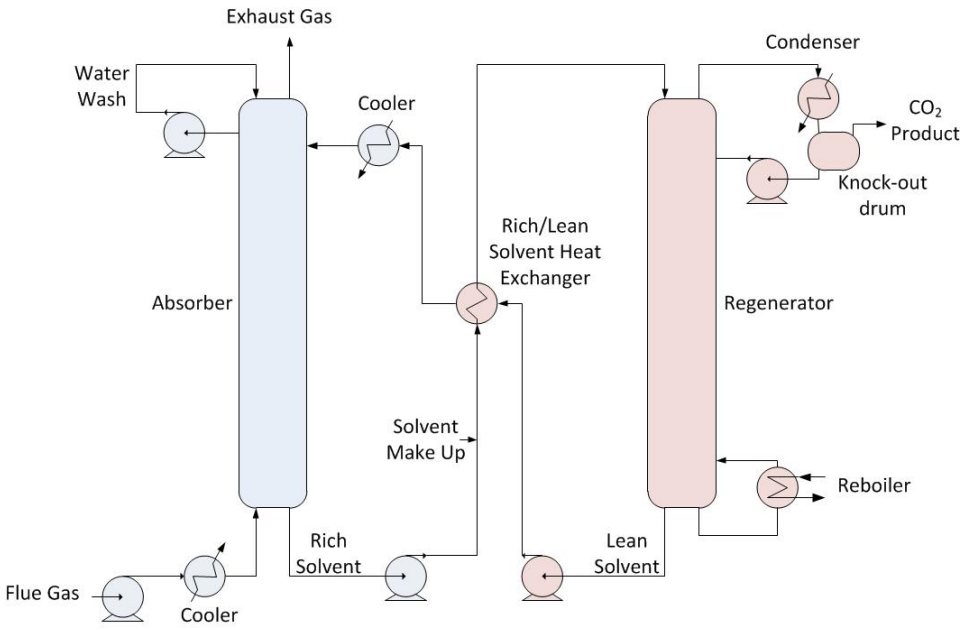

Figure 2.4: Simplified diagram of post-combustion CO_2 capture using absorption (Metz et al. (2005))

Another chemical solvent widely considered is aqueous ammonia which has a lower heat of reaction than amines thus requiring a lower energy for regeneration. Other advantages for it include having a high capacity for CO_2, reduced degradation of solvent and tolerance to O_2. A major drawback is the higher volatility of ammonia which leads to loss of solvent. A chilled ammonia process, operating at low temperature, has been developed by Alstom (Figueroa et al. (2008)).

Physical absorption is generally not considered for post-combustion capture, due to the low CO_2 partial pressure. Regeneration of the solvent requires less

energy than chemical absorption as there is a lower CO_2 and solvent interaction. Examples of physical solvents used for CO_2 capture are Selexol (mixture of dimethyl esthers of polyethylene glycol) and Rectisol (refrigerated methanol). Carbonate solutions and ionic liquids have shown the ability to offer lower energy penalties for regeneration (Harkin et al. (2012), Wappel et al. (2010)).

2.1.5.2 Membrane Separation

Membrane processes involve selective permeation of gases through a porous material. It is driven by pressure difference or CO_2 partial pressure difference (Metz et al. (2005)). High energy penalties compared to amine absorption have been reported due to a high pressure of flue gas required in the feed (Herzog et al. (1991), Sluijs et al. (1992)). For post-combustion CO_2 capture, the use of hybrid systems in which a membrane is used inside a gas-liquid separation system has been considered to improve selectivity (Metz et al. (2005)). An amine solution flows on one side of the membrane and flue gas passes on the other side. These systems would typically be designed to have a high surface to volume ratio. Operational issues such as foaming, flooding, entrainment and channelling can thus be avoided. The overall operation of this type of membrane system is however similar to chemical absorption (Metz et al. (2005)).

2.1.5.3 Adsorption

Adsorption processes are one of the most promising alternatives to CO_2 capture by absorption. They have the potential to overcome the main handicap which is the cost of regeneration. Also, the absence of an aqueous phase means that there is less corrosion.

Adsorption units are typically vessels containing a porous solid, known as the adsorbent which physically/chemically captures CO_2 as the flue gas passes through it. The most common designs of adsorption systems are fixed bed vessels where the entire vessel is filled with a packed bed of adsorbent particles. Once a bed is saturated with CO_2, it can be regenerated either by an increase in temperature, known as *Temperature Swing Adsorption* (TSA) or a decrease in partial pressure *Pressure Swing Adsorption* (PSA). PSA cycles allow for faster regeneration than TSAs but they have lower dynamic capacities. For a continuous operation, multiple beds are used. Larger pressure ratios allow better separation of CO_2. Most fixed bed systems for CO_2 capture need high adsorbent quantities and large vessel sizes. This applies in particular to TSAs in which longer times for regeneration are required for heating and cooling the bed (Metz et al. (2005)). In VSAs (Vacuum Swing Adsorption), in which

regeneration is carried out below atmospheric pressure and PSAs, electrical energy is needed to run vacuum and compression pumps (Pirngruber et al. (2013b), Lee and Sircar (2008)). Electrical energy is however more costly than steam in a power plant. A high CO_2 concentration in the product is difficult to obtain without complex cycle designs which may lead to a greater number of vessels.

Parameters such as the solid adsorbent properties, impurities in the gas and the operating temperature can affect the level of separation. It is desirable that the adsorbent has high CO_2 capacity and selectivity and that kinetics of adsorption and desorption are fast in order to reduce the amount of adsorbent required, reduce the energy for regeneration and to have a high purity product. From an energy balance on the system, a low heat of adsorption and a low heat capacity of the solid would minimize energy for regeneration.

Disadvantages of adsorption systems are linked to their practical implementation and adsorbent suitability. Water and other impurities contained in flue gas could severely affect capture performance. Limitations with the choice of the adsorbent has been a key issue.

2.1.5.4 Challenges associated with CCS

Technical and economic issues restrict the deployment of CCS in the electricity generation industry. With post-combustion CO_2 capture, the flue gas exits the boiler at low CO_2 partial pressures and in presence of impurities. High heat duties are needed for the capture process on large-scale applications such as power plants. A plant with CCS would inevitably require consumption of more fuel than a plant without CCS as CO_2 capture and compression account for a large percentage of running costs.

No economic incentives exist yet for CCS to be applied to the power generation sector. Furthermore, legislation for CO_2 emissions in this sector are fairly deficient globally despite the restriction of building new coal-fired power plants without CCS capability in the UK (Smith (2011)).

The increase in capital and operating costs associated with CCS infrastructure remains a key issue for its implementation. To be economically feasible, higher electricity prices seem unavoidable.

2.1.5.5 Current CCS Projects

Before 2014, there weren't any CCS projects in operation within the electricity generation industry (cf. Table 2.1). However, post-combustion and pre-combustion CO_2 capture plants are being constructed and are scheduled to run

in 2014 (cf. Table 2.2). There are also many planned CCS projects for power generation all over the world. CCS has been applied in particular to natural gas purification and gasification/H_2 production due to higher CO_2 partial pressures and the benefit of the added value for product gases with CO_2 removed. At present, absorption with chemical and physical solvents are the most common technologies.

Table 2.1: Commercial scale CCS projects in operation (Global CCS Institute 2013 (2013))

Project	**Country**	**Year of operation**	**Industry**	**Capture technology**	**Storage**
Val Verde Natural Gas Plants	US	1972	Natural gas	Absorption (amine)	EOR
Enid Fertilizer CO_2-EOR Project	US	1982	H_2/fertiliser production	unknown	EOR
Shute Creek Gas Processing Facility	US	1986	Natural gas	Absorption (Selexol)	EOR
Sleipner CO_2 Injection	Norway	1996	Natural gas	Absorption (amine)	Deep saline aquifer
Great Plains Synfuel Plant and Weyburn-Midale Project	Canada	2000	Gas/liquid fuel from coal	Absorption (Rectisol)	EOR
In Salah CO_2 Storage	Algeria	2004 (suspended since 2011)	Natural gas	Absorption (MDEA)	Deep saline aquifer
Snøhvit CO_2 Injection	Norway	2008	Natural gas	Absorption (amine)	Deep saline aquifer
Century Plant	US	2010	Natural gas	Absorption (Selexol)	EOR
Air Products Steam Methane Reformer EOR Project	US	2013	H_2 production	Adsorption (PSA)	EOR
Petrobras Lula Oil Field CCS Project	Brazil	2013	Natural gas	unknown	EOR
Coffeyville Gasication Plant	US	2013	H_2/fertiliser production	Absorption (Selexol) Adsorption (PSA)	EOR
Lost Cabin Gas Plant	US	2013	Natural gas	Absorption (Selexol)	EOR

Table 2.2: Commercial scale CCS projects in construction (Global CCS Institute 2013 (2013))

Project	**Country**	**Year of operation**	**Industry**	**Capture technology**	**Storage**
Boundary Dam Integrated CCS Demonstration Project	Canada	2014	Power generation (post-combustion)	Absorption (Cansolv)	EOR
Illinois Industrial CCS Project	US	2014	Ethanol production	No capture (compression +dehydration)	Deep saline aquifer
Kemper County IGCC Project	US	2014	Power generation (pre-combustion)	Absorption (Selexol)	EOR
Uthmaniyah CO_2-EOR Project	Saudi Arabia	2014	Natural gas	Absorption (amine)	EOR
ACTL with Agrium CO_2 Stream	Canada	2015	H_2/fertiliser production	unknown	EOR
Gorgon Carbon Dioxide Injection Project	Australia	2015	Natural gas	Absorption (amine)	Deep saline aquifer
Quest	Canada	2015	H_2 production	Absorption (amine)	Deep saline aquifer
ACTL with North West Sturgeon Refinery CO_2 Stream	Canada	2016	Oil refining	unknown	EOR

2.2 Adsorption Separation

The subject of adsorption separation is discussed extensively in literature by Ruthven (1984), Yang (1987), Crittenden and Thomas (1998) and Tien (1984). Information from these sources has been used in the rest of this literature review and it has been summarised.

Important parameters commonly associated with the study of adsorption systems are *capacity*, *selectivity*, *recovery*, *purity* and *productivity* (Yang (1987)). Descriptions are given below for these parameters and other ones associated with CO_2 adsorption:

- **CO_2 capacity (or loading):** It is the amount of CO_2 adsorbed per unit mass/volume of adsorbent.

- **CO_2 selectivity:** The selectivity is the relative amount of CO_2 adsorbed to that of another species. It is generally expressed as the ratio of the loading at equilibrium of the most adsorbed component to that of another component in the mixture.

- **CO_2 recovery:** It is also referred to as *capture/removal rate/efficiency*. It is defined by the amount/flowrate of CO_2 removed from the flue gas as a percentage of the amount/flowrate of CO_2 initially present in the flue gas:

$$\text{CO}_2 \text{ Recovery } \% = 100 \times \frac{\dot{M}_{CO_2}^{cap,in} - \dot{M}_{CO_2}^{cap,out}}{\dot{M}_{CO_2}^{cap,in}} \tag{2.1}$$

  with

  $\dot{M}_{CO_2}^{cap,in}$: molar flowrate of CO_2 at the inlet of CO_2 capture system (mol.s^{-1})

  $\dot{M}_{CO_2}^{cap,out}$: molar flowrate of CO_2 at the outlet of CO_2 capture system (mol.s^{-1})

  Typically, a recovery of 90% or above is targeted for a CO_2 capture process.

- **CO_2 purity:** It is defined by the percentage of CO_2 in the gas leaving the regenerator:

$$\text{CO}_2 \text{ Purity } \% = 100 \times \frac{\dot{M}_{CO_2}^{reg,out}}{\dot{M}_{reg,out}} \tag{2.2}$$

  with

$\dot{M}_{CO_2}^{reg,out}$: molar flowrate of CO_2 at the outlet of sorbent regeneration system ($mol.s^{-1}$)

$\dot{M}_{reg,out}$: total molar flowrate at the outlet of the sorbent regeneration system ($mol.s^{-1}$)

- **Adsorbent productivity:** It is measured by the amount of product or feed mixture processed per unit mass/volume of adsorbent per unit time.
- **Energy required for regeneration:** the heat required for sorbent regeneration is the total heat used in the overall CO_2 capture process. For aborption, this is mainly from the energy required by the reboiler but it can also include heat supplied by independent heat exchangers used to raise the temperature of a gas or solid stream in the process. For example, any additional source of heating in the regenerator also contributes to the heat of regeneration.
- **Sorbent circulation rate/sorbent inventory required**
- **Capital and operating costs:** Capital costs will primarily be dependent on the overall sizes of the processing units used. The operating costs are mainly dependently on the energy required by the entire process and in particular for the heat of regeneration.

The majority of the material covered by Ruthven (1984), Yang (1987), Crittenden and Thomas (1998) and Tien (1984) involves fixed bed operation. CO_2 adsorption processes involving fixed beds have been covered widely. Examples of applications of fixed bed cyclic PSA processes to post-combustion CO_2 capture are given by Kikkinides et al. (1993), Chue et al. (1995) and Zhang et al. (2008) a TSA cycle has been considered by Lee and Sircar (2008). On the other hand, a very small number of commercial applications use moving bed processes. Examples of work carried out in this area for CO_2 capture are given later in section 2.7.

2.3 Adsorption Equilibrium and Loading

2.3.1 Equilibrium Loading and Isotherms

A solute that is adsorbed is known as the adsorbate and the amount of solute adsorbed is known as the *loading*, *capacity* or *uptake*. An adsorption system is said to be at equilibrium when the mass transfer of a solute to the surface of an adsorbent is equal to the mass transfer from the adsorbent surface. The amount

adsorbed at equilibrium depends on the temperature and the concentration of the solutes in the fluid phase.

If the amount of a solute adsorbed at equilibrium per unit mass of adsorbent is measured, at the same temperature, for various solute concentrations in the fluid phase (or solute partial pressures if the fluid is a gas) then an important curve known as the adsorption isotherm is obtained. Typically, as the concentration of the solute in the fluid is increased, the amount adsorbed also increases. As the adsorbent reaches its maximum capacity, it becomes saturated.

For a gas-solid system, the loading of a component i at equilibrium (q_i^*) is a function of temperature (T) and its partial pressure in the fluid (p_i):

$$q_i^* = f\left(T, p_i\right) \tag{2.3}$$

For a single solute i, the total system pressure, P, is equal to p_i. A plot of q_i^* as a function of p_i at a fixed temperature, T, is known as an *isotherm*. Generally, as p_i increases at a given temperature, T, q_i^* increases. Additionally, if T is increased, q_i^* is reduced.

2.3.2 Types of Isotherms

There are five types of isotherms that can be found in detailed literature about adsorption (Yang (1987), Ruthven (1984)). It is known as the BET (Brunauer, Emmett and Teller) classification. Three adsorbent types that have been encountered in the following work are types I, III and V as shown in Figure 2.5.

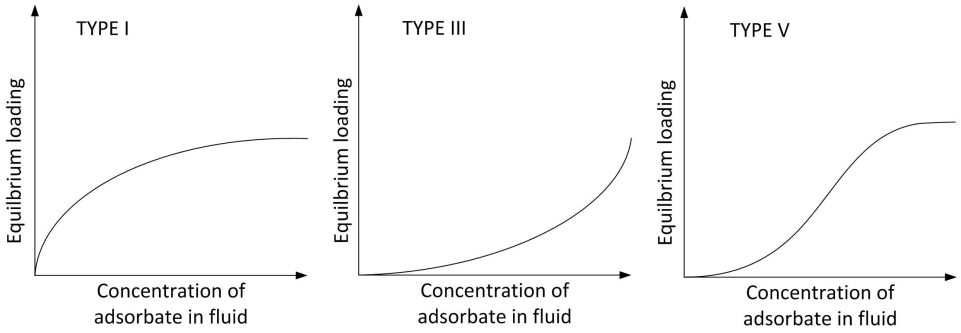

Figure 2.5: Isotherm Types

Type I is the most common type and CO_2 adsorption on most adsorbents is generally of this type. It is commonly represented by the Langmuir model (described in section 2.3.3). Type III and V are common for water adsorption on certain adsorbents. for example, the type V isotherm is observed for water on activated carbon.

2.3.3 Isotherm Models

The isotherm is important for assessing the performance of an adsorbent. A suitable isotherm model is also fundamental for modelling adsorption processes. To develop an isotherm model, equilibrium loadings need to be measured over the required range of temperatures and adsorbate partial pressures. An isotherm model is then fit to this data. To facilitate calculations and to reduce computational time, relatively simplistic isotherm models are desirable. However, the error between experimental equilibrium loadings and those found from the model should be small for greater accuracy.

In the literature for adsorption, there are many isotherm models which are more or less suited for specific adsorbate and adsorbent pairs. Kinetic or thermodynamic equations are mostly used to obtain expressions for the loading at equilibrium as a function of temperature and adsorbate concentration in the gas. In some cases, empirical models derived from fundamental isotherm models are formulated to improve the fit of the predictive model to the experimental data. As well as allowing better understanding of the adsorption behaviour of an adsorbate onto an adsorbent, a model with physical significance can avoid the errors associated with interpolation/extrapolation of experimental data.

The most common isotherm models for a single adsorbed component are shown next along with a model for multiple adsorbed components.

2.3.3.1 Langmuir Model

Many type I isotherms can be represented by the Langmuir model. For initial increases in partial pressure of the adsorbate in the fluid, the equilibrium loading increases steeply but as more of the adsorption sites get filled with adsorbate, the loading levels off. The assumptions for the Langmuir isotherm are that molecules are adsorbed at a fixed number of adsorption sites and that each site can only hold one molecule. In addition to all sites being equivalent, there is no interaction between adsorbed molecules on neighbouring sites.

The equation for the Langmuir model for a single component is:

$$q_i^* = \frac{q_{max,i} b_i p_i}{1 + b_i p_i} \tag{2.4}$$

The loading at saturation should be the same for all temperatures, however the equilibrium constant, b_i, is temperature dependant and it can follow a van 't Hoff expression (Yang (1987)):

$$b_i = b_{i0} \exp\left(\frac{-\Delta H_{ads,i}}{RT}\right) \tag{2.5}$$

with:

q_i^*: equilibrium loading of adsorbate i (mol.kg^{-1})

$q_{max,i}$: maximum/saturated loading of adsorbate i (mol.kg^{-1})

b_i: Langmuir equilibrium constant of i (Pa^{-1})

p_i: partial pressure of adsorbate i in fluid (Pa)

b_{i0}: pre-exponential factor (Pa^{-1})

$\Delta H_{ads,i}$: heat of adsorption of i (J.mol^{-1})

R: ideal gas constant (J.mol^{-1}.K^{-1})

T: temperature (K)

From Equation 2.5, b_i increases as temperature, T, decreases and therefore the loading at a given partial pressure increases.

For very low partial pressures of adsorbate, the Langmuir equation follows the Henry's Law and it is equivalent to a linear isotherm with a slope of $q_{max,i}b_i$:

$$q_i^* = q_{max,i} b_i p_i \tag{2.6}$$

For very high partial pressures of adsorbate, the equilibrium loading reaches the maximum adsorption capacity for the adsorbent:

$$q_i^* = q_{max,i} \tag{2.7}$$

As b_i tends to infinity, the equilibrium loading is constant for all partial pressures of solute in the gas. This corresponds to a *rectangular* or *irreversible* isotherm for which the loading for all partial pressures above zero is $q_{max,i}$.

2.3.3.2 Extended Langmuir Model

The Langmuir isotherm for a single component can be extended for multiple components if the isotherms of the single components can be represented by the Langmuir model. The derivation of the extended Langmuir model follows a similar approach to the single component model and can be found in the literature such as Yang (1987). The equilibrium loading of a component i in a mixture of N adsorbed components is given by:

$$q_i^* = \frac{q_{max,i} b_i p_i}{1 + \sum_{j=1}^{N} b_j p_j} \tag{2.8}$$

with:

q_i^*: equilibrium loading of i (mol.kg^{-1})

$q_{max,i}$: maximum/saturated loading of i (mol.kg^{-1})

b_i: Langmuir equilibrium constant of i (Pa^{-1}) which can be found by Equation 2.5

b_j: Langmuir equilibrium constant of j (Pa^{-1})

p_i: partial pressure of adsorbate in fluid of i (Pa)

p_j: partial pressure of adsorbate in fluid of j (Pa)

From the equation of this model it can be seen that the maximum adsorbed capacity is different for each component. The term, $q_{max,i}$, is more of an empirical term than a parameter of physical significance as the molecules of components adsorbed have different sizes and therefore there would be different saturation loadings for each component. In the derivation of Equation 2.8, $q_{max,i}$ should be the same for all components.

2.4 Kinetics

During adsorption, an adsorbed component moves from the bulk fluid phase outside the adsorbent to the fluid in the pores of the adsorbent. It then fixes to an adsorption site at the adsorbent surface. Simplistically, there are two main resistances to mass transfer which are due to pore diffusion and surface diffusion. In typical adsorption processes, the outside film resistance is small compared with the internal mass transfer resistances. Figure 2.6 shows generalised concentration profiles during adsorption and desorption. It can be seen from this figure that there is a positive mass transfer rate to the adsorbent during adsorption (shown by a positive difference between bulk and pore concentrations) and the opposite is true for desorption (shown by a negative difference between bulk and pore concentrations). By analogy, similar resistances to mass transfer can exist for heat transfer.

The local resistance of transfer of the adsorbate from the fluid in the adsorbent pore to the site is extremely small and it is negligible compared to the transfer rate of the adsorbate from the bulk fluid through the external film of the boundary layer and through the pores inside the adsorbent. Convection of the fluid around the adsorbent is beneficial for improving the overall rate of

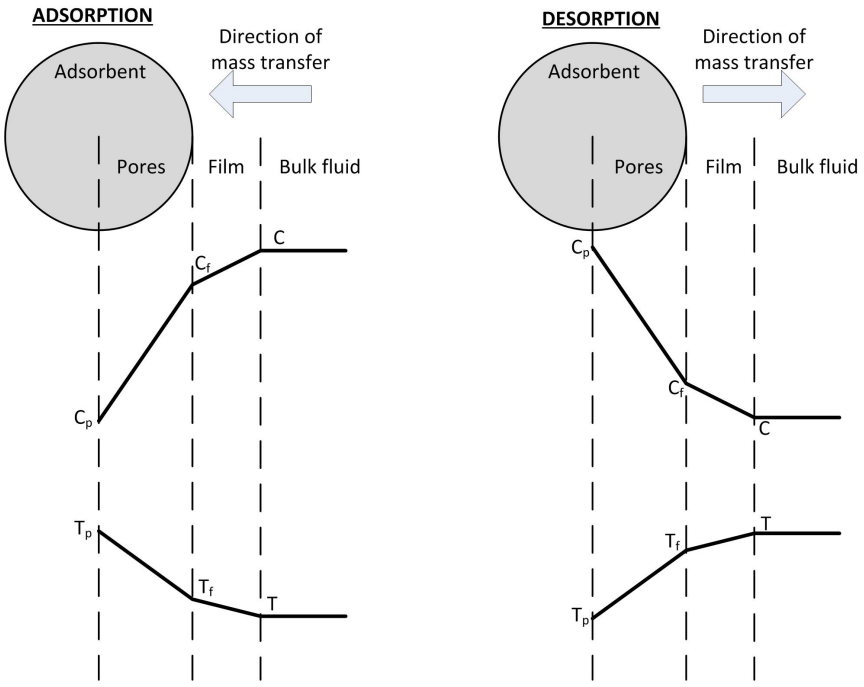

Figure 2.6: Concentration and temperature profiles in the adsorbent and bulk gas phases during adsorption and desorption Yang (1987)

adsorption because the resistance of the film outside the adsorbent is reduced (Yang (1987)).

In a system where there are no such limitations for mass transfer, adsorption is infinitely rapid and the observed loading is the same as the equilibrium loading. In practice, mass and heat transfer rates need to be accounted for in the material and energy balances because adsorption processes are rarely at equilibrium throughout. Slow kinetics lead to larger equipment sizes as the contact time between the adsorbate and adsorbent needs to be increased.

The mass transfer rate for adsorption or desorption is commonly approximated by an expression known as the linear driving force (LDF) model.

It can be expressed in terms of the partial concentration difference between the gas inside and outside the particle:

$$\dot{n}_i = k_i(C_i - C_{p,i}) \tag{2.9}$$

with:

$\dot{n}_i$: mass transfer rate of i to or from the adsorbent per unit volume of adsorbent (mol.m^{-3}.s^{-1})

k_i: LDF mass transfer constant of i based on concentrations (s^{-1})

C_i: concentration of adsorbate i in bulk fluid (mol.m^{-3})

$C_{p,i}$: concentration of adsorbate i in adsorbent pores (mol.m^{-3})

or as the difference in actual loading and equilbrium loading based on the external conditions:

$$\dot{n_i} = k'_i \rho_p (q_i^* - q_i) \tag{2.10}$$

ρ_p: adsorbent particle density (kg.m^{-3})

k'_i: LDF mass transfer constant of i based on loadings (s^{-1})

q_i^*: loading of i at equilibrium (mol.kg^{-1})

q_i: actual loading of i (mol.kg^{-1})

The actual adsorbent loading is a function of the adsorbate concentration inside the pores of the adsorbent whereas the loading at equilibrium is a function of the concentration of adsorbate in the bulk of the fluid. In both cases, the function is known as the isotherm:

$$q_i^* = f\left(T, C_i\right) \tag{2.11}$$

$$q_i = f\left(T, C_{p,i}\right) \tag{2.12}$$

For long adsorption times, it can be shown that k_i and k'_i can be written as:

$$k_i = \frac{15 D_{e,C}}{R_p^2} \tag{2.13}$$

with:

$D_{e,C}$: effective diffusivity of i based on concentrations (m^2.s^{-1})

R_p: adsorbent particle radius (m)

$$k'_i = \frac{15 D_{e,q}}{R_p^2} \tag{2.14}$$

with:

$D_{e,q}$: effective diffusivity of i based on loadings (m^2.s^{-1})

If the isotherm is linear, then

$$D_{e,q} = \frac{D_{e,C}}{\rho_p K} \tag{2.15}$$

K: slope of the linear isotherm (m^3.kg^{-1})

$D_{e,C}$ can be calculated from the molecular diffusion, surface diffusion and Knudsen diffusion within the particles. If molecular diffusion dominates,

$$D_{e,C} = \frac{D_m \varepsilon_p}{\tau} \tag{2.16}$$

where:

D_m: molecular diffusion coefficient ($m^2.s^{-1}$)

ε_p: void fraction of the adsorbent particles (-)

τ: pore tortuosity (-)

In many cases, however, the accuracy of effective diffusivity values found using these equations can be poor and it is instead found empirically from experimental data.

2.5 Methods of Desorption for Adsorption Processes

After the adsorbent has reached some desired approach to saturation during the adsorption step, it needs to be regenerated. Full removal of the adsorbate is energy intensive and hence costly. Therefore, it may be chosen to regenerate the adsorbent only partially each time. The working capacity of the adsorbent is the difference in loading between the end of adsorption and the end of regeneration and this should be maximised without entailing excessive regeneration costs. Desorption is achieved by modifying the temperature or the partial pressure of adsorbed components in the fluid phase such that the amount adsorbed at equilibrium is decreased and any excess component is transferred back to the surrounding fluid phase:

- Increasing the temperature of the adsorption system causes the amount adsorbed at equilibrium to decrease. This method is known as temperature swing adsorption (TSA).

- Decreasing the partial pressure of adsorbed components in the fluid phase also causes a reduction in the amount adsorbed at equilibrium. This method is known as pressure swing adsorption (PSA) and it can be achieved by reducing the overall pressure of the system or by diluting the fluid phase with another component. A combination of both methods can also be used to remove adsorbed components.

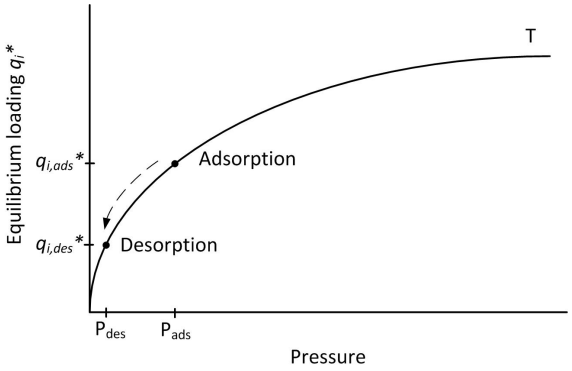

Figure 2.7: Isotherm and equilibrium loadings for pressure swing adsorption

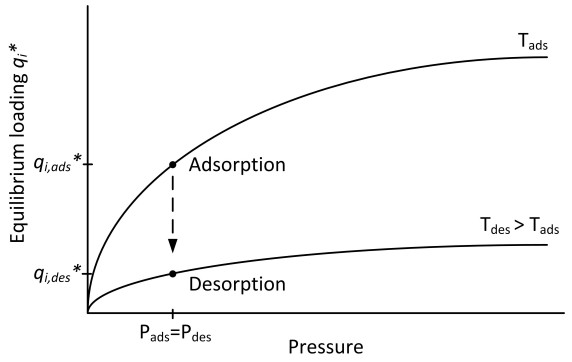

Figure 2.8: Isotherms and equilibrium loadings for temperature swing adsorption

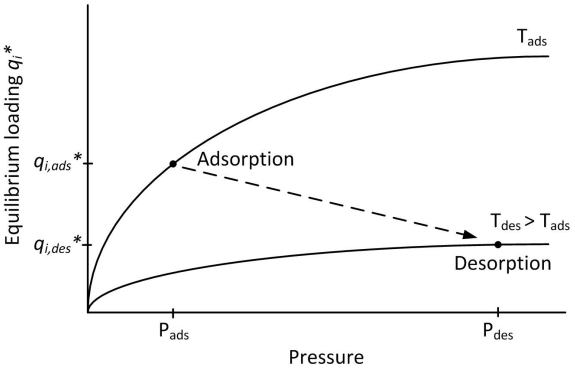

Figure 2.9: Isotherms and equilibrium loadings for temperature swing adsorption using a pure component stream at the desorption pressure

These methods can be graphically represented by using isotherm curves as shown in Figures 2.7-2.10. Figure 2.7 shows how loadings at equilibrium can be reduced using pressure swing adsorption. If the total pressure or partial pressure of the component in the fluid is reduced, equilibrium loadings are also reduced as shown by the isotherm curve. Figure 2.8 shows the isotherms for a temperature swing regeneration process. The temperature of the fluid phase surrounding the adsorbent is raised at constant total pressure. This also causes a drop in the amount loaded at equilibrium. The remaining two figures

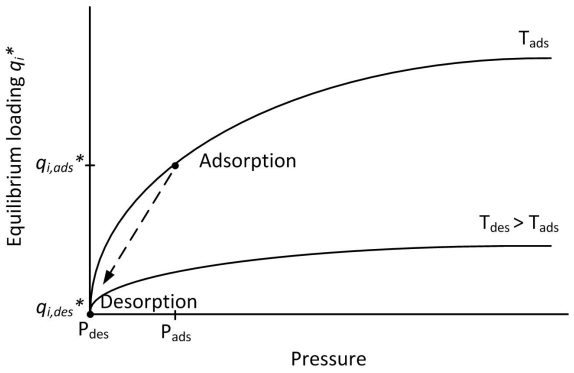

Figure 2.10: Isotherms and equilibrium loadings for temperature swing adsorption using a heated inert stream

(Figures 2.9 and 2.10) show pathways for desorption methods with temperature swing adsorption combined with changes in the partial pressure of the adsorbed components. In Figure 2.9, a pure stream of the adsorbed component is supplied during heating. As a pure stream of adsorbed component is used in the fluid, its partial pressure is equal to the total pressure of the system. The amount adsorbed is therefore higher than in the case of temperature swing adsorption alone (cf. Figure 2.8). Figure 2.10 represents a temperature swing process in which a non-adsorbed component at higher temperature is used to desorb the amount loaded during adsorption. The introduction of the non-adsorbed component is equivalent to reducing the partial pressure of the adsorbed species. Combined with an increase in temperature, this leads to lowering the amount adsorbed.

2.6 Review of Adsorbents for Post-Combustion CO_2 Capture

There are a multitude of adsorbents that have been considered for post-combustion CO_2 adsorption applications. Extensive reviews of these adsorbents are found in the literature (Davidson (2009), Sjostrom and Krutka (2010), Wang et al. (2011b), Sayari et al. (2011), Samanta et al. (2012)). Commonly used commercial adsorbents such as carbon and zeolites are the main ones considered for CO_2 adsorption processes. Many other new adsorbent materials, produced at smaller scale, have been tested under simulated or actual flue gas conditions as well as for CO_2/N_2 binary gas mixtures. Adsorbents that are capable of coping near or above 100°C and in the presence of impurities (e.g. water or SO_x) are prioritized in this literature review.

2.6.1 Physisorbents and Chemisorbents

Physical adsorption (or physisorption) occurs at the surface of a physical adsorbent (or physisorbent). Common examples of physisorbents include activated carbon and zeolites. Physisorption involves the formation of weak bonds from van der Waals or electrostatic forces between adsorbate and adsorbent instead of a stronger chemical bond. Consequently, the heat of adsorption is low and therefore less energy is required for desorption. Selectivity is generally lower than for chemisorbents as the adsorption sites at the surface of the adsorbent are not completely specific to any particular component in the fluid (Davidson (2009)).

Chemical adsorption (or chemisorption) involves a chemical reaction occurring at the surface of a chemical adsorbent (chemisorbent). Stronger ionic or covalent bonds are created between adsorbent and adsorbate. The heat of adsorption is usually substantially higher than for physisorption (Davidson (2009). The rate of adsorption depends on the rate of reaction. Suitable applications would be for low system pressure and at high temperature. Chemisorbents tend to adsorb certain components to a greater extent thus they tend to have a higher selectivity. The main chemisorbents that that are considered for post-combustion CO_2 capture include amine functionalised adsorbents (cf. section 2.6.5) and alkali-carbonate adsorbents (cf. section 2.6.6).

2.6.2 Desirable Adsorbent Properties

It is critical to choose a suitable adsorbent which is well adapted to the application in consideration as highlighted by Drage et al. (2012). Generally, desirable adsorbent properties for CO_2 adsorption are common to many other adsorption applications (Crittenden and Thomas (1998)). The most desirable properties for an adsorbent used for post-combustion CO_2 capture are summarised below:

- **High CO_2 adsorption working capacity:** This is the most important property as it dictates the amount/throughput of adsorbent required during the adsorption step to achieve a desired level of removal of CO_2. Under typical flue gas conditions, an adsorbent with high capacity would minimise the quantity of adsorbent needed as well as the energy required for its regeneration. Sayari et al. (2011) have emphasised that a steep isotherm slope is desired at low partial pressures. However, this is only desirable during adsorption because high CO_2 uptakes are beneficial for relatively low CO_2 partial pressures. The opposite is true for regeneration. Gray et al. (2008) have suggested that only working capacities

above 3 mol.kg^{-1} will have the potential to offer any significant reduction of energy consumed for desorption.

- **Tolerance to impurities:** Impurities found in the flue gas are O_2, H_2O, SO_x, NO_x and trace elements such as heavy metals. The presence of these impurities generally reduces the level of uptake of CO_2 on most adsorbents as there is increased competition for adsorption between CO_2 and the other components. Additionally, some adsorbents can lose their functionality when contaminated by impurities. It is therefore a requirement that the adsorbent can cope with at least low concentrations of contaminants such as water present in the flue gas as their complete removal is not necessarily feasible or it can be costly.

- **Fast kinetics for adsorption/desorption:** A high rate of adsorption is required to reach working capacities close to equilibrium working capacities. For fixed bed columns, low rates of adsorption result in more adsorbent needed and hence larger adsorption beds or shorter cycle times with adsorbent not being used effectively. For moving bed systems, low rates of adsorption can either lead to longer residence times for the adsorbent inside the process (equivalent to larger vessels) or higher throughputs of adsorbent. The overall kinetics for CO_2 adsorption are generally dominated by the mass transfer of gas through the pores of the adsorbent. The binding of adsorbate to the adsorbent is usually very rapid for physisorption. For chemisorbents, the rate of reaction between CO_2 and the reaction site also affects kinetics. Adsorbents and adsorption processes would generally be designed such that overall mass transfer is maximised.

- **Low heat of adsorption:** The value of the heat of adsorption is an indication of the strength of the bond between the adsorbent and the adsorbate. A strong bond makes the desorption of CO_2 more difficult but a weak bond may result in a low adsorption capacity.

- **High CO_2 selectivity:** An adsorbent with high CO_2 selectivity adsorbs CO_2 to a much greater extent than any other component and therefore the CO_2 purity of the product stream would be enhanced. CO_2 compression and transport costs are minimised for adsorbents with high selectivity.

- **Durability and cyclic stability:** High adsorbent functionality can be maintained for adsorbents with greater mechanical strength. Operating conditions such as high flowrates, high temperatures, moisture or vibration should not cause adsorbent degradation after successive adsorption/desorption cycles. In moving bed systems, particle attrition is

a common issue. If the adsorbent is durable, it will require replacement less frequently.

- **Low cost:** For capital costs to be minimised, the adsorbent would need to be cost-effective and of a comparable cost range to MEA solutions. The overall cost of the adsorbent would be minimised if a low throughput of adsorbent is needed and if the adsorbent does not need frequent replacement. More commonly used adsorbents such as activated carbon and zeolites have the lowest cost.

Significant process improvements and cost reduction would be reached if an adsorbent had all the desirable properties cited. However, it is extremely difficult to find an adsorbent with optimal attributes in all areas as some of these are contradictory. For example, some existing adsorbents with high working capacities also have large heats of adsorption. Therefore, adsorbents that may be successfully used for post-combustion CO_2 capture applications would have a good overall performance which can reduce energy and cost penalties. Descriptions follow for adsorbents that are the most considered and the most suitable for post-combustion CO_2 capture. These main types of adsorbents are: carbon based adsorbents, zeolite, amine functionalised adsorbents and alkali-carbonate adsorbents. A list of the types of adsorbents considered for post-combustion CO_2 capture is shown in Figure 2.11.

2.6.3 Carbon Based Adsorbents

Carbonaceous matter (such as wood or coal) can be treated to obtain a material of high porosity and surface area which is known as activated carbon. It has a high porosity, surface area and thermal stability. Other advantages include a low heat of adsorption for desorption (-20 to -30 kJ.mol^{-1}) and relatively rapid kinetics, which are comparable to zeolite (Zhang et al. (2010)).

At low CO_2 partial pressures, CO_2 adsorption capacity and selectivity are lower than for zeolite. Values of capacities found in literature are 0.51 mol.kg^{-1} (at 25°C, CO_2 partial pressure of 0.15 bar) (Kikkinides et al. (1993)) and 0.28 mol.kg^{-1} (at 55°C, CO_2 partial pressure of 0.15 bar) (Chue et al. (1995)). On the other hand, compared to most other adsorbents, activated carbon has a greater CO_2 adsorption capacity at elevated pressure such as for pre-combustion CO_2 capture applications.

Porosity and surface area can be increased to improve the capacity of the adsorbent. This is made possible by modifying the geometry of carbon adsorbents into carbon nanotubes or monoliths as considered by (Cinke et al.

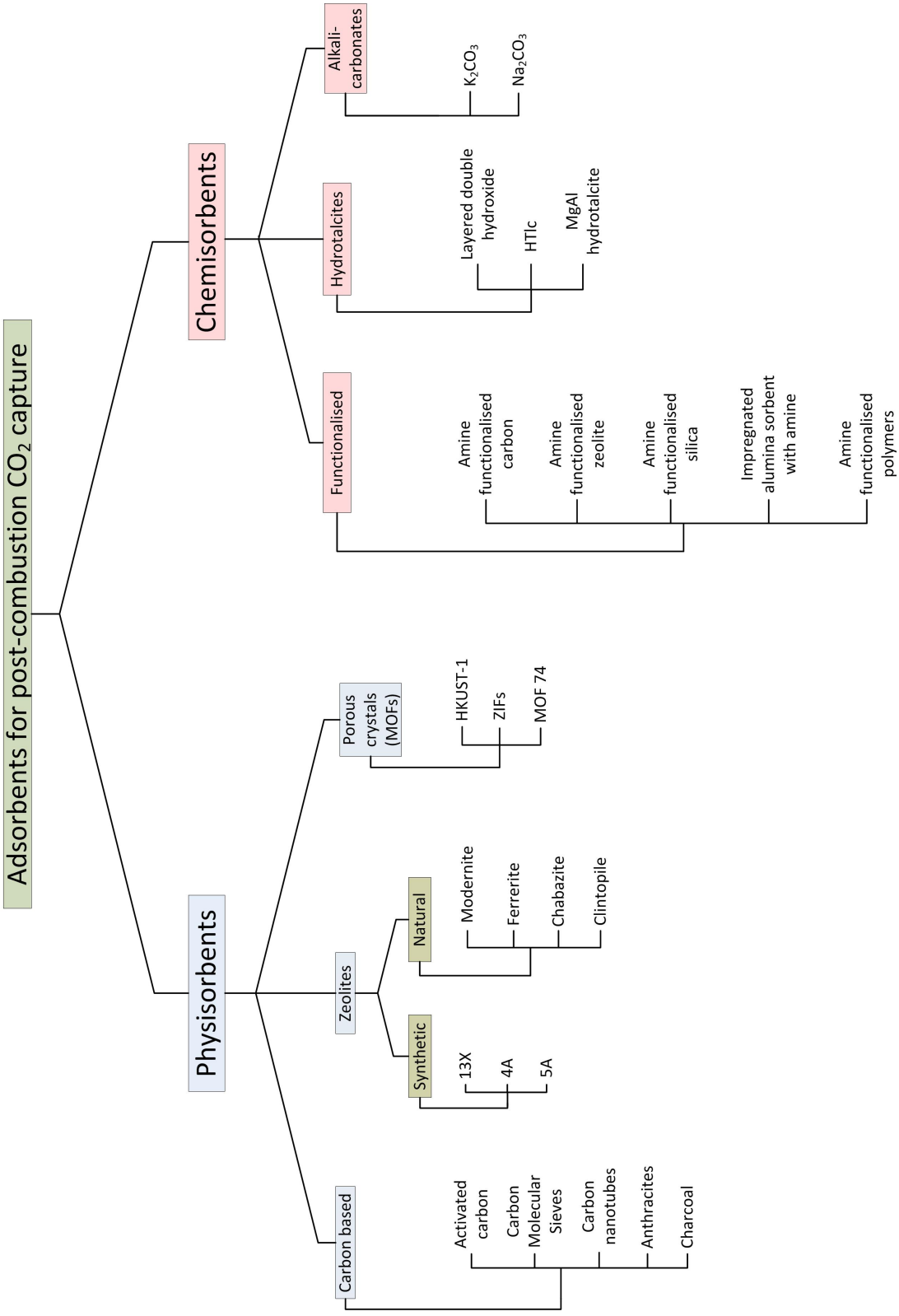

Figure 2.11: Overview of adsorbents

(2003)), (Su et al. (2009)), (Vargas et al. (2011)) and (Ribeiro et al. (2008)). Shen et al. (2010) looked into minimising attrition by the modification of granular activated carbon into spherical beads with higher mechanical strength. Similar isotherm curves to granular activated carbon were obtained with spherical adsorbents. ATMI Inc. have developed a similar spherical adsorbent that has been tested for attrition at bench scale and pilot plant (SRI International (2010)).

A commonly cited disadvantage with activated carbon is its adsorption capacity for impurities, in particular, water. Activated carbon has a particularly strong affinity for water vapour. The water loading is greater than for CO_2 in a saturated vapour stream. The uptake of water can hinder CO_2 capture performance as found by Xu et al. (2011) and Hefti et al. (2013). However, Xu et al. (2011) found that H_2O had a small effect on capture performance of CO_2 as the recovery and purity were nearly constant as relative humidity was increased from 0% to 7%. However, this range of humidity is lower than found for flue gas applications where the flue gas has higher moisture contents. Hefti et al. (2013) measured CO_2 loadings at 1.3 bar partial pressure and in relative humidities of 0%, 40% and 60% for which loadings were 1.25 mol.kg^{-1}, 1 mol.kg^{-1} and 0.5 mol.kg^{-1} respectively. However, loadings at CO_2 partial pressures in flue gas (0.1-0.2 bar CO_2) were not measured.

2.6.4 Zeolite

Zeolite materials (also known as aluminosilicates) are part of the molecular sieve group of adsorbents. Molecular sieves can retain adsorbates based on size exclusion in which only smaller molecules are retained in the pores of the adsorbent. Zeolites are the most used adsorbents for CO_2 capture as, in general, their capacity for CO_2 is higher than activated carbon. CO_2 loading on zeolite is higher than activated carbon at low partial pressures. A wide range of zeolite materials were tested by Harlick and Tezel (2004). It was found that zeolite of the type 13X had the highest capacity of 2.8 mol.kg^{-1} (at 22°C and 0.15 atm partial pressure of CO_2). A similar value of capacity was found by Cavenati et al. (2004). At higher temperatures of 55°C and 110°C, CO_2 loadings fall to 1.93 mol.kg^{-1} and 0.61 mol.kg^{-1} respectively. Harlick and Tezel (2004) observed that adsorption capacity increased for lower silicon to aluminium (Si/Al) ratios in the adsorbent. Zeolite materials with higher Si content have lower CO_2 selectivity but are more hydrophobic.

Generally, without moisture removal from flue gas, zeolite cannot be considered for post-combustion CO_2 capture due to water being preferentially ad-

sorbed over CO_2 and difficulties to regenerate the adsorbent in presence of water (Hefti et al. (2013), Pirngruber et al. (2013a)). As well as for activated carbon, Hefti et al. (2013) compared isotherms for dry CO_2 and a wet stream of CO_2 on zeolite 13X. There was a significant reduction in capacity. At a CO_2 partial pressure of 0.5 bar and 45°C, the loading for dry CO_2 was 4 mol.kg^{-1} which is reduced to 0.2 mol.kg^{-1} at 40% relative humidity. A water removal step prior to CO_2 capture is essential. Furthermore, the structure of the adsorbent pores is destroyed by water as highlighted by Wang et al. (2011a). Attrition of zeolite is higher than activated carbon when used in fluidised beds (Lee et al. (2004)).

2.6.5 Amine Functionalised Adsorbents

The advantages of using amine solvents has led to the idea of using amine groups at the surface of adsorbent materials. In addition to an improvement in CO_2 selectivity, their inclusion offers other advantages such as larger CO_2 loadings at typical flue gas temperature and CO_2 concentrations but also greater tolerance to water. There are two main methods used to develop amine functionalised adsorbents which are amine impregnation and amine grafting. For amine impregnated adsorbents, the interaction between the amine group and the support structure is weak. Of both adsorbents, higher loadings can be achieved for amine impregnated adsorbents. Slow mass transfer to the adsorbent has been reported due to diffusion limitations in the pores filled with amine groups Davidson (2009). Amine grafted adsorbents are characterised by a stronger covalent bond between the amine group and the supporting material. The rate of adsorption is quoted to be high and in some cases as high as for zeolite 13X Davidson (2009).

2.6.5.1 Amine Functionalised Silica

Xu et al. (2002) carried out a study of CO_2 adsorption on a mesoporous silica MCM-41 impregnated with PEI (Polyethylenimine). A loading of 2.16 mol.kg^{-1} was obtained for a 0.15 atm CO_2 at 75°C and a high uptake of 1.52 mol.kg^{-1} was maintained even at a low partial pressure of CO_2 of 0.02 atm. Compared to pure PEI, the capacity and rate of CO_2 adsorption was enhanced by the impregnation of the mesoporous adsorbent. In a subsequent article by the same authors, the same adsorbent had higher CO_2 capacity in the presence of water (Xu et al. (2005)). Other articles by Bacsik et al. (2011), Belmabkhout and Sayari (2010), Wang et al. (2011b) and Liu et al. (2011) find similar results for different types of amine on silica adsorbents. A summary of performances can be found in a review carried out by Sayari et al. (2011). This review also showed

that higher loadings found for amine impregnated adsorbents were attributed to higher amine concentrations than grafted adsorbents. A silica adsorbent with 50% (by mass) loading of a polymeric amine has been tested by Krutka and Sjostrom (2011). The loading at equilibrium was averaged at 2.2 mol.kg^{-1} for an actual flue gas stream with 14% (by volume) of CO_2 at atmospheric pressure. However, it was found that although the adsorbent performed well in batch mode (with 90% capture), it was ineffective in a continuous system due to slow mass transfer kinetics. It is believed that the amine loaded on the adsorbent resulted in strong mass diffusion limitations thereby reducing the mass transfer rate to the adsorption sites.

2.6.5.2 Amine Functionalised Zeolite 13X

It was reported by Jadhav et al. (2007) that zeolite 13X impregnated with 25% by mass MEA at temperatures below 50°C reached a lower CO_2 capacity than pure zeolite 13X. An improvement by adding amine groups to the adsorbent was only achieved at higher temperatures (above 75°C). Additionally, CO_2 performance worsened for higher concentrations of MEA in the adsorbent. The use of amine functionalised zeolite for post-combustion CO_2 capture is limited unless low concentrations of MEA are used to improve the tolerance of this adsorbent to water.

2.6.5.3 Amine Functionalised Activated Carbon

Similar results for CO_2 adsorption on amine functionalised zeolite 13X were found with amine functionalised activated carbon by Bezerra et al. (2011). Activated carbon impregnated with MEA had a lower capacity at 25°C and 0.1 bar CO_2 partial pressure than activated carbon without amine functionalisation. The consequence of adding amine to the pores of the adsorbent was the disappearance of narrow pores which allow physisorption to dominate at low temperature. On the other hand, Guo et al. (2006) found slight improvements at temperatures between 30-60°C for activated carbon impregnated with solutions of potassium hydroxide (KOH), ethylenediamine and ethanol.

2.6.5.4 Other Amine Functionalised Adsorbents

Due to disadvantages in performance for the silica based amine supported adsorbent tested by ADA-Environmental Solutions (Krutka and Sjostrom (2011)), another amine based adsorbent was considered and tested. The support used for the new and more promising adsorbent was a resin. A primary amine was covalently bonded to a cross-linked polystyrene support. The average capacity

at equilibrium of the adsorbent was 2.2 mol.kg^{-1} at 0.15 bar CO_2 and 40°C. The working capacity for this adsorbent was higher than most other adsorbents due to a low CO_2 capacity at higher temperatures albeit with a slightly lower amount adsorbed than amine silica adsorbents at lower temperatures (40-50°C). Other than degradation over many cycles of the adsorbent in the presence of SO_2 (as experienced by all amine functionalised adsobents), the cyclic stability of this adsorbent was high as it maintained its performance over 50 adsorption and desorption cycles. The kinetics of adsorption also showed an improvement over silica adsorbents. Isotherm curves and further adsorbent properties can be found in sections 2.7.1 and 3.7.1 but also in a detailed report by Krutka and Sjostrom (2011). Other amine functionalised adsorbent supports included various other resins, alumina and metal organic frameworks (MOFs).

2.6.6 Alkali-Carbonate Adsorbents

Alkali metal carbonates are chemisorbents that have been considered for post-combustion CO_2 flue gas treatment by several research groups. The performance of these adsorbents has also been tested at pilot-scale. Adsorption and desorption of CO_2 on alkali carbonates occur at higher temperatures than most other adsorbents, between 50°C and 100°C and 120°C and 200°C respectively. Potassium carbonate (K_2CO_3) and sodium carbonate (Na_2CO_3) adsorbents are the most common chemisorbents of this type to have been used. Research projects involving K_2CO_3 have been considered by some of the following groups: Shigemoto et al. (2006) investigated K_2CO_3 on activated carbon, Li et al. (2011) investigated K_2CO_3 on MgO/Al_2O_3, a research team from Southeast University (China) investigated K_2CO_3 on Al_2O_3 (Zhao et al. (2012a), Zhao et al. (2012b), Zhao et al. (2012d), Zhao et al. (2012c), Wu et al. (2013)). A collaboration between the Korea Institute of Energy Research (KIER) and Korea Electric Power Research Institute (KEPRI) (Yi et al. (2007), Park et al. (2009b), Park et al. (2009a), Park et al. (2011), Lee et al. (2011)) used an adsorbent with K_2CO_3 as the alkali. Research Triangle Institute (RTI International) have investigated the performance of Na_2CO_3 adsorbent (Liang et al. (2004), Nelson et al. (2009)).

The reversible carbonation reaction taking place at the surface of the adsorbent is:

$$M_2CO_3(s)+CO_2(g)+H_2O(g) \Leftrightarrow 2MH_2CO_3(s)$$

M represents an alkali metal such as potassium (K) or sodium (Na). These reactions are highly exothermic with heats of reaction of -141 kJ.mol^{-1} and -135 kJ.mol^{-1} K and Na respectively.

For Na_2CO_3, an additional exothermic reaction that also takes place is:

$$Na_2CO_3(s)+0.6CO_2(g)+0.6H_2O(g) \Leftrightarrow 0.4[Na_2CO_3.3NaHCO_3](s)$$

The heat of the reaction is -82 kJ.mol^{-1}.

For these reactions, increasing temperature reduces conversion but it increases the rate of the reaction. Reaction rate is also increased with higher H_2O concentrations. Commonly, it is stated that the rate of reaction between CO_2 and the carbonate is slow. Therefore, support materials such as activated carbon or Al_2O_3 are used to hold K_2CO_3 or Na_2CO_3 to enhance adsorption rate and provide resistance to attrition.

Li et al. (2011) developed and tested a $K_2CO_3/MgO/Al_2O_3$ adsorbent in an entrained bed system at 60°C and 0.1 atm CO_2 partial pressure. The maximum CO_2 loading found was 2.49 mol.kg^{-1}. It was also stated that this adsorbent had high mechanical strength and stability albeit being assessed over only 6 cycles. Zhao et al. (2012a) also tested CO_2 adsorption at similar conditions on nearly the same adsorbent (K_2CO_3/Al_2O_3). The decrease in conversion with temperature and the increase with higher CO_2 and H_2O concentrations were quantified. It was also found that the reaction rate was slow as it took 20 min to reach conversion values at equilibrium. In the following part of the study by the same authors (Zhao et al. (2012b)), it was found that the adsorbent could be regenerated in either N_2, CO_2 or H_2O. Finally the adsorbent was tested in a fluidised bed reactor and the amount of CO_2 captured and released after 80 cycles was stable (Zhao et al. (2012d)).

The main advantages of carbonate adsorbents are that adsorption can be carried out at high temperature and that the presence of water in the gas enhances CO_2 separation. Practical issues found with carbonate based adsorbents are durability, slow reaction kinetics and temperature control due to high levels of heat produced. Additionally, without prior removal of contaminants such as SO_2 or HCl, an irreversible reaction takes place with the carbonate.

Other chemisorbents have the potential to be used for CO_2 capture at even higher temperatures than carbonates. Calcium oxide (CaO), from calcium carbonate or limestone ($CaCO_3$), reacts with CO_2 at 600-700°C and regeneration occurs near 950°C. The carbonation reaction is highly exothermic:

$$CaO(s)+CO_2(g) \Leftrightarrow CaCO_3(s)$$

The heat of reaction is -178 kJ.mol^{-1}. Limestone is an abundant and low cost material. Although relatively rapid reaction kinetics and high capacity are achieved at high temperatures, the adsorbent needs to be replaced frequently as found by Abanades et al. (2005) and Fang et al. (2009). A method for improving the cyclic stability of this adsorbent by using steam to regenerate the adsorbent has been proposed by Fennell et al. (2007).

2.7 Review of Moving bed Adsorption Processes for Post-Combustion CO_2 Capture

Although fixed bed processes for post-combustion CO_2 capture are extensively studied in the literature, there is greater development of moving bed processes from laboratory to pilot plant scale. Three different projects using moving bed systems with amine functionalised adsorbent, activated carbon and potassium carbonate respectively are subsequently highlighted and main results from these studies are also summarised. Findings from other studies using moving bed technologies will also briefly be reviewed.

2.7.1 Moving bed Adsorption and Regeneration Process with a Supported Amine Adsorbent

As well as testing the performance of a wide range of adsorbents, Krutka and Sjostrom (2011) have investigated the integration of these adsorbents in moving bed adsorption cycles. The decision to use amine supported adsorbents over activated carbon and zeolites was due to a lower theoretical regeneration energy which can be explained by the fact that supported amine adsorbents have a higher CO_2 capacity per unit mass of adsorbent therefore less adsorbent is required. In turn, less heat is needed for it to be regenerated. Although water in the gas was tolerated by the chosen adsorbent, the gas underwent a pretreatment step to remove SO_x.

Two pilot scale studies (1 kW in size) were carried out with the same flowrate of flue gas. In both cases, a co-current adsorber was used. The adsorber had a height of 10.7 m and a diameter of 2.5 cm. A fluidised bed with an unspecified size was used as the regenerator. In the regenerator, electric heaters were used for heat input and N_2 was used as the regeneration gas. It is obviously not realistic to use N_2 for the commercial scale plant because a CO_2 product with low purity would be obtained. The flue gas and solid adsorbent flowrates in both cases were near 2×10^{-3} $m^3.s^{-1}$ and 5×10^{-3} $kg.s^{-1}$ respectively. A CO_2 removal of 90% was not maintained in either study. The reasons that were stated were that the arrangement of a co-current adsorber and a fluidised bed desorber did not provide a sufficiently large working capacity. The driving force for separation became too low after a few cycles. Limitations due to mass transfer resistance were also given as a reason for poor CO_2 capture performance as the observed working capacities were less than the working capacities at equilibrium. A different supported amine adsorbent with reduced mass transfer limitations and with a lower loss in CO_2 capacity over time was used instead and

it showed improvements. This adsorbent was a cross-linked polystyrene support with a primary amine functionalised onto the adsorbent. More specific details of the adsorbent such as the BET specific surface area or the amine loading on the adsorbent were not specified. Other similar adsorbents that were tested had an amine loading in the range of 30%-50% wt. Although the targeted level of capture of 90% was not reached, 50% was maintained for several hours of operation. The properties of the improved adsorbent are given in Table 2.3. In subsequent simulations for moving bed processes to be carried out in this thesis, this improved supported amine adsorbent used by Krutka and Sjostrom (2011) is considered. The heat of adsorption for water on the supported amine adsorbent was not provided by Krutka and Sjostrom (2011). As the adsorbent is a chemisorbent which is likely to react with water, a higher heat of adsorption than the heat of condensation found for physisorbents is expected. Therefore, the latent heat of condensation of water (-40.6 kJ.mol^{-1} (Perry et al. (1997))) was not used. Instead, it has been assumed that the heat of adsorption of water is the same as for CO_2 (given in Table 2.3), therefore $\Delta H_{ads,H_2O}$ = -57593.6 J.mol^{-1}. A more accurate value would need to be found in future. Unfortunately, there is a lack of information in the literature on $\Delta H_{ads,H_2O}$ for supported amine adsorbents. Didas et al. (2012) studied the adsorption of water on amine functionalised mesoporous silica adsorbents but they did not report the value of $\Delta H_{ads,H_2O}$. Instead, they hypothesised that water adsorption is dominated by physisorption of water onto the amine groups of the adsorbent. This would imply that no reaction occur between the adsorbent group and water. If this were the case, $\Delta H_{ads,H_2O}$ would have the same value as the latent heat of condensation of water. More work needs to be carried out to find this parameter for the adsorbent in question. For chemisorption, a value of $\Delta H_{ads,CO_2}$ is assumed but if physisorption is assumed, the latent heat of condensation can be used and the sensitivity of this parameter on the results can be tested until a more accurate value is obtained. If the Clausius-Clapeyron equation is used in conjunction to determine the heat of adsorption of water, a value close to the latent heat of water is found.

The scaled up pilot plant (1 MW) is under development by ADA-Environmental Solutions (Krutka et al. (2013)). As it was found that co-current flow in the adsorber was not effective for achieving 90% capture, the design of the adsorber was modified to staged fluidised beds in the adsorber in which the gas and solid flow counter-currently. Heat would be removed in each stage indirectly using cooling water. The driving force for separation will be increased with this new configuration however results for the performance of the overall process have not yet been published.

Table 2.3: Values of parameters of supported amine adsorbent (Krutka and Sjostrom (2011))

Parameter	**Unit**	**Value**
Adsorbent particle density ρ_p	kg.m^{-3}	646
Adsorbent particle size D_p	μm	80-120
Adsorbent heat capacity $c_{p,ads}$	J.kg^{-1}.K^{-1}	1255
Heat of adsorption for CO_2 $\Delta H_{ads,CO_2}$	J.mol^{-1}	-57593.6

2.7.2 Counter-current Adsorption and Regeneration Process with Activated Carbon Adsorbent

Advantages of activated carbon for post-combustion CO_2 capture include low heats of adsorption and some tolerance to contaminants such as SO_x, NO_x and O_2 and water. In a collaboration between SRI International, ATMI Inc., National Carbon Capture Center, University of Toledo and the National Energy Technology Laboratory (NETL), activated carbon has been used in a counter-current column at atmospheric pressure containing structured packing with an adsorption section at the top and a regeneration section at the bottom as shown in Figure 2.12 (SRI International et al. (2011)). This is one of the only studies found that considered the use of counter-current moving beds with internal structured packing for adsorbent distribution. CO_2 is driven off the adsorbent in the regeneration section using a counter-current flow of steam. After leaving the adsorption section, the adsorbent is preheated in a transition region. It is cooled in another transition section after leaving the regeneration section. Finally the adsorbent undergoes dehydration and additional cooling before being recycled back to the adsorber at the top of the column.

In the early stages of this project, the activated carbon was developed by ATMI Inc. specifically for use in moving bed systems. The activated carbon granules have been spherically shaped and the surface is made smooth to minimise adsorbent loss due to attrition. Further properties of the adsorbent and CO_2 adsorption performance were investigated at bench scale (SRI International (2010)). For example, the heat of adsorption and isotherms at different temperatures were measured (cf. Table 2.4). In subsequent simulations for moving bed processes to be carried out in this thesis, this activated carbon used by SRI International (2010) is considered. The heat of adsorption of water on activated carbon was taken from Qi et al. (2000). Values in the range of -43 kJ.mol^{-1} and -50 kJ.mol^{-1} were reported for temperatures between 25°C and 100°C. An average value of $\Delta H_{ads,H_2O}$ = -47 kJ.mol^{-1} was assumed which

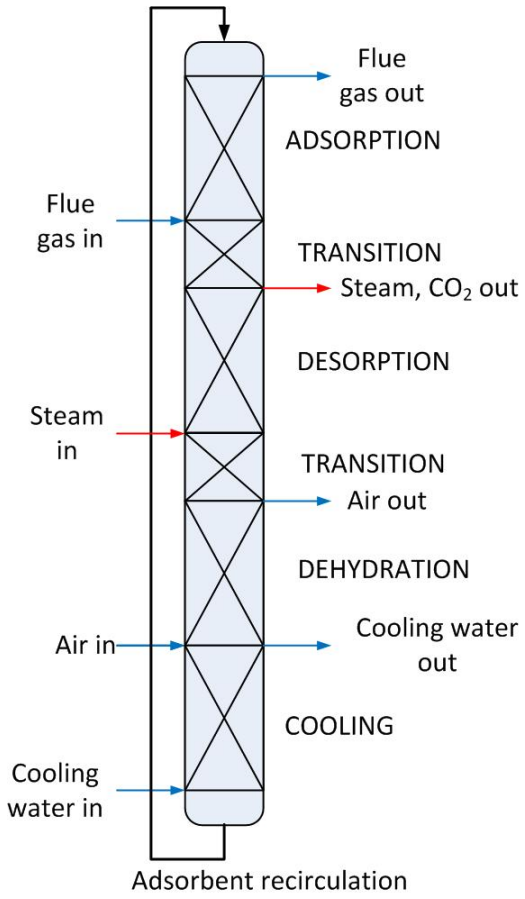

Figure 2.12: Process using activated carbon in a counter-current adsorption system (SRI International et al. (2011))

is also close to the latent heat of condensation of water (-40.6 kJ.mol^{-1} (Perry et al. (1997))) as the adsorbent is a physisorbent. The heat of adsorption for N_2 was not provided by SRI International (2010) therefore a value was taken from Kikkinides et al. (1993) who considered another activated carbon adsorbent: $\Delta H_{ads,N_2}$ = -15.9 kJ.mol^{-1}.

Tests for adsorption and desorption in a laboratory scale counter-current process were carried out. CO_2 removal and purity were above 90% for low flue gas flowrates below 30 L.min^{-1} for 15% vol. CO_2. The size of the equipment was unspecified. The system was subsequently scaled up for a 200 L.min^{-1} inlet flowrate of gas at a CO_2 concentration of 4.5% vol. A CO_2 capture rate above 90% and a high purity of 98% were achieved. This performance was sustained over 130 hours of operation. The next part of the study involved a further scale up to 200 L.min^{-1} with actual flue gas from a pulverised coal fired boiler (SRI International et al. (2012)). Further scale up to 1982 L.min^{-1} has been planned. The adsorption and desorption sections would be 4.57 m in length and the size of the square base is 0.45 m.

Table 2.4: Values of parameters of activated carbon (SRI International (2010))

Parameter	**Unit**	**Value**
Adsorbent particle density ρ_p	$kg.m^{-3}$	1100
Adsorbent particle size D_p	μm	200
BET specific surface area	$m^2.g^{-1}$	1300
Adsorbent heat capacity $c_{p,ads}$	$J.kg^{-1}.K^{-1}$	1000
Heat of adsorption for CO_2 $\Delta H_{ads,CO_2}$	$J.mol^{-1}$	-28000

2.7.3 Moving bed Adsorption and Regeneration Process with Potassium Carbonate Adsorbent

Korea Institute of Energy Research (KIER) and Korea Electric Power Research Institute (KEPRI) have developed a moving bed process using potassium carbonate adsorbent at laboratory and pilot scales. In the co-current adsorber, the carbonation reaction occurs and the regenerator is a fluidised bed in which steam is used to desorb CO_2. The process is represented in Figure 2.13.

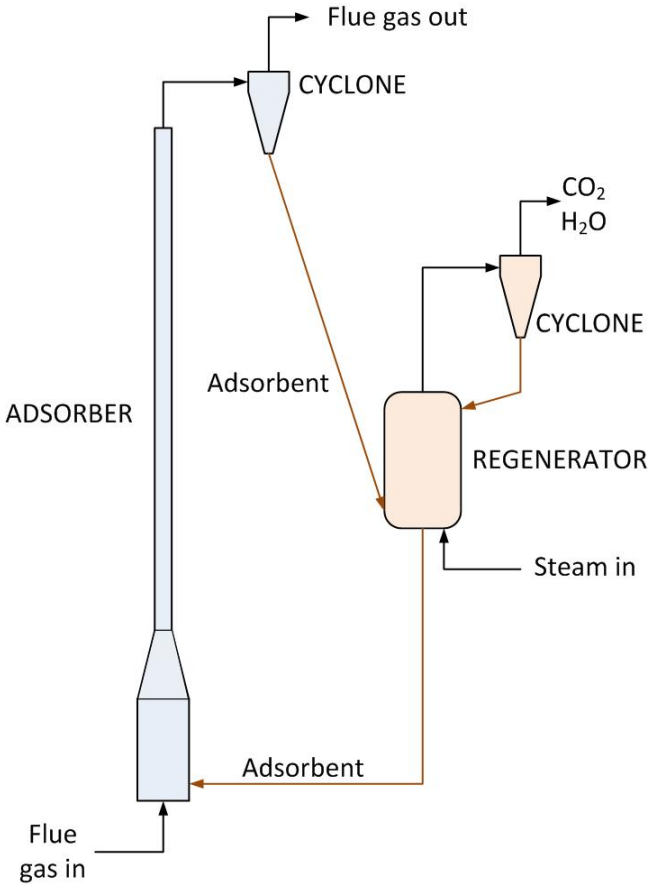

Figure 2.13: Process using carbonate adsorbent in moving bed adsorption system (Park et al. (2009b))

Initially, the adsorbent was tested at a small scale. Simulated flue gas at a flowrate of 2 $m^3.h^{-1}$ was used. The CO_2 capture process was operated for 50 hours and it achieved an average CO_2 removal of 85% (Park et al. (2009b)).

The process was then scaled up to a flue gas flowrate of 0.028 $m^3.h^{-1}$ (Park et al. (2009b)). The height of the co-current adsorber was 13.5 m and the internal diameter was 0.075 m. The height of the fluidised bed regenerator was 2 m and the internal diameter was 0.25 m. Actual flue gas from a coal-fired boiler was used at atmospheric pressure and a CO_2 concentration of 13.5%. The temperature in the adsorber was maintained below 100°C . The temperature in the regenerator was 150°C. For a period of operation of 2 hours, 70% CO_2 removal was maintained. Additional water was added in the adsorber via a gas stream saturated with water to increase the conversion in the carbonation reaction (cf. section 2.6.6).

Further scale-up to a flue gas flowrate of 0.56 $m^3.s^{-1}$ was carried out. The CO_2 removal rate varied from 50-80% with a maximum removal of 85% during a 9 day continuous operation (Park et al. (2011)). Parameters varied during this duration were: temperature of the adsorber, regenerator temperature, moisture content of the flue gas, solid hold-up in the adsorber and the solid circulation flowrate.

2.7.4 Other Studies of Moving bed CO_2 Adsorption Processes

A numerical study of a case for moving bed adsorption with internal heat integration for CO_2 capture was carried out by Kim et al. (2013a). The conceptual process involved the use of a counter-current adsorber and two counter-current desorbers, one of which operates at atmospheric pressure and the other under vacuum. Plate heat exchangers were assumed to be used inside the adsorbers and desorbers. Inside the plate heat exchanger, both gas and solid would flow counter-currently inside one channel whereas water, which is the heat transfer fluid, would flow inside an adjacent channel. Heat was thus transferred through the plates between the channels. The process is represented in Figure 2.14. Zeolite 13X was assumed as a suitable adsorbent in the process and the flue gas was assumed to be a binary mixture of CO_2 and N_2. Water and SO_x were assumed to be removed before CO_2 capture, however no considerations of the effect this had on the performance of the process were given. In Figure 2.14 a base case is shown. Another case was considered in which the cooling water at the outlet of the adsorber was split and only 75% of it was used for steam production in the desorber operating at atmospheric pressure. A CO_2 recovery

of 80% and a purity of 97% were achieved.

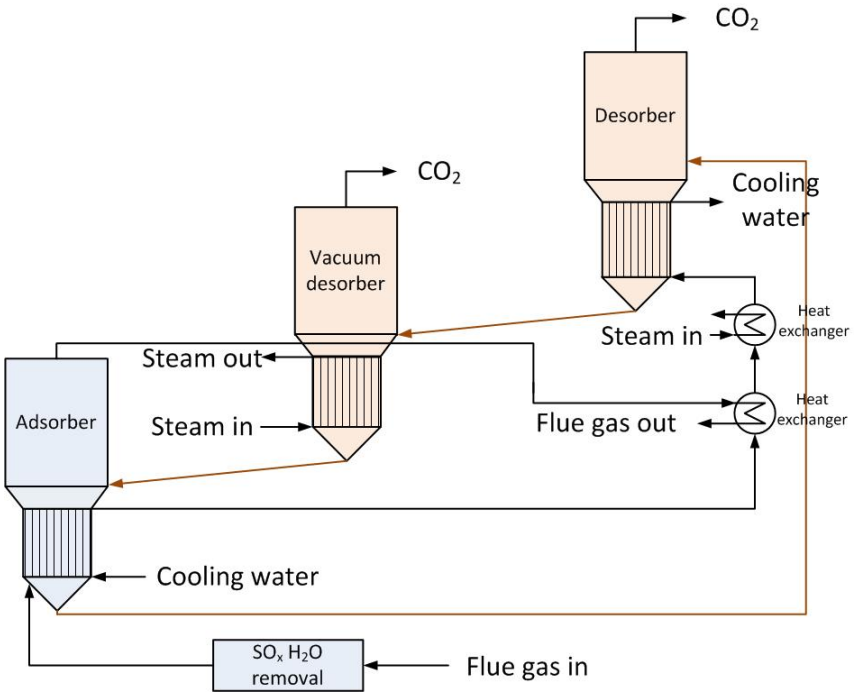

Figure 2.14: Moving bed process with heat integration (Kim et al. (2013a))

However, a few anomalies in the study exist. Values reported for the percentage of energy integration are higher than expected because they have not included the energy required to produce steam for the desorber operating under vacuum. In addition, the energy required to operate the vacuum pump has not been included either. The temperature at which the flue gas enters is 25°C which is below expected flue gas temperature prior to CO_2 capture. The validity of a number of equations used to approximate heat and mass transfer coefficients were not given.

Finally, a sensitivity analysis was carried out for several operating parameters. The parameters varied were adsorber height, desorption temperature and pressure inside the vacuum desorber, cooling water mass flowrate and solid adsorbent mass flowrate. Of these operating parameters, it was found that the desorption temperature inside the vacuum desorber had the greatest effect on CO_2 purity and recovery. The other parameters had a much smaller effect.

Veneman et al. (2012) also considered amine supported adsorbents in a cycle of a fluidised bed adsorber and regenerator. The adsorbent used was Tetraethylenepentamine (TEPA) physically impregnated on silica and Polymethylmethacrylate (PMMA). CO_2 recovery was only 56% on average over a period of one hour. The CO_2 purity of the gas at the outlet of the regenerator was only 9% because N_2 was used for purging. A simulated flue gas at atmospheric pressure with a CO_2 concentration of 6.7% was used and it did

not contain moisture or other impurities. Zhang et al. (2014) also considered a fluidised bed but for CO_2 capture from air with N_2 also being used as the main regeneration purge gas. Rough estimations of heat required to regenerate the adsorbent were performed but again, the CO_2 capture step was the main focus of their work.

Finally, Pirngruber et al. (2013b) have considered the differences between fixed-bed, co-current and fluidised bed TSA processes from a theoretical standpoint. Some interesting practical aspects with TSAs for post-combustion CO_2 capture were put forward. These included water in the flue gas, difficulties in heat exchange between solids and that it would be better to provide heat indirectly via condensing steam in a heat exchanger instead of direct steam contact with the bed of adsorbent. It was pointed out by Pirngruber et al. (2013b) that the driving force for adsorption was higher in a fixed bed than in a fluidised bed because in a fixed bed, the adsorbent would be in equilibrium with the feed gas if the rate of adsorption was rapid and in the absence of a mass transfer zone. However, in a fluidised bed and a co-current system, the adsorbent is in equilibrium with a gas containing a lower concentration of CO_2 than the feed gas because CO_2 is removed from the bulk gas as it flows up the column with the adsorbent. It was then suggested that instead of a single fluidised bed, a cascade of fluidised beds with counter-current flow of solid and gas is more suitable as the adsorbent would be in equilibrium with the feed gas in the first stage. It was also pointed out that adsorption performance is improved for isothermal operation which is more difficult to accomplish in fixed-beds than co-current, counter-current or fluidised beds. They stated that regeneration with pure CO_2 at atmospheric pressure in a fluidised bed is almost impossible however they did not specify whether the adsorbent is heated before being purged with CO_2 or whether CO_2 was used to provide heat to the adsorbent in which case it may well be impossible to regenerate the bed. Additionally, they also ignored the effect of co-adsorbed water. It was stated by Pirngruber et al. (2013b) that for isothermal fixed bed TSAs, existing adsorbents would not be able to offer lower regeneration heat duties than amine absorption. Maximum CO_2 adsorption capacities greater than 6 $mol.kg^{-1}$ were quoted to be necessary. Although only isothermal fixed beds and co-current beds were part of their analysis, counter-current adsorbers were not considered and isothermal operation of the adsorber in the system was assumed to offer the best performance for the overall cycle. As the process of adsorption is exothermic, the adsorbent would require a greater level of heating during regeneration under isothermal operation of the adsorber. Existing adsorbents are to be used in this present work and it will be verified whether adsorption technology can at

least match the performance of amine absorption, if not surpass it.

2.8 Considerations of Energy for Adsorbent Regeneration

As mentioned previously, the heat required to regenerate the sorbent is the primary energy penalty for CO_2 capture. Hoffman et al. (2008) proposed a simple equation for regenerating the adsorbent per unit mass of CO_2 adsorbed:

$$\frac{Q_{reg}}{m_{CO_2}} = \frac{m_{eq}}{m_{CO_2}} c_{p,eq} \Delta T + \frac{c_{p,ads} \Delta T}{q_{CO_2}} + [c_{p,CO_2}(T_2 - T_{ref}) - c_{p,ads}(T_1 - T_{ref})] + \frac{(-\Delta H_{ads})}{m_{CO_2}} \tag{2.17}$$

with:

Q_{reg}: energy required for sorbent regeneration (J)

m_{CO_2}: mass of adsorbed CO_2 (kg)

m_{eq}: mass of equipment (kg)

$c_{p,eq}$: specific heat capacity of equipment ($J.kg^{-1}.K^{-1}$)

ΔT: difference between regeneration and adsorption temperatures ($=T_2 - T_1$) (K)

$c_{p,ads}$: specific heat capacity of adsorbent ($J.kg^{-1}.K^{-1}$)

q_{CO_2}: mass of CO_2 loaded per unit mass of adsorbent ($kg.kg^{-1}$)

c_{p,CO_2}: specific heat capacity of CO_2 ($J.kg^{-1}.K^{-1}$)

T_1: adsorption temperature (K)

T_2: regeneration temperature (K)

T_{ref}: reference temperature (usually 298.15K)(K)

ΔH_{ads}: heat of adsorption per unit mass of CO_2 adsorbed ($J.kg^{-1}$)

The first term on the right-hand side of Equation 2.17 represents the energy used to heat up the equipment (e.g. vessel wall) from T_1 to T_2. This term can be neglected if the adsorbent is directly heated without changing the temperature of the vessel such as for moving beds. The second term on the right-hand of

this equation gives the heat required to heat up the sorbent. The next term in square brackets represents the energy required to heat up the adsorbed CO_2. The final term is the heat of the endothermic reaction associated with the desorption of CO_2 from the solid to the gas.

This proposed equation has some inaccuracies. It assumes that the equipment is heated during regeneration although heat can be transferred to the adsorbent directly. In addition, it does not take into account any heat that can be recovered between heating the adsorbent and cooling the adsorbent. The regeneration heat requirements can be found more rigorously by writing a full energy balance for the system (as will be carried out in the next chapter). It doesn't take into account other adsorbed components such as water. T_{ref} is arbitrary therefore Q_{reg} would change depending on the value of the chosen value of T_{ref}. In addition, the expression inside the square brackets seems unclear to what it represents because the heat capacity of the adsorbent is used stead of the heat capacity of CO_2 at the adsorption temperature.

However, this equation shows if the sorbent has a high specific heat capacity (e.g. amine solvents), a high heat of adsorption and low CO_2 working capacity, then the heat required for regeneration per unit mass of CO_2 captured will be high.

2.9 Conclusions

A lot of research carried out in post-combustion CO_2 adsorption involves developing materials with high capacities of CO_2 however, the effect of the kinetics of CO_2 adsorption and presence of other adsorbed components (e.g. water) is often disregarded.

Moving bed adsorption systems can offer the possibility of reducing costs of the process of capturing CO_2. However, they are also associated with difficulties that hinder their development. These are summarised below:

- Adsorbent attrition
- Loss of adsorbent capacity over time
- Conveying of adsorbent particles
- Heat exchange between solid streams
- Difficulty in running the regenerator at a higher pressure to obtain a CO_2 product requiring less power to compress the CO_2

In the literature, there is more of a focus on the CO_2 capture aspect of the process but the choice of the purge gas used for regenerating the adsorbent is often overlooked. Other practical issues for which little information exists are the strength and cost of the adsorbent used in moving bed systems. Fluidisation considerations and an even distribution of solids can be issues too and these are often not considered in lab-scale equipment. It is important that vessel diameters are not excessively large in practice and this requires dealing with high velocity gas flows. Gas flows can be up to 2 $m.s^{-1}$ in amine absorption columns and similar absorption processes must be run at similar velocities to be commercially viable. The present work aims to explore the potential of the energy saved by using moving bed adsorption systems and it takes some of the difficulties mentioned above into consideration. If there are improvements found for the performance of moving bed CO_2 adsorption technologies over other processes, the difficulties associated with moving bed processes, cited above, could be addressed in the near future. The following chapter presents the construction of the mathematical model used to assess the performance of moving-bed adsorption processes for CO_2 capture.

Chapter 3

Mathematical Modelling of Moving Bed Adsorption Systems

3.1 Introduction

In order to study the performance of a physical or chemical process, a mathematical model may be developed using appropriate assumptions. Results obtained from the model can be helpful but their relevance will strongly depend on the assumptions used to construct the model. This chapter covers the development of material, energy and momentum balances required to analyse the performance of moving bed CO_2 capture systems. The material balance will predominantly give information related to the flow of gas and solid adsorbent through the system and mass transport between them. Similarly, the energy and momentum balances determine temperature and pressure variations within the process.

The adsorption systems considered for modelling in this chapter are:

- Fluidised bed: In the fluidised bed adsorber, the gas is passed upwards through a bed of adsorbent causing the bed to expand at a sufficiently high velocity. In principle, there is improved contact between the gas and solid, as opposed to inside a packed bed. Regenerated adsorbent is continuously added to the system and spent adsorbent is continuously withdrawn at the same rates, as shown in Figure 3.1.

- Co-current bed: In the co-current adsorber, regenerated adsorbent and gas are introduced at the bottom of the adsorber as shown in Figure 3.2. The gas velocity needs to be sufficiently high to entrain the solid upwards through the column. Spent adsorbent and gas are withdrawn at the top of the process. Therefore, gas and solid flow in the same direction.

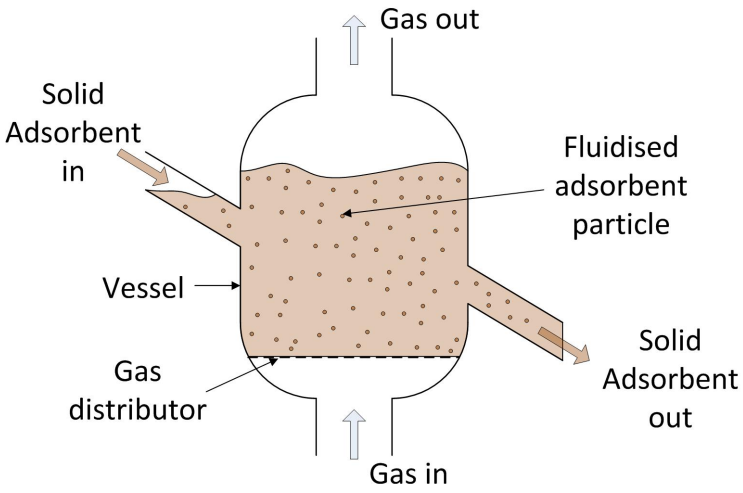

Figure 3.1: Fluidised bed adsorber

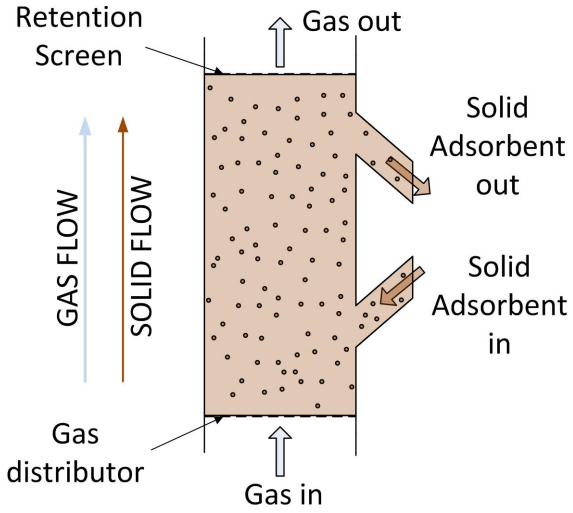

Figure 3.2: Co-current bed adsorber

- Counter-current bed: In the counter-current adsorber, gas is introduced at the bottom of the adsorber and removed at the top as shown in Figure 3.3. Regenerated adsorbent is introduced at the top of the adsorber and spent adsorbent is removed at the bottom. The adsorbent falls through the void spaces inside packing used to slow down the flow of adsorbent such that there is enough contact time between gas and solid phases. The packing material could be small objects randomly placed in the column, known as *random packing* or stacked corrugated and perforated sheets, known as *structured packing*. The gas velocity needs to be sufficiently low such that entrainment of particles, which can also be known as *flooding*, does not occur.

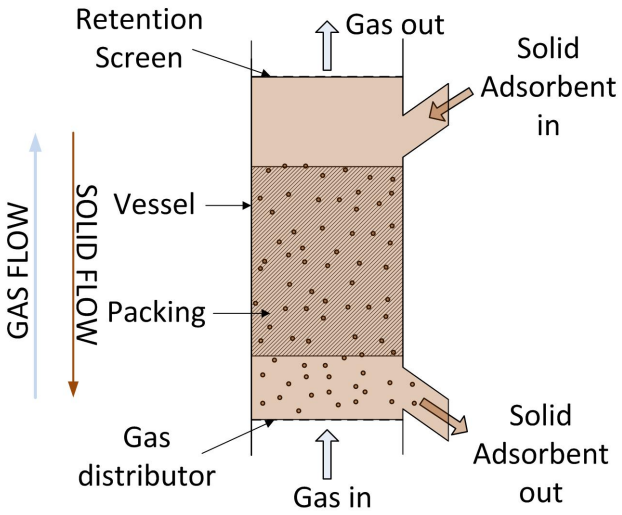

Figure 3.3: Counter-current bed adsorber

Regeneration of the adsorbent can also be achieved in one of these three types of arrangement. The composition of the incoming gas and the adsorbate on the adsorbent may be different, but the design equations will be the same.

3.2 Numerical Methods Used in the Model

3.2.1 Finite Difference Method

The finite difference method is a commonly used numerical approximation for mathematical models. A spatial domain is discretised into a uniform grid in which numerical approximations of the solutions are calculated at the nodes of the grid. After obtaining the set of differential equations from material, energy and momentum balances, the finite difference method can be applied to each node to obtain a set of algebraic expressions. The finite difference method is based on the Taylor series expansion. The derivative terms are approximated by truncating the series with an associated truncation error.

3.2.2 Finite Volume Method

The finite volume method is another numerical approach for solving the mathematical model of a system. The basis of the finite volume method is to divide the spatial domain of interest into discrete control volumes which can also be known as cells. Material, energy and momentum balances are written for an individual cell therefore conservation of material, energy and momentum is ensured for each cell. Errors arise due to discretisation of the spatial domain into individual cells with averaged values of state variables used inside the volume

of each cell. Numerical approximations are used to evaluate integrals. The actual solution for the state variables would change continuously throughout the domain. Therefore the numerical solution for a discretised domain with an infinite number of cells would match the exact solution of the mathematical model.

The finite volume method uses the integral form of the conservation law as opposed to the differential form of the conservation law which is used by the finite difference method. The conservation law can be written to describe conservation of material, energy or momentum in a system. The integral form of the conservation law is given by:

$$\frac{\partial}{\partial t}\int_V u dV + \int_V \nabla . f dV = \int_V q dV \tag{3.1}$$

Using Gauss's theorem, the normal unit vector, $\mathbf{n}$, is introduced,

$$\frac{\partial}{\partial t}\int_V u dV + \int_S f\mathbf{n} dS = \int_V q dV \tag{3.2}$$

The first term on the left-hand side of Equation 3.2 represents the rate of change of u (quantity) in a fixed volume V (control volume). The second term on the left with f (total flux) represents the total flux of u across the control volume of surface S. The term on the right of this equation with q represents the total source term inside V. In the finite volume method, the integral law is applied to a number of control volumes, N_P.

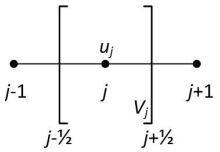

Figure 3.4: 1D control volume

Figure 3.4 shows the vertex centred control volume for a discretised one-dimensional spatial domain. Constant average values for u are assumed inside a control volume:

$$u_j = \frac{1}{|V_j|}\int_{V_j} u dV \tag{3.3}$$

The true flux, f, at the boundaries of the cells can be replaced by a numerical approximation such as a quadrature rule (e.g. midpoint rule, trapezoidal rule or Simpson's rule). A general approximation is given by:

$$\int_V f dV \approx \sum_{j=0}^{N_P} w_j f_j \tag{3.4}$$

where w_j are *weights* and f_j are values of f in a control volume j.

3.2.3 Comparisons of the Finite Difference Method and the Finite Volume Method

The main difference between the finite difference method and the finite volume method is that the state variable is represented over the entire spatial domain with the finite volume method whereas it is only represented at single points of the domain for the finite difference method. Another difference that is often stated between both numerical methods is that there is conservativeness with the finite volume method for each control volume.

In the finite difference method, there exists a truncation error which comes from the Taylor series approximation. If the finite difference method is applied to the mathematical model involving differential equations, there is no longer conservation of material, energy and momentum due to the truncation error. The application of either method to a mathematical model results in the same discretised equations in certain cases.

The mathematical model of moving bed adsorption systems considered in this thesis will use the finite volume approach.

3.2.4 Discretisation and Approximations at the Boundary of a Control Volume

As mentioned in section 3.2.2, the finite volume method is used to calculate solutions inside discretised cells. As averaged values are used inside each cell,

$$\int_{V_j} u dV \approx u_j V_j \tag{3.5}$$

If u_j is taken as the mid-point value in the cell, then this approximation is second-order accurate. These mid-point values can be used to calculate approximations for the wall values. Numerical approximations need to be made for solutions at the boundary of a cell and some of these are shown in sections 3.2.4.1 and 3.2.4.2.

3.2.4.1 Backwards Difference Scheme

Commonly, the values of state variables at the downstream boundary of a cell can be assumed to be the same as the averaged values inside a cell. This scheme is known as the backwards difference method and is equivalent to treating each cell as a Continuous Stirred Tank Reactor (CSTR). For example, referring to

Figure 3.4, the value of u at the position of the cell boundary, $j + 1/2$, would be the same as at the centre of the cell, j. Therefore,

$$u_{j+1/2} = u_j \tag{3.6}$$

The backwards difference scheme is first-order accurate.

3.2.4.2 Central Difference Scheme

The values of the state variables at the boundary of a cell can also be obtained by using the average of the values of the state variables inside the surrounding cells:

$$u_{j+1/2} = \frac{1}{2}u_j + \frac{1}{2}u_{j+1} \tag{3.7}$$

This central difference scheme is second-order accurate. A generalised weighted average scheme can be used to determine values at the cell boundaries:

$$u_{j+1/2} = \alpha u_j + (1 - \alpha)u_{j+1} \tag{3.8}$$

where α is the weight factor. If $\alpha = 1$, the backwards difference scheme is obtained and if $\alpha = \frac{1}{2}$, the central difference scheme is found.

The inlet boundary condition must be specified and at the outlet of the last control volume, $j = N_P$. The value at this boundary can be found from extrapolation from the previous two centre values:

$$u_{N_P+1/2} = (\alpha - 1)u_{N_P-1} + (2 - \alpha)u_{N_P} \tag{3.9}$$

In this work, the generalised weighted average scheme (Equation 3.8) based on the central difference method has been used to calculate cell wall values. Instead of using the backwards difference scheme for the last cell wall value, it is extrapolated using Equation 3.9 for a higher order of accuracy.

3.2.5 Newton-Raphson Method for a Nonlinear System of Equations

The equations resulting from applying the finite volume method require the need for linear or more generally non-linear solution methods to solve them. In non-linear systems of equations, the number of unknown variables in the algebraic balance equations may be very high. A commonly used non-linear system solution method is the Newton-Raphson method.

It is an iterative method which is based on Equation 3.10:

$$x_{n+1} = x_n - \frac{f(x_n)}{f'(x_n)} \tag{3.10}$$

x_{n+1}: solution of the system of equations, f, for the $(n+1)$ iteration

x_n: solution of the system of equations, f, for the previous (n) iteration

f: vector of residuals which is the rearranged form of the equation to be solved

f': Jacobian matrix based on values from the previous iteration x_n

However, the computation of the inverse of the Jacobian matrix f' can be time-consuming therefore Equation 3.10 can be re-written as:

$$f'(x_n)\Delta x_n = -f(x_n) \tag{3.11}$$

With

$$\Delta x_n = x_{n+1} - x_n \tag{3.12}$$

Using Equation 3.11, Δx_n is calculated and the new solution x_{n+1} is found using the previous solution x_n.

$$x_{n+1} = x_n + \Delta x_n \tag{3.13}$$

After a certain number of successive iterations the solutions obtained will converge to the actual solution. The iterations are stopped if the error Δx_n or the root-mean square of the residuals in vector f are below a certain tolerance. Advantages of this method are that convergence is generally obtained rapidly and that it is relatively simple to implement. However, a Jacobian matrix may need to be recalculated for each step and convergence may be poor if the initial guess is far from the actual root. Undesirable solutions may be found by the method if the initial guess is far from the actual solution. The latter is not problematic if a sufficiently close initial guess to the desired solution is chosen and small variations of the unknown variables often exist in most processes considered.

The solution to the vector of errors, Δx_n, can be found by using Gaussian elimination of the augmented matrix until an upper/lower triangular matrix for the Jacobian is found. Back-substitution is carried out until all elements in the vector Δx_n are found.

The following example illustrates how the Newton-Raphson method is used to solve a non-linear system of equations given in the equation below, with unknown variables x_1, x_2 and x_3:

$$
\begin{aligned}
f(x_1, x_2, x_3) &= \begin{pmatrix} f_1(x_1, x_2, x_3) \\ f_2(x_1, x_2, x_3) \\ f_3(x_1, x_2, x_3) \end{pmatrix} \\
&= \begin{pmatrix} 16(x_2 - 2x_1 + 0) + x_1^2 + 1/4 \\ 16(x_3 - 2x_2 + x_1) + x_2^2 + 1/2 \\ 16(0 - 2x_3 + x_2) + x_3^2 + 3/4 \end{pmatrix} = \begin{pmatrix} 0 \\ 0 \\ 0 \end{pmatrix}
\end{aligned} \tag{3.14}
$$

Jacobian matrix:

$$
\begin{aligned}
f'(x_1, x_2, x_3) &= \begin{pmatrix} \frac{\partial f_1}{\partial x_1} & \frac{\partial f_1}{\partial x_2} & \cdots & \frac{\partial f_1}{\partial x_n} \\ \frac{\partial f_2}{\partial x_1} & \frac{\partial f_2}{\partial x_2} & \cdots & \frac{\partial f_2}{\partial x_n} \\ \vdots & \vdots & \ddots & \vdots \\ \frac{\partial f_n}{\partial x_1} & \frac{\partial f_n}{\partial x_2} & \cdots & \frac{\partial f_n}{\partial x_n} \end{pmatrix} \\
&= \begin{pmatrix} -32 + 2x_1 & 16 & 0 \\ 16 & -32 + 2x_2 & 16 \\ 0 & 16 & -32 + 2x_3 \end{pmatrix}
\end{aligned} \tag{3.15}
$$

Applying Equation 3.11:

$$
\begin{pmatrix} -32 + 2x_1 & 16 & 0 \\ 16 & -32 + 2x_2 & 16 \\ 0 & 16 & -32 + 2x_3 \end{pmatrix} \begin{pmatrix} \Delta x_1^0 \\ \Delta x_2^0 \\ \Delta x_3^0 \end{pmatrix} = \begin{pmatrix} -16(x_2 - 2x_1 + 0) - x_1^2 - 1/4 \\ -16(x_3 - 2x_2 + x_1) - x_2^2 - 1/2 \\ -16(0 - 2x_3 + x_2) - x_3^2 - 3/4 \end{pmatrix} \tag{3.16}
$$

With the initial guess:

$$
\begin{pmatrix} x_1^0 \\ x_2^0 \\ x_3^0 \end{pmatrix} = \begin{pmatrix} 0 \\ 0 \\ 0 \end{pmatrix} \tag{3.17}
$$

The following system is obtained:

$$
\begin{pmatrix} -32 & 16 & 0 \\ 16 & -32 & 16 \\ 0 & 16 & -32 \end{pmatrix} \begin{pmatrix} \Delta x_1^0 \\ \Delta x_2^0 \\ \Delta x_3^0 \end{pmatrix} = \begin{pmatrix} -1/4 \\ -1/2 \\ -3/4 \end{pmatrix} \tag{3.18}
$$

After decomposition,

$$\begin{pmatrix} -32 & 16 & 0 \\ 0 & -24 & 16 \\ 0 & 0 & -64/3 \end{pmatrix} \begin{pmatrix} \Delta x_1^0 \\ \Delta x_2^0 \\ \Delta x_3^0 \end{pmatrix} = \begin{pmatrix} -1/4 \\ -5/8 \\ -7/6 \end{pmatrix} \tag{3.19}$$

Solving gives:

$$\begin{pmatrix} \Delta x_1^0 \\ \Delta x_2^0 \\ \Delta x_3^0 \end{pmatrix} = \begin{pmatrix} 5/128 \\ 1/16 \\ 7/128 \end{pmatrix} \tag{3.20}$$

Therefore,

$$\begin{pmatrix} x_1^1 \\ x_2^1 \\ x_3^1 \end{pmatrix} = \begin{pmatrix} x_1^0 + \Delta x_1^0 \\ x_2^0 + \Delta x_2^0 \\ x_3^0 + \Delta x_3^0 \end{pmatrix} = \begin{pmatrix} 0.0391 \\ 0.0625 \\ 0.0547 \end{pmatrix} \tag{3.21}$$

By repeating the steps from Equations 3.11 and 3.13, convergence to the actual solution will be reached.

3.2.6 Gaussian Elimination with a Banded Matrix

After carrying out material and energy balances for each component and each cell volume in addition to momentum balances for each cell, residual expressions are obtained and a numerical Jacobian can be calculated. Gaussian elimination can be carried out to find the unknown error terms Δx_n, as shown in section 3.2.5. However, in order to make the Gaussian elimination procedure and storage of terms in the Jacobian more efficient, the procedure was carried out on the compact band matrix version of the Jacobian instead of the full Jacobian. This matrix has zero elements before and after the left- and right-half band widths. Therefore, carrying out computations on the zero terms and storing them is avoided. For a $n \times n$ band matrix with a total bandwidth of m, it can be stored in a compact form as a $n \times m$ matrix. An example is considered for solving $\mathbf{Ax} = \mathbf{b}$ with $\mathbf{A}$ as the Jacobian and $\mathbf{x}$ as the vector of unknowns. Algorithms for Gaussian Elimination on a full and compact form of the matrix are also shown. A 7×7 band matrix with a total bandwidth of 7 is used.

3.2.6.1 Full Band Matrix

For this example, the values along the diagonal are considered to be the same however, the same procedure works for different values along the diagonals. Figure 3.5 shows the initial $\mathbf{A}$ matrix before Gaussian Elimination. The letters

A, B and C are transformed to zero after carrying out Gaussian Elimination (Algorithm 1). The letters D, E, F, G and Y are transformed to P, Q, R, S respectively after carrying out Gaussian Elimination as shown in Figure 3.6.

Algorithm 1 Gaussian Elimination Algorithm for Full Band Matrix

```
for k := 1 to n − 1 do
    for i := k + 1 to n do
        for j := k + 1 to n do
            A(i, j) = A(i, j) − A(i, k)/A(k, k)×A(k, j)
        end for
        b(i) = x(i) − A(i, k)/A(k, k)×b(k)
    end for
end for
```

	1	2	3	4	5	6	7	x	b
1	D	E	F	G	0	0	0	X	Y
2	C	D	E	F	G	0	0	X	Y
3	B	C	D	E	F	G	0	X	Y
4	A	B	C	D	E	F	G	X	Y
5	0	A	B	C	D	E	F	X	Y
6	0	0	A	B	C	D	E	X	Y
7	0	0	0	A	B	C	D	X	Y

Figure 3.5: Full matrix before Gaussian Elimination

	1	2	3	4	5	6	7	x	b
1	P	Q	R	S	0	0	0	X	Z
2	0	P	Q	R	S	0	0	X	Z
3	0	0	P	Q	R	S	0	X	Z
4	0	0	0	P	Q	R	S	X	Z
5	0	0	0	0	P	Q	R	X	Z
6	0	0	0	0	0	P	Q	X	Z
7	0	0	0	0	0	0	P	X	Z

Figure 3.6: Full matrix after Gaussian Elimination

3.2.6.2 Compact Band Matrix

The compact versions of **A** are shown before and after Gaussian Elimination in Figures 3.7 and 3.8. Algorithm 2, for a compact band matrix, has been used in the model as less values need to be stored and operations are only carried out on non-zero elements.

Algorithm 2 Gaussian Elimination Algorithm for Compact Band Matrix

```
for k := 1 to n − 1 do
    for i := 1 to n − k do
        for j := 1 to n − k do
            A(i + k, j − i) = A(k + i, j − i) − A(i + k, −i)/A(k, 0)×A(k, j)
        end for
        b(i) = b(i) − A(i + k, −i)/A(k, 0)×b(k)
    end for
end for
```

	-3	-2	-1	0	1	2	3	x	b
1	-	-	-	D	E	F	G	X	Y
2	-	-	C	D	E	F	G	X	Y
3	-	B	C	D	E	F	G	X	Y
4	A	B	C	D	E	F	G	X	Y
5	A	B	C	D	E	F	-	X	Y
6	A	B	C	D	E	-	-	X	Y
7	A	B	C	D	-	-	-	X	Y

Figure 3.7: Compact matrix before Gaussian Elimination

	-3	-2	-1	0	1	2	3	x	b
1	-	-	-	P	Q	R	S	X	Z
2	-	-	0	P	Q	R	S	X	Z
3	-	0	0	P	Q	R	S	X	Z
4	0	0	0	P	Q	R	S	X	Z
5	0	0	0	P	Q	R	-	X	Z
6	0	0	0	P	Q	-	-	X	Z
7	0	0	0	P	-	-	-	X	Z

Figure 3.8: Compact matrix after Gaussian Elimination

3.3 Assumptions

The list of assumptions made for the mathematical model for a column are given below. A discussion of each assumption is also given in this section.

- One-dimensional model
- Spherical and identical adsorbent particles
- Cylindrical vessel
- Ideal gas
- Negligible axial dispersion of mass and heat

- Steady state
- Local thermal equilibrium between gas and solid
- Constant mass transfer coefficients
- Non-isothermal and non-adiabatic operation
- No loss of adsorbent in the process
- Constant heats of adsorption

3.3.1 One-dimensional Model

The construction of a 1D model implies that there is only variation of parameters in a single direction in the spatial domain. Variations exist predominantly in the axial direction therefore it will be assumed that the properties of the gas and solid in the radial direction of the bed are the same at a given position in the axial direction. Furthermore, the gas is assumed to be well mixed in the radial direction of the system. It is reasonable to assume that in the practical design of the process, there is good inlet and outlet flow distribution of solid and gas. Maldistribution of flow inside a column can be compensated for with appropriate spacing of devices for redistribution. The use of a 1D model is also chosen for simplicity and because of the interest in obtaining results in the axial direction of a column. The influence of flow in the radial direction is considered low and will not have a great effect on results of a moving bed system. The 1D assumption applies to co-current and counter-current systems but not to a fluidised bed which is treated like a CSTR in which all parameters are the same at all points in the spatial domain. It is therefore assumed that no radial or axial variations exist in a fluidised bed. The use of the 1D model infers that heat is transferred between the process and the surroundings uniformly through the bed in the radial direction if heat is applied at the wall of the bed. To ensure that the temperature is the same at all points in the radial direction at a given axial position in the bed, a large number of tubes inside the column can be used through which cooling/heating fluids circulates instead of heating/cooling at the wall of the column. Averaged properties of the gas, solid and packing are used in the model of the system described at macroscopic level. The large size of the system allows local microscopic phenomena inside the column to be ignored.

3.3.2 Spherical and Identical Adsorbent Particles

For pressure drop and mass transfer purposes, the solid adsorbent particles are treated as mono-sized spherical particles.

3.3.3 Cylindrical Vessel

A cylindrical vessel with constant cross sectional area is considered for the geometry of the column.

3.3.4 Ideal Gas

The moving bed adsorption systems are considered to be at atmospheric pressure, which is low enough to assume that the ideal gas law is applicable. Therefore, it follows that the total concentration of the gas in the bulk gas phase and in the void space inside the particles can be found from the ideal gas law and that the total pressure of the gas is the sum of the partial pressures of the individual components.

3.3.5 Negligible Axial Dispersion

Axial dispersion results from mixing of the gas along the column. It is generally undesirable in adsorption processes as it has a similar effect to mass transfer resistance. Axial dispersion is ignored for the mathematical model but it is considered as an additional resistance which is grouped in the mass transfer rate expression.

3.3.6 Steady State

In more commonly used fixed bed adsorption processes, regeneration of the adsorbent is carried out in the same unit after the gas concentration at the outlet has reached the breakthrough concentration. Therefore, a single fixed-bed adsorption unit cannot be considered at steady state. On the other hand, in moving bed adsorption units, adsorption and regeneration steps do not have to be stopped at any time and each operation can be carried out in separate units. Hence, it is justifiable to study moving bed adsorption processes at steady state.

3.3.7 Local Thermal Equilibrium

At a given axial position in the overall process, it is assumed that the gas and solid phases are at the same temperature and therefore there is no resistance to

heat transfer between gas and solid. This assumption is known as local thermal equilibrium.

3.3.8 Constant Mass Transfer Coefficients

Mass transfer depends on diffusion and possible reactions within the adsorbent particle. Their rates increase as temperature increases. However, this influence is ignored and it is assumed that the mass transfer coefficients are constant. A value in the same order of magnitude as found by Zhang et al. (2010) is used for all components considered. There is uncertainty in the value of the LDF constant in moving bed systems considered. Therefore, constant and typical values for the LDF constant are used and the sensitivity of this parameter is tested instead.

3.3.9 Cooling and Heating Assumptions

If the column is not assumed to be adiabatic, heat exchange is assumed to be carried out either between columns or with a working fluid at a constant temperature T_{ext}, along the column.

3.3.10 Conservation of Adsorbent in the Overall Cycle

In adsorption systems, there is generally a loss of adsorbent functionality as the adsorbent is used many times. This loss results in a reduction in the performance of the overall adsorption process. Replacement of the lost adsorbent is required and therefore there is an economic penalty due to making up adsorbent inventory. Deactivation of the adsorbent leads to the loss of equilibrium capacity or an increase in mass transfer resistance (Ruthven (1984)). Adsorbent deactivation depends on the adsorbent material and structure but also on adverse species in the feed mixture. For example, the presence of moisture and thermal regeneration causes the breakdown of the crystal structure of zeolite adsorbents. Undesirable compounds formed by a reaction between feed mixture constituents and adsorbent material may also accumulate in the pores of the adsorbent. For supported amine adsorbents, evaporation and degradation of the amine at the adsorbent surface may occur due to side reactions between the amine and undesirable components such as SO_2 (Krutka and Sjostrom (2011)). Additionally, for the moving bed systems considered, attrition of the adsorbent after some time is likely to occur due to the adsorbent particles hitting against each other and other surfaces in the system (e.g. vessel wall or internals). The precise knowledge of the loss of adsorbent functionality is not well known and

therefore this factor is not incorporated into the mathematical model of the system. Hence, it is assumed that adsorbent is fully conserved in the overall process. The cost of lost adsorbent can be estimated based on values from literature commonly found for other moving bed systems.

3.3.11 Constant Heats of Adsorption

The heats of adsorption of components ($\Delta H_{ads,i}$) that have been considered in this work are assumed to be constant. The variation of $\Delta H_{ads,i}$ with temperature can be found from the Clausius-Clapeyron equation (Guo et al. (2006), Qi et al. (2000)):

$$\Delta H_{ads,i} = R\frac{(\partial \ln p_i)}{\partial\left(\frac{1}{T}\right)} \tag{3.22}$$

In addition, the heat of adsorption on activated carbon is often found to decrease slightly as the loading of CO_2 and H_2O increase as found by Guo et al. (2006) and Qi et al. (2000) respectively. Qi et al. (2000) also found that $\Delta H_{ads,i}$ of water vapour on activated carbon decreased for rising temperatures. The extent of this drop in $\Delta H_{ads,i}$ was up to 10% over the range of temperature and loadings considered.

As more accurate information on the variation of $\Delta H_{ads,i}$ with respect to temperature and loading has not been currently found for the adsorbents considered in this work, a constant value for $\Delta H_{ads,i}$ has been used. The variation of $\Delta H_{ads,i}$ with temperature and loading is relatively low therefore the impact on the results of this variation would be low but this assumption may need to be verified by a sensitivity analysis.

3.4 Material Balances

The mathematical model of the material balance comprises of:

- the material balance for a gas component
- the material balance for an adsorbed component
- the overall material balance for the gas
- the material balance for the adsorbent
- the adsorption isotherm model for the amount of a component adsorbed at equilibrium
- mass transfer model of the rate of transfer of a component to or from the adsorbent

The material balances will be presented in this section. Isotherm and mass transfer rate models will be shown later in sections 3.7 and 3.9 respectively.

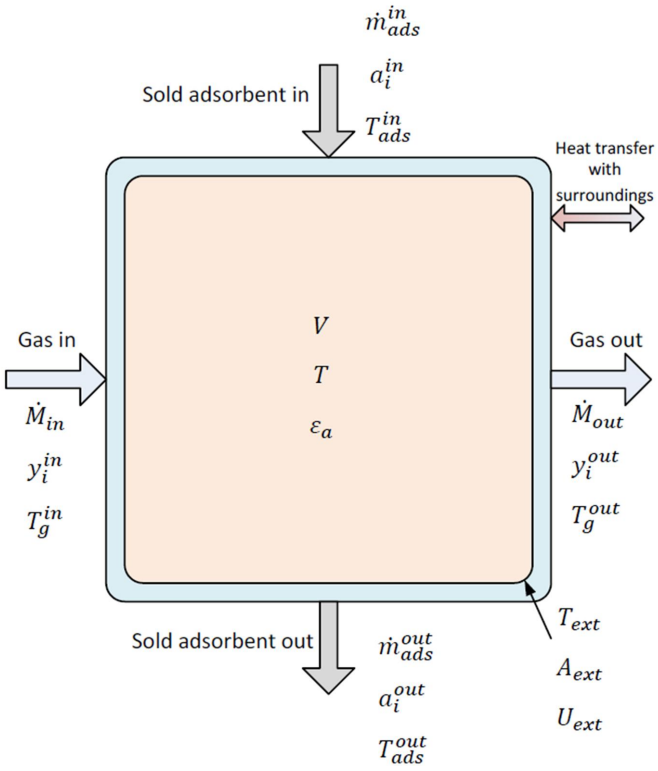

Figure 3.9: Control volume of the systems considered

3.4.1 Material Balance for a Gas Component

For a single control volume (cf. Figure 3.9), the material balance of a component i in the gas phase can be written as:

$$\begin{aligned} &\{\text{Rate of } i \text{ in gas in}\} - \{\text{Rate of } i \text{ in gas out}\} \\ &\quad + \{\text{Rate of generation of } i \text{ in gas}\} \\ &= \{\text{Rate of accumulation of } i \text{ in gas}\} \end{aligned} \tag{3.23}$$

The rate of i generated depends on the rate of i adsorbed or desorbed to or from the adsorbent. The rate of accumulation of i is zero due to the steady state assumption. Equation 3.23 reduces to:

$$\dot{M}_{in} y_i^{in} - \dot{M}_{out} y_i^{out} - \dot{n}_i V \varepsilon_a = 0 \tag{3.24}$$

where:

$\dot{M}_{in}$: molar flowrate of gas at the inlet (mol.s^{-1})

$\dot{M}_{out}$: molar flowrate of gas at the outlet (mol.s^{-1})

y_i^{in}: mole fraction of i in gas at the inlet (-)

y_i^{out}: mole fraction of i in gas at the outlet (-)

$\dot{n}_i$: rate of adsorption/desorption of i to/from the gas per unit volume of the adsorbent (mol.m^{-3}.s^{-1})

V: volume of the control volume (m^3)

ε_a: volume occupied by adsorbent divided by the volume of the control volume (-)

From left to right, the terms on the left-hand side of Equation 3.24 represent the following quantities:

1. The molar flowrate of i in the gas at the inlet of the control volume.
2. The molar flowrate of i in the gas at the outlet of the control volume.
3. The rate of adsorption/desorption of i from/to the gas phase.

3.4.2 Material Balance for an Adsorbed Component

For a single control volume, the material balance of a component i inside the adsorbent can be written as:

$$\begin{aligned} &\{\text{Rate of } i \text{ adsorbed in}\} - \{\text{Rate of } i \text{ adsorbed out}\} \\ &\quad + \{\text{Rate of generation of } i \text{ adsorbed}\} \\ &\quad = \{\text{Rate of accumulation of } i \text{ adsorbed}\} \end{aligned} \tag{3.25}$$

The rate of i generated is given as the rate of i adsorbed or desorbed to or from gas. The rate of accumulation of i is zero due to the steady state assumption. Equation 3.25 can therefore be written as:

$$\dot{m}_{in} a_i^{in} - \dot{m}_{out} a_i^{out} + \dot{n}_i V \varepsilon_a = 0 \tag{3.26}$$

The total amount adsorbed, a_i is the sum of the amount of i adsorbed onto the adsorbent surface and the amount of i contained within the pores of the adsorbent particle (Tien (1984)):

$$a_i = q_i + \frac{\varepsilon_p}{\rho_p} C_{p,i} \tag{3.27}$$

where:

$\dot{m}_{in}$: mass flowrate of adsorbent particles at the inlet (kg.s^{-1})

$\dot{m}_{out}$: mass flowrate of adsorbent particles at the outlet (kg.s^{-1})

ρ_p: adsorbent particle density (kg.m^{-3})

a_i: total amount of i contained in the adsorbent per unit mass of solid adsorbent particle (mol.kg^{-1})

a_i^{in}: total amount of i contained in the adsorbent per unit mass of solid adsorbent particle at the inlet (mol.kg^{-1})

a_i^{out}: total amount of i contained in the adsorbent per unit mass of solid adsorbent particle at the outlet (mol.kg^{-1})

$\dot{n}_i$: rate of adsorption/desorption of i to/from the adsorbate per unit volume of adsorbent (mol.m^3.s^{-1})

V: volume of the control volume (m^3)

ε_a: fraction of the control volume occupied by solid adsorbent particles (volume of solid adsorbent particles per unit volume of the control volume) (−)

q_i: amount of i adsorbed on the surface of the adsorbent per unit mass of adsorbent (mol.kg^{-1})

$C_{p,i}$: concentration of i in the pores of the adsorbent particle (mol.m^{-3})

ε_p: void fraction of the adsorbent particle (volume of void space per unit volume of adsorbent particle) (-)

A typical range for ε_p given by Ruthven (1984) is 0.4-0.6. In the literature, the actual value for the adsorbents considered (supported amine adsorbent, activated carbon and zeolite 13X) were not specified by the authors Krutka and Sjostrom (2011), SRI International (2010) or Cavenati et al. (2004) so value of 0.4 is chosen throughout this work.

From left to right, the terms on the left-hand side of Equation 3.26 represent the following quantities:

1. The molar flowrate of i adsorbed at the inlet of the control volume
2. The molar flowrate of i adsorbed at the outlet of the control volume
3. The rate of adsorption/desorption of i to/from the adsorbed phase

3.4.3 Overall Material Balance for the Gas

The overall gas material balance over the control volume can be written as:

$$\begin{aligned} &\{\text{Rate of gas in}\} - \{\text{Rate of gas out}\} \\ &+ \{\text{Rate of generation of gas}\} \\ &= \{\text{Rate of accumulation of gas}\} \end{aligned} \tag{3.28}$$

The rate of accumulation of gas is zero due to the steady state assumption. However, the rate of generation of gas is the rate of the total amount of gas desorbed from the adsorbent or adsorbed onto the adsorbent if there is a reduction in the amount of gas. This balance is necessary to find the composition of the last component in the mixture and the overall gas flowrates. Therefore Equation 3.28 reduces to:

$$\dot{M}_{in} - \dot{M}_{out} + \sum_{i=1}^{N} \dot{n}_i V \varepsilon_a = 0 \tag{3.29}$$

where:

$\dot{M}_{in}$: molar flowrate of gas at the inlet (mol.s^{-1})

$\dot{M}_{out}$: molar flowrate of gas at the outlet (mol.s^{-1})

N: total number of components (-)

$\dot{n}_i$: rate of adsorption/desorption of i to/from the gas per unit volume of the adsorbent (mol.m^{-3}.s^{-1})

V: volume of the control volume (m^3)

ε_a: volume occupied by adsorbent divided by the volume of the control volume (-)

From left to right, the terms on the left-hand side of Equation 3.29 represent the following quantities:

1. The molar flowrate of gas at the inlet of the control volume
2. The molar flowrate of gas at the outlet of the control volume
3. The total rate of adsorption/desorption of gas

3.4.4 Material Balance for the Adsorbent

For a single control volume, the material balance of the adsorbent can be written as:

$$\begin{aligned} &\{\text{Rate of adsorbent in}\} - \{\text{Rate of adsorbent out}\} \\ &\quad + \{\text{Rate of generation of adsorbent}\} \\ &\quad = \{\text{Rate of accumulation of adsorbent}\} \end{aligned} \tag{3.30}$$

The rate of generation of adsorbent is zero as the solid phase does not undergo any changes. The rate of accumulation of adsorbent is also zero due to the steady-state assumption. Therefore Equation 3.30 reduces to:

$$\dot{m}_{in} - \dot{m}_{out} = 0 \tag{3.31}$$

where:

$\dot{m}_{in}$: mass flowrate of adsorbent particles at the inlet (kg.s^{-1})

$\dot{m}_{out}$: mass flowrate of adsorbent particles at the outlet (kg.s^{-1})

From left to right, the terms on the left-hand side of Equation 3.31 represent the following quantities:

1. The mass flowrate of adsorbent at the inlet of the control volume

2. The mass flowrate of adsorbent at the outlet of the control volume

3.5 Energy Balance

For a single control volume (Figure 3.9), the energy balance for a single stage, can be written as:

$$\begin{aligned} &\{\text{Rate of energy in}\} - \{\text{Rate of energy out}\} \\ &\quad + \{\text{Rate of generation of energy}\} \\ &\quad = \{\text{Rate of accumulation of energy}\} \end{aligned} \tag{3.32}$$

The rate of generation of energy can be expressed in terms of the amounts of energy produced and consumed during adsorption. The rate of accumulation

of energy is zero due to the steady state assumption. Equation 3.32 reduces to:

$$\begin{aligned}
&\dot{m}_{in}c_{p,ads}T_{ads}^{in} + \sum_{i=1}^{N}\dot{M}_i^{in}H_{i,g}^{in} + \sum_{i=1}^{N}\dot{m}_{in}\frac{\varepsilon_p}{\rho_p}C_{p,i}^{in}H_{i,ads}^{in} + \sum_{i=1}^{N}\dot{m}_{in}q_i^{in}H_{i,ads}^{in} \\
&-\dot{m}_{out}c_{p,ads}T_{ads}^{out} - \sum_{i=1}^{N}\dot{M}_i^{out}H_{i,g}^{out} - \sum_{i=1}^{N}\dot{m}_{out}\frac{\varepsilon_p}{\rho_p}C_{p,i}^{out}H_{i,ads}^{out} - \sum_{i=1}^{N}\dot{m}_{out}q_i^{out}H_{i,ads}^{out} \\
&+\sum_{i=1}^{N}\left(\dot{m}_{in}q_i^{in} - \dot{m}_{out}q_i^{out}\right)\Delta H_{ads,i} - U_{ext}A_{ext}\left(T - T_{ext}\right) = 0
\end{aligned} \tag{3.33}$$

where:

$c_{p,ads}$: specific heat capacity of the solid adsorbent particle ($\mathrm{J.kg^{-1}.K^{-1}}$)

T_{ads}^{in}: temperature of the adsorbent at the inlet(K)

$\dot{M}_i^{in}$: molar flowrate of i in the bulk gas at the inlet ($\mathrm{mol.s^{-1}}$)

$H_{i,g}^{in}$: specific molar enthalpy of i in the bulk gas at the inlet ($\mathrm{J.mol^{-1}}$)

$C_{p,i}^{in}$: concentration of i in the pores of the solid adsorbent particle at inlet ($\mathrm{mol.m^{-3}}$)

$H_{i,ads}^{in}$: specific molar enthalpy of i in the pores of the solid adsorbent particle at inlet ($\mathrm{J.mol^{-1}}$)

q_i^{in}: amount of i adsorbed onto the adsorbent at the inlet per unit mass of an adsorbent particle ($\mathrm{mol.kg^{-1}}$)

T_{ads}^{out}: temperature of solid adsorbent at the outlet (K)

$\dot{M}_i^{out}$: molar flowrate of i in the bulk gas at the outlet ($\mathrm{mol.s^{-1}}$)

$H_{i,g}^{out}$: specific molar enthalpy of i in the bulk gas at the outlet ($\mathrm{J.mol^{-1}}$)

$C_{p,i}^{out}$: concentration of i in the pores of the adsorbent particle at outlet ($\mathrm{mol.m^{-3}}$)

$H_{i,ads}^{out}$: specific molar enthalpy of i in the pores of the adsorbent particle at outlet ($\mathrm{J.mol^{-1}}$)

q_i^{out}: amount of i adsorbed onto the adsorbent at outlet per unit mass of an adsorbent particle ($\mathrm{mol.kg^{-1}}$)

$\Delta H_{ads,i}$: specific enthalpy of adsorption of i ($\mathrm{J.mol^{-1}}$)

U_{ext}: overall heat transfer coefficient for heat transfer between material inside the control volume and the cooling/heating fluid ($W.m^{-2}.K^{-1}$)

A_{ext}: surface area for heat transfer between material inside the control volume and the cooling/heating fluid (m^{-2})

T: average temperature of gas and solid in control volume (K).

T_{ext}: average temperature of cooling/heating fluid (K)

N: total number of components ($-$)

From left to right, the terms on the left-hand side of Equation 3.33 represent the following quantities:

1. Rate of transfer of sensible heat of the solid into the control volume

2. Rate of transfer of sensible heat of all components in the bulk gas phase at the inlet of the control volume

3. Rate of transfer of sensible heat of all components in the gas in the pores of the adsorbent at the inlet of the control volume

4. Rate of transfer of sensible heat of all components adsorbed on the solid adsorbent surface at the inlet of the control volume

5. Rate of transfer of sensible heat of the solid at the outlet of the control volume

6. Rate of transfer of sensible heat of all components in the bulk gas phase at the outlet of the control volume

7. Rate of transfer of sensible heat of all components in the gas in the pores of the adsorbent at the outlet of the control volume

8. Rate of transfer of sensible heat of all components adsorbed on the solid adsorbent surface at the outlet of the control volume

9. Rate of transfer of energy due to latent heat of adsorption of all components onto the solid adsorbent inside the control volume

10. Rate of addition/removal of energy by a heat exchanger to/from control volume by heating/cooling fluid

Although the temperatures of the gas and solid are assumed to be the same inside a control volume (cf. section 3.3.7), the temperatures at the boundaries of the control volume may be different if they are flowing in different directions. As a result, the specific molar enthalpies for the bulk gas ($H_{i,g}$) and the adsorbent pores ($H_{i,ads}$) are functions of the temperatures of the bulk gas (T_g) and adsorbent temperatures (T_{ads}) respectively:

$$H_{i,g} = f(T_g) \tag{3.34}$$

$$H_{i,ads} = f(T_{ads}) \tag{3.35}$$

Enthalpy and heat capacities can be approximated by polynomials with coefficients for specific components found from the National Institute of Standards and Technology (2014) database. These coefficients are given in Table 3.1.

$$c_{pi,g} = A + BT_r + CT_r^2 + DT_r^3 + \frac{E}{T_r^2} \tag{3.36}$$

$$H_{i,g} - H_{ref} = AT_r + B\frac{T_r^2}{2} + C\frac{T_r^3}{3} + D\frac{T_r^4}{4} - \frac{E}{T_r} + F - H \tag{3.37}$$

$c_{pi,g}$: gas heat capacity for component i (J.mol^{-1}.K^{-1})

$H_{i,g}$: gas enthalpy for component i (kJ.mol^{-1})

T_r: reduced temperature $T_r = T/1000$ (K), T actual temperature (K)

A, B, C, D, E, F, H: coefficients in polynomials Equations (3.36) and (3.37) (-)

H_{ref}: enthalpy at reference temperature $T_{ref} = 298.15$K (kJ.mol^{-1})

Table 3.1: Coefficients in Equation 3.36 and 3.37

	CO_2	**H_2O**	**N_2**
A	24.99735	30.092	28.98641
B	55.18696	6.832514	1.853978
C	-33.69137	6.793435	-9.647459
D	7.948387	-2.53448	16.63537
E	-0.136638	0.082139	0.000117
F	-403.6075	-250.881	-8.671914
H	-393.5224	-241.8264	0

3.6 Momentum Balance

3.6.1 Momentum Balance for Fluidised Bed Systems

The fluidised bed does not contain packing. Therefore the pressure drop equation for the fluidised bed can be expressed by a force balance on the bed:

$$-\frac{\Delta P}{Z} = (1-\varepsilon)g(\rho_p - \rho_g) \tag{3.38}$$

ΔP: pressure drop in fluidised bed (Pa)

Z: length of section of bed (m)

ε: gas void fraction of the bed (-)

g: acceleration due to gravity (= 9.81 m.s^{-2})

ρ_p: adsorbent particle density (kg.m^{-3})

ρ_g: gas density (kg.m^{-3})

The pressure drop in a fluidised bed increases until the point of minimum fluidisation. After this point, it is roughly constant. At this point, the void fraction and the height of the bed at minimum fluidisation is given by:

$$\varepsilon = \varepsilon_{mf} \tag{3.39}$$

$$Z = L_{mf} \tag{3.40}$$

Commonly, it is assumed that the void fraction and bed height at the point of minimum fluidisation are roughly the same as for a packed bed of solid particles because the amount of space between particles increases only slightly at the start of fluidisation (Kunii and Levenspiel (1991)). In this work, a value of 0.4 (Kunii and Levenspiel (1991)) has been used for ε_{mf} and L_{mf} is chosen as the height of the vessel assuming that it is full with adsorbent.

3.6.2 Momentum Balance for Co-current Systems

It has assumed that the pressure drop in a co-current bed is negligible as the void fraction of adsorbent is significantly lower than in a fluidised bed. However, the actual pressure drop in a co-current column would be close to the pressure drop along a pipe.

3.6.3 Momentum Balance for Counter-current Systems

The mathematical model that was used used to determine the pressure drop inside a counter-current system containing solid particles flowing through structured packing in the opposite direction to a gas stream is described by Stichlmair et al. (1989) for gas/liquid flow through structured packing. The main assumption made is that the solid particles used for adsorption are small enough to behave as a liquid inside the packing.

The main equations of the mathematical model of Stichlmair et al. (1989) used is outlined below:

The equivalent particle diameter of the packing, d_p (m) is expressed using the factional volume occupied by the packing, ε_{pk} (-) and the specific surface area of the packing, a ($\mathrm{m}^2.\mathrm{m}^{-3}$):

$$d_p = \frac{6\varepsilon_{pk}}{a} \tag{3.41}$$

The Reynolds number for the gas phase is expressed in terms of d_p:

$$Re_g = \frac{\rho_g u_g d_p}{\mu_g} \tag{3.42}$$

where:

Re_g: Reynolds number of the gas (-)

ρ_g: density of the gas ($\mathrm{kg.m}^{-3}$)

u_g: superficial gas velocity ($\mathrm{m.s}^{-1}$)

μ_g: gas viscosity (Pa.s)

The friction factor, f_0 (-), for flow past an equivalent single particle of packing is given by:

$$f_0 = \frac{C_1}{Re_g} + \frac{C_2}{Re_g^{1/2}} + C_3 \tag{3.43}$$

C_1, C_2 and C_3 are packing constants (-). Some of these can be found in the specification data from packing suppliers and some constants for structured and random packing are provided by Stichlmair et al. (1989). The Montz structured packing was used in this work due to its large void fraction. Its properties are shown in Table 3.2.

After carrying out a force balance for a single equivalent particle of packing, the pressure drop through the packing containing no solid adsorbent particle is

Table 3.2: Packing constants for Montz structured packing (Stichlmair et al. (1989))

Parameter	**Unit**	**Value**
a	$m^2.m^{-3}$	100
ε_{pk}	-	0.01
C_1	-	3
C_2	-	7
C_3	-	1

given by:

$$-\frac{\Delta P}{Z} = \frac{3}{4} f_0 \frac{1-\varepsilon}{\varepsilon^{4.65}} \frac{\rho_g u_g^2}{d_p} \tag{3.44}$$

ΔP: pressure drop through a section of packing in the column (Pa)

Z: length of section of packing (m)

The solid hold-up, ε_a (-), is the fractional volume occupied by the adsorbent particles in the entire column. With the presence of solid adsorbent particles, the voidage for the gas flow reduces and the equivalent particle diameter, d'_p becomes:

The change in equivalent particle diameter, d'_p, becomes:

$$d'_p = d_p \left(\frac{1-\varepsilon}{\varepsilon_{pk}} \right)^{1/3} \tag{3.45}$$

where

ε: gas voidage after introduction of adsorbent particles

The friction factor, f_0 can be generally expressed in terms of constants A_{f_0} (-) and c (-) as shown by Stichlmair et al. (1989):

$$f_0 = A_{f_0} {Re_g}^c \tag{3.46}$$

with:

$$c = \frac{-C_1/Re_g - C_2/(2Re_g^{1/2})}{f_0} \tag{3.47}$$

The change in friction factor by including hold-up, f'_0 (-), is:

$$f'_0 = f_0 \left(\frac{d'_p}{d_p} \right)^c = f_0 \left(\frac{1-\varepsilon}{\varepsilon_{pk}} \right)^{c/3} \tag{3.48}$$

The holding point in packed beds is the point at which the adsorbent starts to accumulate inside the packing. It was expressed by Stichlmair et al. (1989) as:

$$\varepsilon_a = 0.555 Fr^{1/3} = 0.555 \left(U_s^2 \frac{a}{g\varepsilon^{4.65}} \right)^{1/3} \tag{3.49}$$

Fr: Froude number $(-)$.

U_s: superficial solid velocity $(\mathrm{m.s^{-1}})$ $(= \dot{m}_{in}/(\rho_p A_c))$

A_c: cross sectional area $(\mathrm{m^2})$

g: acceleration due to gravity $(\mathrm{m.s^{-2}})$

The pressure drop with adsorbent present is:

$$-\frac{\Delta P'}{Z} = \frac{3}{4} f_0' \frac{1-\varepsilon}{\varepsilon^{4.65}} \frac{\rho_g u_g^2}{d_p'} \tag{3.50}$$

3.7 Mathematical Models for Isotherms

Isotherm models that have been used are presented in this section. Data for the isotherms have been taken from literature. Isotherm models for the adsorption of three main components: CO_2, H_2O and N_2 on supported amine adsorbent, activated carbon and zeolite 13X follow.

3.7.1 Adsorption Isotherms for a Supported Amine Adsorbent

For the development of the models using the supported amine adsorbent, the adsorption of O_2 and the reaction between O_2 and the amine group at the adsorbent surface were neglected. Additionally, sulphur dioxide (SO_2), nitrogen oxide and particulates should be removed prior to CO_2 removal and their uptake was also neglected. The adsorption of CO_2 and water have been assumed to be independent of one another as there is insufficient data in the literature of multicomponent isotherm models for CO_2 and water adsorption on supported amine adsorbents. Further work in this area is required.

CO_2 Isotherm

The isotherm data for CO_2 adsorption on a supported amine adsorbent was measured by ADA-ES (Krutka and Sjostrom (2011)). In this work, the single component Langmuir model was used to fit the experimental isotherm data for

Table 3.3: Values of parameters for CO_2 on supported amine adsorbent

Parameter	**Unit**	**Value**
A_{max}	$mol.kg^{-1}$	29.901
B_{max}	K^{-1}	-7.69×10^{-3}
$b_{CO_2,0}$	Pa^{-1}	3.99×10^{-12}
$\Delta H_{ads,CO_2}$	$J.mol^{-1}$	-49338.4

multiple temperatures. As shown in Figure 3.10, the model gives a reasonably good prediction of the CO_2 loading at equilibrium for the range of temperatures between 40°C and 120°C. For temperatures higher than 100°C, the predicted equilibrium loading is found to be less accurate in particular at low CO_2 partial pressures. Values of parameters used for the model are shown in Table 3.3.

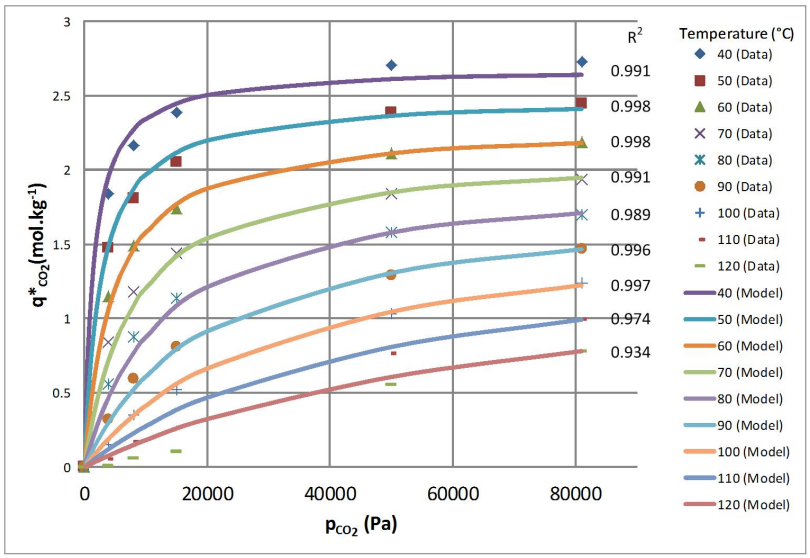

Figure 3.10: CO_2 isotherms at various temperatures for the supported amine adsorbent (data points from Krutka and Sjostrom (2011))

$$q^*_{CO_2} = \frac{q_{max,CO_2}(T) b_{CO_2}(T) p_{CO_2}}{1 + b_{CO_2}(T) p_{CO_2}} \tag{3.51}$$

To give the suitable fitting, the loading at saturation of CO_2 (q_{max,CO_2}) and the affinity constant (b_{CO_2}) were fitted with functions of temperature:

$$q_{max,CO_2}(T) = A_{max} \exp(B_{max} T) \tag{3.52}$$

$$b_{CO_2}(T) = b_{CO_2,0} \exp\left(-\frac{\Delta H_{ads,CO_2}}{RT}\right) \tag{3.53}$$

with:

$q^*_{CO_2}$: equilibrium loading of CO_2 per unit mass of adsorbent (mol.kg^{-1})

q_{max,CO_2}: loading of CO_2 at saturation per unit mass of adsorbent (mol.kg^{-1})

b_{CO_2}: affinity constant for CO_2 in Langmuir isotherm (Pa^{-1})

p_{CO_2}: partial pressure of CO_2 (Pa)

A_{max}: coefficient used in q_{max,CO_2} (mol.kg^{-1})

B_{max}: coefficient used in q_{max,CO_2} (K^{-1})

T: gas temperature (K)

$b_{CO_2,0}$: pre-exponential factor for CO_2 in Langmuir isotherm (Pa^{-1})

$\Delta H_{ads,CO_2}$: heat of adsorption (J.mol^{-1})

R: ideal gas constant (J.mol^{-1}.K^{-1})

N_2 Isotherm

N_2 was assumed to be a non-adsorbing component on the supported amine adsorbent:

$$q^*_{N_2} = 0 \tag{3.54}$$

H_2O Isotherm

The isotherm data for water adsorption was not provided by Krutka and Sjostrom (2011) therefore data for water adsorption on a different supported amine adsorbent was used instead. These were measured by Didas et al. (2012). The Peleg isotherm model (Peleg (1993)) was used to model the water isotherm on the supported amine adsorbent. The isotherm model is shown below and the isotherm curves are represented for different temperatures in Figure 3.11.

$$q^*_{H_2O} = C_{Peleg,1}\left(\frac{p_{H_2O}}{p_{sat}}\right)^{C_{Peleg,3}} + C_{Peleg,2}\left(\frac{p_{H_2O}}{p_{sat}}\right)^{C_{Peleg,4}} \tag{3.55}$$

In this work, the parameters $C_{Peleg,1}$, $C_{Peleg,2}$, $C_{Peleg,3}$, $C_{Peleg,4}$ used for Equation 3.55 were obtained by fitting the model to data given by Didas et al. (2012). The values are given in Table 3.4.

The saturated water vapour pressure can be found from the Antoine equation:

$$p_{sat} = 100000 \times 10^{\left(A_w - \frac{B_w}{T+C_w}\right)} \tag{3.56}$$

The parameters used in Equation 3.56 are given in Table 3.4 and are used from National Institute of Standards and Technology (2014). These parameters were found for temperatures between 20°C and 70°C.

The partial pressure of H_2O can be expressed in terms of the mole fraction or concentration of H_2O in the bulk gas phase:

$$p_{H_2O} = y_{H_2O}P = C_{H_2O}RT \tag{3.57}$$

with:

$q^*_{H_2O}$: equilibrium loading of H_2O per unit mass of adsorbent (mol.kg^{-1})

$C_{Peleg,1}$: coefficient in water isotherm model (mol.kg^{-1})

$C_{Peleg,2}$: coefficient in water isotherm model (mol.kg^{-1})

$C_{Peleg,3}$: coefficient in water isotherm model (-)

$C_{Peleg,4}$: coefficient in water isotherm model (-)

p_{sat}: saturated vapour pressure (Pa)

A_w: coefficient in Antoine equation (-)

B_w: coefficient in Antoine equation (-)

C_w: coefficient in Antoine equation (-)

y_{H_2O}: mole fraction of H_2O in bulk gas phase (-)

C_{H_2O}: concentration of H_2O in bulk gas phase (mol.m^{-3})

Table 3.4: Values of parameters for H_2O on supported amine adsorbent

Parameter	**Unit**	**Value**
$C_{Peleg,1}$	mol.kg^{-1}	6.972
$C_{Peleg,2}$	-	2.998
$C_{Peleg,3}$	mol.kg^{-1}	7.618
$C_{Peleg,4}$	-	0.692
A_w	-	6.20963
B_w	-	2354.731
C_w	-	7.559

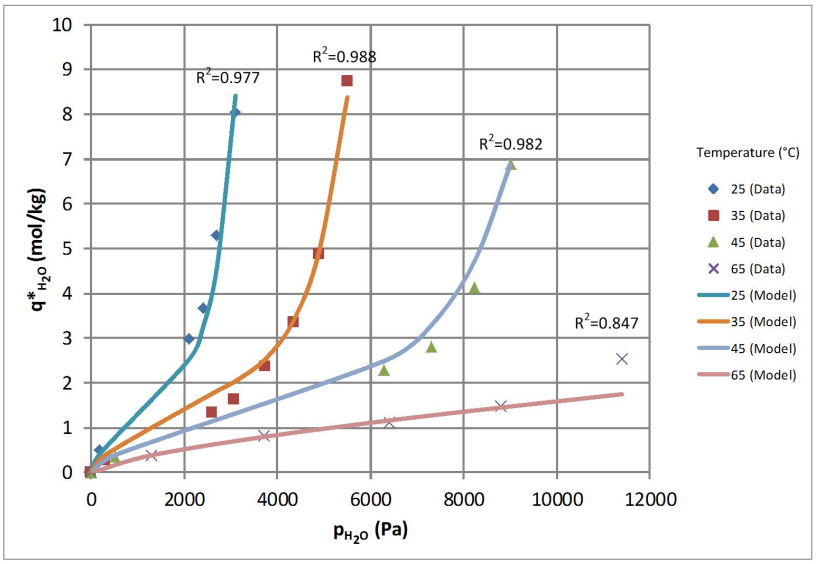

Figure 3.11: H_2O isotherms at various temperatures for an supported amine adsorbent (data points from Didas et al. (2012))

3.7.2 Adsorption Isotherms for an Activated Carbon Adsorbent

CO_2 and N_2 Isotherms

The pure component CO_2 isotherm on the activated carbon produced by ATMI and used by SRI in a counter-current moving bed system was measured at 25C. The pure component N_2 isotherm model was used from Kikkinides et al. (1993). The extended Langmuir isotherm model was then used to represent CO_2 and N_2 isotherms. The adsorption of CO_2 and water have been assumed to be independent of one another as there is insufficient data in the literature of multicomponent isotherm models for CO_2 and water adsorption on activated carbon. Further work in this area is required.

$$q^*_{CO_2} = \frac{q_{max,CO_2}(T) b_{CO_2}(T) p_{CO_2}}{1 + b_{CO_2}(T) p_{CO_2} + b_{N_2}(T) p_{N_2}} \tag{3.58}$$

The affinity constant was found to be a function of temperature:

$$b_{CO_2}(T) = b_{CO_2,0} \exp\left(-\frac{\Delta H_{ads,CO_2}}{RT}\right) \tag{3.59}$$

$$q^*_{N_2} = \frac{q_{max,N_2}(T) b_{N_2}(T) p_{N_2}}{1 + b_{CO_2}(T) p_{CO_2} + b_{N_2}(T) p_{N_2}} \tag{3.60}$$

The loading at saturation of N_2 and the affinity constant were found to be functions of temperature:

$$q_{max,N_2}(T) = l_{N_2,1} - l_{N_2,2}T \tag{3.61}$$

$$b_{N_2}(T) = l_{N_2,3} \exp\left(\frac{l_{N_2,4}}{T}\right) \tag{3.62}$$

with:

b_{N_2}: affinity constant for N_2 in Langmuir isotherm (Pa^{-1})

p_{N_2}: partial pressure of N_2 (Pa)

q_{max,N_2}: loading of N_2 at saturation per unit mass of adsorbent ($mol.kg^{-1}$)

$l_{N_2,1}$: coefficient used in q_{max,N_2} ($mol.kg^{-1}$)

$l_{N_2,2}$: coefficient used in q_{max,N_2} ($mol.kg^{-1}.K^{-1}$)

$l_{N_2,3}$: coefficient used in b_{N_2} (Pa^{-1})

$l_{N_2,4}$: coefficient used in b_{N_2} (K)

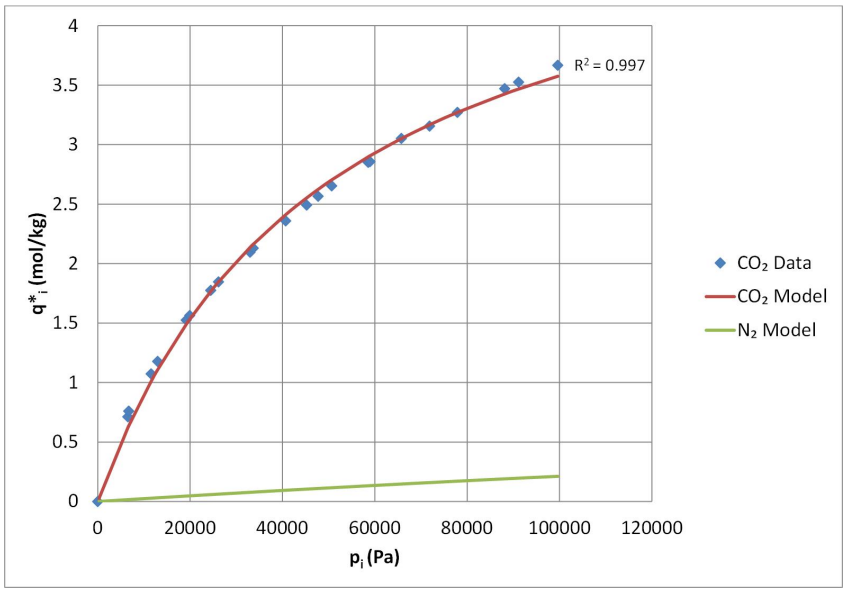

Figure 3.12: CO_2 and N_2 isotherm at 25°C for activated carbon (data points from SRI International et al. (2012))

H_2O Isotherm

The isotherm data for water adsorption on activated carbon was measured by Xu et al. (2011). The isotherm model presented by Mahle (2002) was found

Table 3.5: Values of parameters for CO_2 and N_2 activated carbon

Parameter	Unit	Value
q_{max,CO_2}	$mol.kg^{-1}$	5.3623
$b_{CO_2,0}$	Pa^{-1}	2.48×10^{-10}
$\Delta H_{ads,CO_2}$	$J.mol^{-1}$	-28000
$k_{N_2,1}$	-	4.199
$l_{N_2,2}$	$J.mol^{-1}$	0.0091
$l_{N_2,3}$	-	1.91×10^{-8}
$l_{N_2,4}$	$J.mol^{-1}$	1331.6

to represent the data reasonably well for the conditions considered to obtain the data. The isotherm model is shown below and the isotherm curves are represented for different temperatures in Figure 3.13

$$q^*_{H_2O} = q_{max,H_2O}\frac{\tan^{-1}\left(\frac{p_{H_2O}/p_{sat}}{B_M}\right) - \tan^{-1}\left(-\frac{A_M}{B_M}\right)}{\tan^{-1}\left(\frac{1-A_M}{B_M}\right) - \tan^{-1}\left(-\frac{A_M}{B_M}\right)} \tag{3.63}$$

with:

A_M: constant for H_2O isotherm in Equation 3.63 (-)

B_M: constant for H_2O isotherm in Equation 3.63 (-)

p_{sat}: saturated vapour pressure of water (Pa)

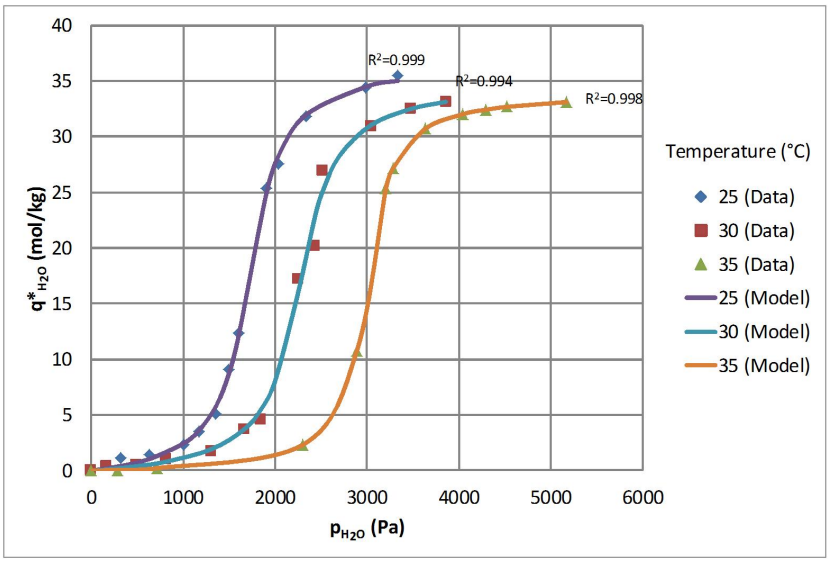

Figure 3.13: H_2O isotherm at various temperatures for activated carbon (data points from Xu et al. (2011))

Table 3.6: Values of parameters for H_2O on activated carbon

Parameter	**Unit**	**Value**
q_{max,H_2O}	mol.kg^{-1}	1.14873
A_M	-	0.533257
B_M	-	0.061782

3.7.3 Adsorption Isotherms for Zeolite 13X

The CO_2 and N_2 isotherms are represented by the extended Langmuir model. Isotherm data for single component CO_2 and N_2 adsorption on zeolite 13X at 40°C and 100°C was found by Mulgundmath et al. (2012). The data for single components was used in the extended Langmuir isotherm. Water was omitted from the isotherm model because there is a strong reduction in capacity for CO_2 adsorption when it is in presence of water (Hefti et al. (2013), Pirngruber et al. (2013a)). Therefore water would need to be removed prior to CO_2 adsorption. The extended Langmuir isotherm model used for component i on zeolite 13X is:

$$q_i^* = \frac{q_{max,i} b_i(T) p_i}{1 + \sum_{i=1}^{N} b_i(T) p_i} \tag{3.64}$$

with:

$$b_i(T) = b_{i,0} \exp\left(-\frac{\Delta H_{ads,i}}{RT}\right) \tag{3.65}$$

The parameters for CO_2 and N_2 are given in Table 3.7. These values were taken from Mulgundmath et al. (2012).

Table 3.7 and Figures 3.14 and 3.15 show the loadings at equilibrium of CO_2 and N_2 on zeolite 13X calculated from Equation 3.64

Table 3.7: Values of parameters for CO_2 and N_2 on zeolite 13X

Parameter	**Unit**	**Value**
q_{max,CO_2}	mol.kg^{-1}	4.095
q_{max,N_2}	mol.kg^{-1}	4.065
b_{0,CO_2}	Pa^{-1}	2.07×10^{-8}
b_{0,N_2}	Pa^{-1}	3.82×10^{-12}
$\Delta H_{ads,CO_2}$	J.mol^{-1}	-21906.56
$\Delta H_{ads,N_2}$	J.mol^{-1}	-33670.04

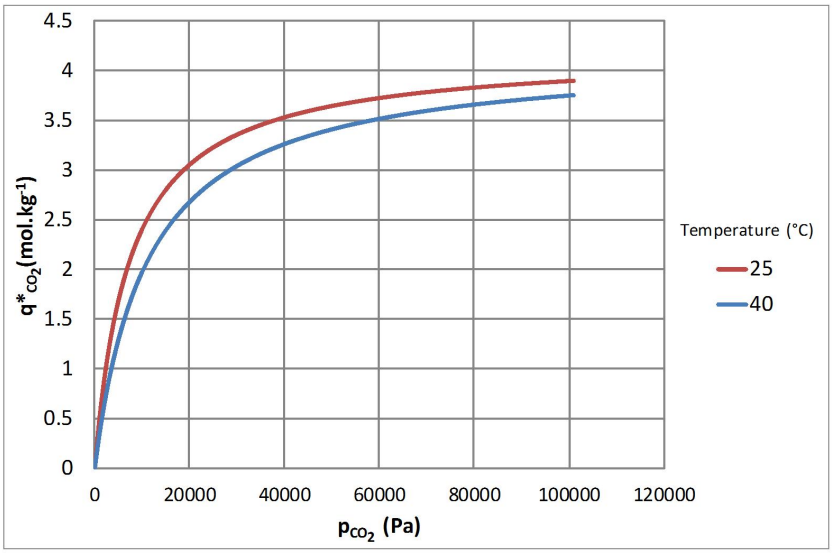

Figure 3.14: CO_2 isotherms at different temperatures for zeolite 13X

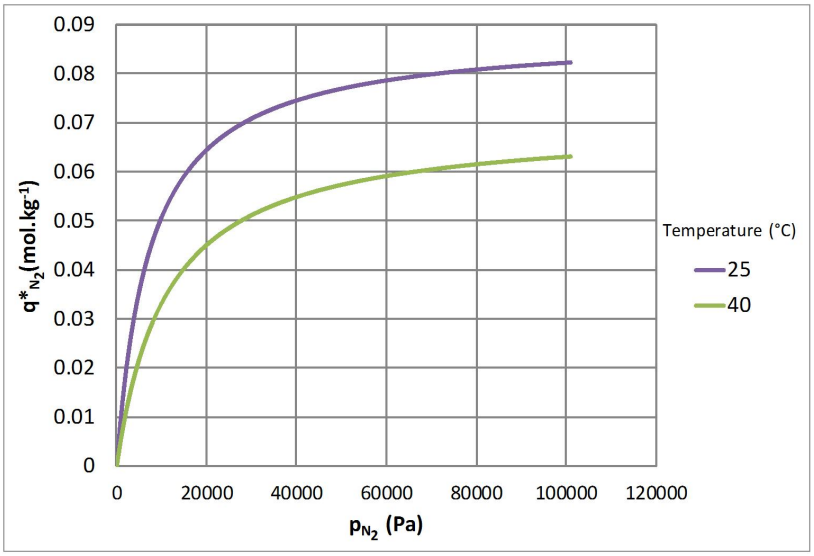

Figure 3.15: N_2 isotherms at different temperatures for zeolite 13X

3.8 Multicomponent Adsorption

A multicomponent isotherm model has not been used in this thesis for the competitive adsorption between H_2O and CO_2 because there was insufficient data in the literature to build a model for the supported amine adsorbent and activated carbon. In addition, for the supported amine adsorbent and activated carbon, a multicomponent model would have added a higher level of complexity to the overall model.

If the H_2 isotherms on activated carbon and the supported amine adsorbent were both of type I (c.f. Figure 2.5), the extended Langmuir model would be suitable (section 2.3.3.2). However, this was not the case therefore another mul-

ticomponent model would be needed. If the gas and adsorbed components are assumed to be thermodynamically ideal, the Ideal Adsorbed Solution Theory (IAST) could be used. However, experimental data would be required to check that the IAST model is adequate. The methodology using IAST is provided below (Yang (1987)):
Raoult's law states that:

$$p_i = y_i P = p_{i,sat} x_i \tag{3.66}$$

with:

p_i: partial pressure of i (Pa)

y_i: mole fraction of i in bulk gas (-)

P: pressure (Pa)

$p_{i,sat}$: saturated vapour pressure of component i (Pa)

x_i: mole fraction of i in adsorbate (-)

$p_{H_2O,sat}$ and $p_{CO_2,sat}$ can be calculated from Gibbs equation:

$$\int_0^{p_{H_2O,sat}} \frac{q^*_{H_2O}}{p_{H_2O}} dp_{H_2O} = \int_0^{p_{CO_2,sat}} \frac{q^*_{CO_2}}{p_{CO_2}} dp_{CO_2} \tag{3.67}$$

with:

$q^*_{H_2O}$: pure component equilibrium loading of H_2O (mol.kg^{-1})

$q^*_{CO_2}$: pure component equilibrium loading of CO_2 (mol.kg^{-1})

and

$$\sum_i^N x_i = 1 \tag{3.68}$$

From Equation 3.66,

$$\frac{p_{H_2O}}{p_{H_2O,sat}} + \frac{p_{CO_2}}{p_{CO_2,sat}} = 1 \tag{3.69}$$

From the isotherms of the individual components, $q^*_{CO_2}(p_{CO_2,sat})$ and $q^*_{H_2O}(p_{H_2O,sat})$ can be calculated.

The mole fractions of both components in the adsorbed phase are deduced from Equation 3.66:

$$x_{CO_2} = \frac{p_{CO_2}}{p_{CO_2,sat}} \tag{3.70}$$

$$x_{H_2O} = \frac{p_{H_2O}}{p_{H_2O,sat}} \tag{3.71}$$

The actual overall loading at equilibrium (q^* (Pa)) is given by:

$$q^* = \frac{1}{\sum_i^N \frac{x_i}{q_i^*(p_{i,sat})}} \tag{3.72}$$

The individual multicomponent loadings are determined from:

$$q^*_{CO_2} = x_{CO_2} q^* \tag{3.73}$$

$$q^*_{H_2O} = x_{H_2O} q^* \tag{3.74}$$

As part of future work, this method could be applied to improve the accuracy of results obtained throughout this thesis. If the competitive nature of the adsorption between CO_2 and H_2O is taken into account, the actual CO_2 loadings found in this work would be lower than isotherm data found for single components. The IAST model would reflect this. The reduction in CO_2 capacity occurs for activated carbon and zeolite 13X as demonstrated by Hefti et al. (2013). On the other hand an improvement in CO_2 loadings have been found with the presence of water (Xu et al. (2005), Guo et al. (2006)) for chemisorbents such as supported amines. The presence of water is found to allow a higher conversion of CO_2 and amine groups and therefore the IAST model would not be adequate.

3.9 Mass Transfer Rate Models

The mass transfer rate model used has been described previously in section 2.4. It involves the use of the linear driving force (LDF) model based on concentrations in the bulk fluid and in the pores of the adsorbent.

$$\dot{n}_i = k_i \left(y_i C - C_{p,i}\right) = k_i \left(y_i \frac{P}{RT} - C_{p,i}\right) \tag{3.75}$$

with:

$\dot{n}_i$: rate of adsorption/desorption of i to/from the gas per unit volume of the adsorbent (mol.m^{-3}.s^{-1})

k_i: mass transfer constant (s^{-1})

y_i: mole fraction of i in the bulk gas (-)

C: concentration of bulk gas (mol.m^{-3})

$C_{p,i}$: concentration of i in adsorbent pores (mol.m^{-3})

P: pressure of bulk gas (Pa)

R: ideal gas constant (J.mol^{-1}.K^{-1})

T: temperature of bulk gas (K)

The mass transfer constant k_i is expressed in terms of the effective diffusivity, $D_{e,C}$ or $D_{e,q}$, and the radius of the adsorbent particle, R_p. However, effective diffusivity, can be difficult to estimate accurately. Kinetic data from experimental measurements give more reliable values. Mass transfer constants are often obtained from the rate of uptake curves which plot the loading of adsorbate against time. However, measurements are generally obtained for samples of adsorbents exposed to gas in a magnetic suspension balance or a fixed-bed of adsorbent.

Zhang et al. (2010) have measured uptake rates at a partial pressure of 0.5 bar of CO_2 on zeolite 13X and activated carbon between 25°C and 55°C. A magnetic suspension balance was used. The LDF model used was based on loadings rather than concentrations as given by Equation 2.10.

Average mass transfer constants for the range of temperatures were $k_i' = 32.6 \times 10^{-4}$ s^{-1} and $k_i' = 21.8 \times 10^{-4}$ s^{-1} for zeolite 13X and activated carbon respectively (Zhang et al. (2010)). Bollini et al. (2012) have fitted an LDF constant to a breakthrough curve representing adsorption of CO_2 in a packed bed of silica supported amine adsorbent. The fitted LDF constant has a value of $k_i' = 12.0 \times 10^{-3}$ s^{-1} at temperatures between 25°C and 45°C. The LDF constant found by Bollini et al. (2012) for the supported amine adsorbent is roughly an order of magnitude higher than for activated carbon and zeolite 13X found by Zhang et al. (2010). Mass transfer is therefore greater for the supported amine adsorbent than activated carbon and zeolite 13X and this is confirmed by their uptake and breakthrough curves.

However, from Equation 2.9, as loadings are used in the mass transfer rate expression instead of concentrations, the LDF constants, k_i, based on a concentration difference is modified to:

$$k_i = k_i' \rho_p \frac{q_i^* - q_i}{C_i - C_{pi}} \tag{3.76}$$

Assuming a linear isotherm for low partial pressures of CO_2, k_i differs from k_i' by a factor of $\rho_p K$, where K is the slope of the isotherm (m^3.kg^{-1}). Using Figure 3.10 to approximate the value of this slope, it is found that $K = 0.5$ m^3.kg^{-1}. Therefore if the LDF constant based on a difference of loadings is $k_i' = 12.0 \times 10^{-3}$ s^{-1}, the LDF constant based on a difference of concentrations is approximately $k_i = 3.9$ s^{-1}.

However, in the literature, there is a great lack of accurate data for the LDF constants for CO_2 adsorption in moving beds with the adsorbents considered. Consequently, there is an uncertainty in the exact value of k_i. Therefore, an approximate value of the same order of magnitude as $k_i = 3.9\ s^{-1}$ is to be used in subsequent simulations. The value used is $k_i = 10\ s^{-1}$ throughout the rest of this work and the effect of the uncertainty of this parameter can be found from a sensitivity analysis. In the future, it would be necessary to find the correct value experimentally.

3.10 Overall Process Model

3.10.1 Mathematical Model of Adsorption or Regeneration Systems

The mathematical model of a full adsorption/regeneration system involves solving the material balance together with the energy and momentum balances for each finite volume. These equations were written for a single finite volume in sections 3.4, 3.5 and 3.6. The symbols used are essentially the same as used previously in these sections but they are written for a finite volume j. The flows of gas and solid for a given stage j, designate the outlet of the stage. These balances are coupled with the isotherm and kinetic rate models. Generally, the system has N components and N_P stages/finite volumes in the column. The flowrates are written for the boundaries of the control volume ($wall$).

For j = 1 to N_P stages and for i = 1 to N-1 components:

$$\left(\dot{M}_{j-1} y_{i,j-1}\right)^{wall} - \left(\dot{M}_j y_{i,j}\right)^{wall} - \dot{n}_{i,j} V_j \varepsilon_a = 0 \tag{3.77}$$

$$\gamma \left(\dot{m}_{j-1} a_{i,j-1}\right)^{wall} - \gamma \left(\dot{m}_j a_{i,j}\right)^{wall} + \dot{n}_{i,j} V_j \varepsilon_a = 0 \tag{3.78}$$

for which γ has a value of either 1 for co-current adsorbent flow or -1 for counter-current flow.

$$\dot{n}_{i,j} = k_{i,j} \left(y_{i,j} C_j - C_{p,i,j}\right) \tag{3.79}$$

For the N^{th} component, if mass transfer for this component is finite, Equations (3.78) and (3.79) are used but if the rate is infinite, the concentration of component N is the same inside and outside the adsorbent pores for which:

$$C_{p,N,j} = y_{N,j} C_j \tag{3.80}$$

and

$$\dot{n}_{N,j} = -\frac{1}{V_j \varepsilon_a} \left(\gamma \dot{m}_{j-1} a^{wall}_{N,j-1} - \gamma \dot{m}_j a^{wall}_{N,j} \right) \tag{3.81}$$

The overall component balance for the gas phase is given by:

$$\dot{M}^{wall}_{j-1} - \dot{M}^{wall}_{j} - V_j \varepsilon_a \dot{n}_{total,j} = 0 \tag{3.82}$$

with

$$\dot{n}_{total,j} = \sum_{i=1}^{N} \dot{n}_{i,j} \tag{3.83}$$

The unknowns for all $j = 1$ to N_P are: $y_{i,j}$ for $i = 1$ to $N-1$, $C_{p,i,j}$ for $i = 1$ to N, $\dot{M}^{wall}_j$, T^{wall}_j and P^{wall}_j.

The mole fraction in the gas phase of component N, is calculated separately after the overall solutions are found for $i = 1$ to $N-1$ and for $j = 1$ to N_P:

$$y_{N,j} = 1 - \sum_{i=1}^{N-1} y_{i,j} \tag{3.84}$$

Referring to Equation 3.33, the temperatures for each stage are given by:

$$\begin{aligned} &\gamma \left(\dot{m}_{j-1} c_{p,ads} T_{j-1} \right)^{wall} + \left(\sum_{i=1}^{N} \dot{M}_{i,j-1} H_{i,j-1} \right)^{wall} \\ &+\gamma \left(\sum_{i=1}^{N} \dot{m}_{j-1} \varepsilon_p C_{p,i,j-1} H_{i,j-1} \right)^{wall} + \gamma \left(\sum_{i=1}^{N} \dot{m}_{j-1} q_{i,j-1} H_{i,j-1} \right)^{wall} \\ &-\gamma \left(\dot{m}_j c_{p,ads} T_j \right)^{wall} - \left(\sum_{i=1}^{N} \dot{M}_{i,j} H_{i,j} \right)^{wall} \\ &-\gamma \left(\dot{m}_j \varepsilon_p C_{p,i,j} H_{i,j} \right)^{wall} - \gamma \left(\sum_{i=1}^{N} \dot{m}_j q_{i,j} H_{i,j} \right)^{wall} \\ &+\gamma \left(\sum_{i=1}^{N} \dot{m}_{j-1} q_{i,j-1} - \dot{m}_j q_{i,j} \right)^{wall} \Delta H_{ads,i} - U_{ext} A_{ext} \left(T_j - T_{ext} \right) = 0 \end{aligned} \tag{3.85}$$

For a counter-current system the pressure at stage j can be found from Equation 3.50. the symbols used are given in section 3.6. P_j and P_{j-1} are the

pressure in stages j and $j-1$ respectively. Explicitly P_j is written as:

$$P_j = P_{j-1} - \Delta x \frac{3}{4} f_0' \frac{1-\varepsilon'}{\varepsilon'^{4.65}} \frac{\rho_g u_g^2}{d_p'} \tag{3.86}$$

For co-current beds, the pressure at stage j is:

$$P_j = P_{j-1} - \Delta x \left(1-\varepsilon\right)\left(\rho_g - \rho_p\right) g \tag{3.87}$$

Pressures at the wall of the stages are found by averaging the pressure at the stages.

There is very little in the literature on mathematical models for moving bed adsorption and even less so applicable to CO_2 capture. However, a material balance was developed by Ruthven (1984) to which the model developed here can been compared. It was written in differential form, axial dispersion was included and it was written for a transient system. However, an energy balance was not carried out by Ruthven (1984).

Kim et al. (2013a) also developed a mathematical model for moving bed CO_2 adsorption systems however, several differences between their model and the one developed in this chapter exist. The balances were written in differential form and they were not written at steady state. Axial dispersion was included in their model however a significant problem with their material and energy balances were that the individual terms in them were not consistent with each other.

3.10.2 Iterative Solving

To solve unknown gas mole fractions ($y_{i,j}$), concentrations inside the adsorbent particle pores ($C_{pi,j}$), molar flowrates at the exit of the cells ($\dot{M}_j$), the temperature (T_j) and pressure (P_j) inside a cell, material, energy and momentum balances were written in a vector form known as the residuals. The numerical Jacobian matrix was then calculated from the residuals according to:

$$f'(x_n) = \frac{f(x_n + \Delta) - f(x_n)}{\Delta} \tag{3.88}$$

with Δ being a small value used for a small change in x_n. Applying Equations (3.11) and (3.13), the Newton-Raphson iterative method was used to find errors between solutions from one iteration to another, Δx_n. Convergence to a solution of the unknowns was found after several iterations and the tolerance limit was reached.

3.10.3 Cycle Formation and Sequential Solving

The mathematical model constructed in section 3.10.1 is applicable to moving bed adsorption columns. However, it can also be extended to moving bed desorbers as well as heat exchangers for gas and solids if they are modelled as another moving bed adsorption column with different boundary conditions. A cycle of adsorbers and desorbers can be constructed by adding columns after the adsorber. After specifying boundary conditions at the inlet of the first adsorption column, the model of the first moving bed adsorption vessel is solved before the solution at the outlet of the system is used as the boundary conditions at the inlet to the subsequent vessels.

3.10.4 Modelling of Heat Exchangers

Independent heat exchangers for the gas or solid adsorbent phases can be modelled as a single column through which solid particles continuously flow and a heat duty is added or withdrawn if the adsorbent requires heating or cooling respectively.

In this work, heat exchangers that involve heat integration between two solid particle streams at different temperatures have been modelled as two single columns with heat transferred either co- or counter-currently between stages. Both sides of the heat exchangers are modelled as columns in which heat can be transferred from one column to another as shown by Figures 3.16 and 3.17. In practice, a small amount of gas could be required to transport the solid adsorbent through the heat exchanger.

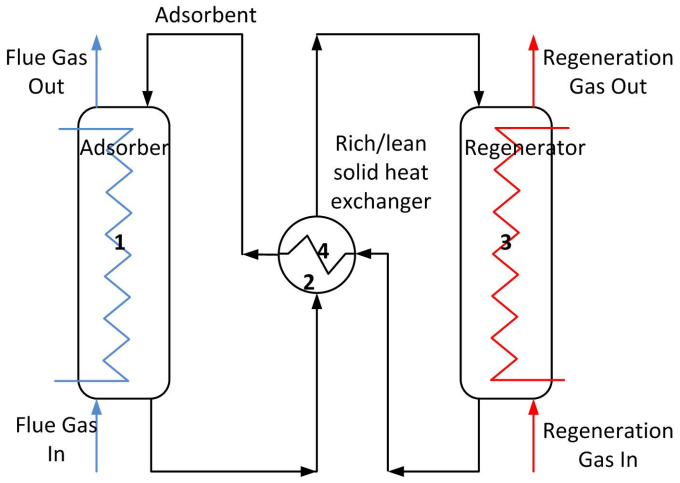

Figure 3.16: Moving bed CO_2 capture process with heat integration

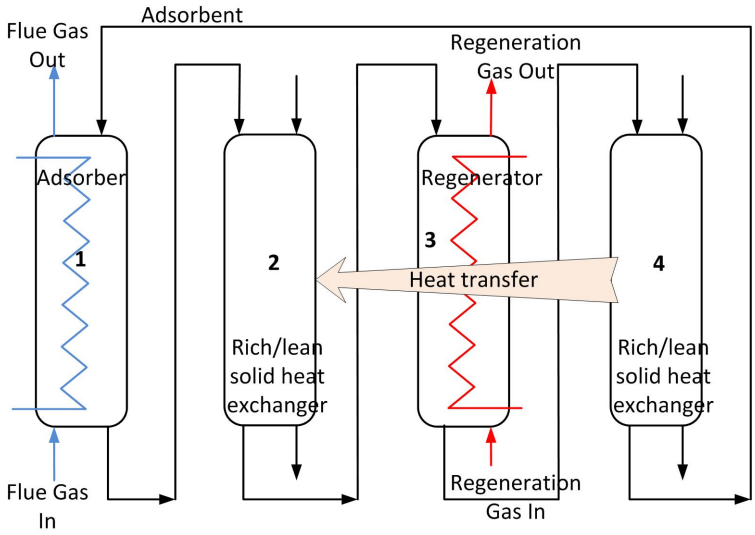

Figure 3.17: Representation of the model of the moving bed CO_2 capture process with heat integration

3.10.5 Overall Cycle Convergence

In moving bed adsorption process cycles, solid adsorbent particles are recycled back to the adsorber after undergoing desorption as shown in Figure 3.16. In order to reach convergence to a solution, a tear stream for the recycle stream can be used for which initial guesses of the properties of the tear stream are used to generate a new updated solution. An iterative process is generally performed to obtain a converged solution for a specified tolerance. Two commonly used methods for the convergence of a process with a recycle stream are *Direct Subsitution* and the *Wegstein method* (Finlayson (2014)).

3.10.5.1 Direct Substitution

With the direct substitution method, an initial guess of the tear stream needs to be specified (y_0) and the new value of the tear stream (y_1) can be calculated by sequentially solving each unit (Finlayson (2014)). Mathematically, it is written as:

$$y_{n+1} = h(y_n) \tag{3.89}$$

with:

y: estimate of the unknown tear stream variable

$h(y)$: calculated value of the tear stream variable from the function given by the mathematical model of the process

n: iteration

3.10.5.2 Wegstein Method

The Wegstein Method is a commonly used technique to accelerate convergence of calculations for processes with recycle streams. It is derived from the secant method as follows (Finlayson (2014)). A new function, f is introduced to represent the error between the value of the unknown variable in the previous iteration and the new value.

$$f(y_n) = y_n - h(y_n) \tag{3.90}$$

$$f(y_{n-1}) = y_{n-1} - h(y_{n-1}) \tag{3.91}$$

Applying the secant method to find the new value, y_{n+1} is:

$$y_{n+1} = y_n - f(y_n)\frac{y_n - y_{n-1}}{f(y_n) - f(y_{n-1})} \tag{3.92}$$

Replacing Equations 3.90 and 3.91 into Equation 3.92 and rearranging gives:

$$y_{n+1} = y_n + (h(y_n) - y_n)(1 - s') \tag{3.93}$$

with:

$$s' = \frac{s}{s-1} \tag{3.94}$$

$$s = \frac{h(y_n) - h(k-1)}{y_n - y_{n-1}} \tag{3.95}$$

The Wegstein method requires two previous iterations which can be a guessed value and the solution obtained from the direct substitution method. If s' is unbounded, oscillations or divergence may occur. The Wegstein method becomes a direct substitution method if $s' = 0$. Other methods for accelerating convergence could also be used. In the Wegstein method, each unknown variable of the recycle stream is iterated individually. The Broyden Method can be used to estimate all unknown variables simultaneously using a matrix that is adjusted after each iteration (Kelley (2003)).

In the model of this work for the application to the CO_2 cyclic capture process, the direct substitution method is used for the first three iterations in order to avoid divergence from the solution early on in the first few iterations. The Wegstein method is used thereafter. If the absolute error, found using the Wegstein method, increases from one iteration to another, the solution from direct substitution is used instead.

3.11 Summary

In this chapter, the mathematical models of the adsorption systems considered have been presented:

- Three types of moving bed adsorbers (fluidised bed, co-current and counter-current) were presented and described.
- The numerical methods and techniques used to solve the model were presented. The finite volume method is used to discretise the equations of the mathematical model and a weighted average is used to calculate the values at the boundaries of a control volume. The Newton-Raphson method is used to solve the unknown variables in the model.
- The assumptions used to create the mathematical model were given and justified.
- The material, energy and momentum balances were established.
- Isotherm models are shown for the components present (N_2, CO_2 and H_2O) on three adsorbents considered in this work (supported amine adsorbent, activated carbon and zeolite 13X). The linear driving force model for the mass transfer rate was used.
- Finally, the model of the overall process is shown and how the overall cycle can be solved has been presented.

The mathematical model that has presented in this chapter was constructed in Excel and Visual Basic for Applications (VBA). This can be found on the accompanying CD. The mathematical model allows simulations to be carried out on a commercial CO_2 capture process for flue gas from a full scale coal fired power plant. In the following chapters, simulations using the constructed mathematical model have been carried out to assess the performance of moving bed adsorption processes.

Chapter 4

Numerical and Analytical Solutions

4.1 Introduction

Previously in Chapter 3, material balances for components in the gas and adsorbate were established. Numerical techniques to solve the model were also shown. If the model is simple, analytical solutions can be found. Analytical solutions have been presented in literature on adsorption, however these solutions are common for simplified cases such as linear or rectangular isotherms, trace component or a binary mixture (Ruthven (1984), Tien (1984)). Recent work on adsorption modelling rarely use these types of isotherm models. In this chapter, analytical solutions for co- and counter-current beds are found. A brief example is used to verify that under certain assumptions, the numerical solution concurs with the analytical one.

4.2 Assumptions

Assumptions that were already made in section 3.3 are used in addition to the following ones:

- Isothermal system
- Binary mixture of CO_2 and N_2. Only CO_2 is adsorbed
- CO_2 is in trace concentrations therefore the gas molar flowrate is constant

4.3 Analytical Model of a Co-current Bed

For the analytical solutions, the gas and adsorbate material balances given by Equations 3.24 and 3.26 can be rewritten in a differential form.

Under the assumptions above, the material balance for component $i = CO_2$ in the gas phase, reduces to:

$$-\dot{M}\frac{dy_i}{dx} - A_c\varepsilon_a\dot{n}_i = 0 \tag{4.1}$$

Given that the mass flowrate of adsorbent is constant, the material balance for CO_2 adsorbed is given by:

$$-\dot{m}\frac{da_i}{dx} + A_c\varepsilon_a\dot{n}_i = 0 \tag{4.2}$$

where:

$\dot{M}$: total molar flowrate of gas (mol.s^{-1})

$\dot{m}$: mass flowrate of adsorbent particles (kg.s^{-1})

y_i: mole fraction of CO_2 (-)

a_i: amount of CO_2 contained in the adsorbent per unit mass of solid adsorbent particle (mol.kg^{-1})

$\dot{n}_i$: rate of adsorption of CO_2 per unit volume of adsorbent (mol.m^{-3}.s^{-1}))

A_c: cross sectional area of the bed (m^2)

ε_a: volume fraction occupied by solid adsorbent particles ($-$)

x: axial position (m)

The rate of mass transfer can be given by the LDF equation in terms a difference of loadings:

$$\dot{n}_i = k_i'\rho_p(q_i^* - q_i) \tag{4.3}$$

where:

k_i': mass transfer constant of CO_2 (s^{-1})

ρ_p: adsorbent particle density (kg.m^{-3})

q_i^*: equilibrium loading of CO_2 (mol.kg^{-1})

q_i: loading of CO_2 (mol.kg^{-1})

Introducing a new variable for simplification:

$$k'_{i,A_c\varepsilon_a} = k'_i A_c \varepsilon_a \rho_p \tag{4.4}$$

Combining Equations 4.1 and 4.2:

$$\dot{M}\frac{dy_i}{dx} = -\dot{m}\frac{da_i}{dx} \tag{4.5}$$

Assuming that the amount of CO_2 contained in the pores is much smaller than the amount loaded,

$$a_i = q_i \tag{4.6}$$

Integrating Equation 4.5 between the bed inlet ($x = 0$), y_i^0 and any axial position x, y_i:

$$q_i = q_i^0 - \frac{\dot{M}}{\dot{m}}(y_i - y_i^0) \tag{4.7}$$

Combining Equations 4.1 and 4.7:

$$\dot{M}\frac{dy_i}{dx} = -k'_{i,A_c\varepsilon_a}\left(q_i^* - \left(q_i^0 - \frac{\dot{M}}{\dot{m}}(y_i - y_i^0)\right)\right) \tag{4.8}$$

The equation for the Langmuir isotherm for CO_2 is:

$$q_i^* = \frac{q_{max,i} b_i y_i P}{1 + b_i y_i P} \tag{4.9}$$

$$\dot{M}\frac{dy_i}{dx} = -k'_{i,A_c\varepsilon_a}\left(\frac{q_{max,i} b_i y_i P}{1 + b_i y_i P} - \left(q_i^0 - \frac{\dot{M}}{\dot{m}}(y_i - y_i^0)\right)\right) \tag{4.10}$$

Integrating Equation 4.10 from the inlet to the outlet of the system gives:

$$\frac{\dot{m}}{\dot{M} b_i P}\left(\left(-\frac{1 + b_i P y_1}{y_2 - y_1}\right)\ln\left(\frac{y_i - y_1}{y_i^0 - y_1}\right) + \left(\frac{1 + b_i P y_2}{y_2 - y_1}\right)\ln\left(\frac{y_i - y_2}{y_i^0 - y_2}\right)\right) = -\frac{k'_{i,A_c\varepsilon_a}}{\dot{M}}x \tag{4.11}$$

A quadratic equation results after integration which has roots:

$$y_1 = \frac{-\left(q_{max,i} b_i P - q_i^0 b_i P + \frac{\dot{M}}{\dot{m}} - \frac{\dot{M}}{\dot{m}} y_i^0 b_i P\right) + \sqrt{\Delta^0}}{2\frac{\dot{M}}{\dot{m}} b_i P} \tag{4.12}$$

$$y_2 = \frac{-\left(q_{max,i} b_i P - q_i^0 b_i P + \frac{\dot{M}}{\dot{m}} - \frac{\dot{M}}{\dot{m}} y_i^0 b_i P\right) - \sqrt{\Delta^0}}{2\frac{\dot{M}}{\dot{m}} b_i P} \tag{4.13}$$

The discriminant is:

$$\Delta^0 = \left(q_{max,i}b_iP - q_i^0 b_i P + \frac{\dot{M}}{\dot{m}} - \frac{\dot{M}}{\dot{m}}y_i^0 b_i P\right)^2 + 4\frac{\dot{M}}{\dot{m}}b_i P\left(q_i^0 + \frac{\dot{M}}{\dot{m}}y_i^0\right) \quad (4.14)$$

Equation 4.11 indirectly gives the analytical profile of the CO_2 mole fraction in the co-current bed.

4.4 Analytical Model of a Counter-current Bed

The material balance of adsorbate is given by:

$$\dot{m}\frac{da_i}{dx} + A_c\varepsilon_a\dot{n}_i = 0 \quad (4.15)$$

Combining Equations 4.1 and 4.15 gives:

$$\dot{M}\frac{dy_i}{dx} = \dot{m}\frac{da_i}{dx} \quad (4.16)$$

The length of the bed is L (m). Integrating Equation 4.16 from any axial position (x) to the gas outlet ($x = L$), which is the position at which adsorbent enters the counter-current bed:

$$q_i = q_i^L + \frac{\dot{M}}{\dot{m}}(y_i - y_i^L) \quad (4.17)$$

Therefore by using Equations 4.1 and 4.17,

$$\dot{M}\frac{dy_i}{dx} = -k'_{i,A_c\varepsilon_a}\left(q_i^* - \left(q_i^L + \frac{\dot{M}}{\dot{m}}(y_i - y_i^L)\right)\right) \quad (4.18)$$

$$\dot{M}\frac{dy_i}{dx} = -k'_{i,A_c\varepsilon_a}\left(\frac{q_{max,i}b_i y_i P}{1 + b_i y_i P} - \left(q_i^L + \frac{\dot{M}}{\dot{m}}(y_i - y_i^L)\right)\right) \quad (4.19)$$

Integrating Equation 4.19 between the bed inlet ($x = 0$), y_i^0 any axial position (x), y_i:

$$-\frac{\dot{m}}{\dot{M}b_iP}\left(\left(-\frac{1 + b_iPy_1}{y_2 - y_1}\right)\ln\left(\frac{y_i - y_1}{y_i^0 - y_1}\right) + \left(\frac{1 + b_iPy_2}{y_2 - y_1}\right)\ln\left(\frac{y_i - y_2}{y_i^0 - y_2}\right)\right) = -\frac{k'_{i,A_c\varepsilon_a}}{\dot{M}}x \quad (4.20)$$

The roots of a resulting quadratic are:

$$y_1 = \frac{-\left(q_{max,i}b_iP - q_i^L b_i P - \frac{\dot{M}}{\dot{m}} + \frac{\dot{M}}{\dot{m}}y_i^L b_i P\right) + \sqrt{\Delta^L}}{-2\frac{\dot{M}}{\dot{m}}b_i P} \tag{4.21}$$

$$y_1 = \frac{-\left(q_{max,i}b_iP - q_i^L b_i P - \frac{\dot{M}}{\dot{m}} + \frac{\dot{M}}{\dot{m}}y_i^L b_i P\right) - \sqrt{\Delta^L}}{-2\frac{\dot{M}}{\dot{m}}b_i P} \tag{4.22}$$

The discriminant is:

$$\Delta^L = \left(q_{max,i}b_iP - q_i^L b_i P - \frac{\dot{M}}{\dot{m}} + \frac{\dot{M}}{\dot{m}}y_i^L b_i P\right)^2 + 4\frac{\dot{M}}{\dot{m}}b_i P\left(-q_i^L + \frac{\dot{M}}{\dot{m}}y_i^L\right) \tag{4.23}$$

However the roots obtained are functions of y_i^L which is unknown. Therefore Equation 4.24 needs to be solved for y_i^L and this solution can be used to find the roots y_1 and y_2. Integrating Equation 4.19 between y_i^0 and y_i^L gives:

$$-\frac{\dot{m}}{\dot{M}b_iP}\times\left(\left(-\frac{1+b_iPy_1}{y_2-y_1}\right)\ln\left(\frac{y_i^L-y_1}{y_i^0-y_1}\right)+\left(\frac{1+b_iPy_2}{y_2-y_1}\right)\ln\left(\frac{y_i^L-y_2}{y_i^0-y_2}\right)\right) = -\frac{k'_{i,A_c\varepsilon_a}}{\dot{M}}L \tag{4.24}$$

Equation 4.20 indirectly gives the analytical profile of the CO_2 mole fraction in the counter-current bed.

4.5 Parameters

To compare the solutions given by the analytical and numerical results, the following parameters in Table 4.1 were chosen in the analytical and numerical model. The value of 0.5 for α chosen corresponds to a central difference method and a relatively high number of discretisations is chosen to compare numerical solutions to analytical ones.

Table 4.1: Parameters used to obtain analytical and numerical solutions

Parameter	**Unit**	**Value**
P	Pa	101325
T	°C	25
ε	-	0.3
ρ_p	kg.m^{-3}	1000
k_i'	s^{-1}	0.1
A_c	m^2	19.635
L	m	10
q_i^0 (co-current)	mol.kg^{-1}	0
q_i^L (counter-current)	mol.kg^{-1}	0
$\dot{M}$	mol.s^{-1}	7931.03
$\dot{m}$	kg.s^{-1}	6000
$q_{max,i}$	mol.kg^{-1}	3.1514
b_i	Pa^{-1}	1.66×10^{-5}
α	-	0.5
Number of discretisations	-	64

4.6 Results and Discussion

Simulations were carried out with parameters in Table 4.1 to obtain numerical results for the profiles in co-current and counter-current single adsorbers. These were compared with the analytical solutions. Four inlet mole fractions of CO_2 were considered (1×10^{-5}, 0.01, 0.15, 0.5). Results are shown in Figures 4.1, 4.2, 4.3, 4.4 for the co-current bed and in Figures 4.5, 4.6, 4.7, 4.8 for the counter-current bed.

The numerical and analytical solutions are very close for $y_i^0 = 1\times10^{-5}$ and $y_i^0 = 0.01$ due to the assumption about trace concentrations being applicable. For $y_i^0 = 0.15$ and $y_i^0 = 0.5$, the molar flowrate of gas changes more significantly as CO_2 is adsorbed. Therefore the assumption about trace concentrations is no longer valid for analytical solutions and it results in a greater deviation with the numerical solution.

Although analytical solutions are relatively rapid to obtain and exploit, they require more assumptions to be made if a simple solution is wanted. However, work shown in the rest of this thesis involves phenomena that would make the analytical solution difficult to obtain. For example, not only CO_2 is adsorbed, but also water and N_2 and it is inaccurate to assume that the system is isothermal for the given heats of adsorption of CO_2 and water. Therefore, the numerical model presented previously in Chapter 3 is used.

This analysis has also shown that a lower final mole fraction is reached for

the counter-current bed as there is a greater driving force for adsorption than the co-current bed. This can be seen from Figures 4.1-4.8.

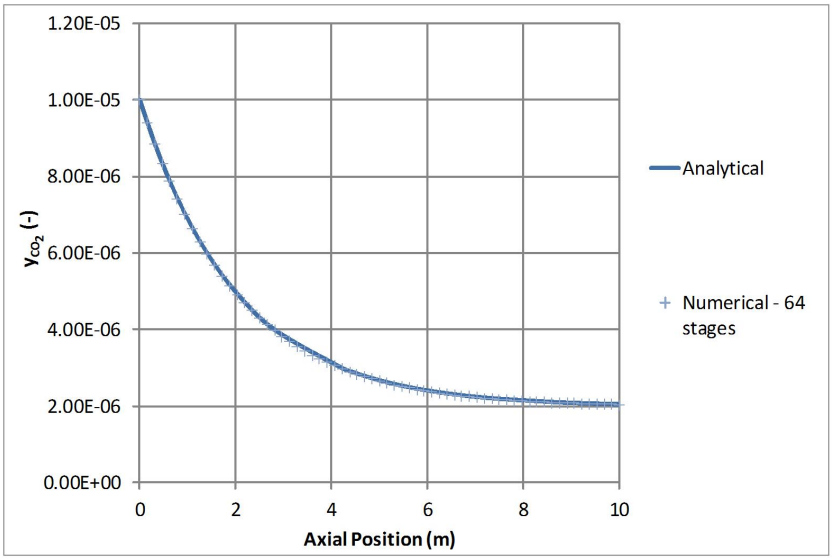

Figure 4.1: CO_2 mole fraction profiles in a co-current system for $y_i^0 = 1\times10^{-5}$

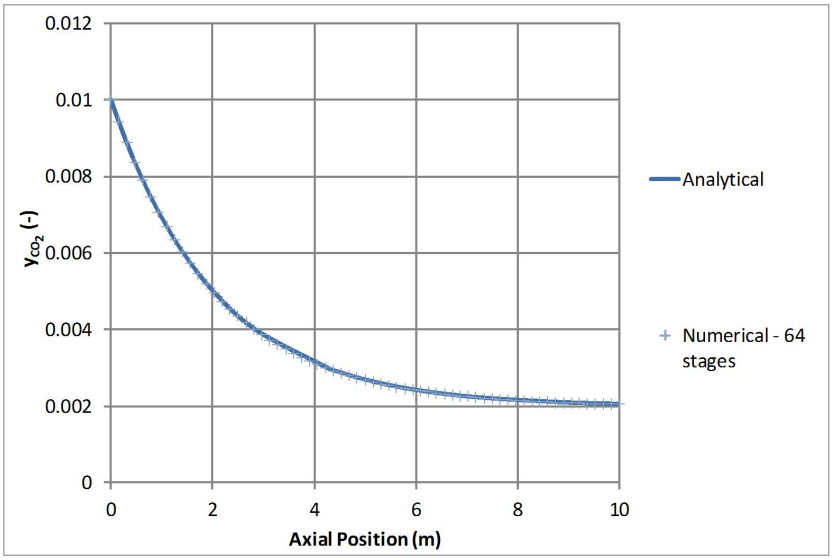

Figure 4.2: CO_2 mole fraction profiles in a co-current system for $y_i^0 = 0.01$

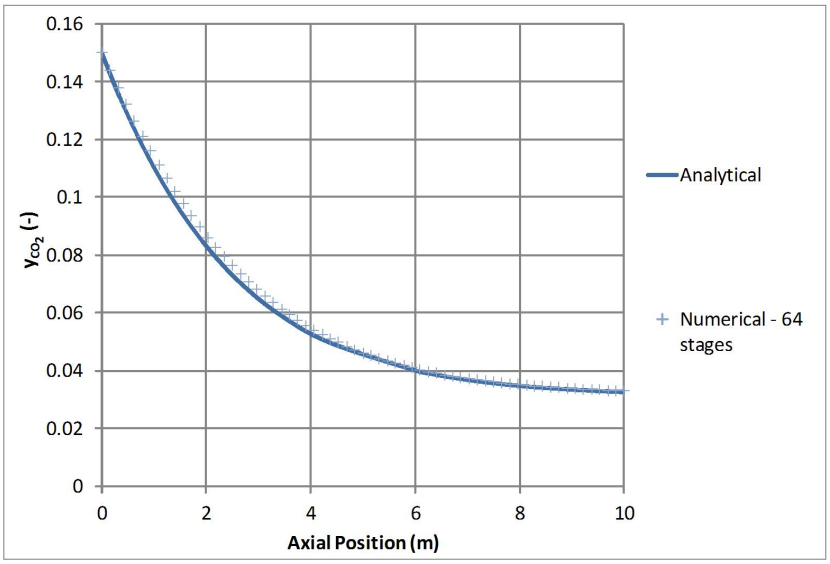

Figure 4.3: CO_2 mole fraction profiles in a co-current system for $y_i^0 = 0.15$

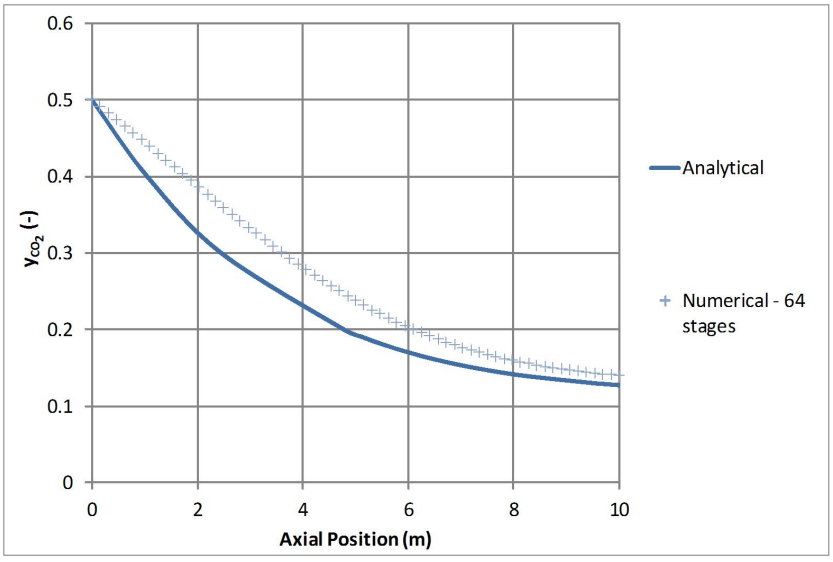

Figure 4.4: CO_2 mole fraction profiles in a co-current system for $y_i^0 = 0.5$

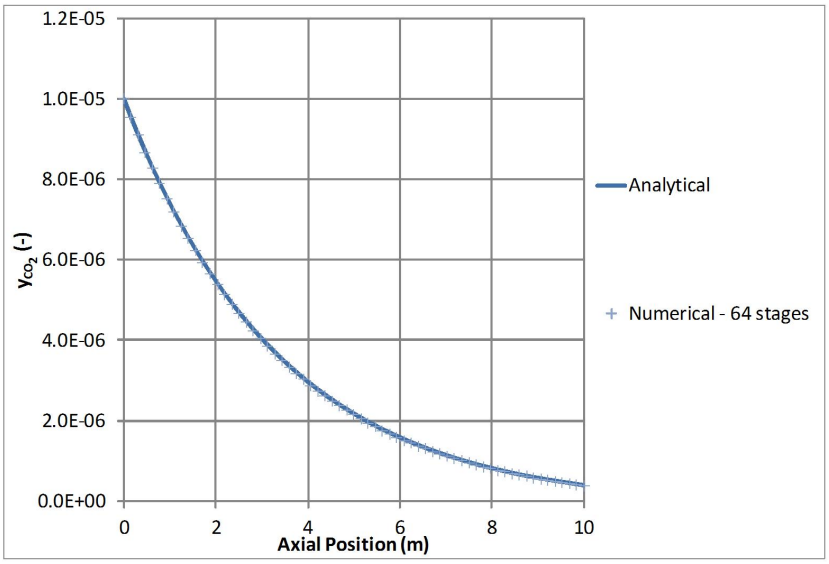

Figure 4.5: CO_2 mole fraction profiles in a counter-current system for $y_i^0 = 1\times10^{-5}$

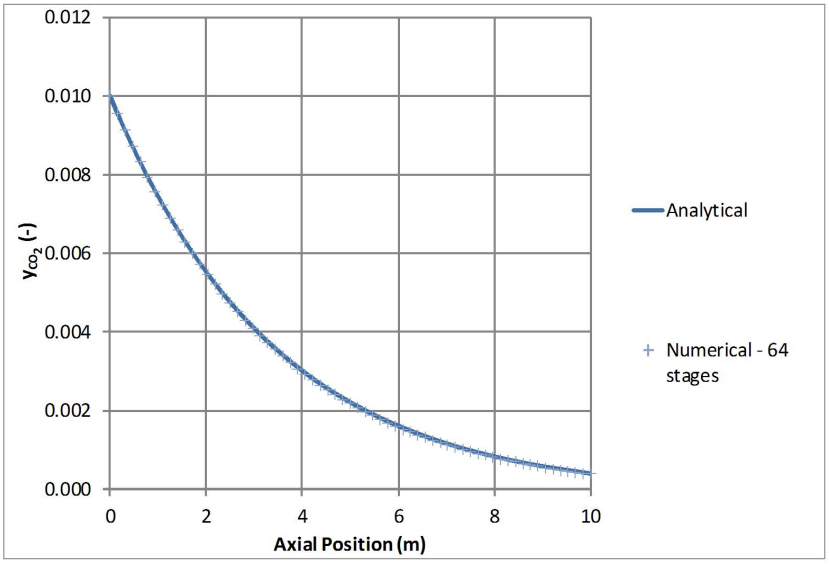

Figure 4.6: CO_2 mole fraction profiles in a counter-current system for $y_i^0 = 0.01$

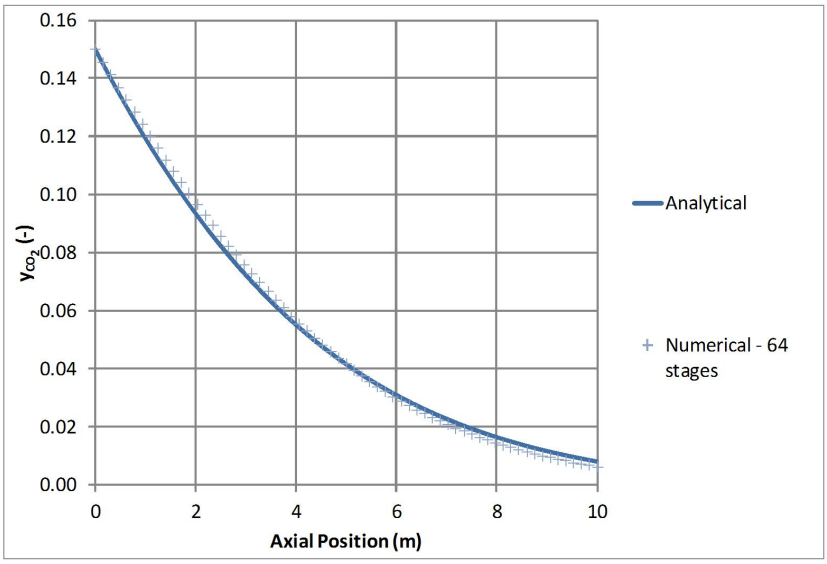

Figure 4.7: CO_2 mole fraction profiles in a counter-current system for $y_i^0 = 0.15$

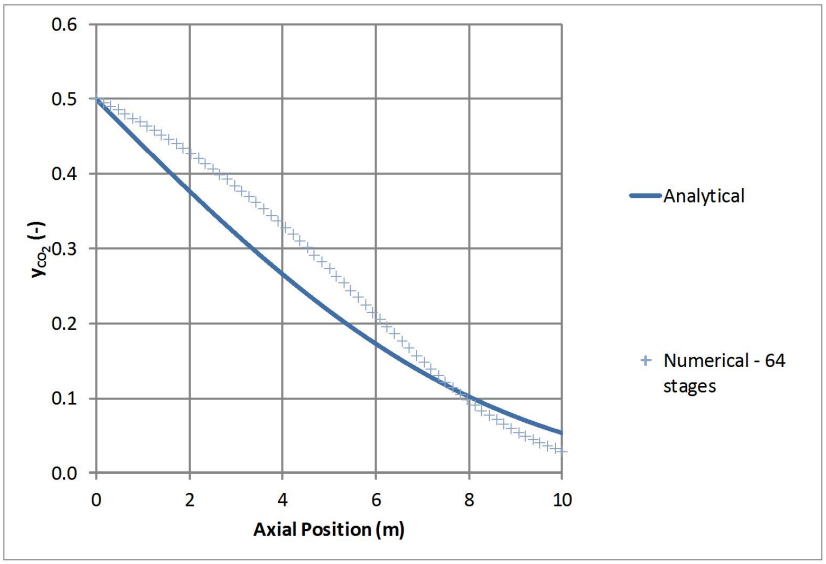

Figure 4.8: CO_2 mole fraction profiles in a counter-current system for $y_i^0 = 0.5$

Chapter 5

Fluidisation Limits for Moving Bed Systems

5.1 Introduction

It is important to determine what column diameter is required to achieve co-current, counter-current or fluidised bed operation for a set of adsorbent properties and gas flowrate used.

In this chapter, the requirements for the adsorbent particle size will be determined for the three modes of operation and for columns with a given diameter. It is assumed that the gas flows vertically upwards in the column. In addition, it has been assumed in this chapter that there is no interaction between adsorbent particles (i.e. they do not clump together).

5.2 Minimum Fluidisation Velocity

For a fluidised bed, the superficial gas velocity in an adsorption bed must be above the minimum fluidisation velocity. Starting from a fixed-bed of particles, incipient fluidisation occurs when the bed starts to expand as the velocity of the gas and the drag force on the particle increase to compensate for the weight of the bed (Kunii and Levenspiel (1991)). The distance between the particles increases and the particles are suspended in the gas. Mixing of the gas phase is promoted at the point of minimum fluidisation because the voidage in the bed increases and the gas travels more freely through the bed than in a fixed bed. However, to obtain a high level of mixing of solid particles, the velocity of the gas must be higher than the minimum fluidisation velocity so that the particles will be in motion. The pressure drop through the bed stabilises at the point of minimum fluidisation. The total frictional force on the particles equals

the effective weight of the bed because the particles are just suspended. The pressure drop at minimum fluidisation is then given previously by Equation 3.38 (Kunii and Levenspiel (1991)). The pressure drop in a fixed bed is commonly given by the Ergun equation:

$$-\frac{\Delta P}{Z} = 150\frac{\mu_g u_g}{D_p^2}\frac{(1-\varepsilon)^2}{\varepsilon^3} + 1.75\frac{1-\varepsilon}{\varepsilon^3}\frac{\rho_g u_g^2}{D_p} \tag{5.1}$$

ΔP: pressure drop (Pa)

Z: length of section of bed (m)

μ_g: gas velocity (Pa.s^{-1})

D_p: particle diameter (m)

ε: void fraction (-)

u_g: superficial gas velocity (m.s^{-1})

ρ_g: gas density (kg.m^{-3})

At the point of minimum fluidisation (mf), the pressure drop of the initially fixed bed equals the pressure drop of the newly fluidised bed. Equating Equations (3.38) and (5.1) for the minimum fluidisation point and rearranging for the minimum fluidisation velocity for a known particle diameter D_p gives Equation 5.2:

$$u_{mf} = \frac{-150\frac{\mu_g}{D_p^2}\frac{1-\varepsilon_{mf}}{\varepsilon_{mf}^3} + \sqrt{\left(150\frac{\mu_g}{D_p^2}\frac{1-\varepsilon_{mf}}{\varepsilon_{mf}^3}\right)^2 - 4\frac{1.75}{\varepsilon_{mf}^3}\frac{\rho_g}{D_p}(-g(\rho_p-\rho_g))}}{2\frac{1.75}{\varepsilon_{mf}^3}\frac{\rho_g}{D_p}} \tag{5.2}$$

u_{mf}: superficial gas velocity at minimum fluidisation (m.s^{-1})

ε_{mf}: void fraction at minimum fluidisation (-)

ρ_p: particle density (kg.m^{-3})

The minimum fluidisation velocity must be positive therefore the positive root of the quadratic found is used in Equation 5.2.

The void fraction of the bed at minimum fluidisation can be approximated by the following expression found by Broadhurst and Becker (1975):

$$\varepsilon_{mf} = 0.586\phi^{-0.72}\left(\frac{\mu_g^2}{\rho_g(\rho_p-\rho_g)gD_p^3}\right)^{0.029}\left(\frac{\rho_g}{\rho_p}\right)^{0.021} \tag{5.3}$$

ϕ: sphericity of the adsorbent (in this work, it is assumed to have a value of 1) (-)

The main requirement for operating a fluidised bed is that the superficial gas velocity must be greater than the minimum fluidisation velocity. For a fixed adsorbent diameter, D_p, and gas flowrate, $\dot{V}_g$, the maximum allowable column diameter to achieve the criteria of minimum fluidisation is given by:

$$D_{mf} = \sqrt{\frac{4\dot{V}_g}{\pi u_{mf}}} \tag{5.4}$$

D_{mf}: maximum diameter (m)

$\dot{V}_g$: gas volumetric flowrate ($m^3.s^{-1}$)

u_{mf}: minimum fluidisation velocity ($m.s^{-1}$)

Alternatively, if both the column diameter and the gas flowrate are fixed, the adsorbent particle diameter would need to be reduced such that the point of minimum fluidisation is found. Equations (3.38) and (5.2) would need to be solved for the diameter of the particle at the point of minimum fluidisation.

5.3 Terminal Settling Velocity

There is an upper limit on fluidised bed operation and that is when the gas flow is high enough to pick up and transport particles out of the top of the moving bed. This occurs when the gas flowrate approaches the particle terminal velocity.

The terminal velocity of an object is attained when the drag force and the buoyancy forces acting on an object are equal to the gravitational force of the object. Above the terminal settling gas velocity, the adsorbent will continue moving upwards in the gas. It is the maximum velocity that the particle can reach, relative to the gas, before it is entrained in the gas and transported outside of the fluidised bed system. If the particle is carried out, the drag force acting on the particle exceeds the gravitational force of the particle. After applying a force balance on a single spherical adsorbent particle, at equilibrium, the terminal velocity of a particle (u_t) is written as:

$$u_t = \sqrt{\frac{4D_p\left(\rho_p - \rho_g\right)g}{3c_D\rho_g}} \tag{5.5}$$

u_t: terminal settling velocity ($m.s^{-1}$)

c_D: drag coefficient (-)

The drag coefficient, c_D, is a function of the particle Reynolds number, Re_p:

$$Re_p = \frac{\rho_g u_t D_p}{\mu_g} \tag{5.6}$$

Different expressions of c_D are used depending on whether the flow is in the laminar, intermediate or turbulent flow regime. It is therefore commonly expressed as a function of Re_p. To avoid using an iterative procedure to calculate u_t, the method of Haider and Levenspiel (1989) uses an expression based on non-dimensional terminal velocity (u_t^*) and particle diameter (D_p^*) numbers as shown by Equations (5.8)-(5.9).

$$D_p^* = D_p \left(\frac{\rho_g \left(\rho_p - \rho_g\right) g}{\mu_g^2} \right)^{1/3} \tag{5.7}$$

$$u_t^* = \left(\frac{18}{\left(D_p^*\right)^2} + \frac{0.591}{\left(D_p^*\right)^{0.5}} \right)^{-1} \tag{5.8}$$

$$u_t = u_t^* \left(\frac{\rho_g^2}{\mu_g(\rho_p - \rho_g)g} \right)^{-1/3} \tag{5.9}$$

D_p^*: dimensionless particle diameter (-)

u_t^*: dimensionless terminal settling velocity (-)

The column diameter for which the particles would reach the terminal velocity is given by:

$$D_t = \sqrt{\frac{4\dot{V}_g}{\pi u_t \varepsilon}} \tag{5.10}$$

D_t: column diameter at terminal velocity (m)

For column diameters below D_t, the adsorbent would be entrained by the gas.

5.4 Fluidisation Limits for Moving bed Adsorbers

The superficial gas velocity in the column needs to be compared to the minimum fluidisation and terminal settling velocities in order to find out in which

mode the bed operates. The superficial gas velocity and real solid velocity are dependant on the volumetric flowrates of the gas and solid respectively:

$$u_g = \frac{\dot{V}_g}{(\pi/4)D_C^2} \tag{5.11}$$

$$u_s = \frac{\dot{m}_{in}/\rho_p}{\varepsilon_a(\pi/4)D_C^2} \tag{5.12}$$

u_s: real solid velocity (m.s^{-1})

D_C: column diameter (m)

$\dot{m}_{in}$: mass flowrate of adsorbent (kg.s^{-1})

ε_a: volume fraction of adsorbent in the bed (-)

Table 5.1 shows the individual constraints on each type of moving bed adsorption system. The fluidised bed must operate above the points of minimum fluidisation but below entrainment. The co-current bed requires high velocities so that the adsorbent is entrained by the flow of the gas. Finally, the counter-current system requires that the gas superficial velocity is low enough to ensure that the solid flows downwards without being entrained.

Table 5.1: Constraints on the superficial gas velocity for different moving bed systems

	Constraint
Counter-current	$u_g<u_t$
Co-current	$u_g>u_t$
Fluidised bed	$u_{mf}<u_g<u_t$

In Table 5.1, there is an overlap in the velocity conditions of the fluidised bed and the counter-current bed. Although both systems need to operate below the terminal settling velocity, the void fraction is different in these systems. Although adsorbent is withdrawn in a fluidised bed, there is an accumulation or back-up of adsorbent. However, in a counter-current bed, adsorbent continuously drops and is withdrawn without being accumulated. Therefore, the adsorbent volume fraction, ε_a, would be higher in the fluidised bed than in a counter-current or co-current bed. Kunii and Levenspiel (1991) have quoted values of ε_a in entrained fluidised beds which operate similarly to co-current beds. Three regions in an entrained fluidised bed as given by Kunii and Levenspiel (1991) are:

- At the bottom of the bed, adsorbent accumulates as it enters the bed. ε_a is the highest in this region. A range of 0.2-0.4 was given for ε_a.
- There is an intermediate zone in which ε_a is roughly constant, $\varepsilon_a = 0.2$.
- At the top of the bed, ε_a is significantly lower in the region of 0.02-0.05.

Values of ε_a in a counter-current system with packing were not found in the literature. Instead, Equation 3.49 for liquid hold-up in structured packing is assumed to be valid for solid particles too. Resulting from this assumption, values were found to be typically in the same region as for the top of the entrained bed (ε_a in the 0.02-0.05 range). Values of specific cases for the adsorbents considered in this work are shown in Table 5.2.

5.5 Limits on the Solid Velocity in a Counter-current Bed

The solid velocity in a counter-current bed which does not contain structured packing, u_s, must be less than the velocity at which the solid particle would settle, u_{sett}, which is given by:

$$u_{sett} = u_t - \frac{u_g}{\varepsilon} \tag{5.13}$$

u_{sett}: settling velocity of the adsorbent ($\mathrm{m.s^{-1}}$)

u_t: terminal settling velocity of the adsorbent ($\mathrm{m.s^{-1}}$)

ε: void fraction of the bed (-)

If the solid velocity, u_s, is higher than the settling velocity, u_{sett}, structured packing is needed to slow down the drop of the particles. If $u_s \leq u_{sett}$, no structured packing is required, but it can be used to slow down the adsorbent so that the adsorbent volume fraction in the column, ε_a, is increased which may be beneficial if kinetic rates of adsorption are slow.

5.6 Fluidisation Limits for the Adsorber

The vessel size used for the adsorber in the fluidisation calculations is the same as the absorber in the amine process developed by Fisher et al. (2005). A similar flue gas flowrate and composition as Fisher et al. (2005) has also been

used. Tables 5.2 and 5.3 show the gas and solid properties used in the adsorber with different adsorbents. Averaged values of the gas density and viscosity were taken from National Institute of Standards and Technology (2014). The adsorbent particle densities used were taken from literature. The density of the supported amine adsorbent was given by Krutka and Sjostrom (2011), the activated carbon density was given by SRI International (2010) and that of zeolite 13X, by Cavenati et al. (2004).

Table 5.2: Column and gas parameters and gas velocity in the adsorber for different adsorbents

	Unit	Supported amine adsorbent	Activated carbon	Zeolite 13X
Column				
D_C	m	10	10	10
L	m	15	15	15
Gas		Flue gas	Flue gas	Flue gas
T_g^{in}	°C	40	40	40
P_{in}	Pa	101325	101325	101325
ρ_g	$kg.m^{-3}$	1.15	1.15	1.15
μ_g	$kg.m^{-1}.s^{-1}$	1.8×10^{-5}	1.8×10^{-5}	1.8×10^{-5}
$\dot{M}_{in}$	$mol.s^{-1}$	5607.5	5607.5	5607.5
$\dot{V}_g$	$m^3.s^{-1}$	144.1	144.1	144.1
u_g	$\mathbf{m.s^{-1}}$	**1.83**	**1.83**	**1.83**
Contact time	s	8.2	8.2	8.2

Table 5.3: Adsorbent parameters used for different adsorbents to match the terminal velocity

	Unit	Supported amine adsorbent	Activated carbon	Zeolite 13X
Solid				
ρ_p	$kg.m^{-3}$	646	1100	1130
D_p	mm	0.52	0.37	0.36
ε_{mf}	-	0.406	0.407	0.404
u_{mf}	$\mathbf{m.s^{-1}}$	**0.07**	**0.06**	**0.06**
u_t	$\mathbf{m.s^{-1}}$	**1.86**	**1.86**	**1.84**

Figures 5.1, 5.2 and 5.3 show the bed diameters needed as a function of particle sizes for supported amine adsorbent, activated carbon and zeolite 13X respectively. From these graphs, it is shown that to operate as a counter-current

bed or a fluidised bed, the particle diameter of the supported amine adsorbent should be greater than 0.52 mm, greater than 0.36 mm for activated carbon and greater than 0.37 mm for zeolite 13X. For a given adsorbent, a particle diameter smaller than the one specified would result in a co-current bed. In the literature, Krutka and Sjostrom (2011) and SRI International (2010) used adsorbent diameters of 0.1 mm and 0.2 mm respectively. For the gas flowrate used inside the column of a diameter of 10 m, the gas velocity is higher than the terminal velocity and the adsorbent would be entrained. Therefore, for counter-current operation, the adsorbent diameters that were chosen by Krutka and Sjostrom (2011) and SRI International (2010) are too small and must be increased for the gas flowrate and column size given by Fisher et al. (2005). In the pilot plant tests carried out by Krutka and Sjostrom (2011), the adsorber used was a co-current bed with a smaller adsorbent particle size.

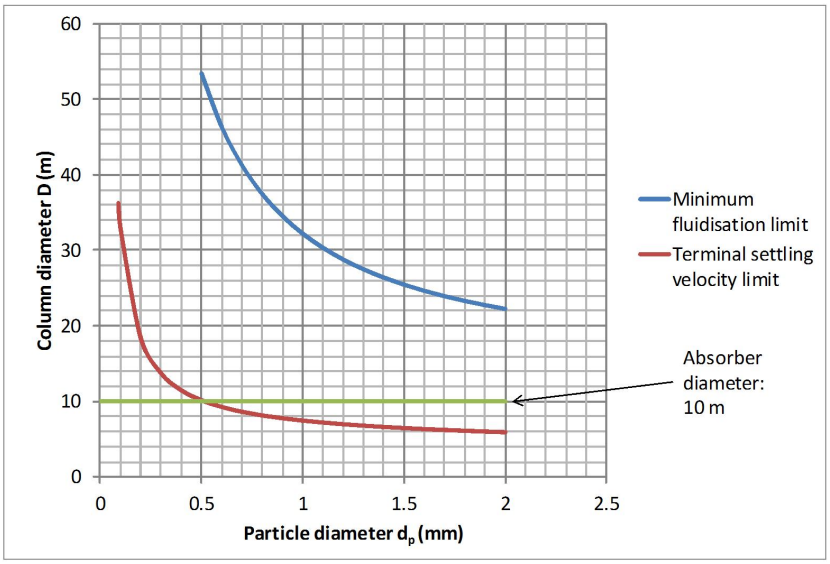

Figure 5.1: Diameters of the adsorber at minimum fluidisation and for the terminal settling velocity as a function of particle size of supported amine adsorbent ($\rho_p = 646$ kg.m^{-3})

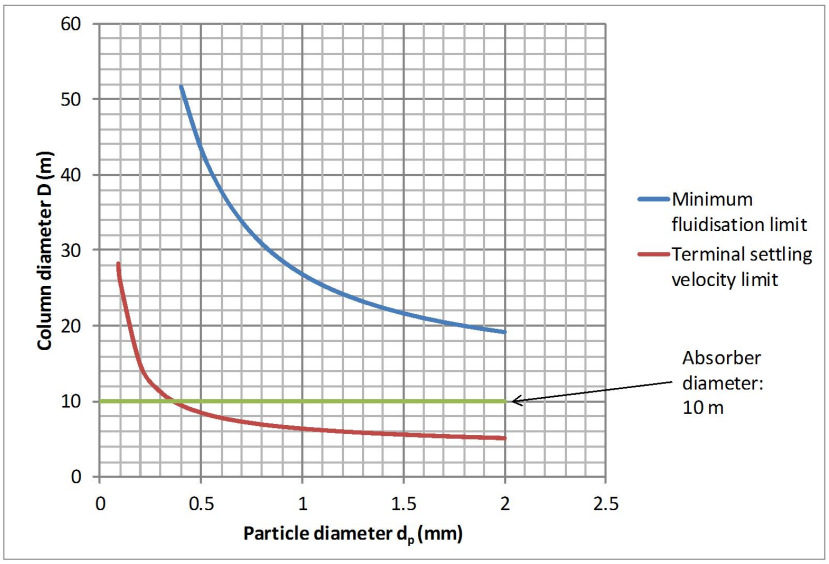

Figure 5.2: Diameters of the adsorber at minimum fluidisation and for the terminal settling velocity as a function of particle size of activated carbon (ρ_p = 1100 kg.m^{-3})

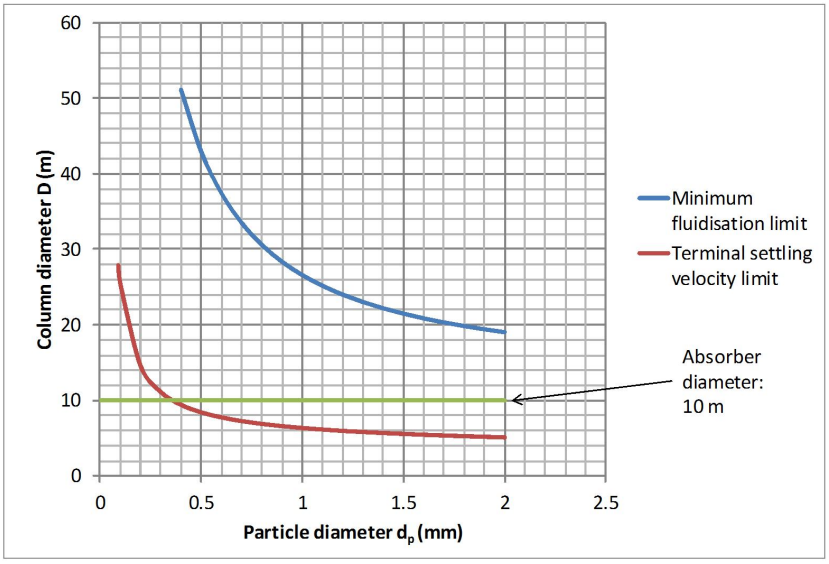

Figure 5.3: Diameters of the adsorber at minimum fluidisation and for the terminal settling velocity as a function of particle size of zeolite 13X (ρ_p = 1130 kg.m^{-3})

Alternatively, for a counter-current bed or a fluidised bed, the column size would need to be increased for smaller particle sizes but this isn't really an option because column sizes greater than in amine absorption processes are unwanted due to higher capital costs. For example, Delgado et al. (2011) carried out a study for CO_2 capture in a VSA process. They used a gas velocity of 0.1 m.s^{-1} which would lead to a column with an extremely large diameter.

If a smaller column diameter is required, Figures 5.1, 5.2 and 5.3 also show

the requirements of the particle size up to 1 mm. For example, if a 8 m bed diameter is specified, the supported amine adsorbent would need to be 0.84 mm in size, the activated carbon would need to be 0.57 mm in size and zeolite 13X would need to be 0.56 mm in size.

Although increasing the adsorbent particle size would allow counter-current or fluidised bed operation, the mass transfer coefficient of components, k_i, is negatively affected by an increase in particle diameter as shown by Equation 2.13. The mass transfer constant drops if the adsorbent size increases because of higher mass transfer resistance. Due to the current uncertainty in the mass transfer constant of components, the extent of the impact of larger particle diameters is not yet known. More experimental data on adsorption rates are required to determine if the particle size limitations are problematic or not. In this work, a sensitivity analysis around the mass transfer rate is performed instead.

Yang and Hoffman (2009) also considered fluidisation limits in a fluidised bed adsorber from flue gas exiting a 500 MW power plant. The flue gas flowrate was similar to the one used in this work and by Fisher et al. (2005) in the amine absorption process. An amine enriched adsorbent quoted to have a relatively high CO_2 loading (6 mol.kg^{-1}) was used. It resulted in a lower mass flowrate of adsorbent than for the supported amine adsorbent considered in this work. In the study by Yang and Hoffman (2009), a total cross-sectional area of 83.7 m^2 was used, as compared with a cross-sectional area of 78.5 m^2 by Fisher et al. (2005). These are very close, showing that equivalently sized vessels can be used for both approaches. Results provided by Yang and Hoffman (2009) are summarised in Table 5.2. For closer comparison between Tables 5.2, 5.3 and 5.4, the basis of the bed diameter has been changed to a circular diameter by keeping the cross-sectional area the same. The superficial gas velocity is between the minimum fluidisation velocity and the terminal settling velocity which confirms that their moving bed operates as a fluidised bed.

Table 5.4: Parameters and velocities of an adsorber (Yang and Hoffman (2009))

	Unit	Supported amine adsorbent
Column		
D_C	m	10.325
L	m	9.15
Gas		Flue gas
T_g^{in}	°C	65
P_{in}	Pa	122000
ρ_g	kg.m^{-3}	1.28
μ_g	kg.m^{-1}.s^{-1}	1.8×10^{-5}
$\dot{M}_{in}$	mol.s^{-1}	4919
$\dot{V}_g$	m^3.s^{-1}	113.3
u_g	**m.s^{-1}**	**1.35**
Contact time	s	14.29
Solid		
ρ_p	kg.m^{-3}	880
D_p	mm	0.6
$\dot{m}_{in}$	kg.s^{-1}	81.7
$\dot{V}_s$	m^3.s^{-1}	0.093
ε_{mf}	-	0.40
u_{mf}	**m.s^{-1}**	**0.12**
u_t	**m.s^{-1}**	**2.6**

5.7 Fluidisation Limits for a Regenerator

As for the adsorber, there are similar rules and constraints around sizing the regenerator diameter. However, this depends on the regeneration gas flowrate, which is yet to be determined. If no regeneration gas is used or if the gas flowrate is very low, the regenerator would operate as a counter-current bed.

5.8 Conclusions

Properties such as the gas and particle densities, gas viscosity and particle diameter are key to allowing moving bed systems to operate as either co-current, counter-current or fluidised beds. A high gas velocity coupled with a low adsorbent density and particle size are suitable conditions for co-current adsorption systems. On the other hand, the opposite is more favourable for counter-current and fluidised beds. Fluidised beds differ from counter-current beds due to significantly higher void fractions in counter-current beds.

Calculations of minimum fluidisation and terminal settling velocities were

carried out to find out how the adsorbent would flow in a moving bed. For a given adsorbent, vessel size and gas conditions, the adsorbent particle diameter would need to be modified to allow the adsorbent to descend or be entrained by the gas. Finally, it must be pointed out that the analysis in this chapter was carried out for a single particle, assuming that it does not interact with other particles or equipment. A more accurate analysis which takes into account the influence of these factors could be carried out in future work.

Chapter 6

Analysis of an Adsorber

6.1 Introduction

This chapter presents the results obtained from simulations of standalone counter-current, co-current and fluidised bed adsorbers using three types of adsorbents: supported amine adsorbent, activated carbon and zeolite 13X. The properties of the three adsorbents used have been provided in the literature outlined previously in section 2.7 and the properties of zeolite 13X are shown in this chapter. The mathematical model and isotherms for CO_2, water and N_2 on the adsorbents have been provided already in section 3.7.

Various operating parameters have been investigated and comparisons will be made against a counter-current base case where supported amine adsorbent is used to capture at least 90% of CO_2 in the flue gas. The properties of temperature, mole fractions and loadings of components inside the column will be shown for different operating conditions.

The adsorber is treated as a standalone unit so that its operation can be investigated on its own without having to consider how the regenerator works. This interaction will be covered later in Chapter 8. Hence, properties such as incoming adsorbent loading and temperature can be varied arbitrarily. The impact of the following conditions and parameters are deemed to be the most influential on CO_2 capture performance:

- Type of the moving bed adsorber
- Type of adsorbent
- Mass flowrate of adsorbent
- Mass transfer constant
- Mole fraction of CO_2 in the flue gas

- Mole fraction of water in the flue gas
- Concentration of CO_2 in the adsorbent at the inlet
- Concentration of water in the adsorbent at the inlet
- Molar flowrate of flue gas
- Inlet flue gas temperature
- Inlet adsorbent temperature
- Heat removed from the adsorber

A sensitivity analysis on a single adsorber is carried out in this chapter for the parameters and conditions cited above. In each case the values at the base case are fixed and the investigated parameter is varied within a certain range around the base case value.

6.2 Adsorber Base Case

6.2.1 Base Case Conditions

A base case chosen for the analysis consists of a single adsorber using counter-current flow and the supported amine adsorbent. For the base case, 92% of CO_2 is removed from the flue gas. A diagram of the single adsorber is given in Figure 6.1 and values of the operating and simulation parameters that were used are given in Table 6.1.

Fisher et al. (2005) have provided details on a post-combustion CO_2 capture system using an amine absorber from a 500 MW coal-fired power plant. For the base case, adsorber operating conditions and vessel size have been replicated for comparison. The only significant changes that were made for the system were to use an adsorbent instead of a liquid amine solution and the feed flue gas temperature was reduced to 40°C instead of 55°C. It was assumed that there was no heat lost or gained through external heat transfer for the base case. Flue gas temperatures of or lower than 40°C are often quoted and used (Krutka et al. (2013)). In addition, a lower gas temperature is more favourable for adsorption. The flue gas is saturated with water vapour as it enters the adsorber because it is assumed that SO_2 is removed in a wet flue gas desulfurisation scrubber before CO_2 capture. Although O_2 is also considered to be present in the flue gas by Fisher et al. (2005), only CO_2, N_2 and water are considered here for the adsorber as O_2 is present at a lower concentration (roughly 5 mol%).

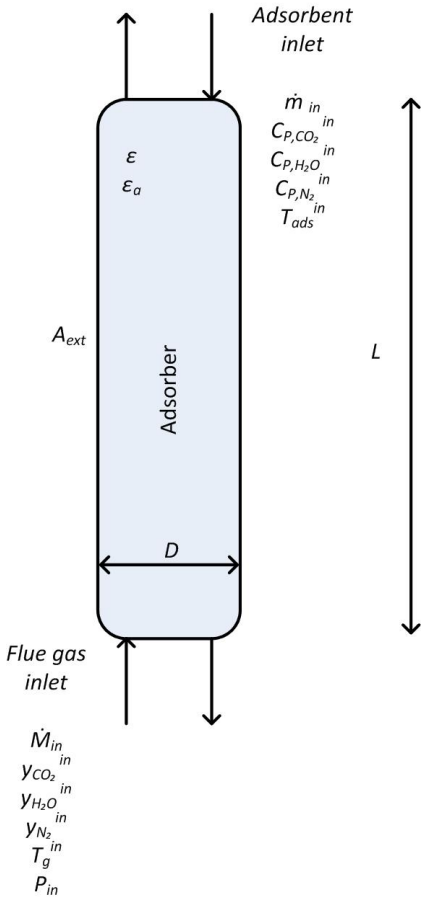

Figure 6.1: Single Adsorber (Counter-current)

The pores of the incoming adsorbent were assumed to be saturated with water vapour (at 40°C, the water vapour pressure is 7310 Pa which is equivalent to a concentration of 2.84 mol.m^{-3} for which the water loading at the inlet is 10.17 mol.kg^{-1}). It was assumed that the adsorbent does not contain any CO_2 prior to entering the adsorber. The remaining pore space was assumed to be occupied by N_2 so that the total internal pressure was equal to atmospheric pressure.

A total flue gas flowrate of 655.7 kg.s^{-1} (576 m^3.s^{-1} at 40°C and 1 atm) was split up into four parallel absorbers by Fisher et al. (2005). The volume fraction occupied by the adsorbent in the counter-current adsorber, ε_a, was calculated by the method developed by Stichlmair et al. (1989) as described in section 3.6.3 and it has a value of 0.046. The column contains structured packing occupying a volume fraction of 0.01.

The adsorption study was therefore based around an adsorber with the same height and diameter as a typical amine adsorber. The mass flowrate of adsorbent was chosen to give at least 90% CO_2 removal from the flue gas.

The choice of the LDF mass transfer constant of CO_2 was justified earlier

Table 6.1: Parameters used for the base case adsorber

Parameter	Unit	Value
L	m	15
D_C	m	10
ε_a	-	0.046
ε_p	-	0.4
ε_{pk}	-	0.01
P_{in}	Pa	101325
T_g^{in}	°C	40
M_{in}	mol.s^{-1}	5607.5
$\dot{m}_{in}$	kg.s^{-1}	375
$y_{CO_2}^{in}$	-	0.1233
$y_{H_2O}^{in}$	-	0.07
$y_{N_2}^{in}$	-	0.8067
k_{CO_2}	s^{-1}	10
k_{H_2O}	s^{-1}	10
k_{N_2}	s^{-1}	10
A_{ext}	m^2	0
C_{p,CO_2}^{in}	mol.m^{-3}	0
C_{p,H_2O}^{in}	mol.m^{-3}	2.84
C_{p,N_2}^{in}	mol.m^{-3}	36.10
$q_{CO_2}^{in}$	mol.kg^{-1}	0
$q_{H_2O}^{in}$	mol.kg^{-1}	10.17
$q_{N_2}^{in}$	mol.kg^{-1}	0
T_{ads}^{in}	°C	40
Number of discretisations	-	100
α	-	0.75

in section 3.9. The same value of this LDF constant was assumed for water and N_2 due to lack of exact values that have not been provided by Krutka and Sjostrom (2011) for the supported amine adsorbent. These values would need to be measured experimentally in future work.

Finally, the solver choices of the number of discretisations and weight factor, α, were chosen for the base case to give a high enough accuracy and for faster convergence. If a greater number of discretisations were chosen, a solution with lower error could be obtained at the expense of longer computational times. Oscillatory profiles were found if a higher weight factor was used.

The profiles are given as a function of the distance, x, in the column of length, L, from the flue gas inlet.

6.2.2 Profiles for the Adsorber Base Case

Figure 6.2 shows the profiles of the mole fraction of CO_2, water and N_2 along the counter-current adsorber. The mole fraction of CO_2 in the bulk gas drops towards the gas product end as CO_2 is removed from the flue gas whereas that of water and N_2 generally increases. The mole fraction of water in the bulk gas increases towards the gas product end of the adsorber because the temperature in this region is highest (cf. Figure 6.4) and therefore the amount of water that the flue gas can hold increases. In conjunction to a drop in the mole fraction of water at the gas outlet, the mole fraction of N_2 which remained constant in the majority of the column, now increases slightly at the gas outlet because the levels of CO_2 and water decrease. It was assumed that N_2 is not loaded on the adsorbent as shown in Figure 6.3 and any amount of N_2 removed from the bulk flue gas is contained within the pores of the adsorbent.

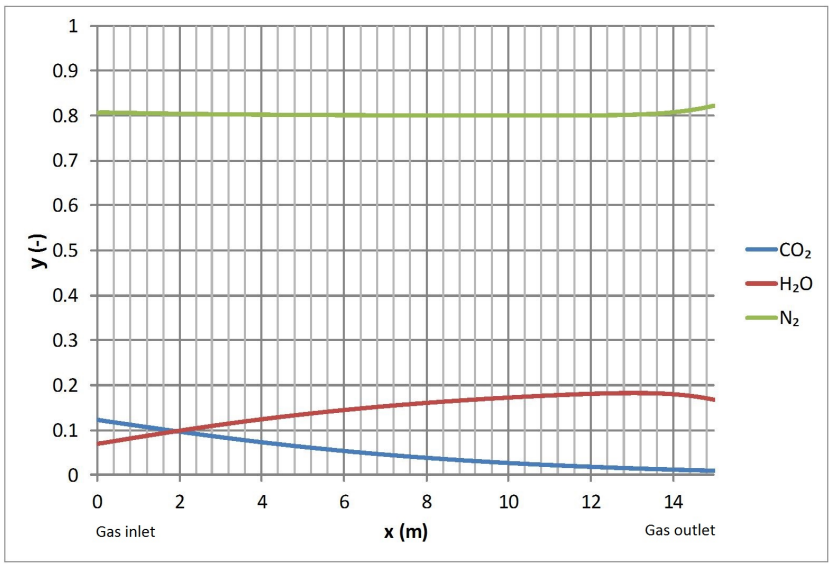

Figure 6.2: Mole fraction profiles for a counter-current adsorber with amine supported adsorbent and pores saturated with water

The profiles of the loadings of all components are shown in Figure 6.3 where the adsorbent inlet is at $x = 15$ m. The CO_2 loading increases down the column whereas the water loading initially increases as cooler adsorbent enters but it then drops as the temperature of the adsorbent rises down the column (cf. Figure 6.4).

There is a net loss of water from the adsorbent down the column that ends up in the flue gas product. However, at the adsorbent inlet, the adsorbent picks up water as it travels downwards and the heat released by the adsorption of CO_2 is greater than the heat consumed in desorbing water. CO_2 and water are adsorbed at the gas outlet as shown in Figure 6.3 which explains why the

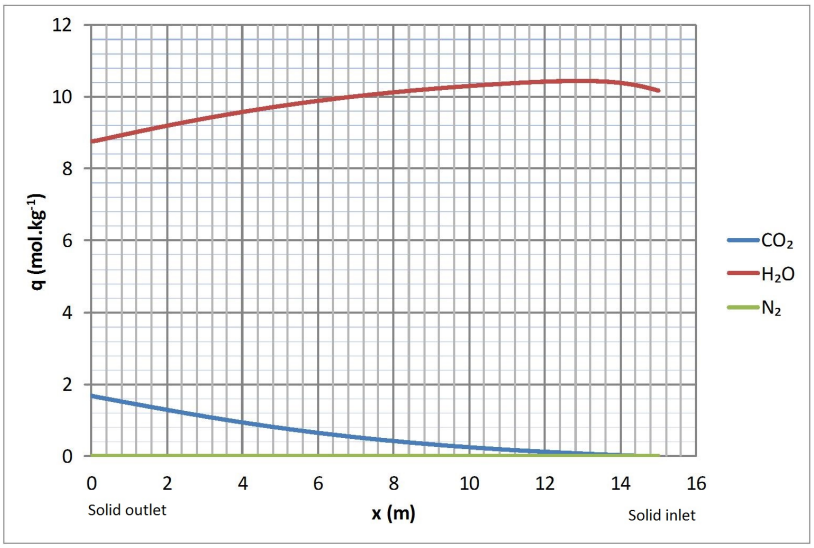

Figure 6.3: Loading profiles for a counter-current adsorber with amine supported adsorbent and pores saturated with water

temperature profiles of the adsorbent increases as it enters the column as shown in Figure 6.4. The adsorbent temperature drops as more and more water is desorbed from the adsorbent. As the adsorbent leaves the adsorber, it is cooled by the gas at the inlet.

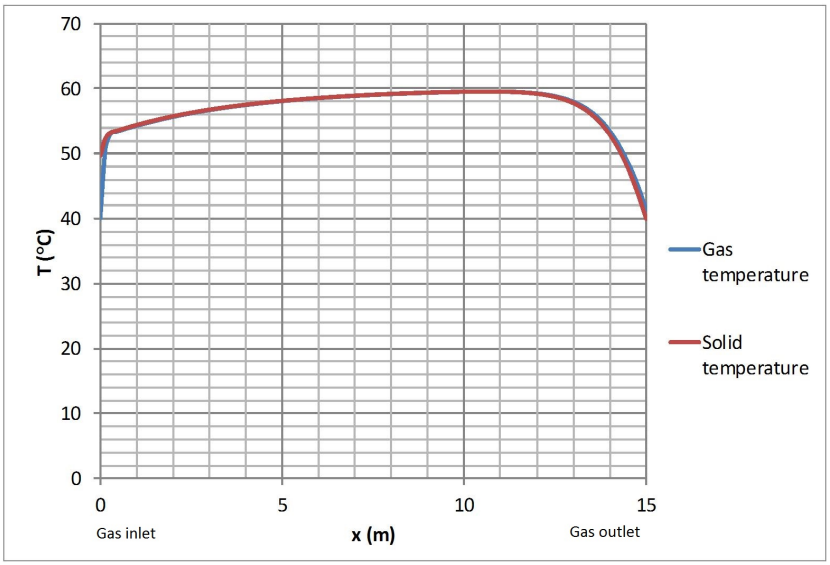

Figure 6.4: Temperature profiles for a counter-current adsorber with amine supported adsorbent and pores saturated with water

It is expected that the amount of material removed from the bulk gas is taken up by the adsorbent therefore the variation of the gas flowrate of CO_2 and water echo the variation in adsorbate flowrate of CO_2 and water as shown in Figure 6.5.

The pressure profile in the counter-current adsorber containing structured

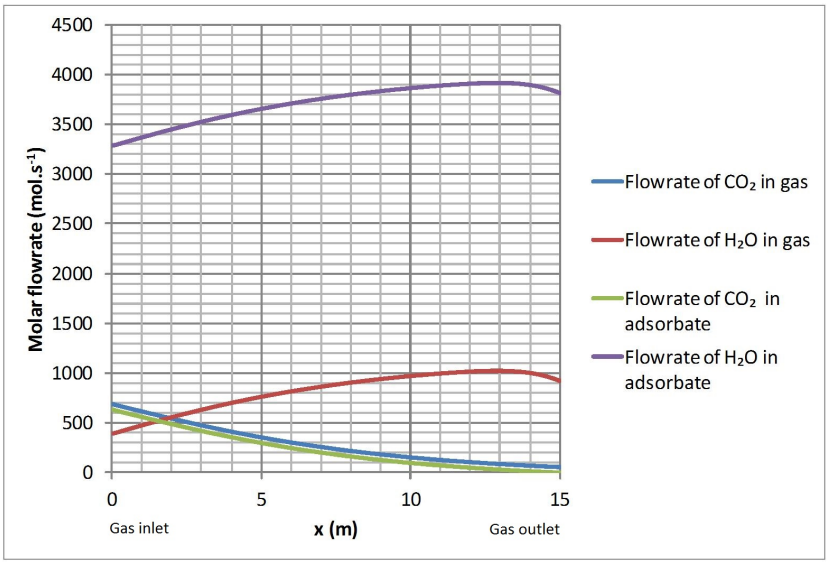

Figure 6.5: Profiles of molar flowrate and adsorbate flowrate of components in the flue gas for a counter-current adsorber with amine supported adsorbent and pores saturated with water

packing is shown in Figure 6.6. There is a linear decrease in the pressure as given by Equation 3.50 used in the model for pressure drop. Overall, there is a relatively low pressure drop of 5% in the counter-current adsorber.

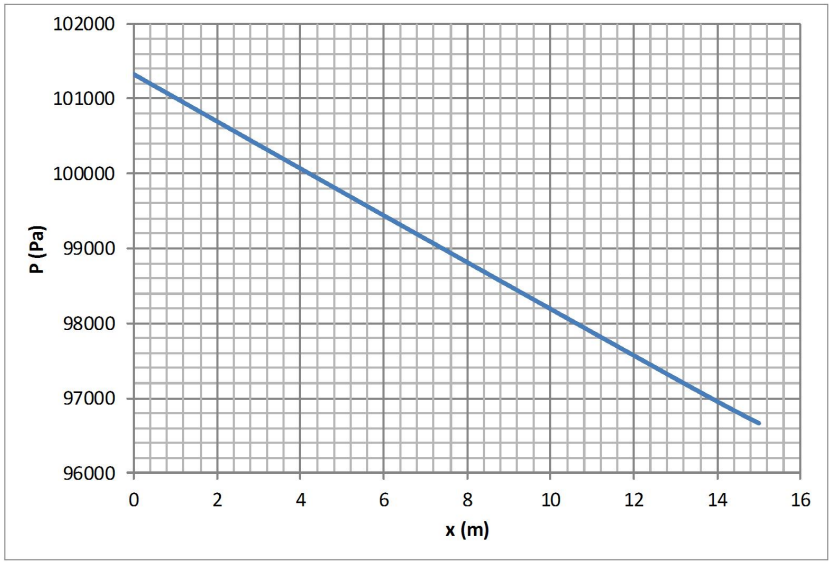

Figure 6.6: Pressure profile for a counter-current adsorber with amine supported adsorbent and pores saturated with water

Unfortunately, as there is a very small amount of literature available on moving bed CO_2 adsorption, the profiles inside the adsorber that have been shown in this section, could not be compared to other work in the literature. However, the observed trends can be explained in relation to the variations of

concentrations of components and temperature inside the column. Therefore, the profiles found are justified.

6.3 Impact of Isotherm Model Errors on the Adsorber

In Figure 3.10, it was seen that the isotherm model (Equations 3.51-3.53) had a relatively poor fit with the corresponding data at the limits of the temperature range at which measurements were taken. For example, at 110°C and 120°C, the coefficient of determination, R^2, was lower than for other temperatures. Similarly, the water isotherm model had an even lower accuracy for the temperatures considered in particular at higher temperatures. The isotherm models therefore imply lower confidence on some of the results in this chapter. However, the R^2 values in all cases are greater than 0.9, so the results are therefore not altogether unreasonable. From Figure 3.10, at 40°C, the equilibrium loading is overestimated by the model. Therefore, the actual CO_2 loading obtained in the column would be lower than the modelled CO_2 loading. The CO_2 profile curve would be slightly higher than shown in Figure 6.2 and the CO_2 loading profile would be below the one shown in Figure 6.3. The temperature profile would shift downwards too because the temperature raise in the bed would be lower as a lower rate of exothermic heat would be generated.

In this case, the temperature in the adsorber does not exceed 110°C. The confidence in the results for CO_2 adsorption is better than for the regenerator which operates at a higher temperature.

6.4 Effect of the Type of Adsorber

As a comparison to the counter-current column, the model was also run in co-current and fluidised bed modes with the same parameters except that in the fluidised bed, the solid adsorbent fraction $\varepsilon_a = 0.4$ is used because more adsorbent is held up inside it. The same volume fraction used for the counter-current bed was assumed for the co-current bed.

Profiles of the CO_2 mole fraction in the counter-current, co-current and fluidised bed adsorbers are shown in Figure 6.7. The CO_2 mole fraction reached at the gas outlet of the counter-current system is lower than for the co-current and fluidised beds because the amount of CO_2 loaded onto the adsorbent (at $x = 0$) is greater than in a co-current or a fluidised bed system (at $x = L$) as shown in Figure 6.8.

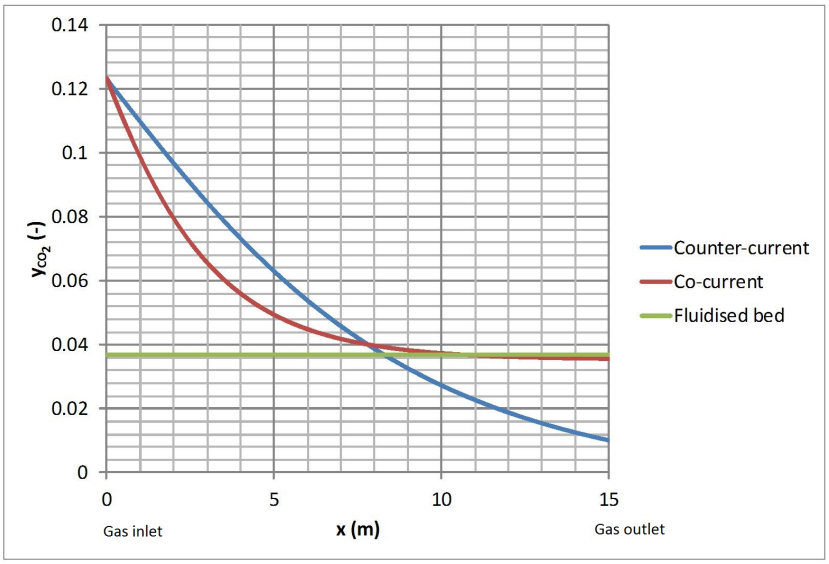

Figure 6.7: Mole fraction profiles of CO_2 for counter-current, co-current and fluidised bed adsorbers with amine supported adsorbent and pores saturated with water

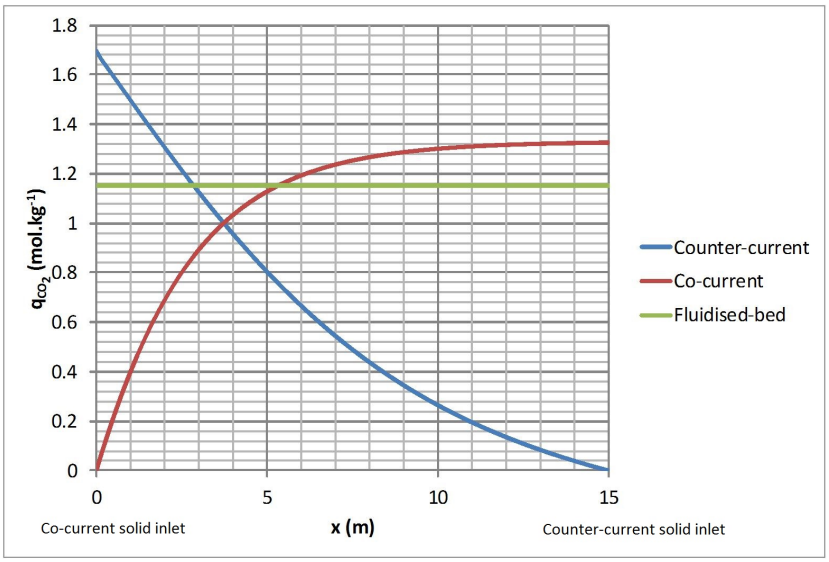

Figure 6.8: CO_2 loading profiles for counter-current, co-current and fluidised bed adsorbers with amine supported adsorbent and pores saturated with water

Comparing the counter-current mode to the co-current mode, overall, there is a greater difference between adsorbent pore and bulk gas concentrations of CO_2 throughout the counter-current bed (cf. Figures 6.9 and 6.10). In the co-current case, the mole fraction of CO_2 reaches a plateau as the same CO_2 concentration is reached inside and outside the adsorbent pores (cf. Figure 6.10). For a counter-current adsorber, the loading in a counter-current bed continues to increase as the adsorbent reaches the bottom of the column (cf. Figure 6.11). The loading in a co-current bed is limited by the equilibrium

loading as shown in Figure 6.12 for which a portion of the co-current bed near the gas outlet is not used for separation where the concentration in the bulk gas approaches the pore concentration (cf. Figure 6.10).

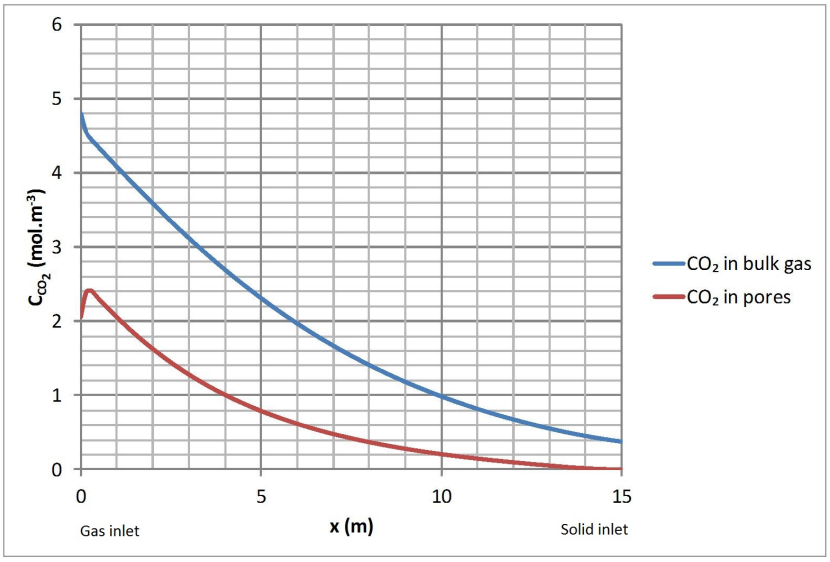

Figure 6.9: CO_2 concentration profiles in a counter-current adsorber with amine supported adsorbent and pores saturated with water

In Figure 6.10, the CO_2 bulk gas concentration drops from the inlet to the outlet as it is adsorbed. On the other hand, the CO_2 pore concentration increases for the adsorbent initially not containing CO_2 as CO_2 moves from the bulk gas into the adsorbent pores.

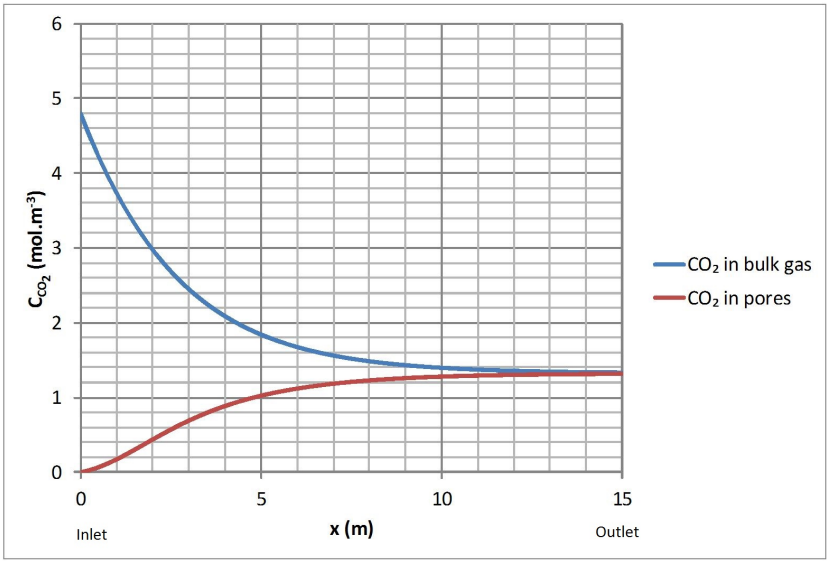

Figure 6.10: CO_2 concentration profiles in a co-current adsorber with amine supported adsorbent and pores saturated with water

Figure 6.11 shows that there is a drop in the equilibrium CO_2 loading as

the adsorbent enters at the top of the counter-current column. This effect is due to the temperature of the column being at its highest as shown in Figure 6.13. However, as the mole fraction is higher nearer to the gas inlet (bottom of the column), the CO_2 equilibrium loading increases.

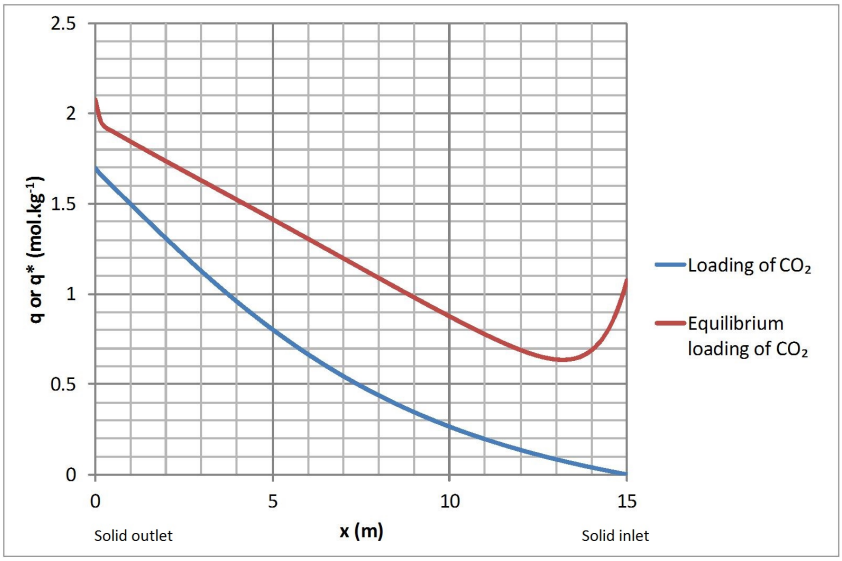

Figure 6.11: CO_2 loading profiles in a counter-current adsorber with amine supported adsorbent and pores saturated with water

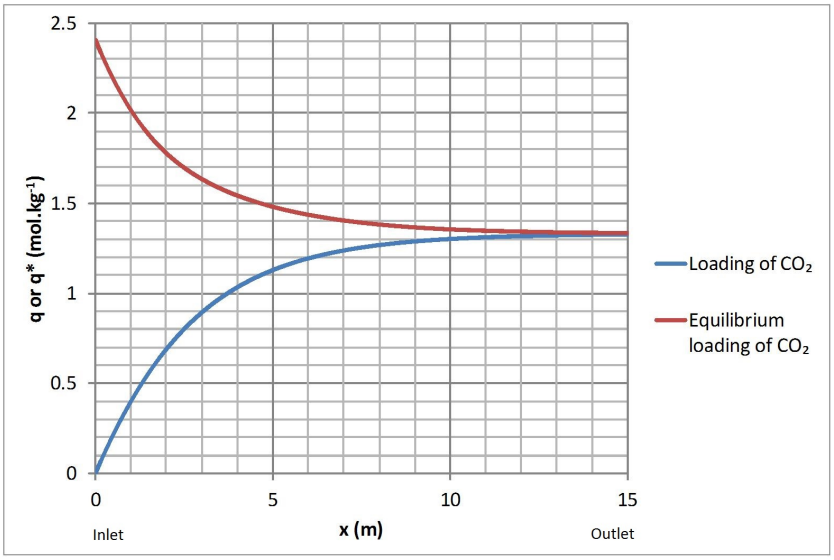

Figure 6.12: CO_2 loading profiles in a co-current adsorber with amine supported adsorbent and pores saturated with water

As the adsorbent leaves at the bottom of the counter-current adsorber ($x = 0$), it is cooled by inlet flue gas at a lower temperature entering the adsorber. This is shown in the adsorbent temperature profile in Figure 6.13. This causes the loading to increase and there is a sudden reduction in the concentration of CO_2 in the adsorbent pores shown in Figure 6.9 at the gas inlet.

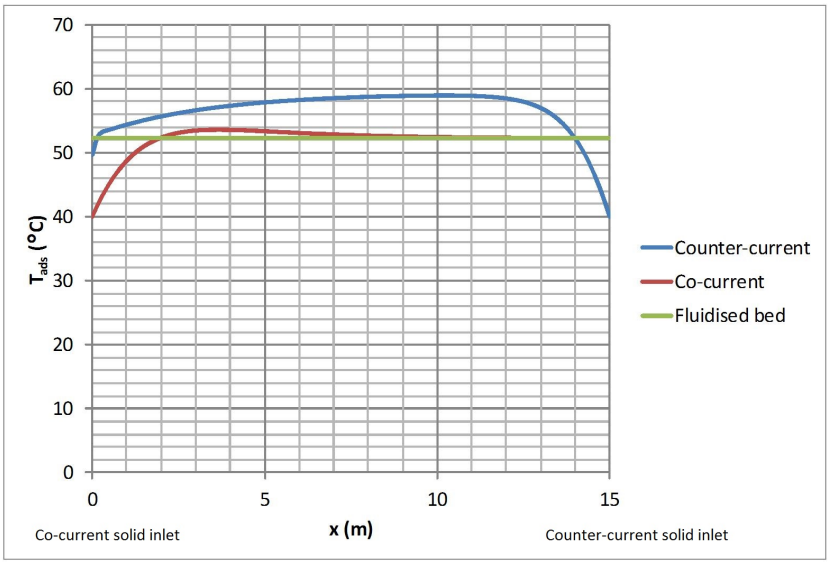

Figure 6.13: Adsorbent temperature profiles for counter-current, co-current and fluidised bed adsorbers with amine supported adsorbent and pores saturated with water

By keeping the same conditions as for the counter-current adsorber (except a higher adsorbent fraction, ε_a, of 0.4 in the fluidised bed), the counter-current adsorber gives a better CO_2 recovery over co-current and fluidised beds by 20.1% and 29.6% respectively as shown in Table 6.2. Additionally, under the same conditions as for a counter-current adsorber, a supported amine adsorbent flowrate of 975 kg.s^{-1} would be required for a co-current adsorber to achieve a 90% CO_2 recovery. This is 2.6 times larger than for the counter-current adsorber.

Table 6.2: CO_2 recoveries (molar basis) for supported amine adsorbents in three different beds

	Counter-current	Co-current	Fluidised bed
CO_2 recovery	92.1%	72.0%	71.0%

6.5 Effect of the Adsorbent

This section compares profiles in adsorbers for the supported amine adsorbent and activated carbon for adsorbent pores saturated with water. Results for zeolite 13X are found for dry flue gas and adsorbent.

The adsorbent parameters used in the simulations (particle density ρ_p, heat capacity of the adsorbent $c_{p,ads}$ and the heats of adsorption, ΔH_{ads}) were taken

from literature. For the supported amine adsorbent, these were provided by Krutka and Sjostrom (2011) and they are given in Table 2.3. The values for activated carbon are taken from SRI International et al. (2011) and are provided in Table 2.4. The properties of zeolite 13X are given in Table 6.3. For activated carbon, the volume fraction of the adsorbent is $\varepsilon_a = 0.033$ and for zeolite 13X, $\varepsilon_a = 0.032$ (Equation 3.49).

Table 6.3: Values of parameters for zeolite 13X (Cavenati et al. (2004), Chan et al. (2012))

Parameter	**Unit**	**Value**
Adsorbent particle density ρ_p	$kg.m^{-3}$	1130
Adsorbent particle size d_p	μm	1600
Adsorbent heat capacity c_{pads}	$J.kg^{-1}.K^{-1}$	836
Heat of adsorption for CO_2 ΔH_{CO_2}	$J.mol^{-1}$	-37222

The profiles for CO_2 mole fractions inside a counter-current adsorber are shown in Figure 6.14. The difference between the variations of the mole fraction of CO_2 in the activated carbon and the supported amine adsorbent can be seen. The drop in CO_2 in the bulk gas is larger at the inlet of the column for the supported amine adsorbent. This is attributed to higher CO_2 loadings, particularly at the gas inlet in the column (cf. Figure 6.16). On the other hand, the CO_2 loading is lower for activated carbon at the bottom of the counter-current adsorber which is why there is a smaller reduction in CO_2 concentration in the bulk gas at the gas inlet. Of the three adsorbents considered, the supported amine adsorbent gives the highest CO_2 capacities at 40°C and a CO_2 partial pressure of 12493 Pa for the inlet flue gas (cf. Figure 6.15).

The temperature profiles for the column with the base case flowrate of supported amine adsorbent and activated carbon (with pores saturated with water) are shown in Figure 6.17. Higher temperatures are reached for the supported amine adsorbent because of higher heats of adsorption of CO_2 and because a higher rate of CO_2 is adsorbed with this adsorbent than activated carbon.

As opposed to the counter-current bed, for which the profiles of CO_2 in the gas are different for both adsorbents, the co-current adsorber profiles for both adsorbents show similar trends as shown in Figure 6.18. CO_2 in the gas drops rapidly at the inlet of the column but as the CO_2 loading reaches the equilibrium loading at the outlet of the adsorber, CO_2 is no longer adsorbed and the mole fraction of CO_2 stagnates but does not drop any further. As more CO_2 is adsorbed in the counter-current bed, the mole fraction of CO_2 at the gas outlet is higher for the co-current bed than the counter-current bed (cf.

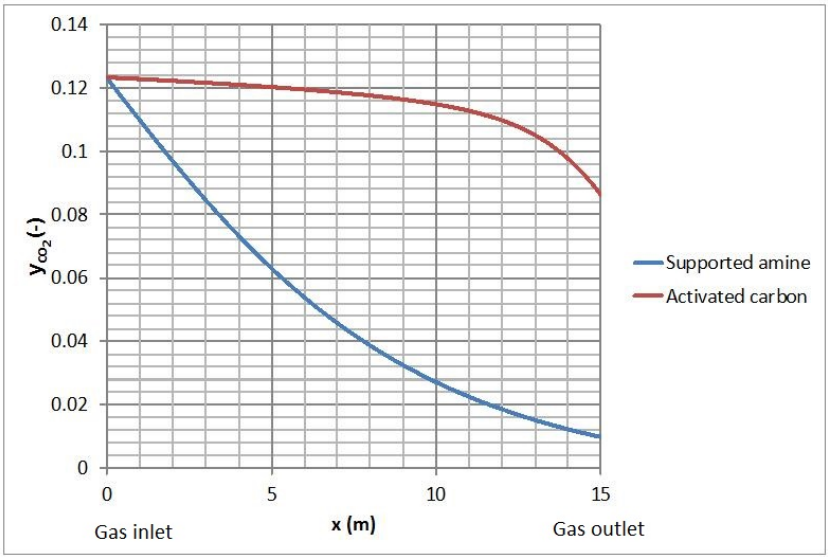

Figure 6.14: CO_2 mole fraction profiles for a counter-current adsorber with amine supported adsorbent and activated carbon (pores saturated with water)

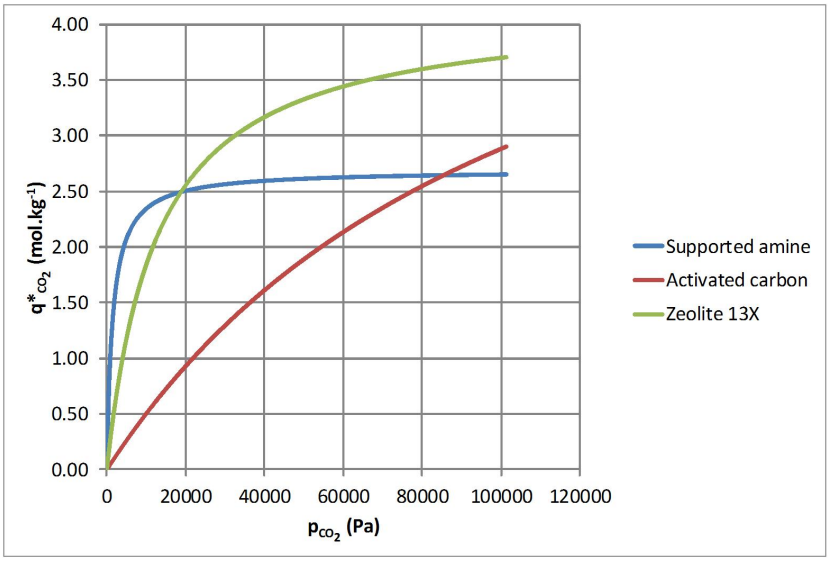

Figure 6.15: CO_2 isotherms for three adsorbents at 40°C

Figures 6.14 and 6.18).

As the supported amine adsorbent gives the highest CO_2 loading at the given flue gas conditions, less adsorbent is required to attain the desired level of CO_2 captured. Table 6.4 shows the additional flowrates of activated carbon and zeolite 13X required. In the case of zeolite 13X, no water is present in the gas or the adsorbent.

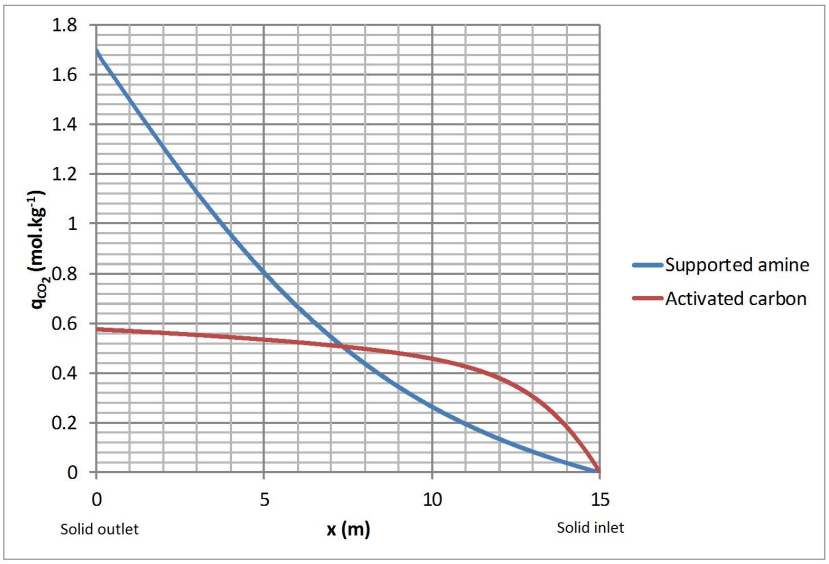

Figure 6.16: CO_2 loading profiles for a counter-current adsorber with amine supported adsorbent and activated carbon (pores saturated with water)

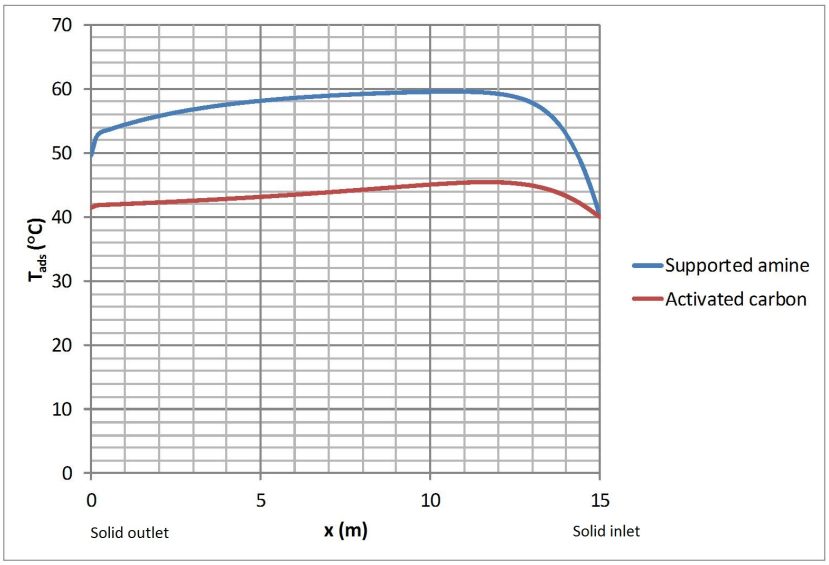

Figure 6.17: Adsorbent temperature profiles for a counter-current adsorber with amine supported adsorbent and activated carbon (pores saturated with water)

Table 6.4: Adsorbent flowrates required to attain 92.1% CO_2 capture

	Supported amine adsorbent	Activated carbon	Zeolite 13X
$\dot{m}_{in}$ (mol.kg^{-1})	375	1447.5	675

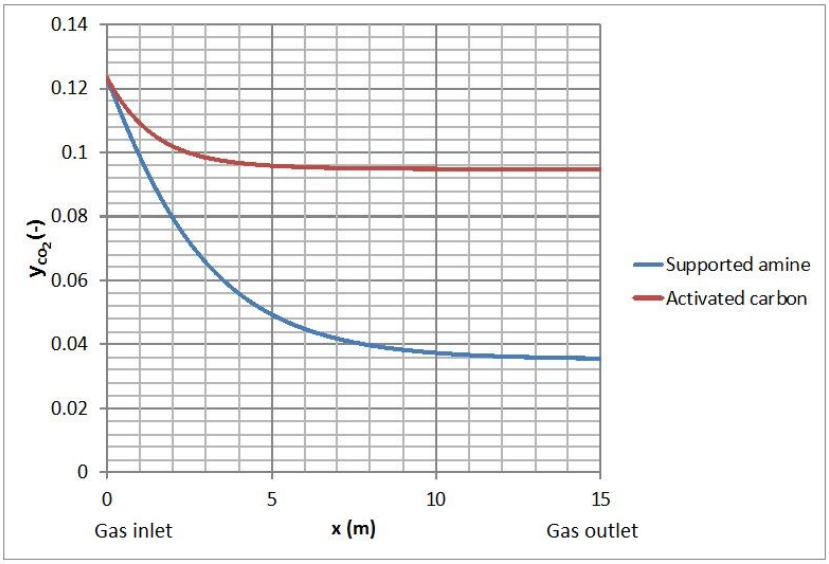

Figure 6.18: CO_2 mole fraction profiles for a co-current adsorber with amine supported adsorbent and activated carbon (pores saturated with water)

6.6 Fluidised Bed Adsorbers

Previously in section 6.4, it was shown that the performance of a single fluidised bed adsorber is poor compared with a counter-current one. However, it is technically possible to split a large fluidised bed into a number of smaller units where gas and solid are cascaded from one unit to another.

Fluidised beds typically have a higher adsorbent volume fraction (ε_a) inside the bed than co-current and counter-current systems. Kunii and Levenspiel (1991) have reported a typical value of $\varepsilon_a = 0.4$ which has been used for the fluidised bed simulations in this work.

Figures 6.19 and 6.20 show the results for multiple fluidised beds put in series with the gas and solid moving co-currently and counter-currently between them. The results show that it is possible to reach above 90% capture if at least three counter-current fluidised beds with the amine supported adsorbent are used as shown in Figure 6.20. This is an interesting finding because Krutka et al. (2013) modified their initial co-current adsorber (Krutka and Sjostrom (2011)) to a counter-current system of four fluidised beds in series. However, their choice of using four fluidised beds was not explained but it is possible that they also found that a low number of fluidised beds would be necessary to achieve a process which performs better.

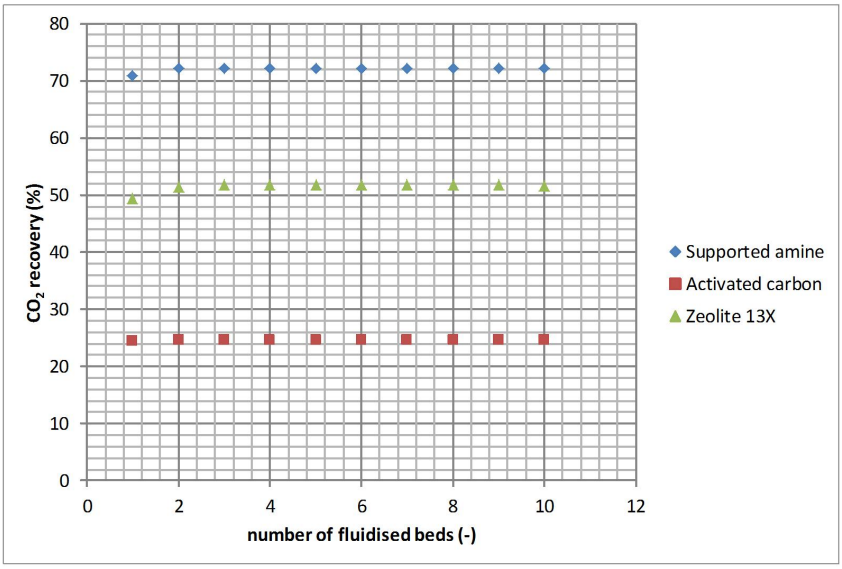

Figure 6.19: Effect of number of co-current fluidised beds in the adsorption column on recovery ($\varepsilon_a = 0.4$)

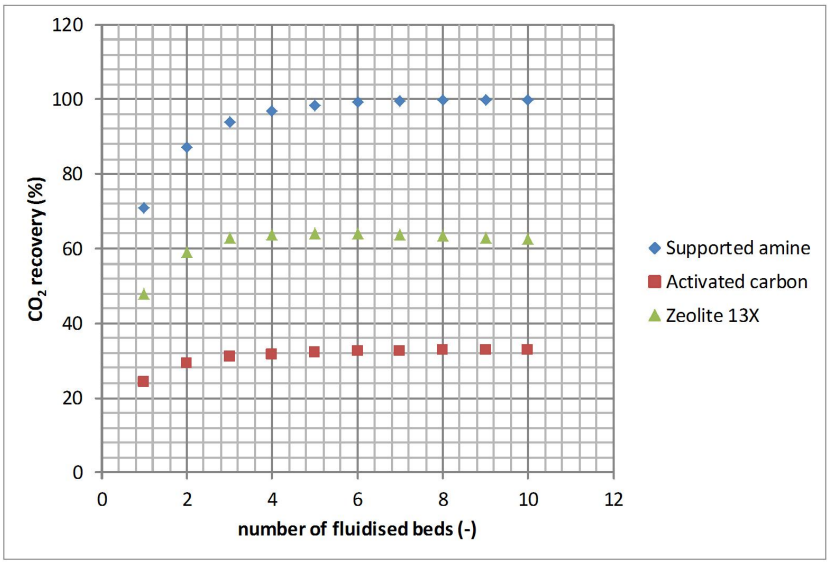

Figure 6.20: Effect of number of counter-current fluidised beds in the adsorption column on recovery ($\varepsilon_a = 0.4$)

For the co-current adsorber, there is only a small improvement offered by more than four fluidised beds in series as CO_2 recovery reaches 70%. For counter-current fluidised beds using the supported amine adsorbent, CO_2 recovery continues to increase for each additional fluidised bed added to the system whereas a limit is reached for after four beds with activated carbon and zeolite 13X. A true counter-current bed would be obtained for an infinite number of counter-current fluidised beds. However, difficulties in their practicalities of design may cause co-current and fluidised bed systems to be considered as viable options despite their lower CO_2 separation performance.

6.7 Effect of Adsorbent Flowrate

The effect of the variation of the flowrate of supported amine adsorbent, activated carbon and zeolite 13X (without water in flue gas or in the adsorbent pores) is shown in Figure 6.21. It can be seen that for a CO_2 removal of 90%, the minimum mass flowrates required for the amine supported adsorbent, activated carbon and zeolite 13X need to be 350 kg.s^{-1}, 1350 kg.s^{-1} and 650 kg.s^{-1} respectively.

A drop in CO_2 recovery for zeolite 13X is observed for adsorbent flowrates around 100 kg.s^{-1} due to a change in temperature profiles within the counter-current bed as shown in Figure 6.22. The heat capacity rate of the incoming gas and the solid can be represented by $\dot{m}_{in}c_{p,ads}$ and $\dot{M}_{in}c_{p,g}$ respectively with $c_{p,ads}$ (J.kg^{-1}.K^{-1}) and $c_{p,g}$ (J.mol^{-1}.K^{-1}) being the adsorbent and gas specific

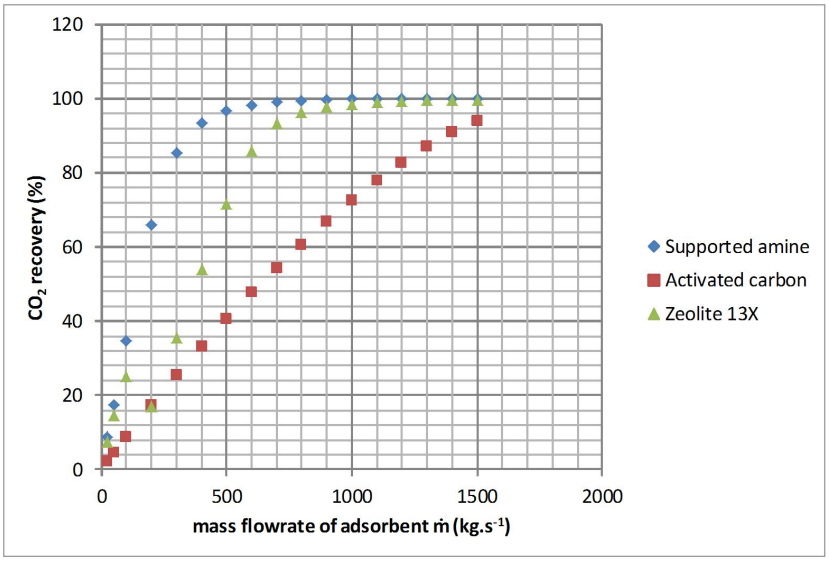

Figure 6.21: Effect of adsorbent flowrate on recovery for three different adsorbents

heat capacities. If $\dot{m}_{in}c_{p,ads} < \dot{M}_{in}c_{p,g}$, the gas is the main contributor to the movement of heat in the column and heat is preferentially moved towards the gas outlet. The temperature near the gas inlet remains closer to the flue gas temperature at the inlet which in this case is 40°C. The maximum temperature in the column is reached closer to the gas outlet for high gas flowrates/low adsorbent flowrates. The peak in the gas outlet temperature, shown in Figure 6.23 shows the significance of the carrying capacity of the gas for low adsorbent flowrates.

As the adsorbent flowrate increases, more CO_2 is adsorbed and the maximum temperature reached in the column increases. High temperatures are shifted to the gas inlet which is also the solid outlet. If $\dot{m}_{in}c_{p,ads} > \dot{M}_{in}c_{p,g}$, the main contributor to the movement of heat is now the solid. Heat is moved towards the solid outlet which is also the gas inlet for a counter-current bed. As the temperature at the solid outlet is now high, the CO_2 capacity reduces which leads to a reduction in the CO_2 recovery (cf. Figure 6.21). Further increases in $\dot{m}_{in}c_{p,ads}$ reduces the temperatures reached in the column as the additional adsorbent cools the column down.

There is no peak observed in the gas outlet temperature for the supported amine adsorbent. It drops as the mass flowrate of adsorbent used increases as shown in Figure 6.24. Therefore, there is no drop in CO_2 recovery observed for increasing adsorbent flowrates of this adsorbent. This is because the adsorbent enters wet and is dried in the flue gas, causing temperatures to drop. The heat released by the adsorption of CO_2 is not sufficient to counteract the heat of desorption of water.

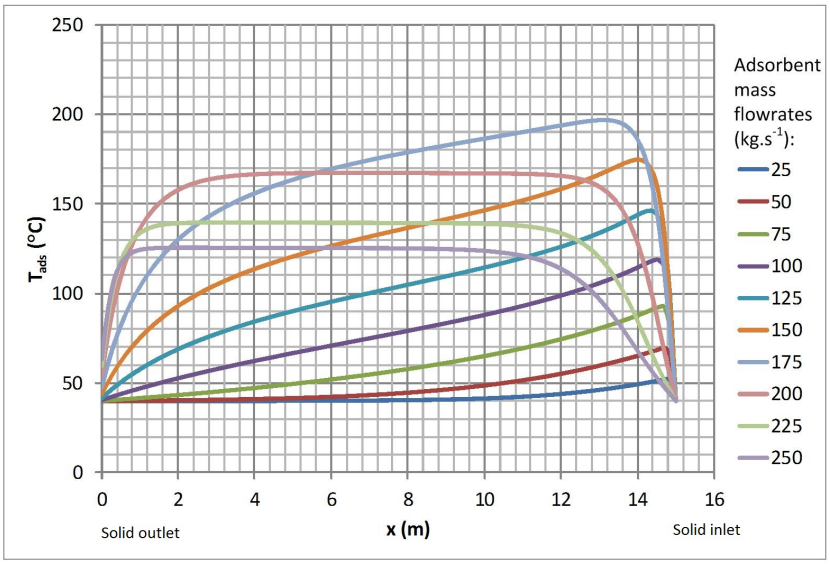

Figure 6.22: Adsorbent temperature profiles for a counter-current adsorber with zeolite 13X

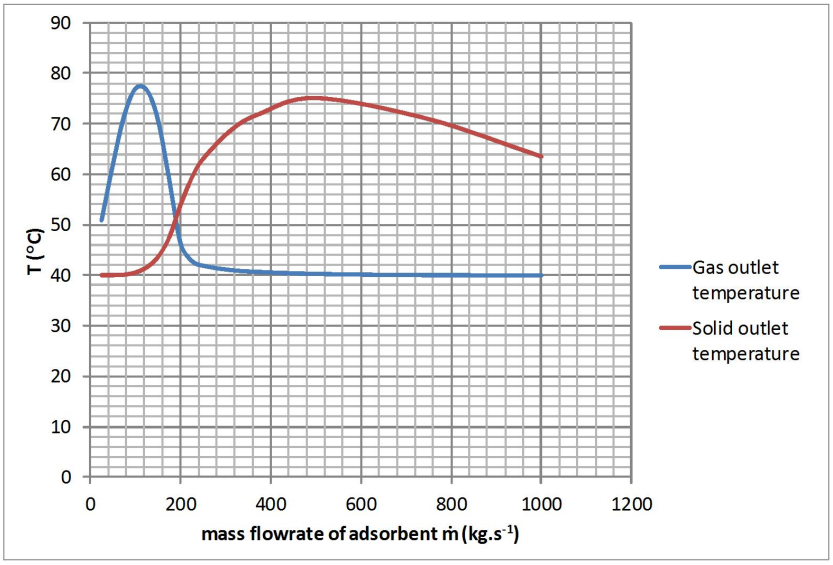

Figure 6.23: Gas and solid outlet temperatures for a counter-current adsorber with zeolite 13X

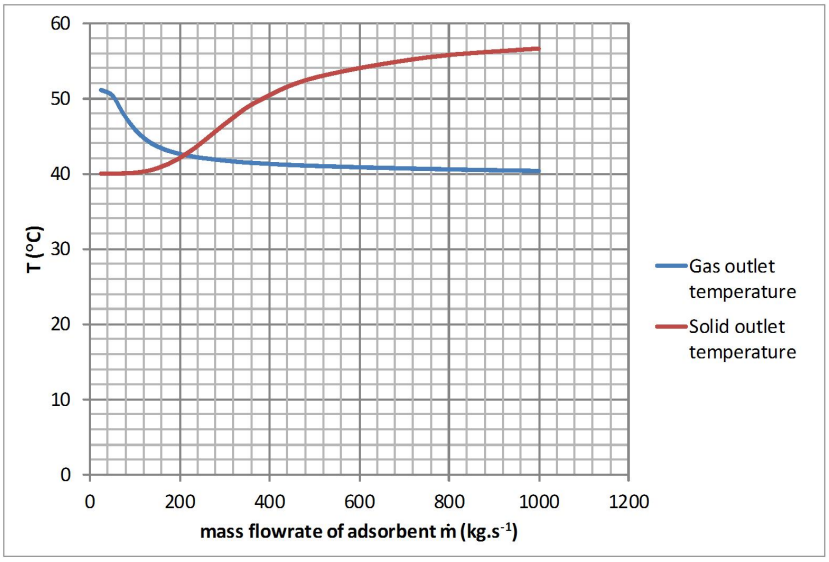

Figure 6.24: Gas and solid outlet temperatures for a counter-current adsorber with supported amine adsorbent (pores saturated with water)

Comparison of adsorbent flowrates with literature

Some information on adsorbent and gas flowrates used in moving bed CO_2 adsorption systems has been provided in the literature. A summary is shown in Table **??**. The required flowrate of activated carbon used by SRI International et al. (2013) has not been given and therefore no comparison with their work was made here.

Although the conditions used by the authors cited in Table 6.5 differ from work carried out here, a general comparison between flowrates can be made. The ratios of flue gas flowrate to adsorbent flowrate are similar for this work and for work carried out by Krutka and Sjostrom (2011). However, they found a lower CO_2 recovery. For zeolite 13X, a greater flowrate of adsorbent is required for the present work because a higher CO_2 loading was found by Kim et al. (2013a). The CO_2 loading found by Kim et al. (2013a) is in the order of 3.3 $mol.kg^{-1}$ at a partial pressure of 13000 Pa and 25°C. The gas temperature used for this work is higher (40°C) which is also why a lower loading was achieved.

Table 6.5: Literature values for adsorbent flowrates required

Adsorbent	Direction	CO_2 partial pressure (Pa)	Flue gas flowrate ($m^3.s^{-1}$)	Adsorbent flowrate ($kg.s^{-1}$)	**Ratio flue gas: adsorbent flowrate ($m^3.s^{-1}$:$kg.s^{-1}$)**	Reference
Supported amine adsorbent	co-current	6789	2.11×10^{-3}	5×10^{-3}	**1:2.37**	Krutka and Sjostrom (2011)
Amine impregnated silica	co-current	12463	9.5×10^{-5}	0.04×10^{-3}	**1:0.42**	Veneman et al. (2012)
Supported amine adsorbent (this work)	co-current	15200	144	375	**1:2.6**	-
Zeolite 13X	counter-current	13172	0.55	0.8	**1:1.44**	Kim et al. (2013a)
Zeolite 13X (this work)	counter-current	12463	144	375	**1:4.7**	-

6.8 Effect of CO_2 Mass Transfer Constant

It has been assumed that the mass transfer constants for all components considered are the same and this remains the case in this section. The sensitivity of the mass transfer constant of CO_2 is tested in this section.

Previously in Chapter 3, the rate of adsorption of a component, given by Equations 3.77 and 3.79 showed that the general term used for the rate of CO_2 adsorbed is dependent on $V\varepsilon_a k_{CO_2}$.

Figure 6.25 shows that for the amine supported adsorbent and for sufficiently high mass transfer constants (k_{CO_2}>10 s^{-1}), CO_2 recoveries are greater than 90%. For k_{CO_2}>20 s^{-1}, CO_2 recoveries are closer to 100% which indicates that adsorption is no longer limited by kinetics but by the equilibrium loading. Similar trends are obtained for activated carbon and zeolite 13X. However, for these adsorbents, the mass flowrate of adsorbent is insufficient to reach 100% capture even for high mass transfer constants.

For zeolite 13X, recoveries are over-predicted if only 100 discretisations are used for values of k_{CO_2} greater than 10 s^{-1}. The numerical error drops significantly for a larger number of discretisations and 1000 discretisations were used instead. This error is due to larger rises in temperature in the column for this adsorbent which therefore requires a larger number of control volumes for an accurate solution to be attained.

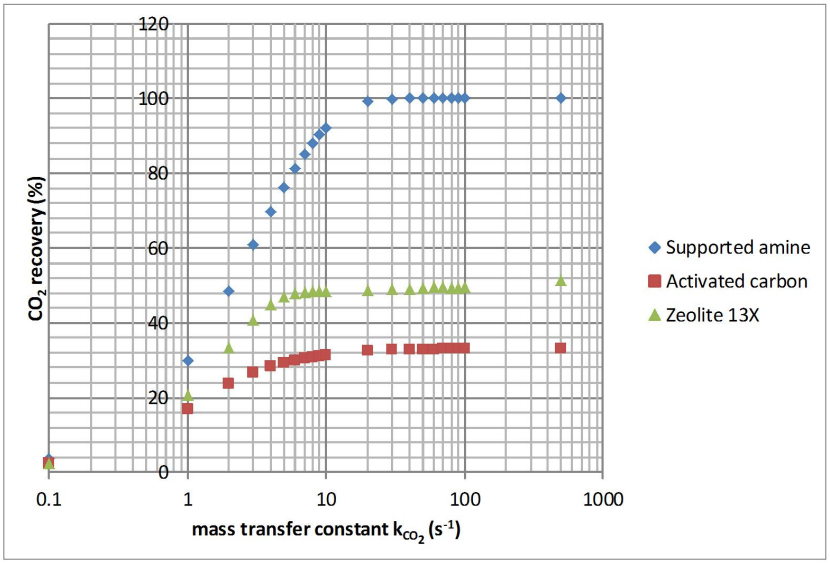

Figure 6.25: Effect of mass transfer constant on recovery for three different adsorbents

Figure 6.25 also shows that the performance of the adsorber is severely reduced if k_{CO_2}<10 s^{-1}. Low mass transfer rates would lead to higher adsorbent flowrates required to reach the desired level of CO_2 recovery as shown in Figure

6.26. For example, if k_{CO_2} has a value of 1 s^{-1} instead of 10 s^{-1}, the supported amine adsorbent flowrate needs to be roughly 16 times higher. This means that the performance of the system is highly dependant on getting the correct value of k_{CO_2}. It also means that from a mass transfer point of view, a system with a high value of ε_a (i.e. fluidised bed) would be beneficial over one with a lower ε_a (i.e. co-current or counter-current beds) as this would bring similar benefits to running the column with high k_{CO_2} values because it is the overall value of $V\varepsilon_a k_{CO_2}$ that is important.

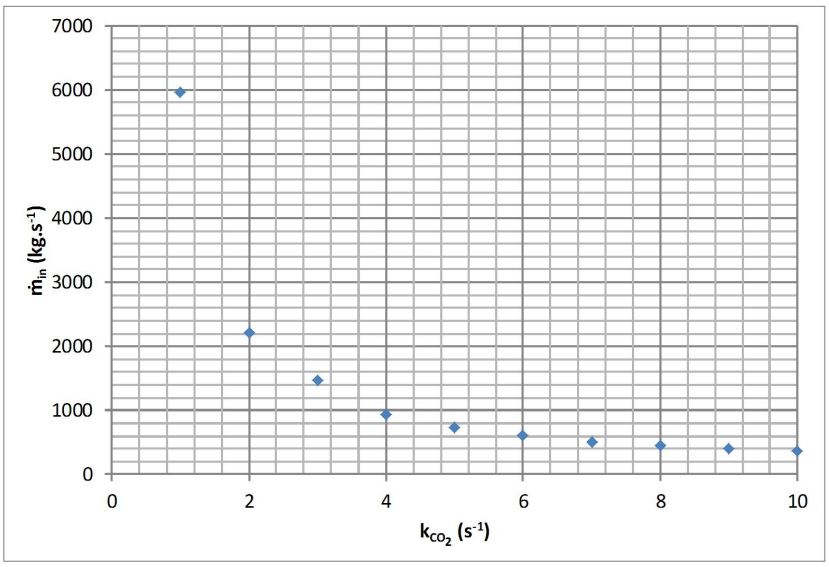

Figure 6.26: Impact of the CO_2 mass transfer constant on the mass flowrate of supported amine adsorbent required to obtain 92.1% CO_2 recovery

6.9 Effect of CO_2 Mole Fraction in the Inlet Flue Gas

In this section, the effect on the CO_2 recovery of the CO_2 mole fraction in the inlet flue gas is investigated. For a given adsorbent flowrate, Figure 6.27 shows that as more CO_2 is present in the flue gas, the CO_2 recovery drops for all three adsorbent considered. The flowrate of adsorbent is also insufficient as the CO_2 mole fraction in the flue gas is increased. The decrease in CO_2 recovery is also partly due to rising temperatures inside the adsorber for increasing CO_2 levels in the flue gas. More heat is given off as more CO_2 is adsorbed in the column. The increase of the mole fraction of CO_2 in the flue gas leads to higher amounts of CO_2 initially adsorbed as the adsorbent enters the system. However, for larger mole fractions of CO_2 in the flue gas, an increase in heat generated from adsorption is associated with this higher loading as the adsorbent enters

the adsorber. Figure 6.28 shows that if the level of CO_2 in the gas increases, the temperature rise is the highest near the solid inlet where the amount of CO_2 adsorbed rises sharply.

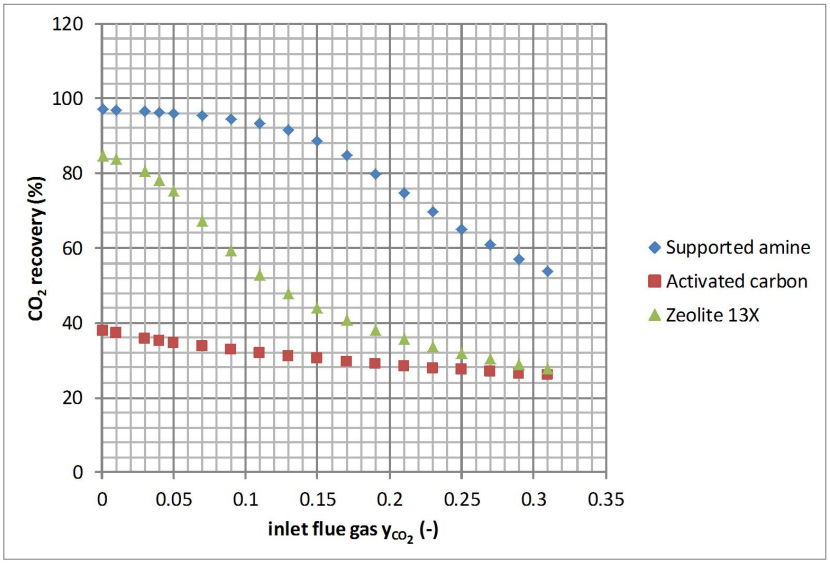

Figure 6.27: Effect of the mole fraction of CO_2 in the inlet flue gas on recovery

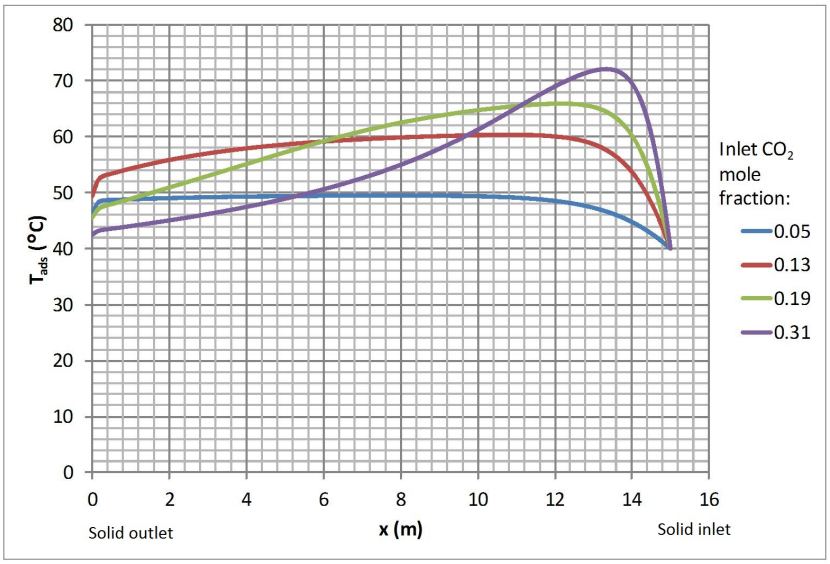

Figure 6.28: Adsorbent temperature profiles for various CO_2 mole fractions in the gas inlet for a counter-current adsorber with amine supported adsorbent (pores saturated with water)

The difference of the isotherms for each adsorbent also contributes to the drop in CO_2 recovery. Activated carbon has a CO_2 isotherm which is closest to a linear isotherm as shown in Figure 6.15. CO_2 loading therefore continues to increase as the partial pressure of CO_2 increases. However, for the supported amine adsorbent, above a partial pressure of about 15000 Pa, the CO_2 isotherm

approaches the maximum CO_2 loading given by the isotherm. Therefore, unlike activated carbon, there is no increase in loading as the CO_2 partial pressure increases. The CO_2 recovery drops more sharply for the supported amine adsorbent because CO_2 loading is not substantially increased for higher CO_2 concentrations in the feed gas whereas loading continuously increases for higher CO_2 concentrations in the feed when activated carbon is used. CO_2 recovery is more maintainable and therefore it drops less rapidly as the CO_2 concentration in the feed gas increases (cf. Figure 6.27). In addition, CO_2 removal does not decrease as much for activated carbon because of lower maximum temperatures reached in the adsorber.

6.10 Effect of Water in the Inlet Flue Gas

The effect of the mole fraction of water in the inlet flue gas is investigated here. Zeolite 13X is not included in this analysis because it is not suitable for CO_2 adsorption in the presence of moisture.

As with increased CO_2 levels in the gas, CO_2 recovery drops if the flue gas contains high levels of moisture as shown in Figure 6.29. Less water is desorbed from the adsorbent initially with its pores saturated with water for higher mole fractions of water in the bulk flue gas as shown in Figure 6.30. Therefore, higher temperatures are reached in the adsorber if the flue gas contains less water as shown in Figure 6.31.

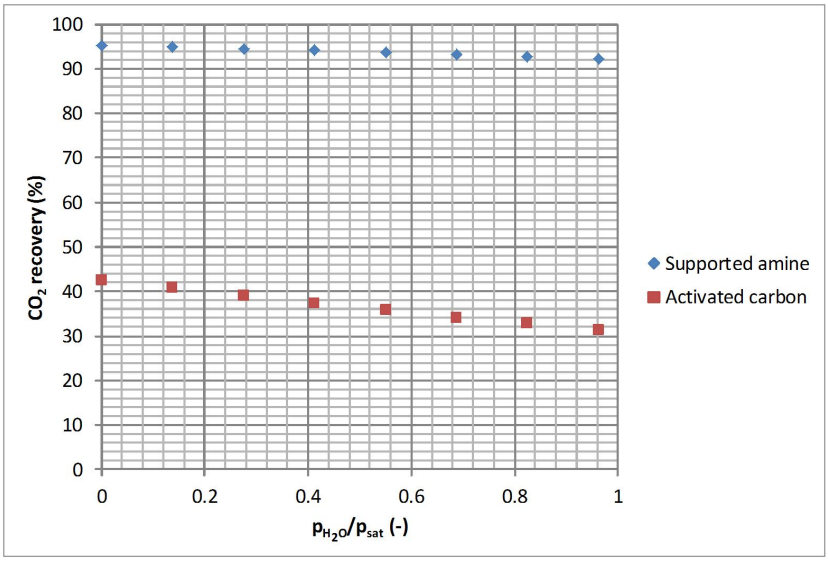

Figure 6.29: Effect of the relative humidity of the inlet flue gas on recovery

The drop in CO_2 recovery for increasing mole fractions of water in the flue gas is low because the uptake of CO_2 and water were considered to be indepen-

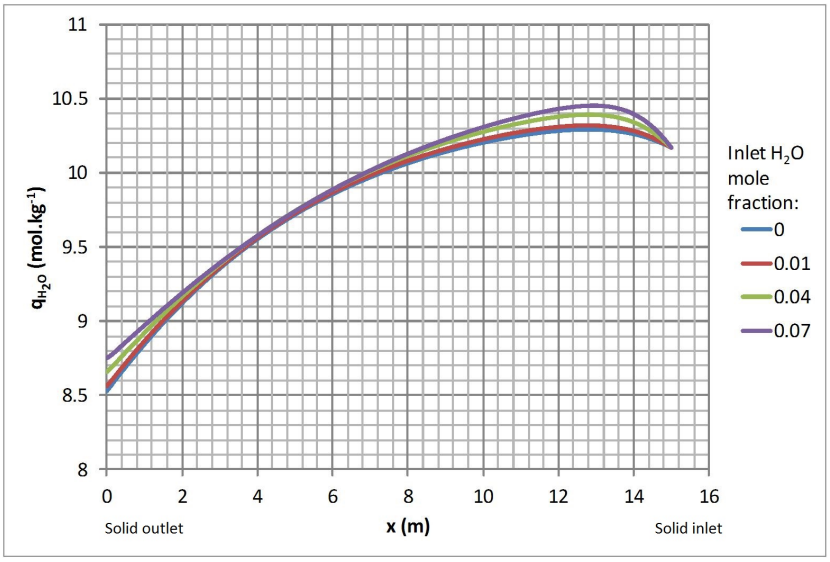

Figure 6.30: Water loading profiles for a counter-current adsorber with amine supported adsorbent for various inlet gas mole fractions of water

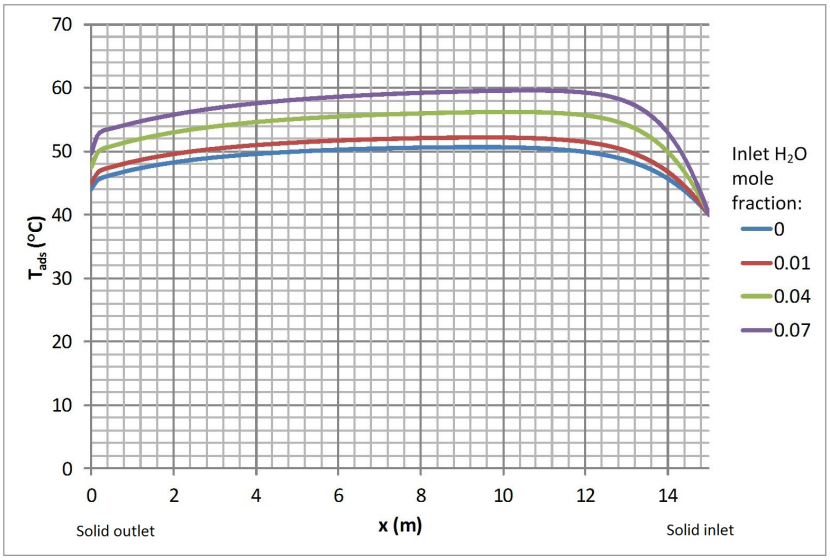

Figure 6.31: Adsorbent temperature profiles for a counter-current adsorber with amine supported adsorbent for various inlet gas mole fractions of water

dent of each other rather than being competitive. Therefore, the reduction in the CO_2 recovery observed in Figure 6.29 is mainly a temperature effect. An accurate isotherm model for CO_2 in the presence of water would be required for a better prediction of the influence of water in the flue gas.

6.11 Effect of Pre-loaded CO_2

Figure 6.32 shows that the initial loading of CO_2 on the adsorbents entering the counter-current adsorber, needs to be minimised to reach the highest levels

of CO_2 removal. For inlet pore concentrations greater than 5 mol.m^{-3}, CO_2 which is preloaded before entering the adsorber is desorbed into the flue gas. This is shown by a negative recovery in Figure 6.32. A comparison between two cases with and without pre-loaded CO_2 is shown in Table 6.6. If the adsorbent has an initial loading of CO_2 of 1.148 mol.kg^{-1} (corresponding to an inlet CO_2 concentration of 0.7 mol.m^{-3}), CO_2 recovered drops significantly by 49%. Of the three adsorbents, this is the largest drop in recovery.

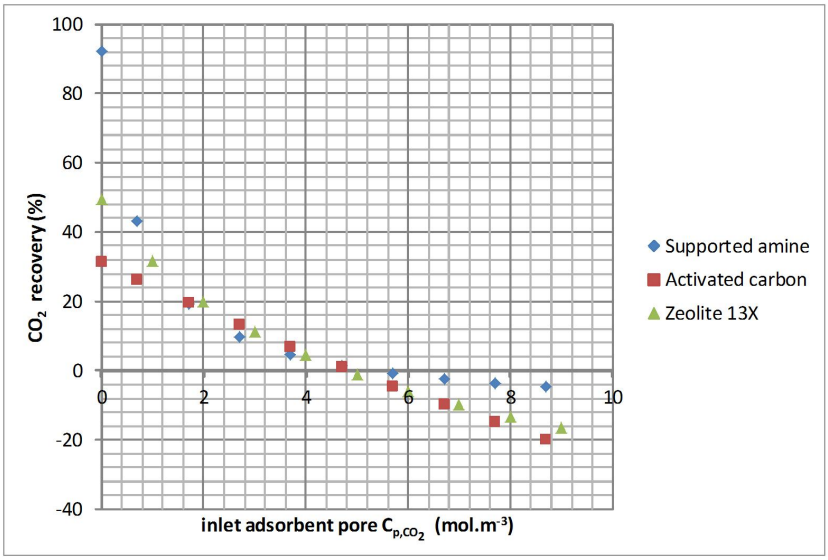

Figure 6.32: Effect of the inlet CO_2 concentration in adsorbent pores on CO_2 recovery for the three different adsorbents

Table 6.6: Cases with and without preloaded CO_2 on the supported amine adsorbent

	Without preloaded CO_2	With preloaded CO_2
C^{in}_{p,CO_2} (mol.m^{-3})	0	0.7
q_{CO_2} (mol.kg^{-1})	0	1.148
CO_2 recovery	92%	43%

The main reason for a lower CO_2 recovery if CO_2 is pre-loaded on the adsorbent at the adsorbent inlet (top of the column) is because the capacity of the adsorbent is reduced. Therefore, a higher adsorbent flowrate would be required to achieve a higher CO_2 recovery.

The reduction in CO_2 recovery is also due to a lower driving force for adsorption (i.e. a lower difference between the pore concentration and bulk gas concentration) in the adsorber if the adsorbent entering is pre-loaded with CO_2 as shown in Figure 6.33. For adsorbent initially containing no pre-loaded CO_2

entering the counter-current adsorber, the driving force is highest near the gas inlet. On the other hand, if $C^{in}_{p,CO_2} = 5$ mol.m^{-3}, the driving force is greatest at the gas outlet.

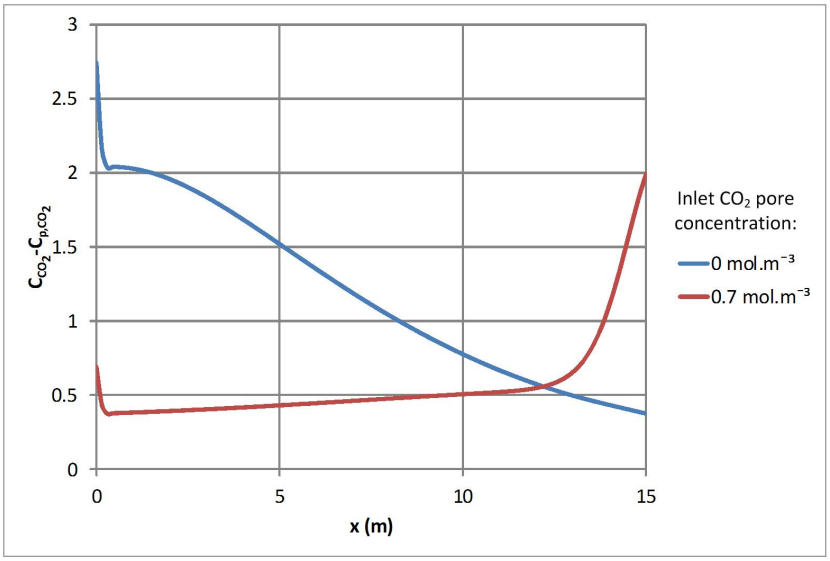

Figure 6.33: Difference between bulk gas and pore CO_2 concentrations for adsorbent pores with and without CO_2 preloaded

6.12 Effect of Pre-loaded Water

The influence of preloaded water in the pores of the supported amine adsorbent and activated carbon is shown in Figure 6.34. Preloading the adsorbents with water has the opposite effect to preloading it with CO_2. CO_2 removal is higher for adsorbents preloaded with water prior to entering the adsorber as less water would be adsorbed in the adsorber, thus reducing the amount of exothermic heat produced and hence also reducing the maximum temperatures reached.

If the adsorbents do not contain any water prior to entering the counter-current column, there is a similar trend observed for the CO_2 profiles for the supported amine adsorbent and activated carbon as shown in Figure 6.35. As cooler flue gas enters the column, CO_2 is adsorbed and its mole fraction drops slightly. However, the temperature of the adsorbent increases due to the release of heat from the adsorption of CO_2 and water which causes the desorption of CO_2 and an increase in concentration in the gas. The mole fraction of CO_2 increases above the inlet mole fraction of CO_2 after which it falls sharply at the gas outlet where cooler adsorbent enters the column. Correspondingly, there is a sharp increase in CO_2 loading as the adsorbent enters the column at the gas outlet. This trend is not observed for zeolite 13X due to the absence of water from the feed gas.

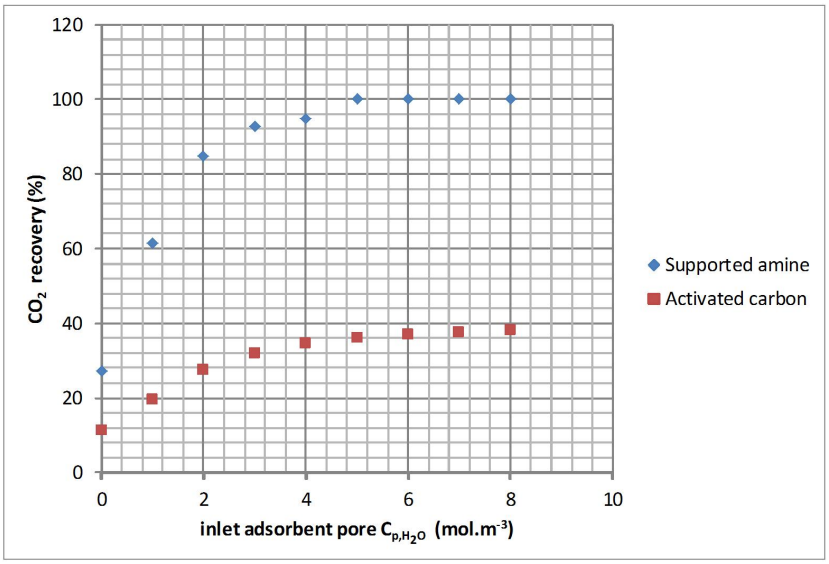

Figure 6.34: Effect of initial water concentration in adsorbent pores on CO_2 recovery for supported amine and activated carbon adsorbents

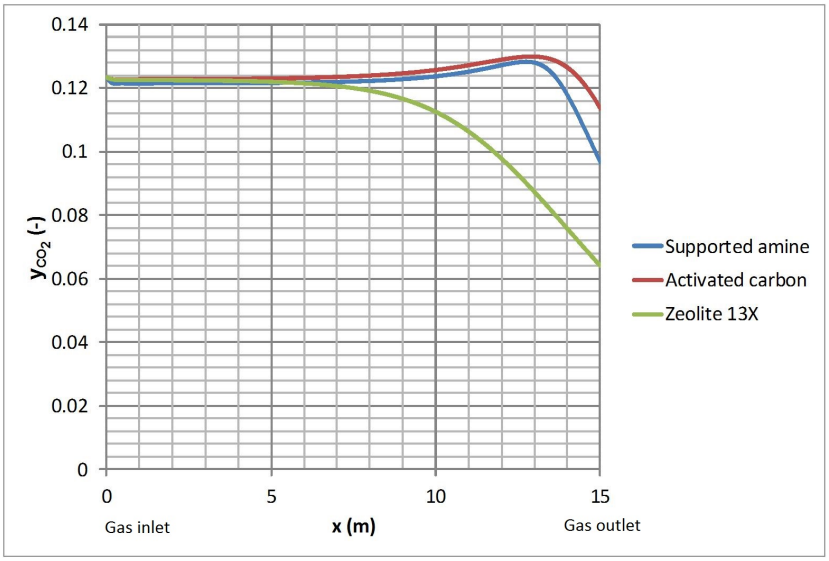

Figure 6.35: CO_2 mole fraction profiles for a counter-current adsorber with amine supported adsorbent, activated carbon and zeolite 13X (pores do not contain any water)

From Figure 6.36, a temperature as high as 103°C is reached if the adsorbent contains no water before entering the adsorber. If the adsorbent pores are saturated with water, the highest temperature reached is close to 60°C (cf. Figure 6.13). The increased temperatures in the adsorber lead to lower CO_2 uptakes as given by the CO_2 isotherms shown previously in section 3.7.

More CO_2 is removed in a co-current adsorber than a counter-current adsorber if the supported amine adsorbent used is not preloaded with water as shown in Figure 6.37 due to higher temperatures reached inside the counter-current

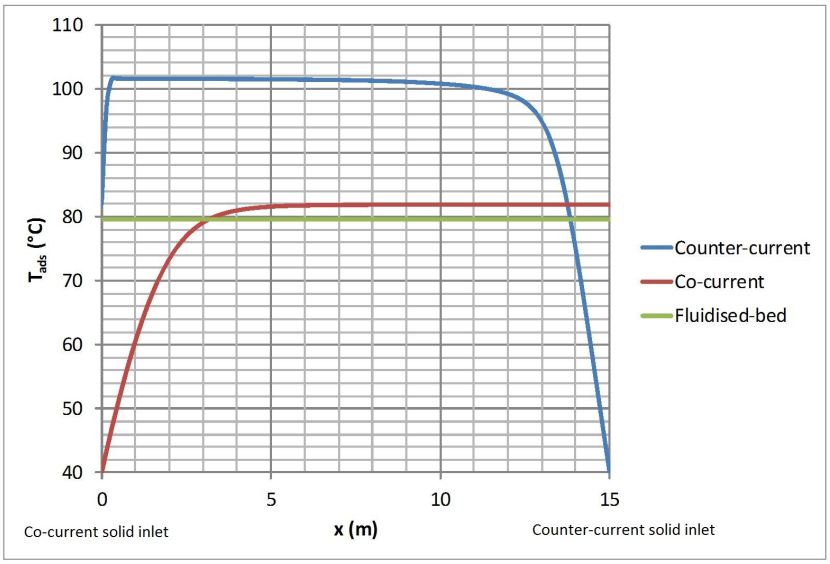

Figure 6.36: Adsorbent temperature profiles for counter-current, co-current and fluidised bed adsorbers with amine supported adsorbent (pores do not contain any water)

adsorber.

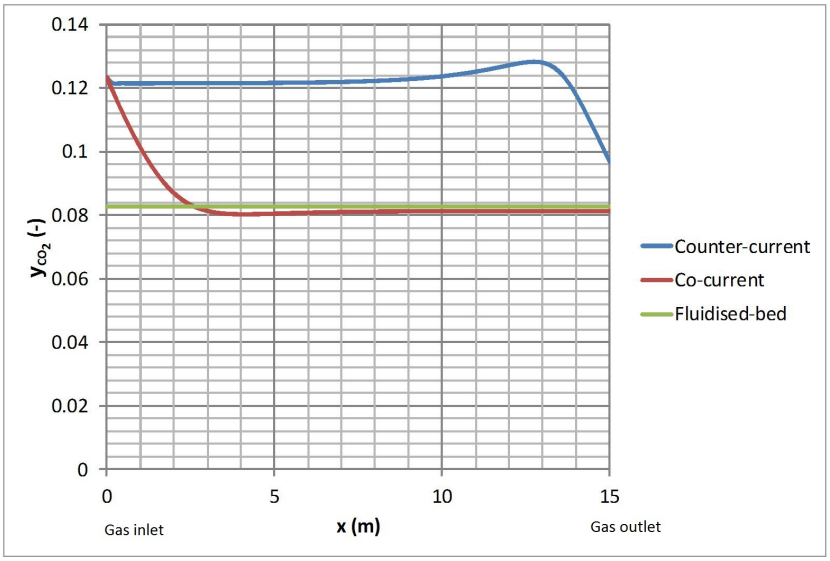

Figure 6.37: Mole fraction profiles of CO_2 for counter-current, co-current and fluidised bed adsorbers with amine supported adsorbent (pores do not contain any water)

The CO_2 concentration profiles for the bulk gas and the pores for initially dry supported amine adsorbent are shown in Figure 6.38. It can be seen that adsorption occurs at the inlet and outlet of the bed only where the CO_2 concentration in the gas is greater than the pore concentration. Locations at which the concentration in the bulk gas and in the pores are the same and constant also correspond to positions at which the temperature in the adsorber is the

highest.

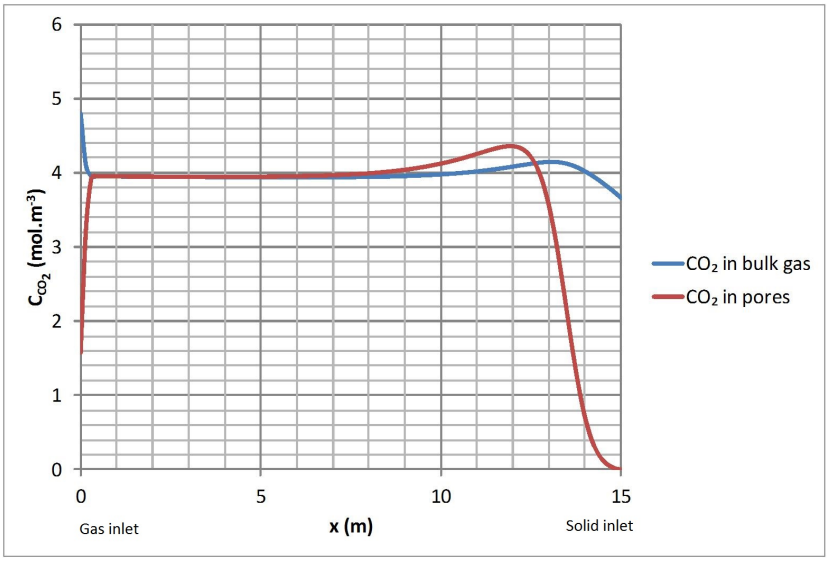

Figure 6.38: CO_2 concentration profiles in a counter-current adsorber with amine supported adsorbent (pores do not contain any water)

If the adsorbent pores do not contain water before entering the adsorber, water is adsorbed and its mole fraction decreases as shown in Figure 6.39. On the other hand, if the adsorbent pores are saturated with water, water is desorbed from the adsorber as shown in Figure 6.40 and heat is consumed thereby counteracting the heat produced simultaneously during the adsorption of CO_2. As a result lower temperatures are achieved in the adsorber if the adsorbent is preloaded with water.

If the adsorbent is saturated as the adsorbent enters, the pore concentration of water still increases as water is adsorbed at the gas outlet which is shown by a higher bulk gas concentration than the pore concentration (cf. Figure 6.41). At the gas inlet, however, the concentration of water in the pores is greater than in the bulk gas causing the water to be desorbed. Overall, the water mole fraction in the bulk gas rises as shown in Figure 6.40.

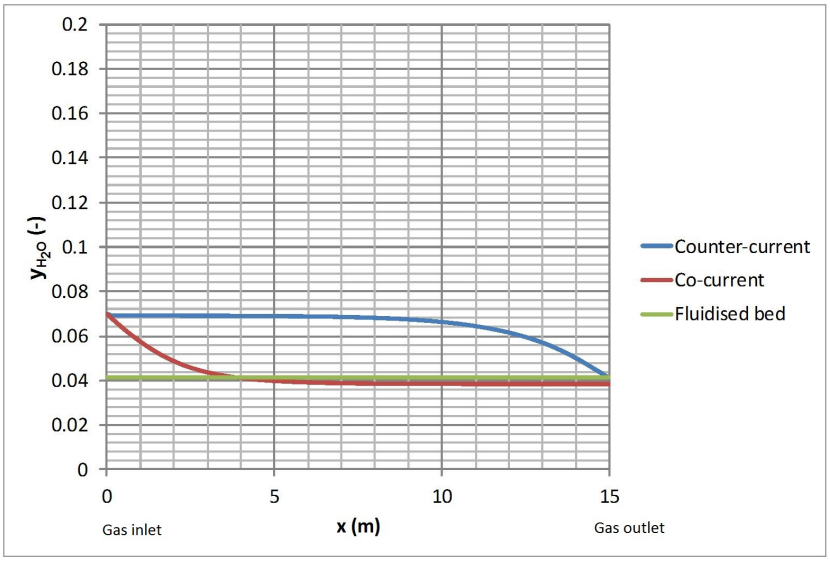

Figure 6.39: Mole fraction profiles of water for counter-current, co-current and fluidised bed adsorbers with amine supported adsorbent (pores do not contain any water)

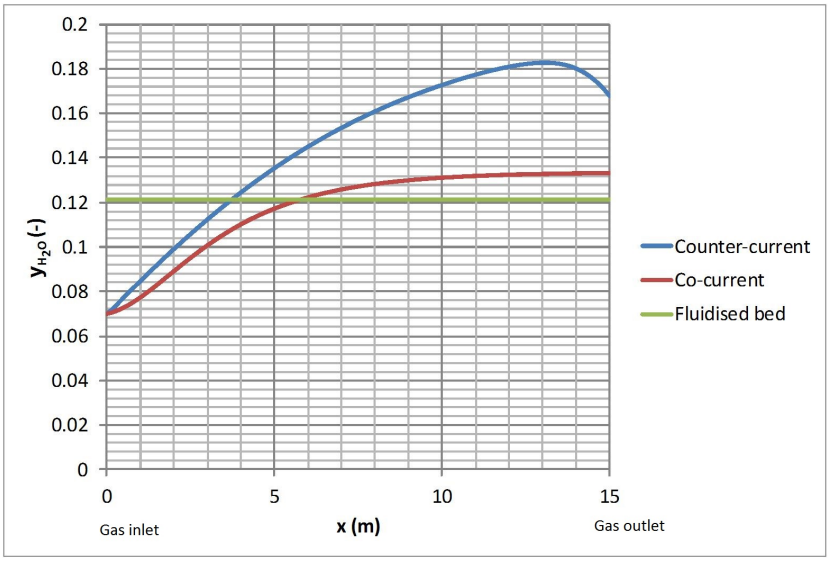

Figure 6.40: Mole fraction profiles of water for counter-current, co-current and fluidised bed adsorbers with amine supported adsorbent and pores saturated with water

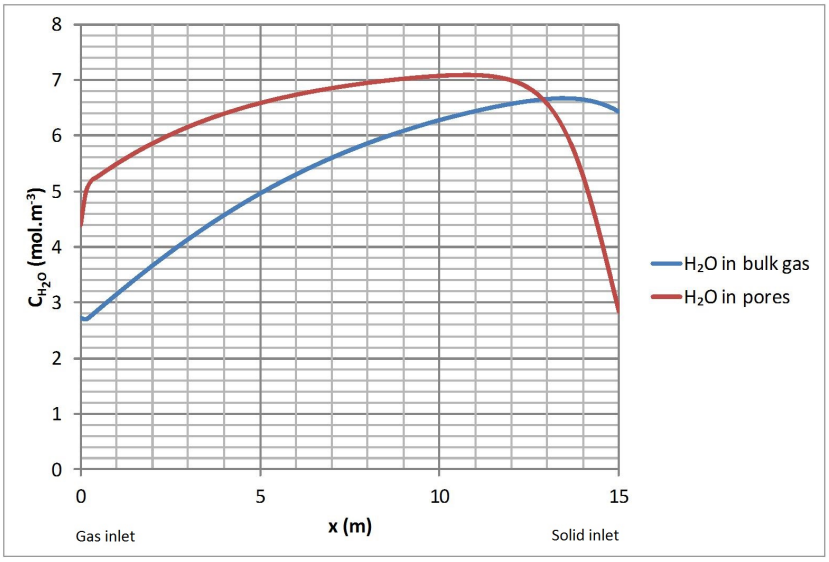

Figure 6.41: Water concentration profiles in a counter-current adsorber with amine supported adsorbent and pores saturated with water

6.13 Effect of Molar Flowrate of Flue Gas

Without considering the impact that higher flowrates of flue gas would have on the flow of the adsorbent (e.g. entrainment) as described in Chapter 5, the effect of higher flue gas flowrates on the CO_2 recovery is assessed in this section.

If the molar flowrate of gas into the counter-current adsorber is increased whilst maintaining the same CO_2 mole fraction in the inlet gas, a higher rate of CO_2 must be processed by the adsorbent. As the molar flowrate of the inlet flue gas is increased for a constant adsorbent flowrate, the CO_2 recovery reduces more sharply for zeolite 13X than the other adsorbents due to higher temperatures reached in the adsorber with this adsorbent (cf. Figure 6.42). As the supported amine adsorbent and activated carbon arriving into the adsorber are saturated with water, the temperature is more controlled than for zeolite 13X as heat is given off as water is desorbed therefore the drop in CO_2 recovery with the supported amine adsorbent and activated carbon is less sharp than for zeolite 13X.

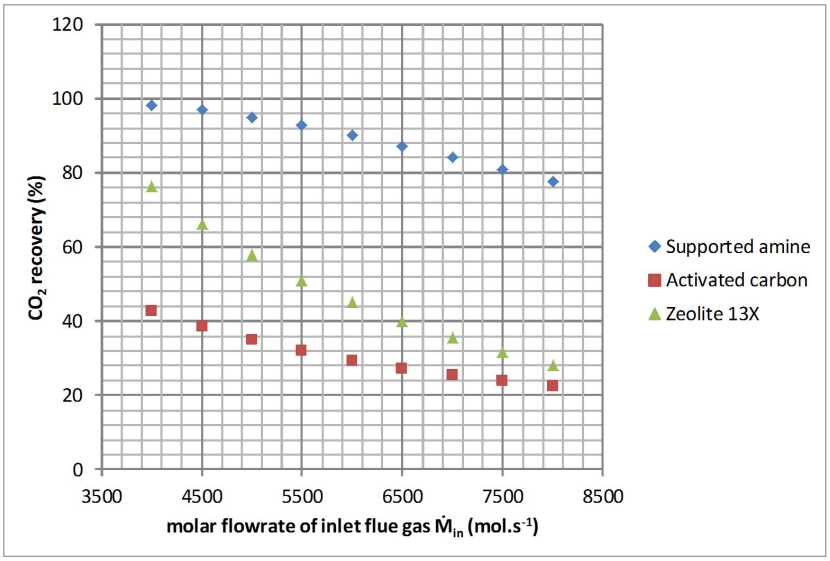

Figure 6.42: Effect of molar flowrate of gas on recovery for three different adsorbents

6.14 Effect of Inlet Flue Gas Temperature

There is a very small effect of the inlet gas temperature on CO_2 capture for all three adsorbents in a counter-current bed, as shown in Figure 6.43. In a sensitivity analysis carried out by Øi (2007) for the effect of the gas temperature in an amine absorption process, it was found that there was a greater drop in CO_2 recovery if the flue gas were to be introduced at higher temperatures.

Reported values include a recovery of 89% at 30 °C but only a 84% for 50°C. Due to a higher heat capacity rate of the adsorbent ($\dot{m}_{in}c_{p,ads} = 242$ kW.K^{-1}) compared to that of the gas ($\dot{M}_{in}c_{p,g} = 165$ kW.K^{-1}), the temperature in the adsorber is dominated by the adsorbent temperature as shown in Figure 6.44. The temperature of the adsorbent and hence the CO_2 loading is only affected by the flue gas temperature near the gas inlet where the adsorbent leaves the system. Due to kinetic limitations, the region close to the gas feed where most of the difference in temperature occurs has little effect on the resulting CO_2 removed.

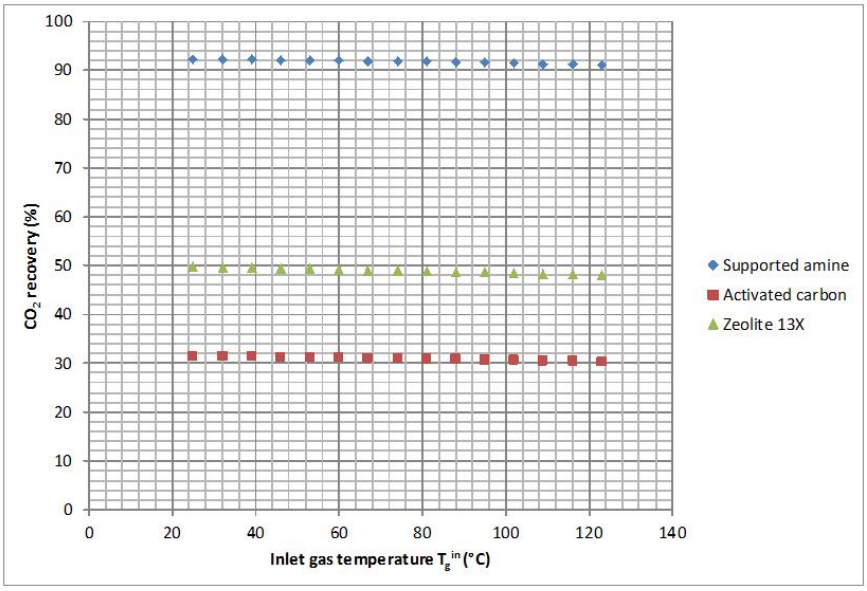

Figure 6.43: Effect of inlet gas temperature on recovery for three different adsorbents

The gas is saturated with water at the inlet gas temperature used for the base case (the relative humidity is 100%). However, as the inlet gas temperature has been increased, the inlet gas to the adsorber contains the same mole fraction of water and therefore the flue gas is no longer saturated with water. Consequently, water that is pre-adsorbed has a greater tendency to be desorbed into the gas at higher temperature. The heat given off during the desorption of water encourages a lower temperature which compensates for the higher inlet adsorbent temperature. This is another reason why the CO_2 recovery is not affected much by higher inlet gas temperatures. Another analysis could have been done in which the relative humidity of the flue gas at the inlet is held at 100%.

For flue gas temperatures of 25°C and 123°C, the CO_2 loading profiles and the profiles of the loading at equilibrium are shown in Figures 6.45 and 6.46 respectively. The loadings q_{CO_2}, are similar for both temperatures and the

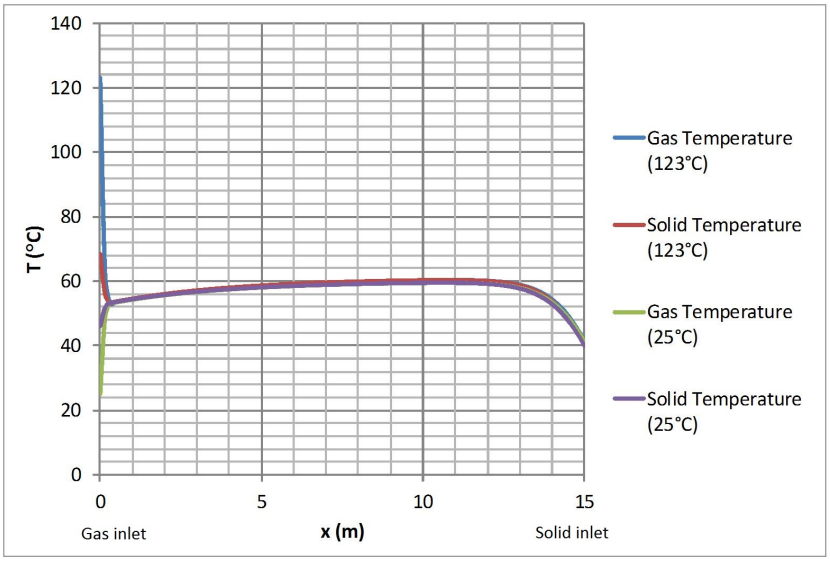

Figure 6.44: Adsorbent temperature profiles for a counter-current adsorber with amine supported adsorbent (pores saturated with water) inlet flue gas temperatures of 123°C and 25°C

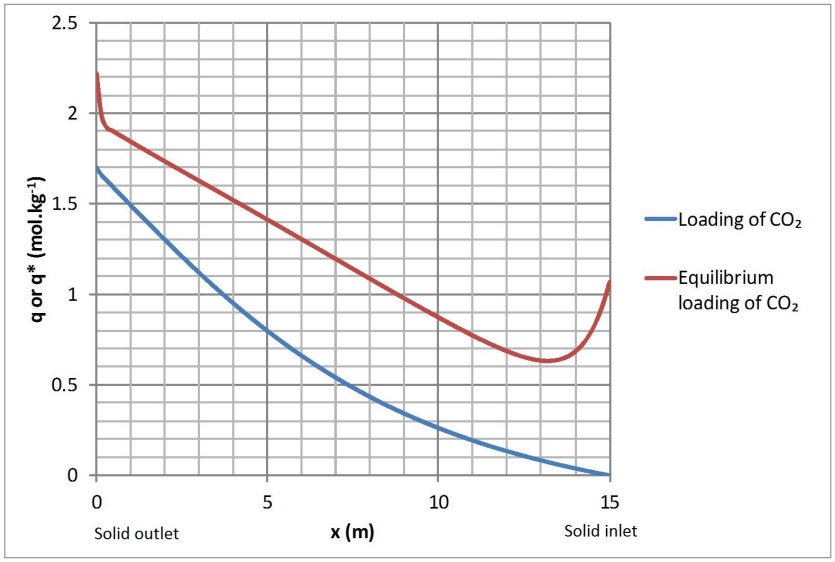

Figure 6.45: CO_2 loading profiles in a counter-current adsorber with supported amine adsorbent and pores saturated with water for flue gas entering at 25°C

equilibrium loadings, $q^*_{CO_2}$, are similar in the majority of the column except at the gas inlet where it drops for the higher temperature. The equilibrium loading is lower than the actual loading for flue gas entering the column at 123°C which indicates that CO_2 is desorbed at the gas inlet.

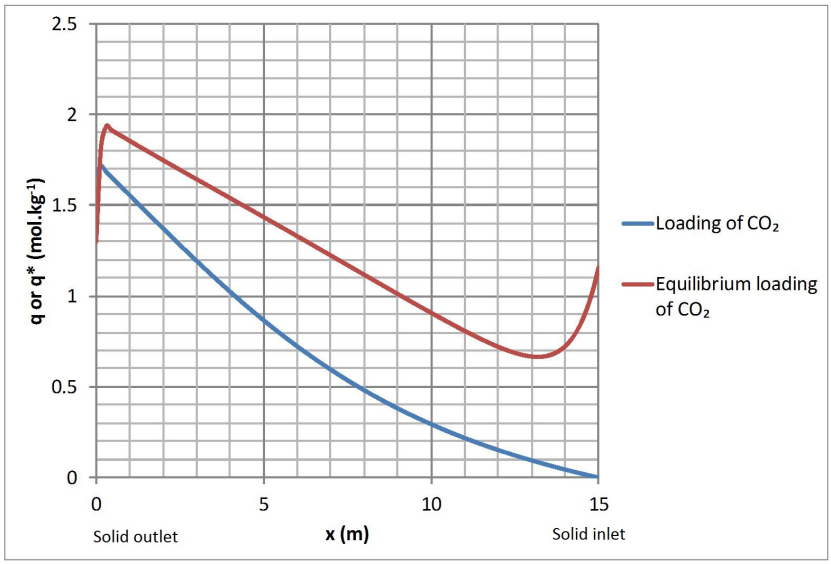

Figure 6.46: CO_2 loading profiles in a counter-current adsorber with supported amine adsorbent and pores saturated with water for flue gas entering at 123°C

6.15 Effect of Inlet Adsorbent Temperature

The temperature of the adsorbent entering the adsorber has a great impact on CO_2 capture in particular for the amine supported adsorbent. For example, it can be seen from Figure 6.47, that for adsorbent entering at 40°C, a removal of 92% can be reached whereas only 57% is reached for a temperature of 60°C. Although higher inlet temperatures also negatively affect activated carbon and zeolite 13X, the extent of reduction in CO_2 removal is lower than for the supported amine adsorbent due to much lower CO_2 capacities at higher temperature associated with this adsorbent. For effective CO_2 separation in the adsorber, the adsorbent needs to be cooled before entering the adsorber.

For the supported amine adsorbent and the activated carbon base case, it is assumed that the pores of the adsorbents are saturated with water as the adsorbent enters the adsorber. However, as the temperatures of the adsorbents are increased, the pores are below saturation and therefore less water is desorbed from the adsorbent. This encourages higher temperatures inside the adsorber. This is another reason why the CO_2 recovery drops sharply at higher inlet adsorbent temperatures (cf. Figure 6.47). Alternatively, the concentration of the adsorbent pores could have been adjusted such that the relative humidity of the pores is held constant at 100% for increasing adsorbent temperatures.

The difference in profiles of the equilibrium loading and the actual loadings for adsorbent entering at a low and high temperature is shown in Figures 6.48 and 6.49. Not only are the loadings higher at the lower temperature but adsorption occurs in the entire column as opposed to primarily at the gas inlet

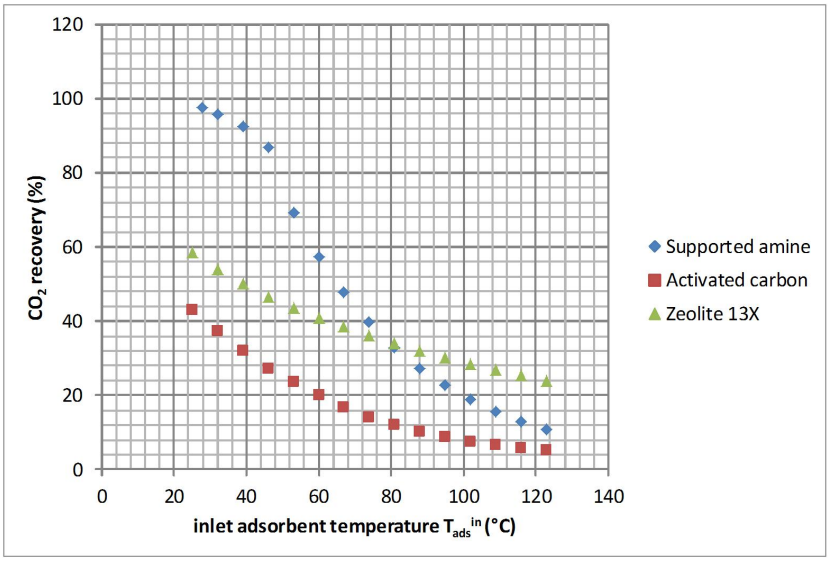

Figure 6.47: Effect of inlet adsorbent temperature on recovery

and outlet at 123°C as shown in Figure 6.49.

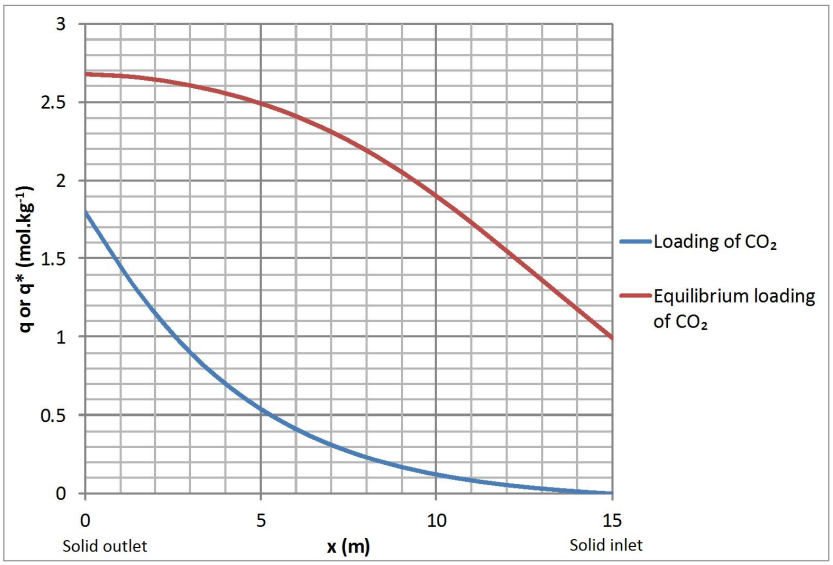

Figure 6.48: CO_2 loading profiles in a counter-current adsorber with supported amine adsorbent and pores saturated with water for adsorbent entering at 27°C

The difference in adsorbent temperature profiles for inlet adsorbent temperatures of 27°C and 123°C is shown in Figure 6.50. The adsorbent temperature increases overall if the adsorbent enters at 27°C. The adsorbent temperature increases initially as the adsorbent enters at 123°C and it stays constant in most of the column, however, it drops at the gas inlet as it comes into contact with gas entering at lower temperature.

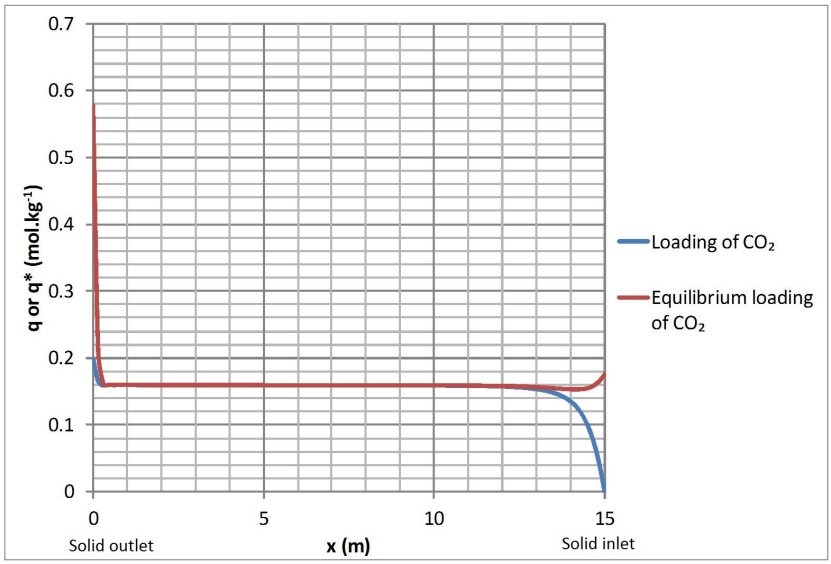

Figure 6.49: CO_2 loading profiles in a counter-current adsorber with supported amine adsorbent and pores saturated with water for adsorbent entering at 123°C

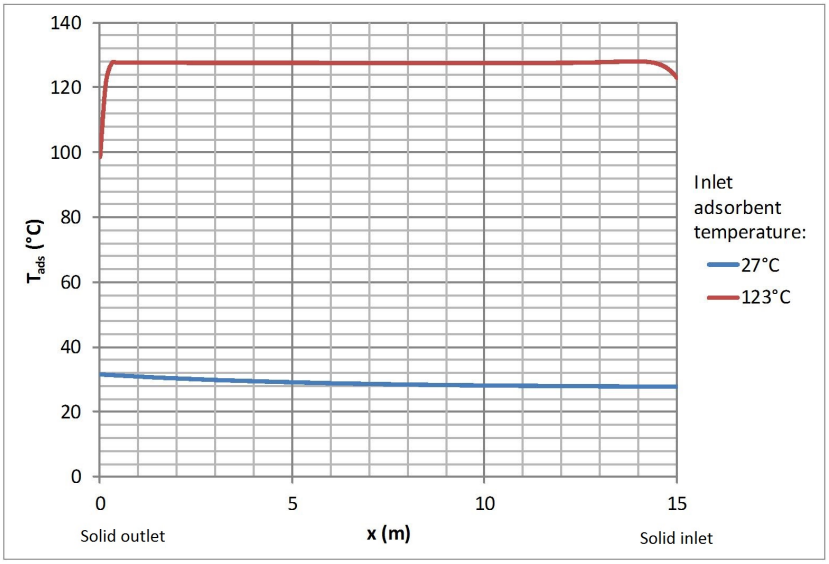

Figure 6.50: Adsorbent temperature profiles in a counter-current adsorber with supported amine adsorbent and pores saturated with water for inlet adsorbent temperatures of 27°C and 123°C

6.16 Effect of Heat Removal from the Adsorber

The rate of heat removed from the adsorber, Q, has been included in the energy balance given by Equation 3.33. It is given as:

$$Q = -U_{ext} A_{ext} (T - T_{ext}) \tag{6.1}$$

Increasing the rate of heat removed from the adsorber is shown to offer small improvements of CO_2 recovery for the amine supported adsorbent and the activated carbon (cf. Figure 6.51).

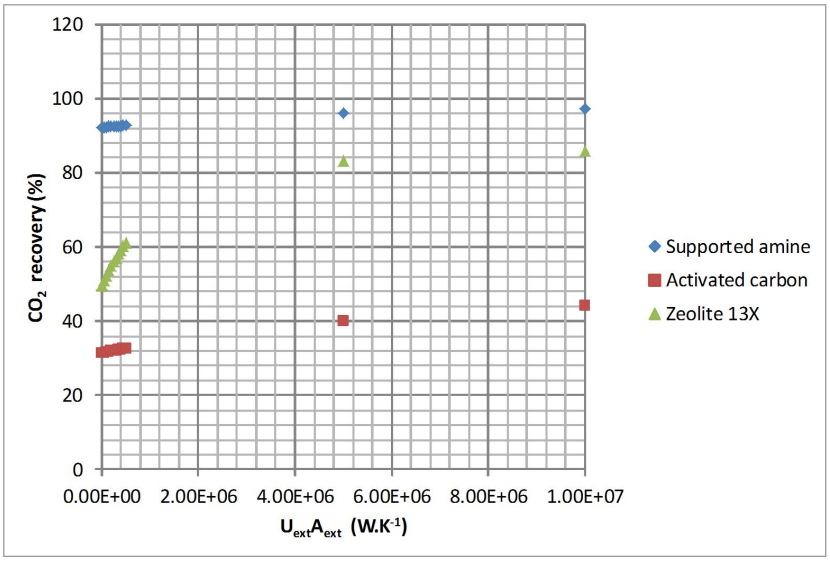

Figure 6.51: Effect of the product of the overall heat transfer coefficient and area on recovery

The ambient coolant is at T_{ext}=25°C. For any significant amount of heat removed from the adsorber, a very large value of $U_{ext}A_{ext}$ is likely to be required. This would correspond to an isothermal adsorber. This may result in excessive capital cost penalties for only small improvements in CO_2 capture performance. Alternatively, reducing the temperature of the adsorbent before entering the adsorber may offer better CO_2 capture performance.

The removal of heat has a greater positive effect on a system using zeolite 13X for which there is a larger increase in the temperature of the adsorbent. With a sufficiently high $U_{ext}A_{ext}$ value, CO_2 can be increased from 48% with no heat removal to 82% if $U_{ext}A_{ext} = 10^7$ W.K^{-1}.

The effect of the removal of heat is shown by the temperature profiles in Figure 6.52. The shape of the temperature profiles changes significantly as more heat is removed and the adsorbent leaves the adsorber at lower temperatures. The temperature rises less abruptly as the adsorbent enters the column. For a high $U_{ext}A_{ext}$ value of 10^7 W.K^{-1}, the temperature in the adsorber drops at the adsorbent inlet despite heat being produced as CO_2 is adsorbed at this location. The temperature then gradually increases. Nearly half of the bed operates below the gas/solid inlet temperature which allows higher CO_2 loadings but as more CO_2 is adsorbed, the heat produced exceeds the heat removed near the gas inlet.

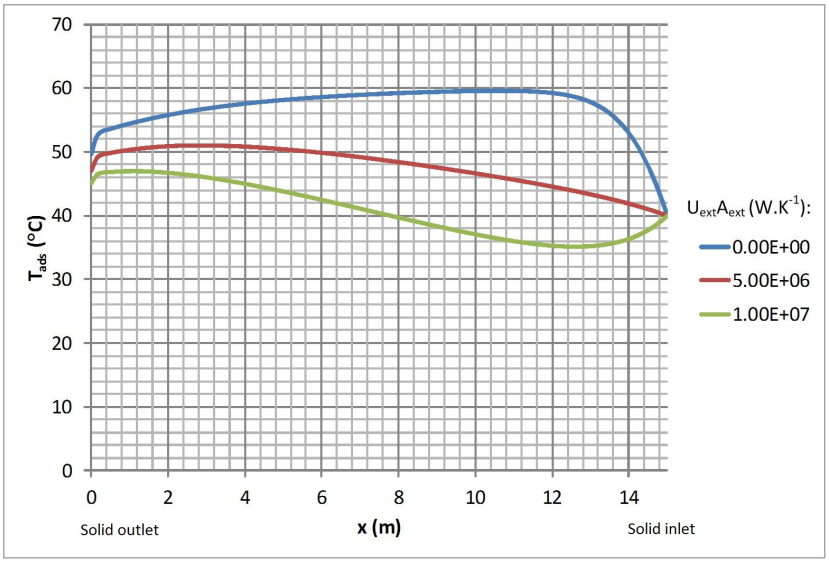

Figure 6.52: Adsorbent temperature profiles for a counter-current adsorber with amine supported adsorbent (pores saturated with water) for various $U_{ext}A_{ext}$ values

6.17 Conclusions

Profiles of concentrations, loadings, temperatures and pressure inside a counter-current adsorber have been shown for a supported amine adsorbent that does not contain CO_2 prior to entering the column. It has been found that as CO_2 is adsorbed, water is desorbed because the adsorbent enters the column pre-loaded with water and the temperature in the adsorber increases. The performance of the supported amine adsorbent has been compared against activated carbon and zeolite 13X adsorbents inside moving bed adsorbers.

Sensitivity analyses have been carried out for a number of conditions and a wide range of parameters. This has enabled us to find out which of these would affect the performance of the adsorber the most. These studies also allow us to find out which inlet conditions would be preferable when the full moving bed CO_2 adsorption cycle is analysed later in Chapter 8.

Some of the most important findings from this chapter are summarised:

- A counter-current adsorber or a series of counter-current fluidised beds allow higher CO_2 recoveries than a co-current adsorber or a single fluidised bed adsorber for a given flowrate of adsorbent. The adsorbent flowrate would need to be increased significantly in co-current and fluidised beds to achieve a high CO_2 recovery.

- The supported amine adsorbent gives the highest CO_2 loadings at the conditions at which the flue gas enters the adsorber. This adsorbent

allows higher CO_2 recoveries for a given mass flowrate of adsorbent than activated carbon or zeolite 13X (under dry conditions).

- As it has been assumed that water is adsorbed non-competitively with CO_2 onto the supported amine adsorbent and activated carbon, its presence improves the CO_2 removal from the flue gas because the temperature in the adsorber is lowered due to water being desorbed.

- The mass transfer rate has an important effect on CO_2 removal in a counter-current adsorber. Accurate values for the mass transfer constant would need to be measured because this parameter would influence greatly the mass flowrate of adsorbent or the size of the column required.

- The adsorbent plays a greater role in the movement of heat than the gas because its heat capacity rate is larger than for the gas. Therefore, in order to reach higher CO_2 recoveries, it is more important that the adsorbent is cooled before entering the counter-current adsorber than the gas.

In the following chapter, a similar analysis is carried out for a single regenerator.

Chapter 7

Analysis of a Regenerator

7.1 Introduction

After having analysed a standalone adsorber previously in Chapter 6, a similar analysis for a standalone regenerator is carried out in this chapter. For a chosen base case regenerator, the flowrate and properties of the adsorbent used at the inlet are the same as those found from the outlet of the base case adsorber used in Chapter 6. The regenerator gas used for the base case is steam but mixtures of steam and pure CO_2 have also been considered. The impact of the parameters on adsorbent regeneration performance to be investigated are:

- Type of the moving bed regenerator
- Type of adsorbent
- Mass flowrate of adsorbent
- Mass transfer constant
- Mole fraction of CO_2 in the regeneration gas
- Inlet loading of CO_2 in the adsorbent
- Molar flowrate of regeneration gas
- Inlet regeneration gas temperature
- Inlet adsorbent temperature
- Heat added to the regenerator

To evaluate the performance of the regenerator, the following parameters are considered:

- CO_2 removed from the adsorbent which is the percentage of CO_2 removed from the inlet adsorbent:

$$CO_2 \text{ removed } \% = 100 \times \frac{\dot{m}_{in} q^{in}_{CO_2} - \dot{m}_{out} q^{out}_{CO_2}}{\dot{m}_{in} q^{in}_{CO_2}} \tag{7.1}$$

- Wet purity of CO_2 is the percentage of CO_2 (on a molar basis) in the outlet regeneration gas containing water:

$$CO_2 \text{ wet purity } \% = 100 \times y^{out}_{CO_2} \tag{7.2}$$

- Dry purity of CO_2 is the percentage of CO_2 (on a molar basis) in the outlet regeneration gas without water:

$$CO_2 \text{ dry purity } \% = 100 \times \frac{y^{out}_{CO_2}}{y^{out}_{CO_2} + y^{out}_{N_2}} \tag{7.3}$$

7.2 Regenerator Base Case

7.2.1 Base Case Conditions

The base case for the analysis of the standalone regenerator is a counter-current regenerator with supported amine adsorbent. Pure steam is used as the regenerator gas at the inlet. 96% of adsorbed CO_2 is removed in the base case regenerator. A diagram of the single regenerator is given in Figure 7.1 and values of the operating and simulation parameters that were used are given in Table 7.1.

The same vessel size as Fisher et al. (2005) for the regenerator in the amine absorption process was used for the standalone regenerator of the adsorbent. Fisher et al. (2005) used one absorber for one regenerator and a similar configuration is used here where one regenerator is used to regenerate the adsorbent coming from an adsorber. The flowrate of steam used as the regeneration gas was chosen such that 96% of CO_2 is removed from the adsorbent. In this moving bed regenerator, steam is fed directly into the column whereas in amine absorption, steam is supplied to a reboiler which heats the amine solution.

Although the same packing is assumed in the regenerator as for the adsorber, the hold-up of solid in the regenerator is higher than in the base case adsorber as hold-up was found to increase for higher adsorbent superficial velocities, according to Equation 3.49.

The pore concentrations of CO_2, C^{in}_{p,CO_2}, water, C^{in}_{p,H_2O} , and N_2, C^{in}_{p,N_2} are the same as those at the outlet of the base case adsorber (Chapter 6). The

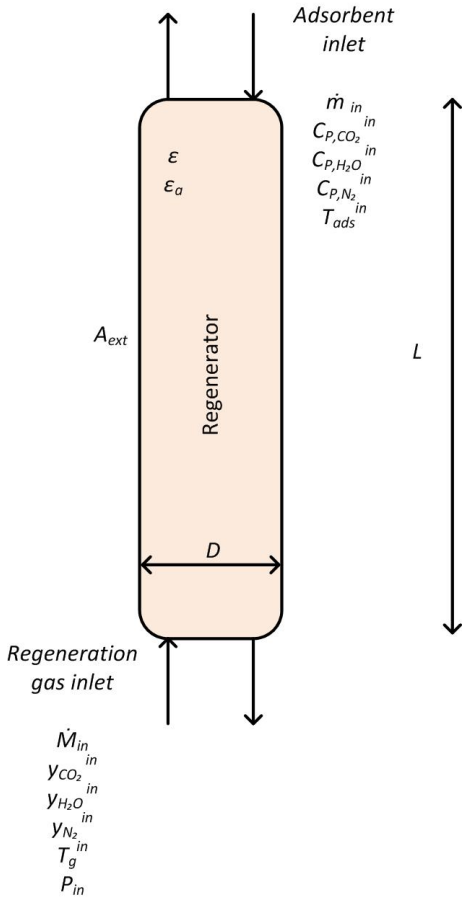

Figure 7.1: Single Regenerator (Counter-current)

incoming adsorbent temperature, T_{ads}^{in}, has been chosen to be high enough so that steam in the regeneration gas does not condense on the adsorbent.

The same LDF constants as for the base case adsorber have been assumed for the base case regenerator. Due to insufficient experimental data available for calculating k_i values, the same value as for the base case adsorber has been assumed and the effect of a variation in this mass transfer coefficient was investigated.

Finally, the solver choices for the number of discretisations and the weight factor, α, are the same as for the base case adsorber in Chapter 6.

7.2.2 Profiles for the Regenerator Base Case

The CO_2 loading increases slightly as adsorbent enters the regenerator at $x =$ 10 m (cf. Figure 7.2) because the gas contains the highest concentration of CO_2 at the gas outlet and the temperature of the adsorbent is lowest as it enters the regenerator (cf. Figure 7.3). However, as the temperature of the adsorbent in the regenerator increases and the concentration of CO_2 in the gas drops as the adsorbent leaves the regenerator (at the gas inlet in Figure 7.4), the

Table 7.1: Parameters used for the base case regenerator

Parameter	**Unit**	**Value**
L	m	10
D_C	m	6
ε_a	-	0.092
ε_p	-	0.4
ε_{pk}	-	0.01
P_{in}	Pa	101325
T_g^{in}	°C	100
M_{in}	mol.s^{-1}	1000
$\dot{m}_{in}$	kg.s^{-1}	375
$y_{CO_2}^{in}$	-	0
$y_{H_2O}^{in}$	-	1
$y_{N_2}^{in}$	-	0
k_{CO_2}	s^{-1}	10
k_{H_2O}	s^{-1}	10
k_{N_2}	s^{-1}	10
A_{ext}	m^2	0
C_{p,CO_2}^{in}	mol.m^{-3}	2.06
C_{p,H_2O}^{in}	mol.m^{-3}	4.36
C_{p,N_2}^{in}	mol.m^{-3}	30.46
$q_{CO_2}^{in}$	mol.kg^{-1}	0.45
$q_{H_2O}^{in}$	mol.kg^{-1}	0.95
$q_{N_2}^{in}$	mol.kg^{-1}	0
T_{ads}^{in}	°C	89.0
Number of discretisations	-	100
α	-	0.75

CO_2 loading drops as the adsorbent reaches the bottom of the counter-current adsorber, as shown in Figure 7.2. Steam is used as the regeneration gas and it is adsorbed therefore the loading of water increases. The amount of adsorbed N_2 remains at zero because it is assumed that this component is non-adsorbable but it is present within the pores of the incoming adsorbent. Profiles of the mole fraction of CO_2 water and N_2 in the base-case regenerator are shown in Figure 7.4. Because CO_2 is desorbed, its mole fraction in the gas increases. On the other hand, water is adsorbed so its mole fraction drops in the bulk gas.

Temperature profiles of the adsorbent and gas are shown in Figure 7.3. The solid temperature increases as it passes through the regenerator. As adsorbent enters the column at a lower temperature than the regeneration gas, its temperature increases to meet the gas temperature. In addition, there is a release of heat in the regenerator because the overall amount of CO_2 and

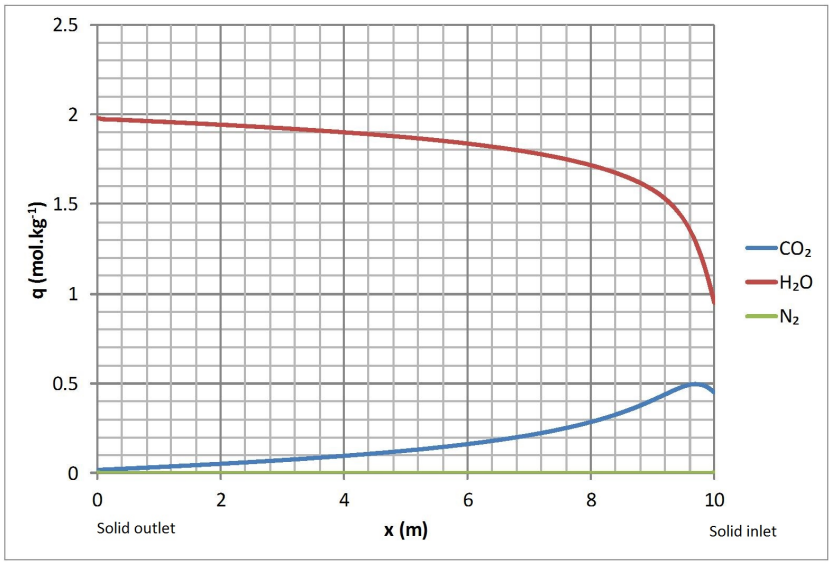

Figure 7.2: Loading profiles for a counter-current regenerator with amine supported adsorbent

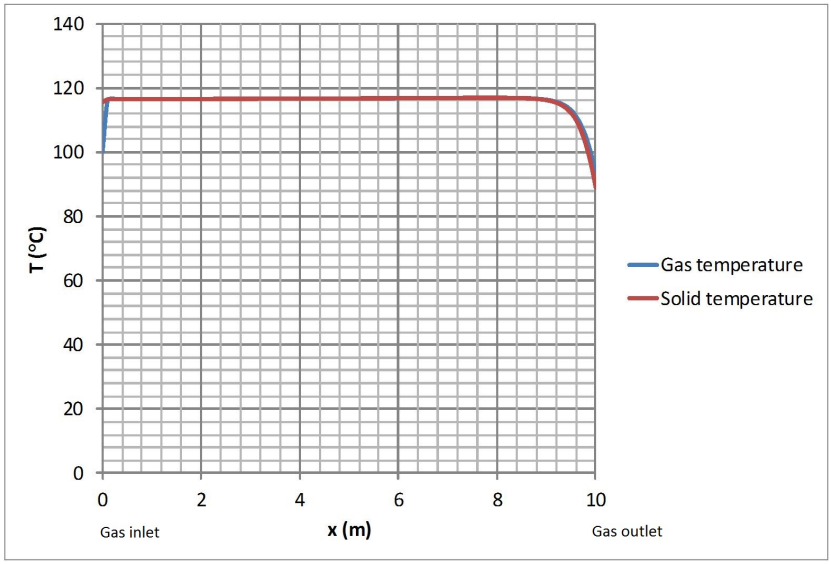

Figure 7.3: Temperature profiles for a counter-current regenerator with amine supported adsorbent

water adsorbed increases as shown by Figure 7.5. This also contributes to the overall rise in temperature of the solid and gas to above the steam and solid inlet temperatures. A similar trend in the adsorbent temperature profile was found for a counter-current regenerator of zeolite 13X (Kim et al. (2013a)). The temperature of the adsorbent used increased as it was indirectly heated with steam.

The pressure drop profile for the regenerator is shown in Figure 7.6. A lower pressure drop is found in the regenerator than for the adsorber considered in Chapter 6 (Figure 6.6) because the velocity of the gas is higher in the

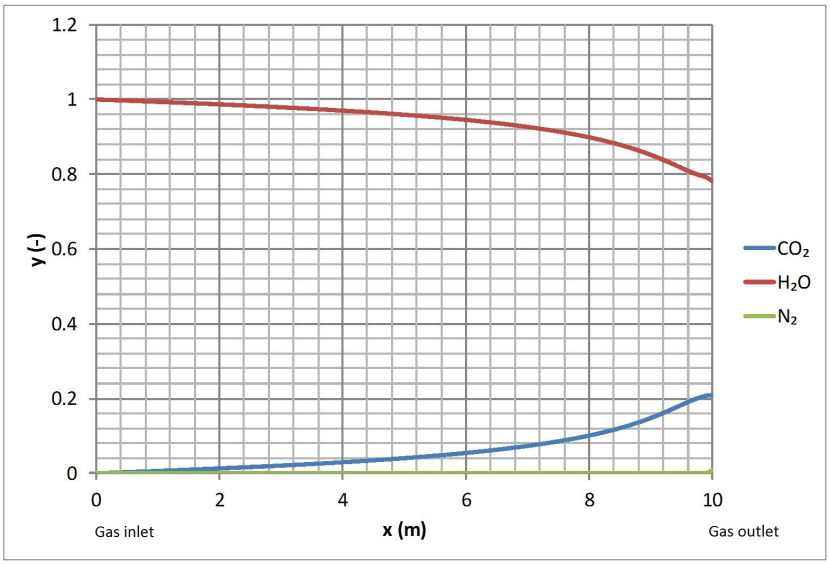

Figure 7.4: Mole fraction profiles for a counter-current regenerator with amine supported adsorbent

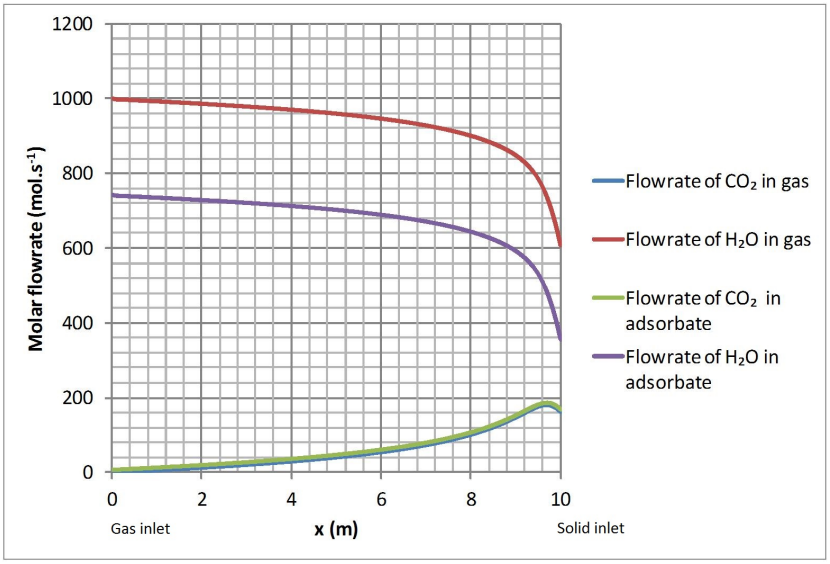

Figure 7.5: Profiles of flue gas molar flowrate for a counter-current regenerator with amine supported adsorbent

regenerator than the adsorber.

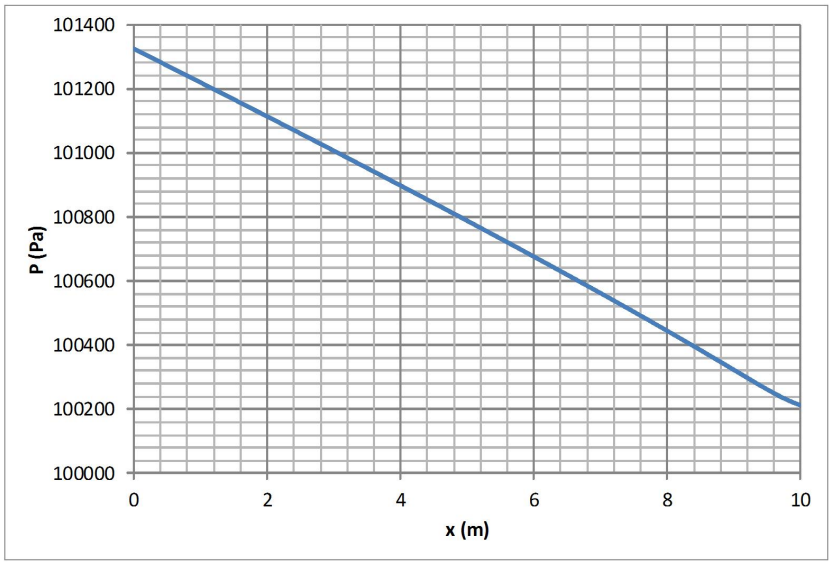

Figure 7.6: Pressure profile for a counter-current regenerator with amine supported adsorbent

7.3 Impact of Isotherm Model Errors on the Regenerator

In section 6.3, it was seen that the error between the modelled and measured CO_2 isotherm values in Figure 3.10 were relatively high for temperatures above 100°C. As the regenerator operates above this temperature, it is conceded that there is a higher uncertainty in the results found in this chapter than for the adsorber studied in Chapter 6. At higher temperatures, the CO_2 equilibrium loadings are overestimated by the isotherm model (Equations 3.51-3.53). Therefore, the performance of the regenerator is somewhat underestimated because the loadings achieved at the given regenerator temperatures should in fact be lower than predicted by the isotherm model. The curve for the CO_2 loading profile in Figure 7.2 should thus be positioned slightly lower. Consequently, the curve for the CO_2 mole fraction profile in Figure 7.4 would in fact be positioned slightly higher as more of the CO_2 would be driven off from the adsorbent.

From Figure 3.11, it is unsure how large the uncertainty is for the modelled isotherm values because of the lack of measured data above 65°C.

7.4 Effect of the Type of Regenerator

In the co-current regenerator, the adsorbent is added at a temperature of 100°C instead of 89°C for the counter-current regenerator, to avoid the condensation of steam at the gas inlet.

Table 7.2 compares the performance of the three types of moving bed regenerators with the same inlet conditions specified in Table 7.1. In each of these cases the adsorbent is the supported amine adsorbent and the same flowrate of pure steam as for the counter-current regenerator is used. The percentage of CO_2 desorbed and the wet purity of CO_2 for the counter-current regenerator are significantly higher than co-current and fluidised bed regenerators.

Table 7.2: CO_2 recoveries and purities (molar basis) for supported amine adsorbents in three different regenerators

	Counter-current	Co-current	Fluidised bed
CO_2 removed	95.8%	57.2%	47.9%
wet CO_2 purity	20.9%	8.0%	10.6%
dry CO_2 purity	95.8%	89.9%	92.0%

The profiles for the CO_2 mole fraction and loading in the three regenerators can be compared in Figures 7.7 and 7.8 respectively. For the co-current bed, the CO_2 mole fraction increases but stagnates towards the gas outlet because the CO_2 loading has reached the equilibrium loading limited by the CO_2 concentration in the bulk gas (as shown in Figure 7.9). For the counter-current bed, the mole fraction continues to increase towards the gas outlet and there is a greater reduction in CO_2 loading as the adsorbent travels down the column. The equilibrium CO_2 loading at the adsorbent outlet ($x = 10$ m) is zero as shown on Figure 7.10 which allows the actual loading to be lower than for the co-current regenerator. Temperature profiles for the three types of regenerators can be compared in Figure 7.11. The adsorbent temperature at the outlet of the co-current regenerator reaches a higher temperature than for the counter-current and fluidised bed regenerators because the adsorbent has been introduced at a higher temperature.

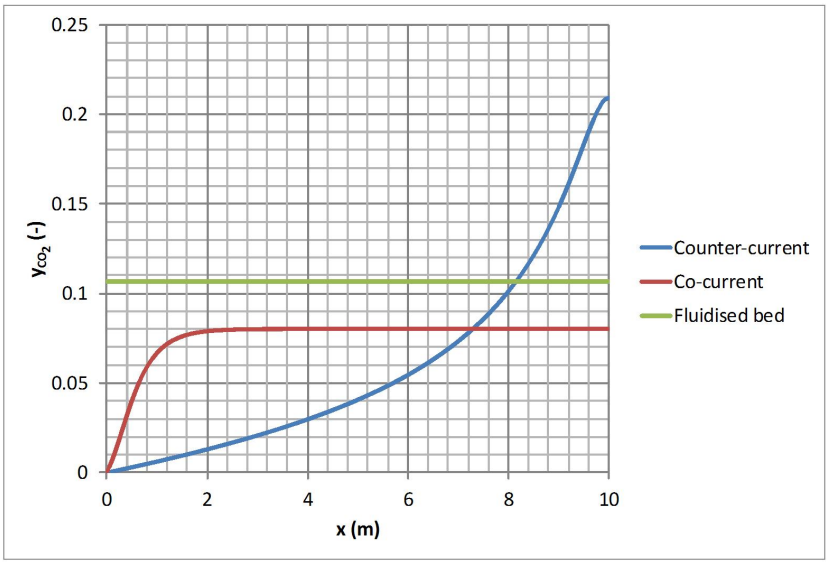

Figure 7.7: Mole fraction profiles of CO_2 for counter-current, co-current and fluidised bed regenerators with amine supported adsorbent

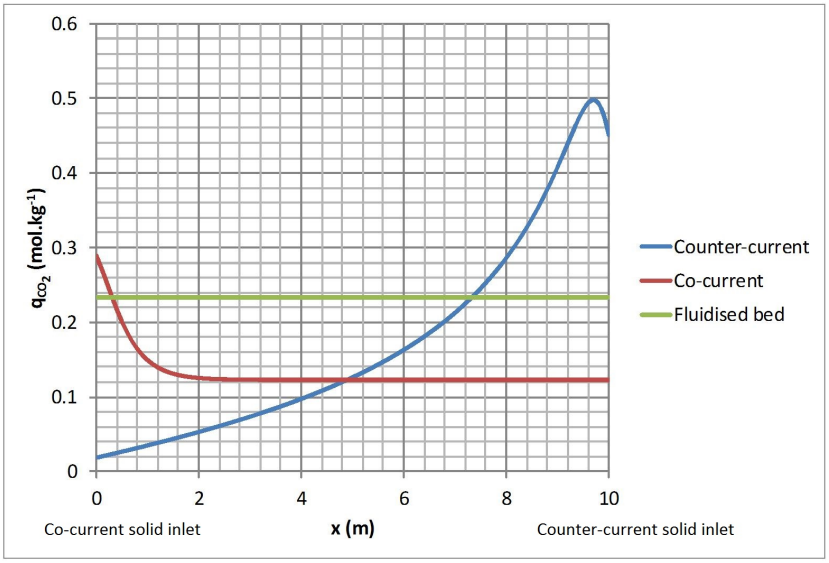

Figure 7.8: CO_2 loading profiles for counter-current, co-current and fluidised bed regenerators with amine supported adsorbent

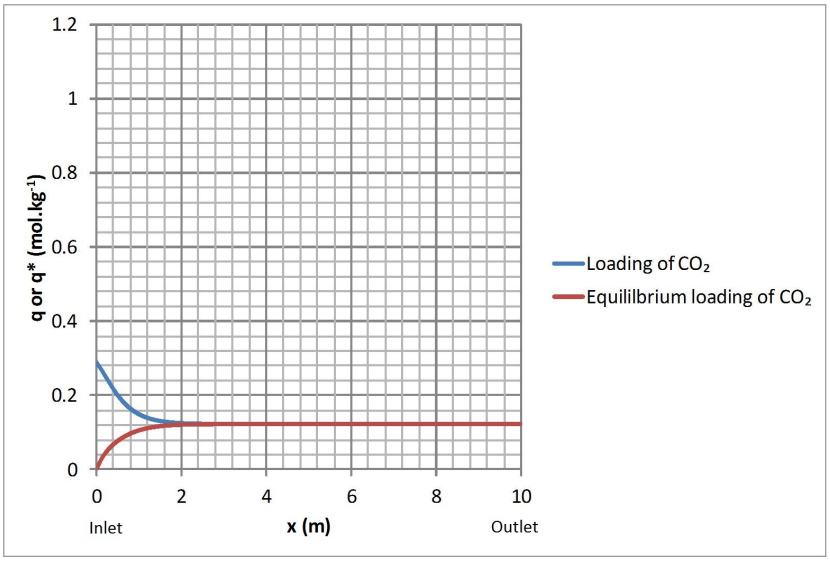

Figure 7.9: CO_2 loading and equilibrium loadings in a co-current regenerator with supported amine adsorbent

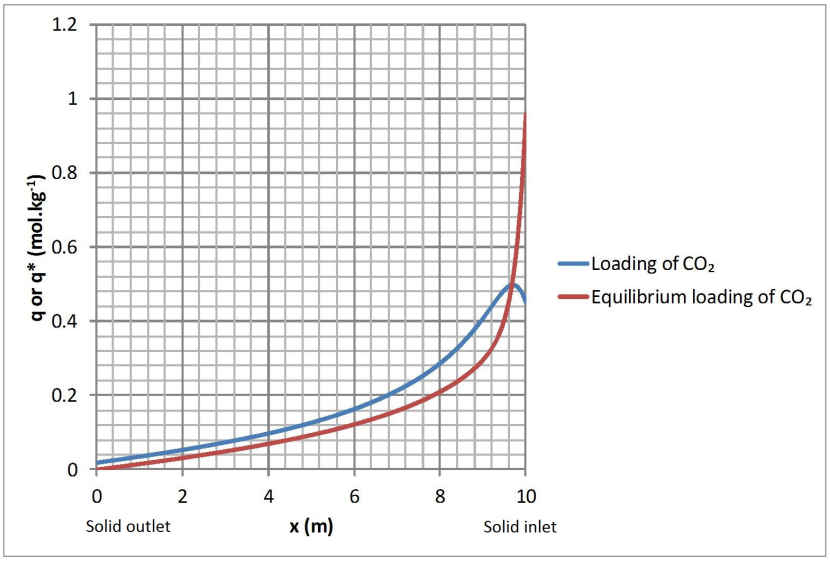

Figure 7.10: CO_2 loading and equilibrium loadings in a counter-current regenerator with supported amine adsorbent

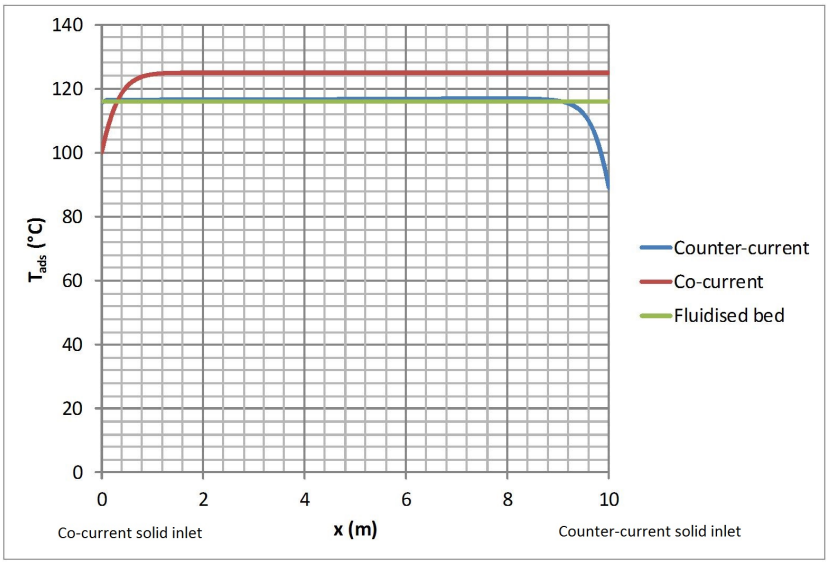

Figure 7.11: Adsorbent temperature profiles for counter-current, co-current and fluidised bed regenerators with supported amine adsorbent

7.5 Effect of the Adsorbent

This section compares profiles for activated carbon and the supported amine adsorbent in a counter-current regenerator. The supported amine adsorbent and activated carbon are mostly considered in this chapter because steam is used as the regeneration gas and it is unsuitable to use for regenerating zeolite 13X. Therefore an analysis of using a hot stream of CO_2 as regeneration gas for zeolite 13X will be made later in section 7.15 in this chapter.

For activated carbon in a counter-current regenerator, most of the inlet adsorbent and regeneration gas conditions were used as in Table 7.1. However, the mass flowrate of activated carbon in the adsorber has been increased to 1447.5 kg.s^{-1} in order to achieve 92.1% CO_2 capture in the adsorber (cf. Table 6.4). The same adsorbent mass flowrate is therefore used for the single counter-current regenerator with activated carbon that is studied in this section. The volume fraction of the activated carbon adsorbent in the counter-current regenerator is $\varepsilon_a = 0.158$ (cf. Equation 3.49). The adsorbent at the outlet of the single adsorber would contain different pore concentrations than the supported amine adsorbent (in Table 7.1). These new values are shown in Table 7.3. A higher steam flowrate has been chosen to remove more CO_2 from the adsorbent in the regenerator. Therefore, for all cases involving the counter-current regenerator with activated carbon, the parameters in Table 7.1 have been used except that the parameters shown in Table 7.3 have been replaced with new values also shown in Table 7.3. For the fluidised bed regenerator with activated carbon, the same parameter values as for the counter-current regenerator with activated carbon are used except that the volume fraction of adsorbent is replaced with $\varepsilon_a = 0.4$. For the co-current regenerator using activated carbon, the same parameter values as for the counter-current regenerator with activated carbon are used except that the inlet adsorbent temperature is 100°C.

Due to the adsorption of N_2 on activated carbon, a low dry CO_2 purity is found. SRI International et al. (2013) have considered activated carbon in a moving bed adsorption cycle however, to improve the CO_2 purity, they considered removing N_2 from the adsorbent before desorbing CO_2.

The performances of activated carbon in the counter-current, co-current and fluidised bed regenerators are shown in Table 7.4). As for the supported amine adsorbent, the counter-current regenerator offers the best performance.

Figure 7.12 shows that the mole fraction reached at the outlet of the regenerator is higher than for the supported amine adsorbent. This can be explained by lower CO_2 loadings on activated carbon than the supported amine adsorbent as shown by the isotherms on Figure 7.13. Therefore, more CO_2 remains in the

Table 7.3: Parameters used for activated carbon in the single counter-current regenerator

Parameter	**Unit**	**Value**
$\dot{M}_{in}$	mol.s^{-1}	1650
$\dot{m}_{in}$	kg.s^{-1}	1447.5
ε_a	-	0.158
C^{in}_{p,CO_2}	mol.m^{-3}	4.19
C^{in}_{p,H_2O}	mol.m^{-3}	3.5
C^{in}_{p,N_2}	mol.m^{-3}	30.17
$q^{in}_{CO_2}$	mol.kg^{-1}	0.17
$q^{in}_{H_2O}$	mol.kg^{-1}	0.53
$q^{in}_{N_2}$	mol.kg^{-1}	0.06

Table 7.4: Performance of the three types of regenerators with activated carbon

	Counter-current	Co-current	Fluidised bed
CO_2 removal	91.4%	46.5%	39.0%
wet CO_2 purity	52.4%	13.0%	15.7%
dry CO_2 purity	69.5%	53.6%	51.8%

bulk gas with activated carbon and therefore, the gas contains a higher mole fraction of CO_2.

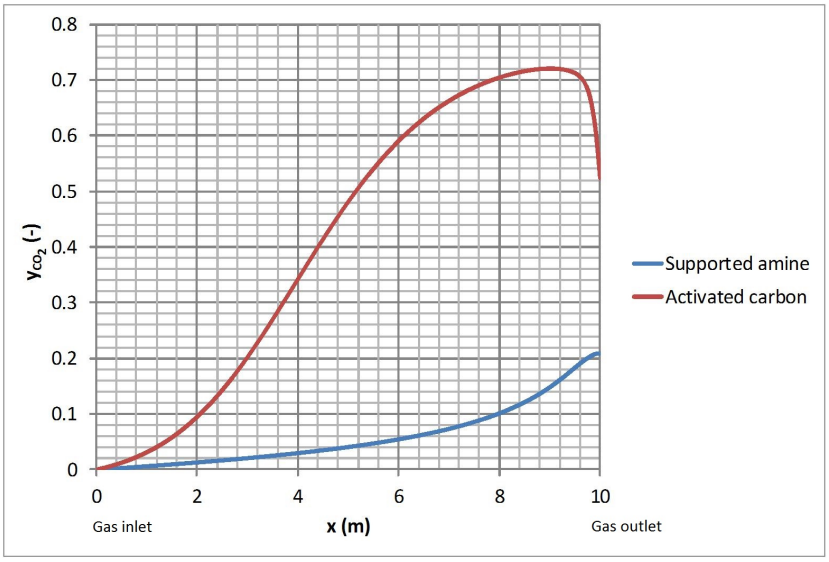

Figure 7.12: CO_2 mole fraction profiles for a counter-current regenerator with supported amine adsorbent and activated carbon

As the adsorbent enters the regenerator at $x = 10$ m on Figure 7.14, the CO_2 loading rises due to high mole fractions of CO_2 in near the gas outlet. But

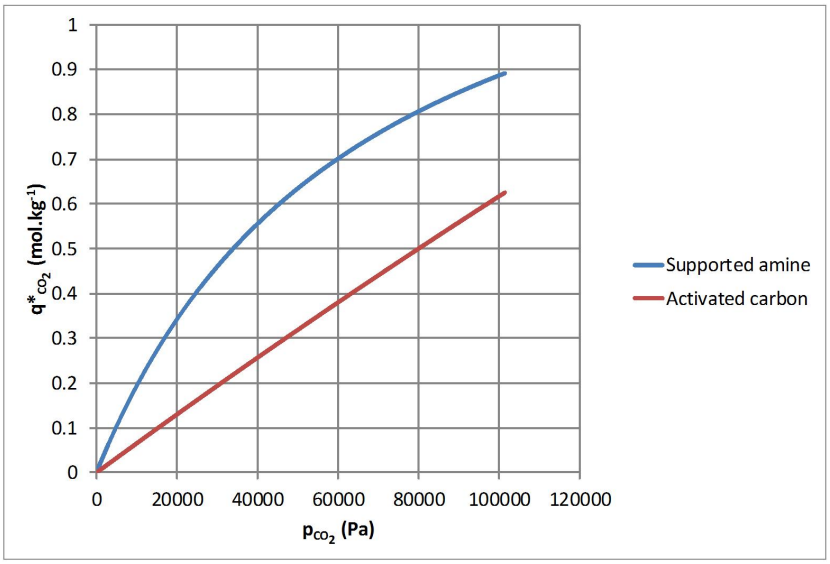

Figure 7.13: CO_2 isotherms for the supported amine adsorbent and activated carbon at 120°C

as the adsorbent travels towards the bottom of the regenerator, near the gas inlet, the regeneration gas has a lower CO_2 concentration because it consists mainly of steam. Therefore, the CO_2 loading drops.

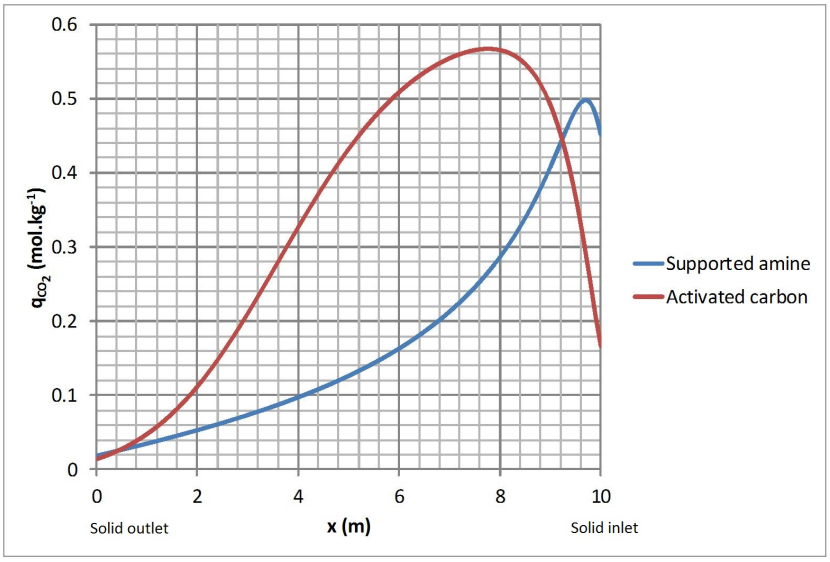

Figure 7.14: CO_2 loading profiles for a counter-current regenerator with supported amine adsorbent and activated carbon

Unlike for the supported amine adsorbent, the temperature of the activated carbon continues to increase as the adsorbent reaches the gas inlet. This occurs due to the water that is adsorbed as shown by the water loading profile in Figure 7.16 which has a trend which matches with the trend of the temperature profile. More water is loaded onto the activated carbon than the supported amine adsorbent and therefore more exothermic heat is released. The loading profile

of water on the amine supported adsorbent flattened as the adsorbent reached the bottom of the column (the gas inlet) as shown in Figure 7.2 and a flat temperature profile resulted for the exiting adsorbent at the bottom of the regenerator.

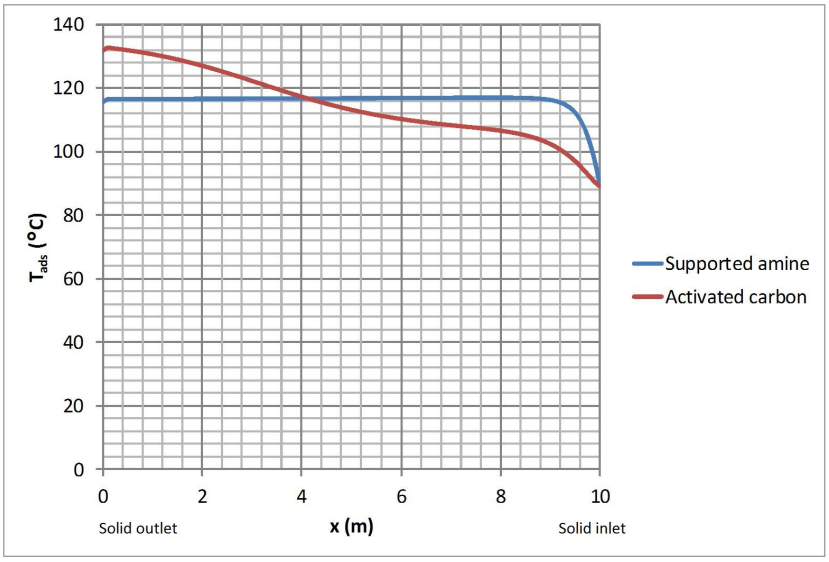

Figure 7.15: Adsorbent temperature profiles for a counter-current regenerator with supported amine adsorbent and activated carbon

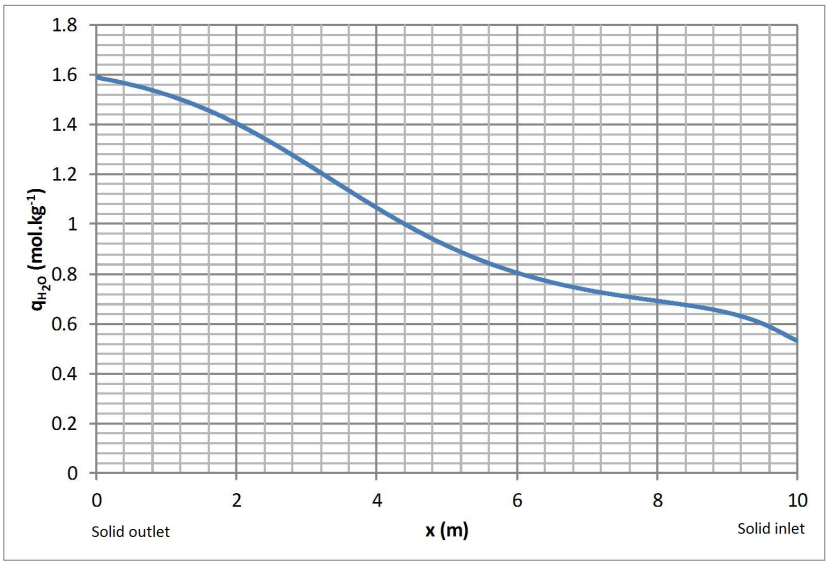

Figure 7.16: Water loading profile for a counter-current regenerator with activated carbon

7.6 Fluidised Bed Regenerators

The effect of dividing the column into equal sized fluidised bed regenerators is considered in this section. The same adsorbent inlet conditions and steam flowrate are assumed as for the regenerator base case (section 7.2.1).

As with the counter-current series of fluidised bed adsorbers, the best performance is found for a counter-current series of fluidised bed regenerators because greater CO_2 removals from the adsorbent and CO_2 purities are found (cf. Figures 7.17-7.22.

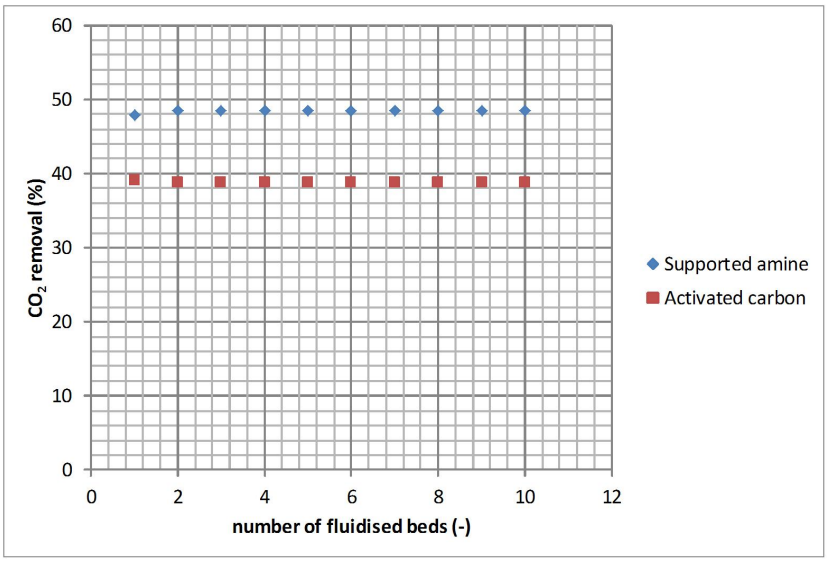

Figure 7.17: Effect of the number of co-current fluidised beds in the regeneration column on CO_2 removal from the adsorbent ($\varepsilon_a = 0.4$)

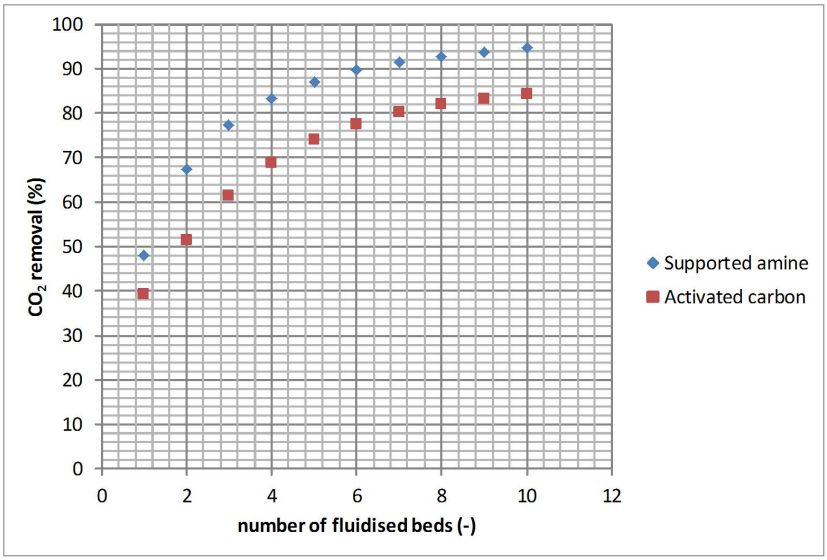

Figure 7.18: Effect of the number of counter-current fluidised beds in the regeneration column on CO_2 removal from the adsorbent ($\varepsilon_a = 0.4$)

A series of counter-current regenerators is particularly more effective for desorbing CO_2 than co-current fluidised bed regenerators because the adsorbent leaving the co-current regenerator is essentially at equilibrium with the regeneration gas outlet stream containing CO_2. The adsorbent leaving the counter-current regenerator is closer to equilibrium with gas containing a lower concentration of CO_2 if pure steam is used to regenerate the adsorbent.

The wet and dry CO_2 purities are enhanced in a series of counter-current fluidised bed regenerators. The wet CO_2 purities for co- and counter-current fluidised beds can be compared in Figures 7.19 and 7.20. Results for dry CO_2 purities are shown in Figures 7.21 and 7.22. The improvement in purities for counter-current systems can be explained by the fact that the loading of CO_2 on the adsorbent at the outlet is lower than for co-current systems, hence more CO_2 is desorbed into the regeneration gas in a counter-current regenerator. Wet and dry purities are therefore higher due to the additional rate of CO_2 desorbed from the adsorbent over a co-current series of fluidised beds.

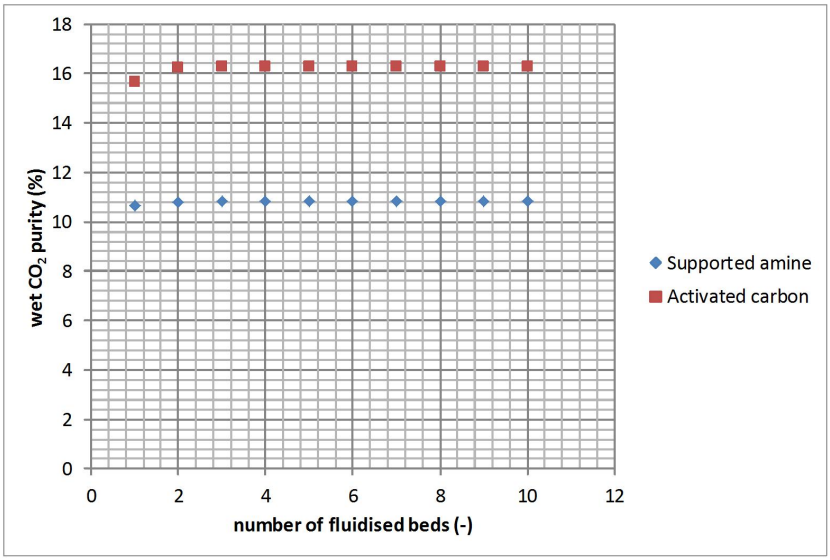

Figure 7.19: Effect of the number of co-current fluidised beds in the regeneration column on the wet purity of CO_2 in the regeneration gas outlet ($\varepsilon_a = 0.4$)

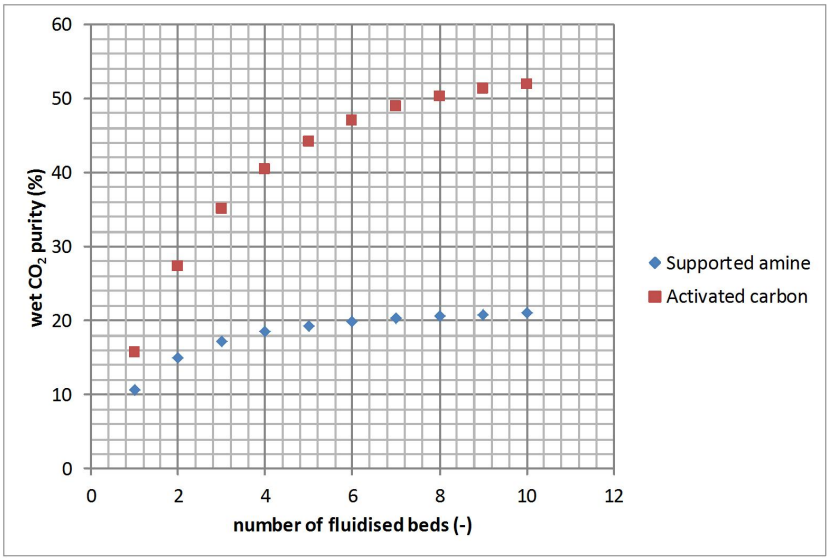

Figure 7.20: Effect of the number of counter-current fluidised beds in the regeneration column on the wet purity of CO_2 in the regeneration gas outlet ($\varepsilon_a = 0.4$)

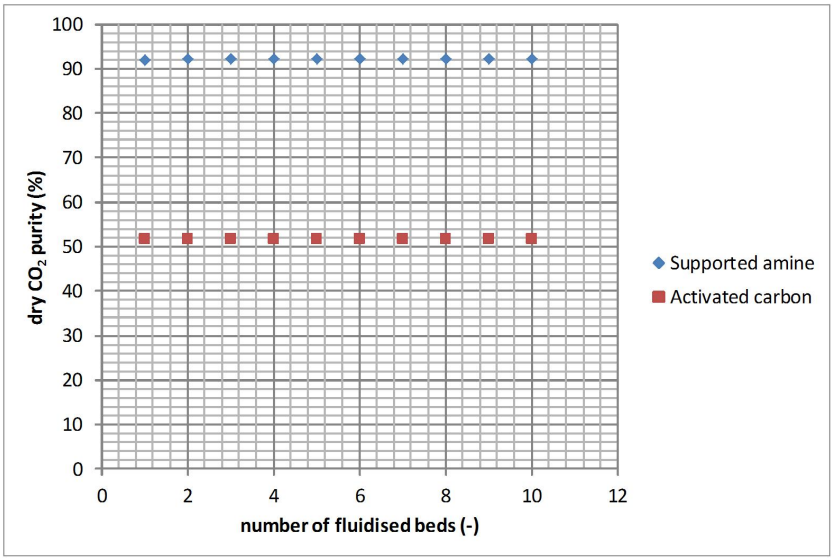

Figure 7.21: Effect of the number of co-current fluidised beds in the regeneration column on the dry purity of CO_2 in the regeneration gas outlet ($\varepsilon_a = 0.4$)

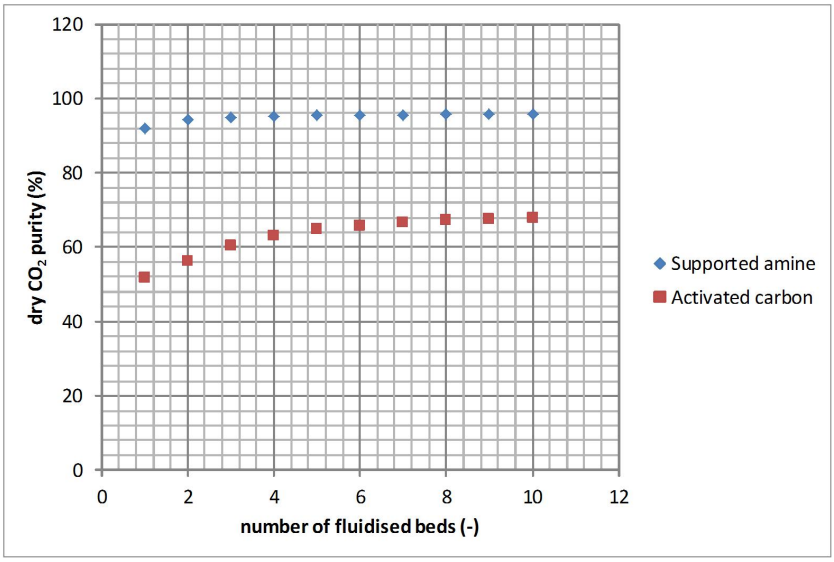

Figure 7.22: Effect of the number of counter-current fluidised beds in the regeneration column on the dry purity of CO_2 in the regeneration gas outlet (ε_a = 0.4)

7.7 Effect of Adsorbent Flowrate

The variation in the CO_2 removal from the supported amine adsorbent and activated carbon as a function of the mass flowrate of adsorbent is shown in Figure 7.23. The same steam flowrate as the regenerator base case was used and it is held constant. Increasing the mass flowrate of the adsorbent leads to a drop in the amount of CO_2 removed from the adsorbent because a higher flowrate of steam would be required to regenerate the adsorbent better.

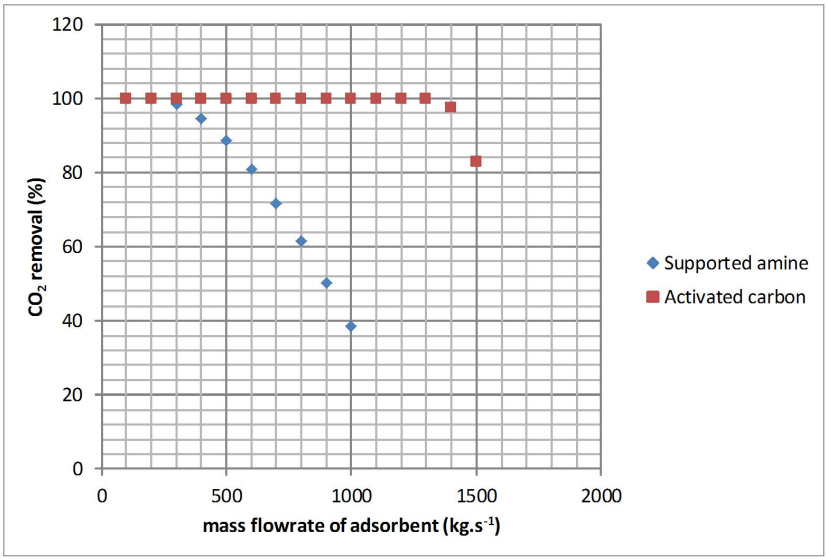

Figure 7.23: Effect of the mass flowrate of adsorbent on CO_2 removal from the adsorbent

The wet purity of CO_2 increases for higher adsorbent flowrates (cf. Figure 7.24) because more water would be adsorbed in the regenerator for higher adsorbent flowrates. Therefore, less water would be present in the outlet gas from the regenerator.

The plot of the dry CO_2 purity as a function of adsorbent flowrate show that the dry CO_2 purity drops for high adsorbent mass flowrates (cf. Figure 7.25) therefore, more N_2 is desorbed for higher mass flowrates of adsorbent. This is shown also by a drop in the wet CO_2 purity for the highest mass flowrates of adsorbent considered in Figure 7.24.

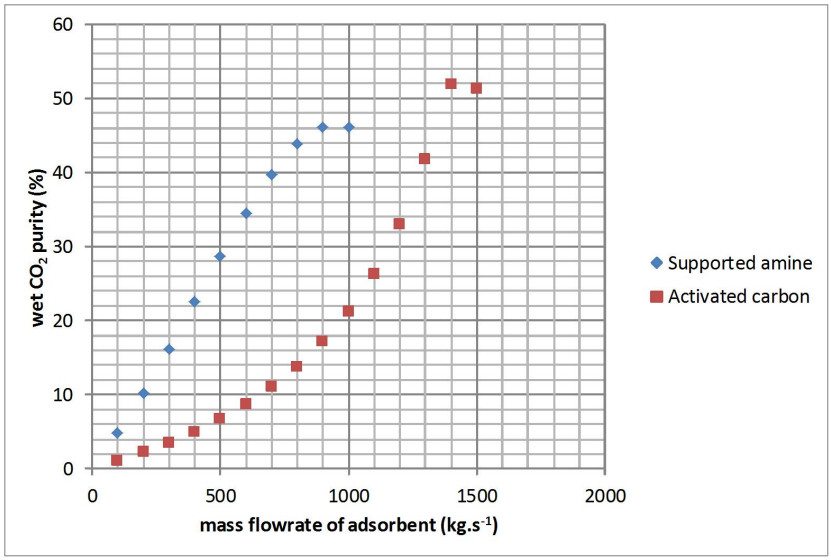

Figure 7.24: Effect of the mass flowrate of adsorbent on the wet purity of CO_2 in the regeneration gas outlet

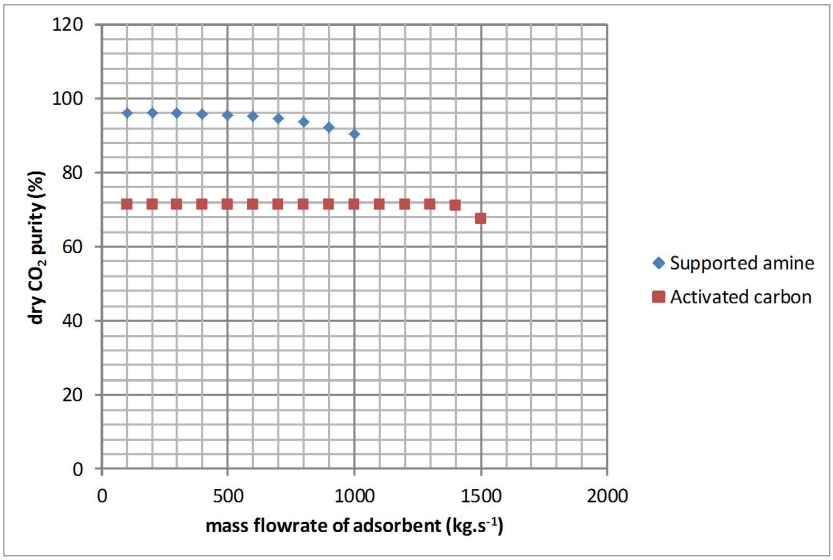

Figure 7.25: Effect of the mass flowrate of adsorbent on the dry purity of CO_2 in the regeneration gas outlet

7.8 Effect of CO_2 Mass Transfer Constant

The mass transfer constants of components CO_2, water and N_2 remain the same as each other but the effect of a variation in this parameter is considered in this section.

The effect of the mass transfer constant, k_{CO_2}, on the CO_2 removal from the adsorbent is shown in Figure 7.26. For the regenerator, the LDF expression for CO_2 (Equation 3.79) represents the rate of transfer of CO_2 from the pores of the adsorbent to the bulk gas phase. From Figure 7.26, for the supported

amine adsorbent, nearly full CO_2 removal is reached if $k_{CO_2} > 20$ s^{-1}.

For activated carbon, CO_2 removal from the adsorbent increases from $k_{CO_2} = 0.1$ s^{-1} to $k_{CO_2} = 20$ s^{-1}. However there is an unexpected drop in CO_2 removal for $k_{CO_2} > 20$ s^{-1}. This occurrence means that there is a greater CO_2 loading at the adsorbent outlet for $k_{CO_2} > 20$ s^{-1} than for lower k_{CO_2} values. This could either be due to a higher temperatures in the regenerator for $k_{CO_2} < 20$ s^{-1} than for $k_{CO_2} > 20$ s^{-1} or it could mean that the pore concentration of CO_2 at the adsorbent outlet is lower for $k_{CO_2} < 20$ s^{-1} than for $k_{CO_2} > 20$ s^{-1}. For example, considering $k_{CO_2} = 20$ s^{-1} and $k_{CO_2} = 500$ s^{-1}, the difference in adsorbent temperatures at the adsorbent outlet for for these two values of k_{CO_2} is small, as shown in Figure 7.27. Therefore, as shown in Figure 7.28, the lower CO_2 pore concentrations for $k_{CO_2} = 20$ s^{-1} leads to reduced CO_2 loadings. For $k_{CO_2} = 500$ s^{-1}, the higher pore concentration at the adsorbent outlet can be explained by higher CO_2 concentrations in the bulk gas, in proximity to the adsorbent outlet as shown in Figure 7.29.

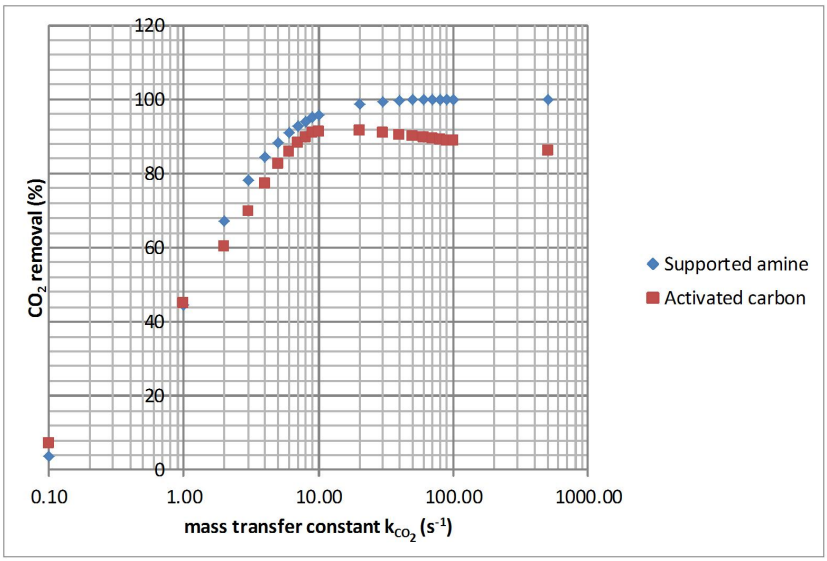

Figure 7.26: Effect on CO_2 removal of mass transfer constant for two different adsorbents

For low values of k_{CO_2}, less CO_2 would be removed from the adsorbent in the regenerator for both adsorbents. Therefore, the wet CO_2 purity is low as shown in Figure 7.30. For activated carbon, the wet CO_2 purity is higher than for the supported amine adsorbent because the outlet regeneration gas contains a higher mole fraction of CO_2 compared to water whereas the outlet regeneration gas for the supported amine adsorbent contains more water than CO_2. After removing water from the outlet regeneration gas for the regenerator using activated carbon, the higher presence of N_2 in the gas leads to lower dry CO_2 purities than for the supported amine adsorbent as shown in Figure 7.31.

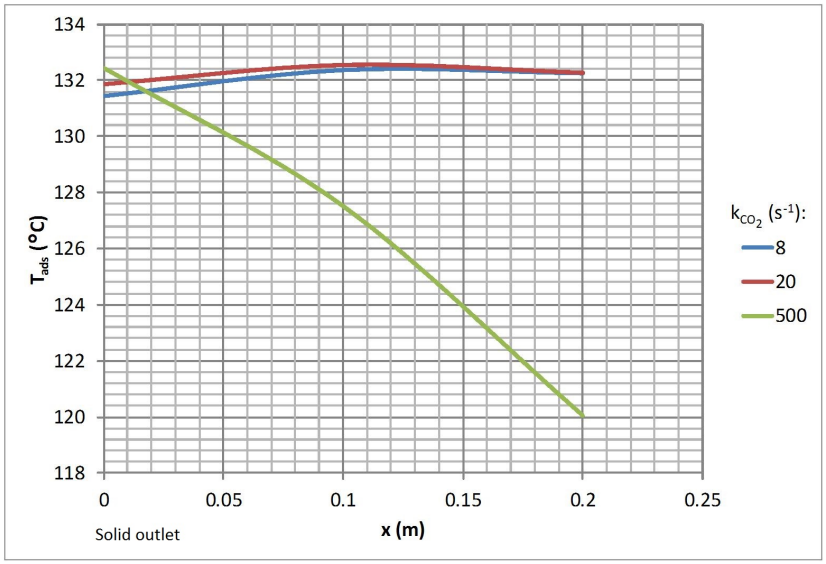

Figure 7.27: Adsorbent temperature profiles for various k_{CO_2} values at the adsorbent outlet from the counter-current regenerator with activated carbon

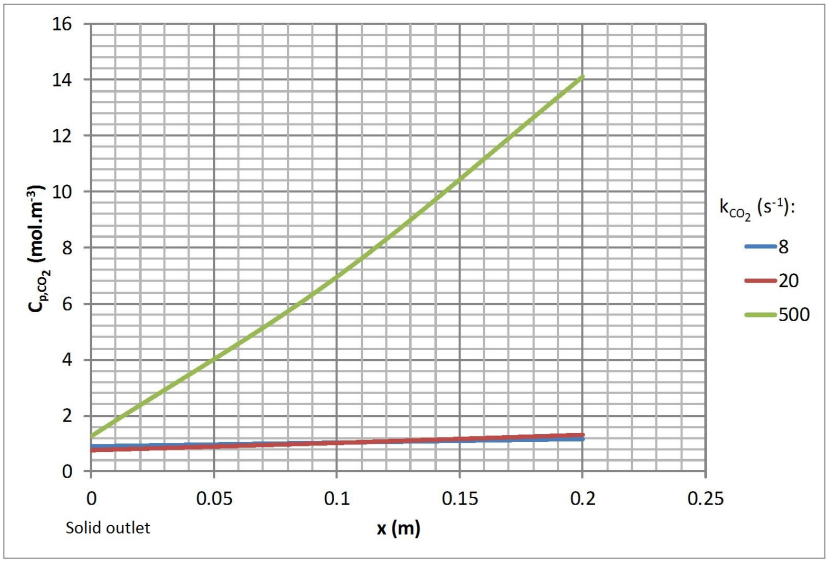

Figure 7.28: CO_2 pore concentration profiles for various k_{CO_2} values at the adsorbent outlet from the counter-current regenerator with activated carbon

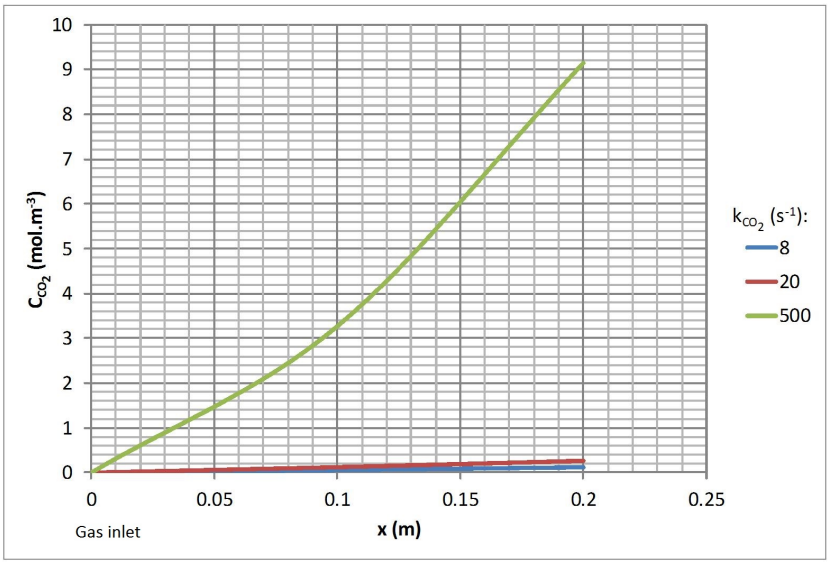

Figure 7.29: Profiles of CO_2 concentration in bulk gas for various k_{CO_2} values at the adsorbent outlet from the counter-current regenerator with activated carbon

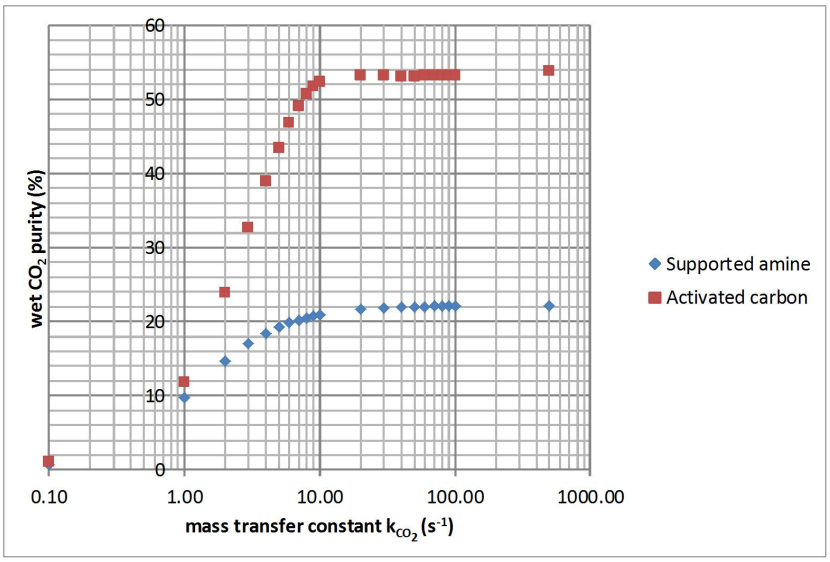

Figure 7.30: Effect on wet CO_2 purity of mass transfer constant for two different adsorbents

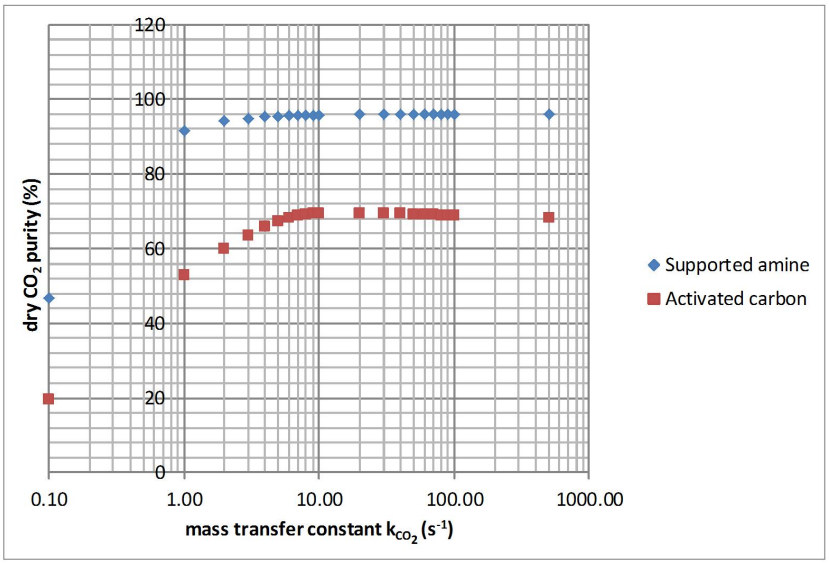

Figure 7.31: Effect on dry CO_2 purity of mass transfer constant for two different adsorbents

7.9 Effect of CO_2 in the Regeneration Gas

The objective of using a regeneration gas is to remove adsorbate from the adsorbent. It is typically introduced at a high temperature and it has the purpose of elevating the temperature in the bed and purging off adsorbate. For many CO_2 adsorption processes, CO_2, steam and N_2 are considered as regeneration gases.

At first thought, hot CO_2 is a logical choice because the CO_2 purity of the gas product would not be compromised. However, at low temperatures, there is a possibility that CO_2 would be adsorbed in the regenerator instead of being desorbed. Groups that have considered CO_2 as the regeneration gas include Krutka et al. (2013), Kim et al. (2013a), Yang and Hoffman (2009) and Zhang et al. (2014). Other groups such as SRI International (2010) have considered steam which can be condensed with a high purity CO_2 product remaining. The objective of capturing CO_2 is to obtain a CO_2 product with high purity and therefore regeneration with N_2 is not suitable. In this section, the overall flowrate of regneration gas is maintained the same as for the regenerator base case but the effect of having CO_2 in the regeneration gas, containing steam, is analysed.

As shown in Figure 7.32, instead of CO_2 being desorbed, it is actually adsorbed if pure CO_2 at an inlet temperature of 100°C is used for regenerating the supported amine and activated carbon. The presence of CO_2 in the regeneration steam reduces CO_2 removal from the adsorbent. Pure steam allows the highest removal of CO_2 for both adsorbents.

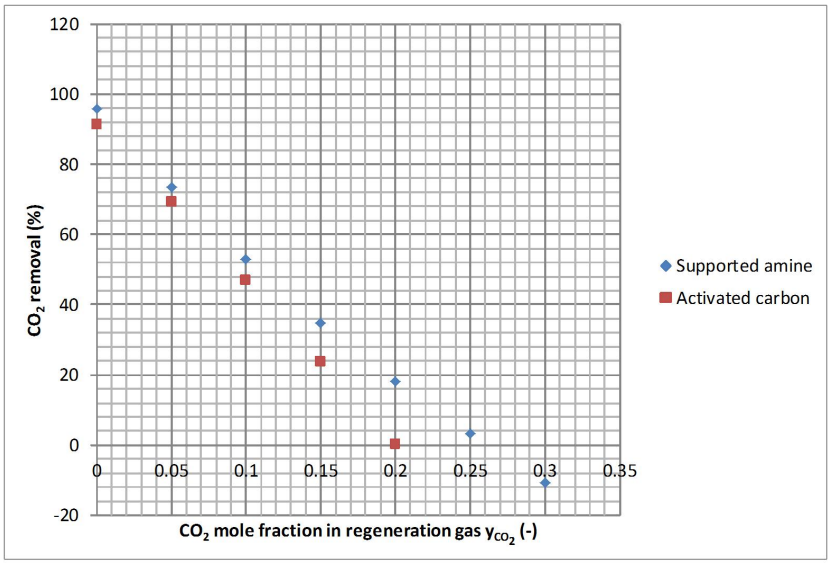

Figure 7.32: Effect of CO_2 mole fraction in the regeneration gas on CO_2 removal from the adsorbent

The purity of the gas at the outlet of the regenerator increases when higher concentrations of CO_2 are used in the regeneration gas as shown in Figures 7.33 and 7.34. If pure steam is used, the wet purity of CO_2 is low for both adsorbents because the gas contains a high concentration of water.

If water in the gas is condensed, the gas at the outlet of regenerator is of high CO_2 purity for the supported amine adsorbent as shown by the dry purity values in Figure 7.34. For activated carbon, the dry gas at the outlet of the regenerator contains higher concentrations of N_2 because it is adsorbed along with CO_2. As N_2 is assumed not to be adsorbed for the supported amine, the dry CO_2 purity is much higher.

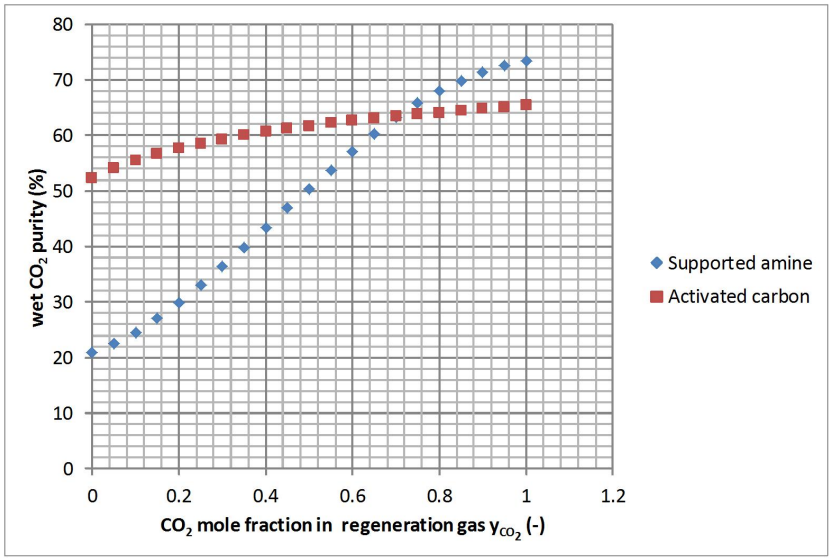

Figure 7.33: Effect of CO_2 mole fraction in the regeneration gas on the wet purity of CO_2 in the regeneration gas outlet

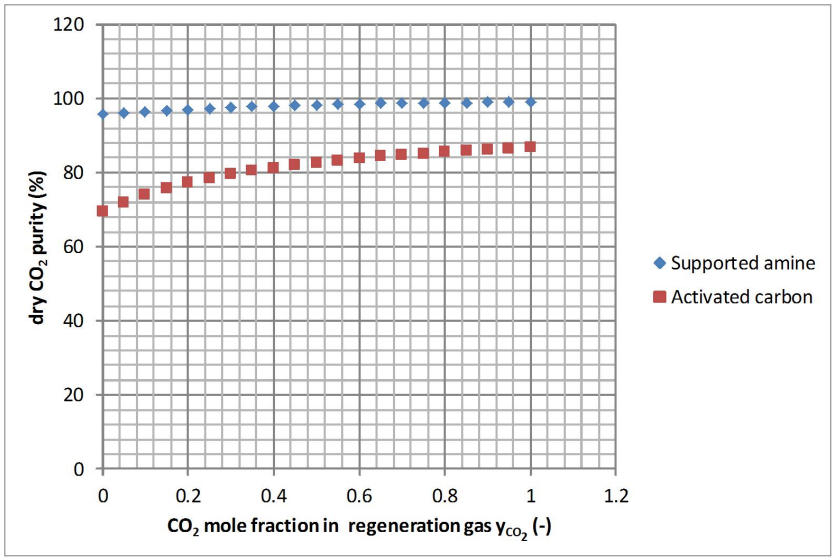

Figure 7.34: Effect of CO_2 mole fraction in the regeneration gas on the dry purity of CO_2 in the regeneration gas outlet

7.10 Effect of the CO_2 Loading at the Adsorbent Inlet

The effect of higher CO_2 loadings on the adsorbent at the inlet to the countercurrent regenerator is investigated in this section for the supported amine adsorbent and activated carbon.

Higher CO_2 loadings on the adsorbents at the inlet to the regenerator lead to a lower percentage of CO_2 removed from the adsorbent as shown in Figure 7.35. This can be explained from the isotherms shown in Figure 7.13. For higher CO_2 loadings, the regeneration gas would contain more CO_2 which makes it more difficult to achieve lower CO_2 loadings for the adsorbent leaving the regenerator. The lower CO_2 removal from the activated carbon can also be explained by the isotherms in Figure 7.13. For a given inlet CO_2 loading, the regeneration gas would contain a higher mole fraction of CO_2 for activated carbon and therefore the CO_2 loading on the adsorbent would be higher than for the supported amine adsorbent.

Regenerating adsorbent which contains higher CO_2 loadings, produces a gas with high concentrations of CO_2. Therefore there is an increase in the wet and dry CO_2 purities for higher CO_2 loadings at the adsorbent inlet as shown in Figures 7.36 and 7.37. The wet purity of CO_2 is lower than for supported amine adsorbent because the regeneration gas contains more water than with activated carbon which has a regeneration gas containing higher concentrations of N_2. For both adsorbents, the dry CO_2 purity increases for higher CO_2 inlet

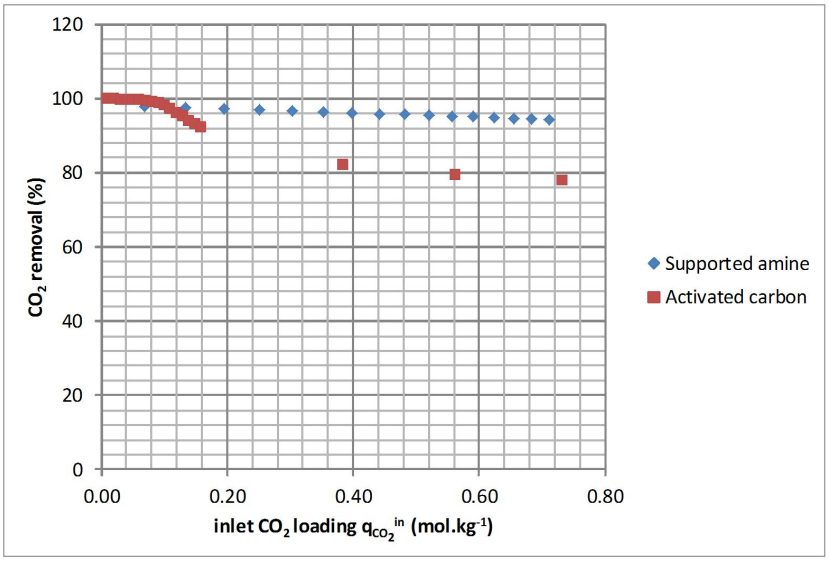

Figure 7.35: Effect on CO_2 removal of the concentration of CO_2 in the adsorbent at the inlet

loadings because the adsorbent pores would contain relatively high proportions of CO_2 to N_2.

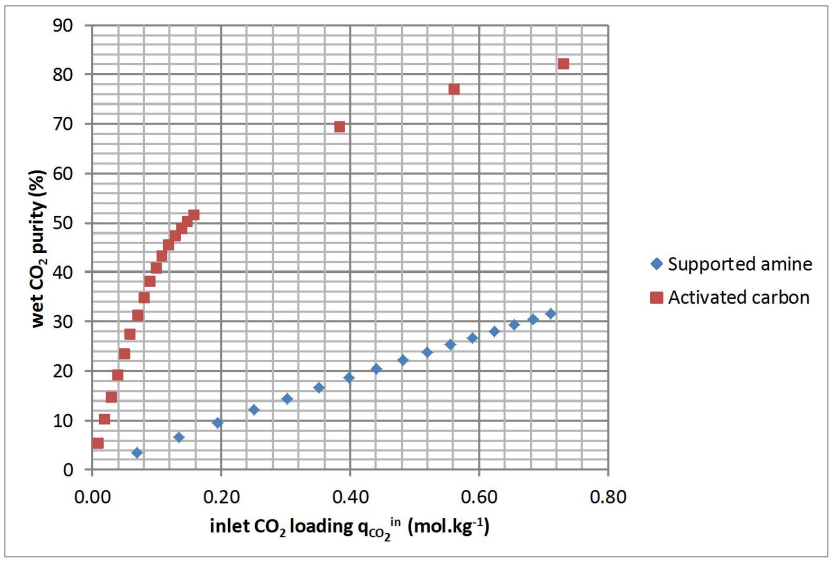

Figure 7.36: Effect on wet CO_2 purity of the concentration of CO_2 in the adsorbent at the inlet

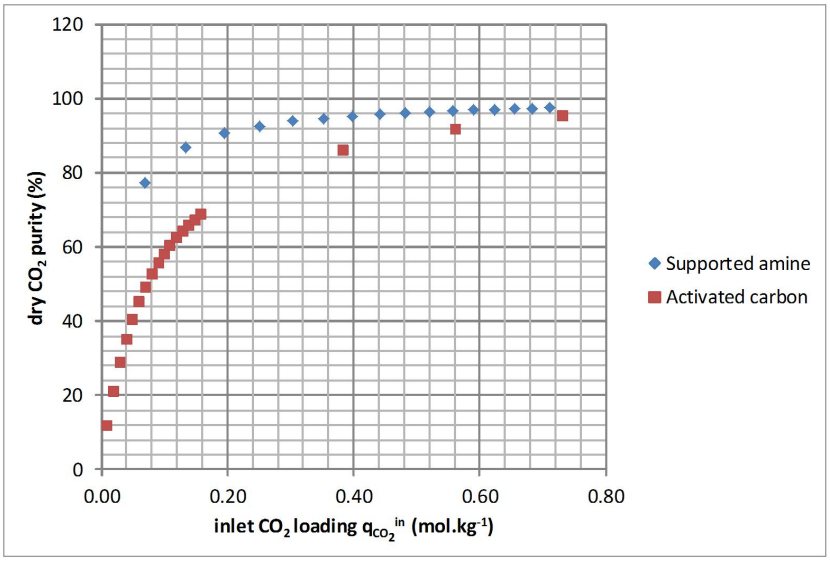

Figure 7.37: Effect on dry CO_2 purity of the concentration of CO_2 in the adsorbent at the inlet

7.11 Effect of the Molar Flowrate of Steam

In this section, the effect of increasing the flowrate of steam into the regenerator is considered for the supported amine adsorbent and activated carbon. In the single counter-current regenerator that has mainly been considered in this chapter, steam is used to supply heat to the adsorbent and to purge the adsorbed CO_2. The influence of adding more steam directly into the regenerator on the CO_2 removal from the adsorbents considered, is shown in Figure 7.38. For the supported amine adsorbent, a very small percentage of adsorbed CO_2 is removed for molar flowrates of steam lower than 200 mol.s^{-1}. The CO_2 removal increases sharply for steam flowrates between 200-1000 mol.s^{-1}. For activated carbon, the CO_2 removal is low for molar flowrates of steam below 1000 mol.s^{-1}. Therefore, if the flowrate of steam is insufficient, the adsorbent temperature is not high enough to desorb CO_2.

The effect of the steam flowrate on the wet and dry CO_2 purities is shown in Figures 7.39 and 7.40 respectively. For the supported amine adsorbent, the wet CO_2 purity increases for flowrates of gas in the range of 200-400 mol.s^{-1} and for activated carbon, the wet CO_2 purity increases for flowrates of gas in the range of 1000-1600 mol.s^{-1} because CO_2 removal from the adsorbent is increased for these flowrates (cf. Figure 7.38). If the steam flowrate is increased further, the wet CO_2 purity of the gas drops because of the higher amount of water present in the gas at the outlet of the regenerator which dilutes CO_2.

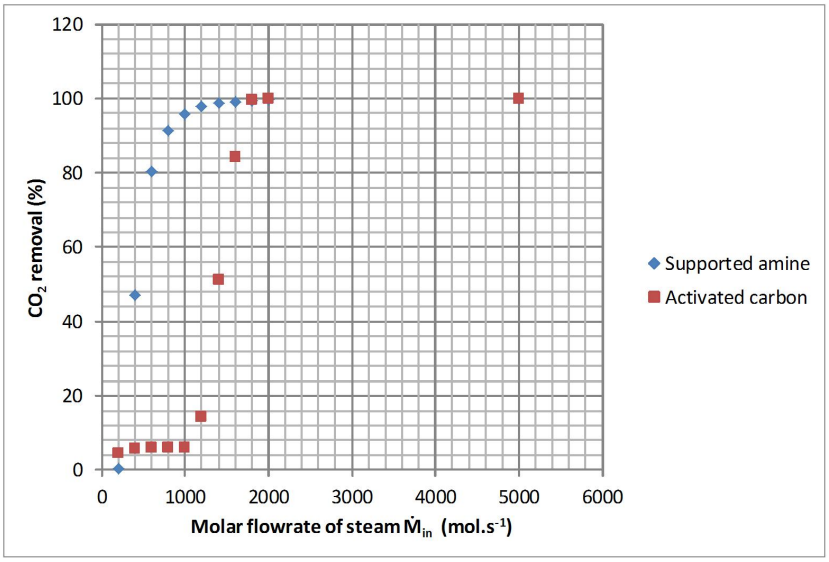

Figure 7.38: Effect of the molar flowrate of steam on CO_2 removal from the adsorbent

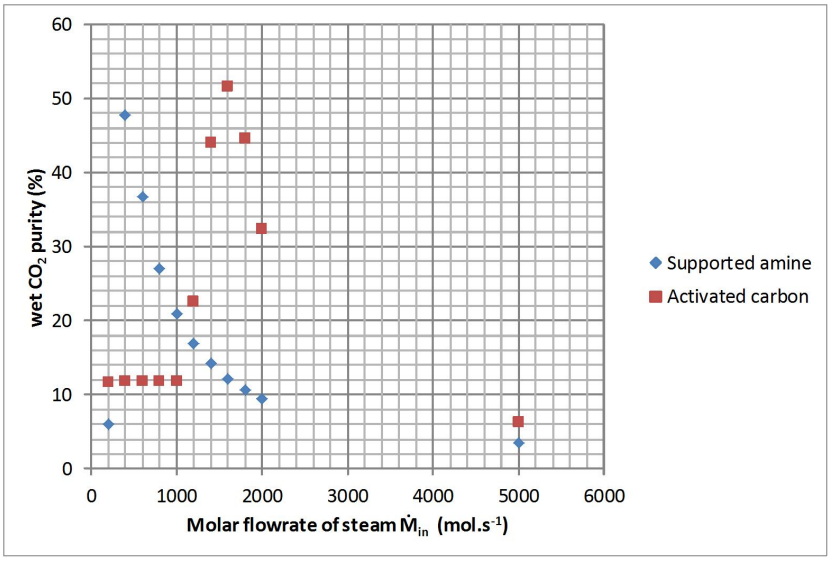

Figure 7.39: Effect of the molar flowrate of steam on the wet purity of CO_2 in the regeneration gas outlet

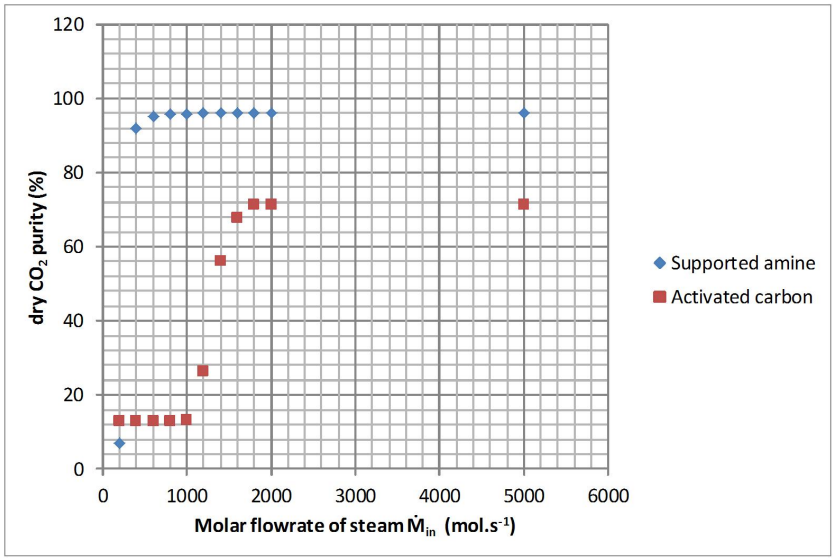

Figure 7.40: Effect of the molar flowrate of steam on the dry purity of CO_2 in the regeneration gas outlet

7.12 Effect of Inlet Steam Temperature

The temperature of the steam at the inlet to the regenerator has been increased up to 120°C in this section. In section 6.14, it was found that the inlet flue gas temperature for the adsorber has a very small effect on CO_2 recovery. Similarly, the temperature of the steam at the inlet to the regenerator also has a very small effect on CO_2 removal from the adsorbent as shown in Figure 7.41. The heat capacity rate of the gas, $\dot{M}_{in}c_{p,g}$, is lower than the heat capacity rate of the solid, $\dot{m}_{in}c_{p,ads}$, due to significantly higher mass flowrates of adsorbent compared to the regeneration gas. Therefore, the gas has a smaller contribution in the movement of heat in the regenerator. The inlet steam temperature also has an insignificant effect on the CO_2 wet and dry purities as shown in Figures 7.42 and 7.43.

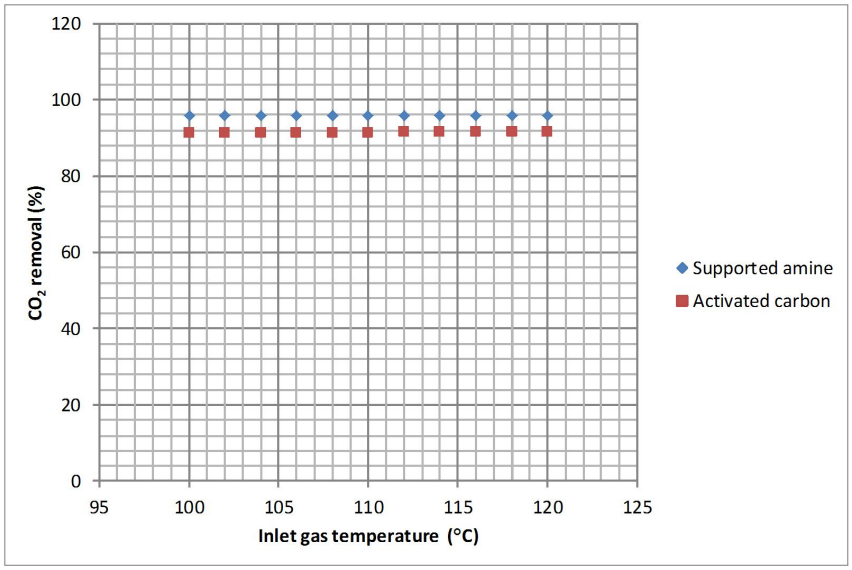

Figure 7.41: Effect of the inlet steam temperature of adsorbent on CO_2 removal from the adsorbent

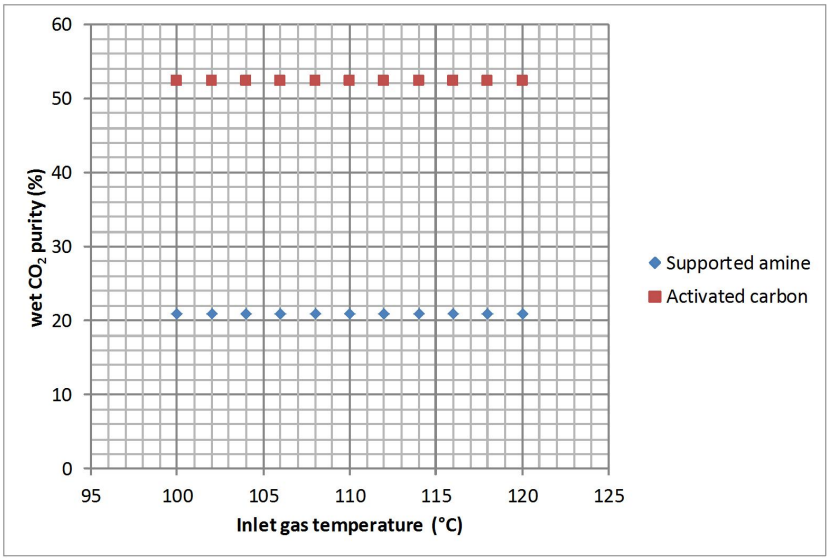

Figure 7.42: Effect of the inlet steam temperature on the wet purity of CO_2 in the regeneration gas outlet

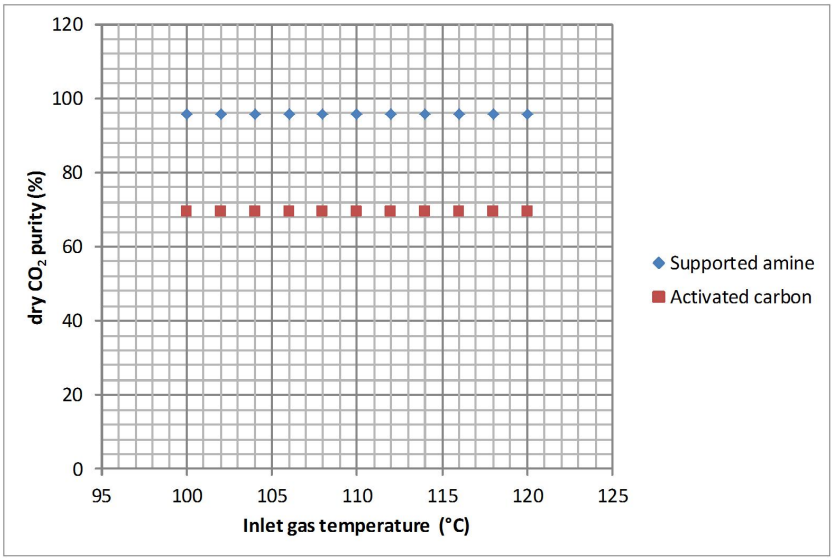

Figure 7.43: Effect of the inlet steam temperature on the dry purity of CO_2 in the regeneration gas outlet

7.13 Effect of Inlet Adsorbent Temperature

In this section, the counter-current base case regenerator is considered with supported amine adsorbent and activated carbon but adsorbent temperatures are increased to find out the effect this has on CO_2 removal and purities.

The adsorbent must be introduced into the regenerator at a temperature above which water in the regeneration gas condenses onto the adsorbent. Therefore the gas in the regenerator must be below a relative humidity of 100%. The relative humidity is the ratio between the partial pressure of water in the gas

and the saturated vapour pressure given by Equation 3.56. Therefore the partial pressure of water must be below the saturated vapour pressure. It was found that, to avoid condensation, the supported amine adsorbent had to be introduced at a temperature of at least 89°C. For the counter-current regenerator using activated carbon, the regeneration gas inside the regenerator contains lower mole fractions of water than for the supported amine adsorbent, therefore the adsorbent can be introduced at a lower temperature of 47°C without steam condensing.

Higher inlet adsorbent temperatures for activated carbon increase the level of CO_2 removed from the adsorbent as shown in Figure 7.44. To achieve CO_2 removals from the adsorbent greater than 90%, activated carbon should be introduced at a temperature of at least 89°C. The CO_2 removal for the lowest temperature for which the supported amine adsorbent can be introduced (89°C) is already high (95.8%) but it increases further for higher inlet adsorbent temperatures too. Therefore, for both adsorbents, increasing the adsorbent temperature gives a greater removal of the CO_2 adsorbed.

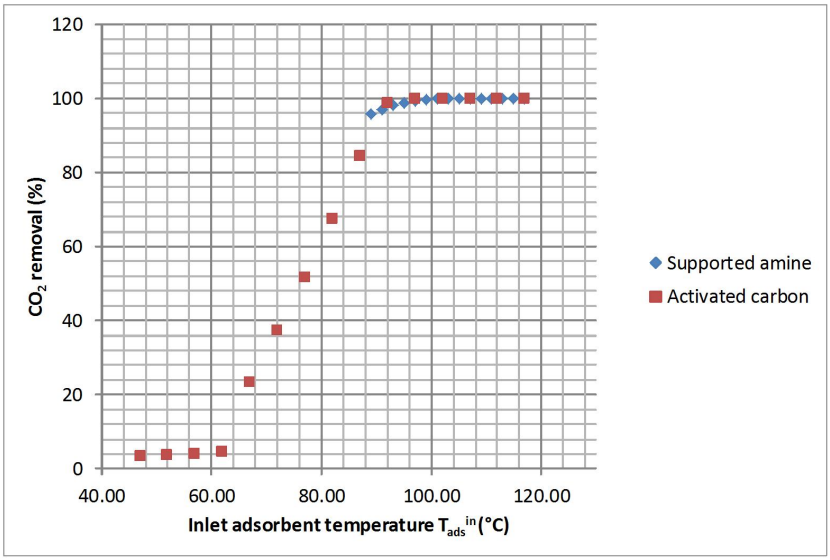

Figure 7.44: Effect on CO_2 removal of the inlet adsorbent temperature

For supported amine adsorbent, the wet CO_2 purity drops for higher inlet adsorbent temperatures because more water and N_2 is desorbed (cf. Figure 7.45). The dry CO_2 purity drops with increasing inlet adsorbent temperatures due to more N_2 being desorbed (cf. Figure 7.46).

For activated carbon, the wet CO_2 purity increases significantly between 62°C and 87°C as more CO_2 is removed from the adsorbent. For temperatures higher than 87°C, more water and N_2 also desorb which reduces the wet CO_2 purity (cf. Figure 7.45). The dry CO_2 purity drops for temperatures above

87°C due to more N_2 being desorbed (cf. Figure 7.46).

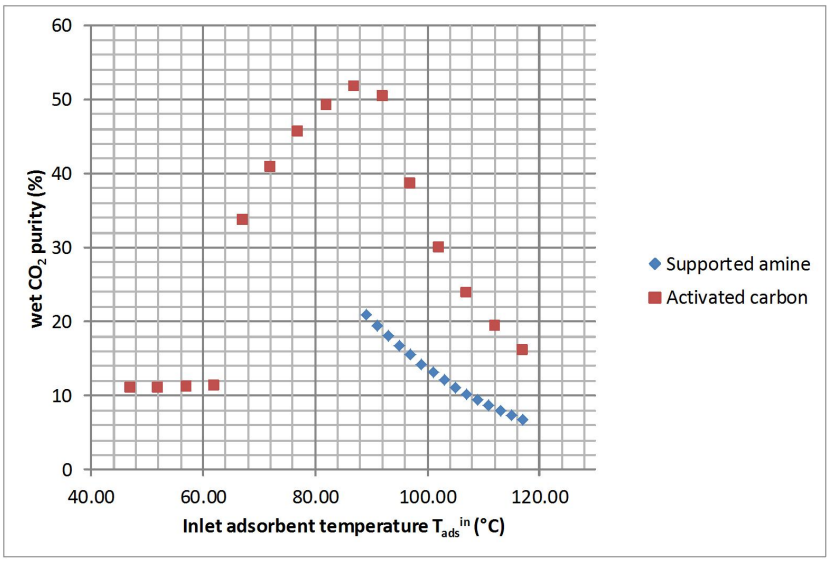

Figure 7.45: Effect on wet CO_2 purity of the inlet adsorbent temperature

Figure 7.46

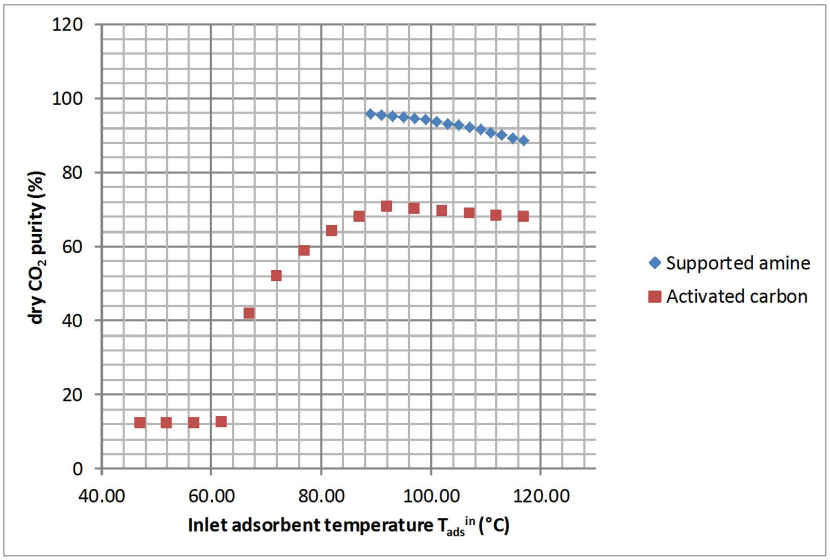

Figure 7.46: Effect on dry CO_2 purity of the inlet adsorbent temperature

7.14 Effect of Heat Addition to the Regenerator

In the base case for the regenerator, the only source of external heat supplied to the regenerator is from the regeneration gas which is steam. However, additional heat can also be supplied to the regenerator by external heating, which

can increase the temperature of the adsorbent to desorb more CO_2. The same equation as Equation 6.1 can be used to quantify the rate of heat added to the regenerator. For this analysis, the ambient temperature of the heat source to the regenerator is chosen to be T_{ext}=120°C.

Figure 7.47 shows the effect on the CO_2 removal from the adsorbent by increasing $U_{ext}A_{ext}$ in the regenerator. U_{ext} is the overall heat transfer coefficient of the external heater in the regenerator and A_{ext} is the surface area for external heat exchange. By increasing $U_{ext}A_{ext}$ for the supported amine adsorbent, the temperature of the adsorbent in the regenerator increases therefore more of the CO_2 previously adsorbed is desorbed.

For activated carbon, a similar trend is found for the CO_2 removal from the adsorbent as a function of $U_{ext}A_{ext}$ up to $U_{ext}A_{ext} = 1{\times}10^6$ W.K^{-1}. There is an unexpected drop in CO_2 removal for $U_{ext}A_{ext} > 1{\times}10^6$ W.K^{-1} (cf. Figure 7.47). This is explained by a drop in the temperature of the adsorbent leaving the regenerator (at $x = 0$ m), for increasing values of $U_{ext}A_{ext}$, as shown in Figure 7.48. At the adsorbent outlet, the activated carbon reaches temperatures higher than 130°C for $U_{ext}A_{ext} = 0$ W.K^{-1} which is higher than T_{ext}=120°C. Therefore, for high values $U_{ext}A_{ext}$, the adsorbent is actually being cooled by the external heater at the adsorbent outlet rather than being heated. This causes more CO_2 to remain loaded onto the adsorbent and therefore there is a drop in CO_2 removal from the adsorbent.

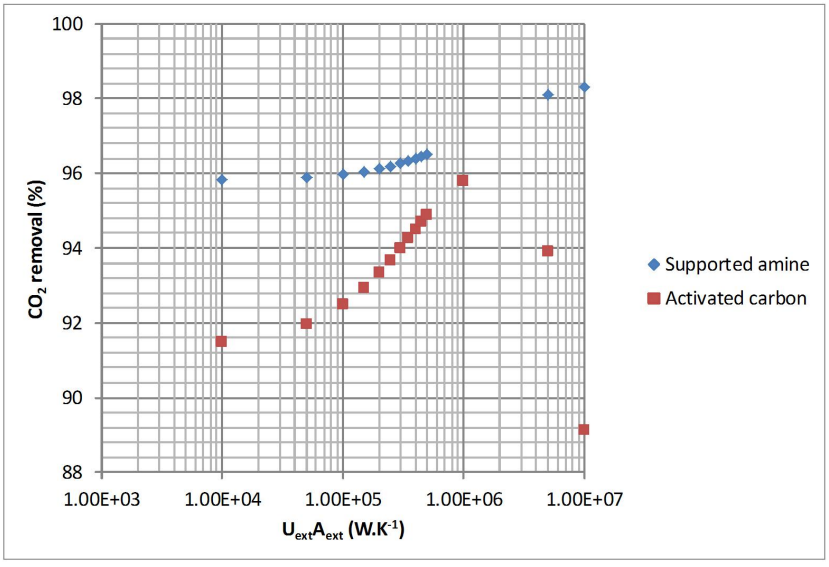

Figure 7.47: Effect of the overall heat transfer coefficient and area on CO_2 removal from the adsorbent

The variation in wet and dry purities of CO_2 with increasing $U_{ext}A_{ext}$ values is shown in Figures 7.49 and 7.50 respectively. The wet CO_2 purity remains constant for both adsorbents but there is a drop in wet CO_2 purity for activated

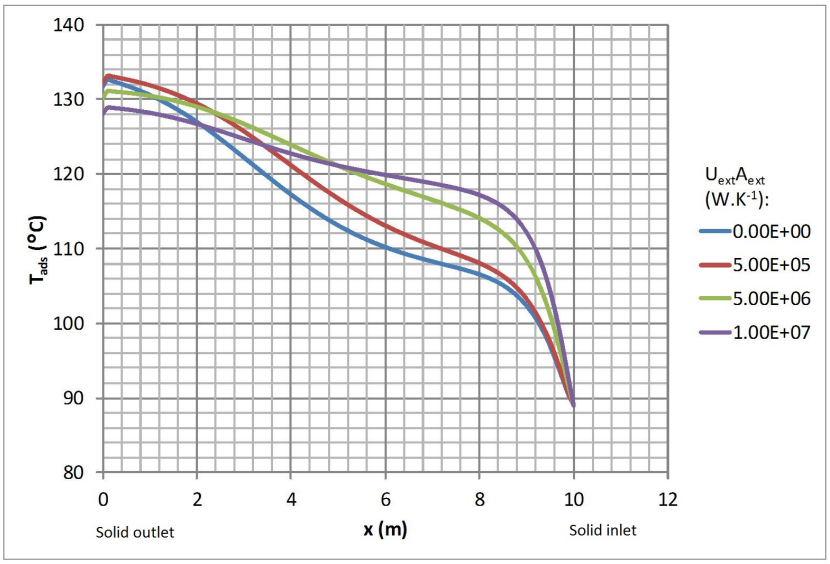

Figure 7.48: Adsorbent temperature profiles for a counter-current regenerator with activated carbon for various $U_{ext}A_{ext}$ values

carbon above $U_{ext}A_{ext} = 1{\times}10^{6}$ W.K^{-1} because of the drop in CO_2 removal found in Figure 7.47. Therefore, the mole fraction of CO_2 in the outlet gas from the regenerator drops for $U_{ext}A_{ext} > 1{\times}10^{6}$ W.K^{-1} which reduces the wet CO_2 purity.

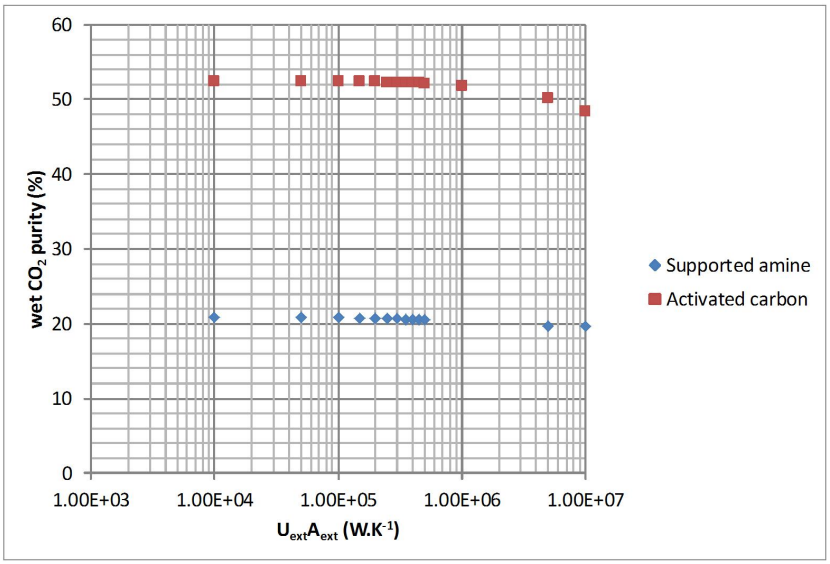

Figure 7.49: Effect of the overall heat transfer coefficient and area on the wet purity of CO_2 in the regeneration gas outlet

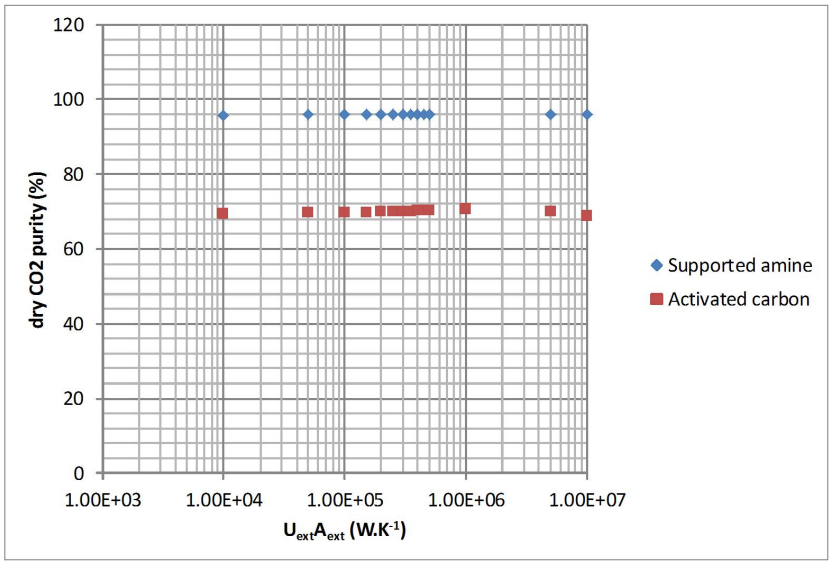

Figure 7.50: Effect of the overall heat transfer coefficient and area on the dry purity of CO_2 in the regeneration gas outlet

7.15 Inadequacy of Zeolite 13X

It was mentioned previously in section 2.6.4, that if zeolite 13X is in presence of water, the CO_2 loading would drop unless it is fully removed after regeneration of the adsorbent. If N_2 is used as a regeneration gas, the gas at the outlet of the regenerator would be of low CO_2 purity. Therefore neither water or N_2 are suitable gases to regenerate zeolite 13X. Although a pure stream of CO_2 at high temperature can also be considered, the isotherms shown in Figure 7.51, show why it is not possible to desorb CO_2 with a pure CO_2 stream at a temperature of 120°C at which the adsorbent leaves the regenerator. The CO_2 loading at the bottom of the regenerator is higher than at the bottom of the adsorber therefore more CO_2 has been adsorbed inside the regenerator.

With the supported amine adsorbent and the activated carbon, the presence of water lowers the CO_2 partial pressure during regeneration which allows higher CO_2 working capacities. This is not the case for zeolite 13X as water is assumed to be absent.

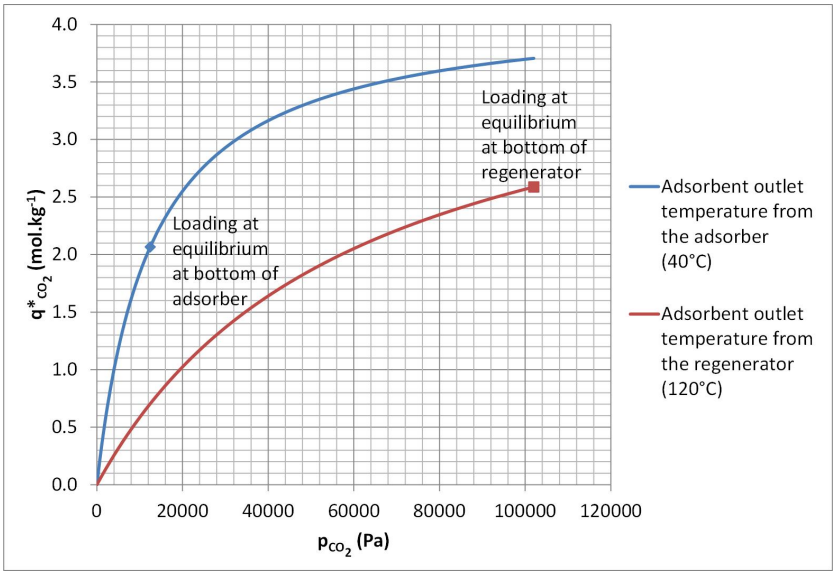

Figure 7.51: CO_2 isotherms for the supported amine adsorbent at adsorption and regeneration temperatures

The moving bed system proposed by Kim et al. (2013a) carries out desorption in two stages: at atmospheric pressure and under vaccuum. However, a regeneration gas is not used in either stage. Instead, steam is used to heat the adsorbent indirectly without coming into contact with the adsorbent, through a plate heat-exchanger. The CO_2 desorbed in the first stage at atmospheric pressure was only able to remove 29 mol% of the loaded CO_2. It therefore seems necessary that desorption under vacuum must be carried out to remove a greater percentage of CO_2 which may be more costly than using heat from steam in a power plant.

7.16 Conclusions

In this chapter, profiles of concentrations, loadings, temperatures and pressure inside a counter-current regenerator have been presented for an supported amine adsorbent. Some of these profiles have been compared to a similar regenerator using activated carbon. Sensitivity analyses have been carried out on a counter-current regenerator for a range of parameters to find out which of these would have a greater influence on improving the desorption of CO_2.

The most important findings from this chapter are given below:

- A counter-current regenerator or a series of counter-current fluidised bed regenerators offer higher removals of adsorbed CO_2 from the adsorbent than co-current or single fluidised bed regenerators due to the equilibrium conditions at the adsorbent outlet.

- The adsorbent needs to be introduced at a high enough temperature not only to improve CO_2 removal but to avoid the condensation of steam if it is used as the regeneration gas.

- CO_2 removal from the adsorbent is greatly improved by higher steam flowrates into the regenerator. More steam is needed to desorb CO_2 from activated carbon than the supported amine adsorent because a higher mass flowrate of activated carbon is required to achieve a 90% CO_2 recovery in the adsorber.

- Although zeolite 13X is suitable for capturing CO_2 after water removal from flue gas, it is not possible to desorb CO_2 using a hot stream of CO_2 at 120°C. Steam or N_2 are not suitable as regeneration gases for this adsorbent. For this reason it will not be considered further in this thesis.

- The purity of CO_2 in the outlet gas from the regenerator using activated carbon is significantly lower than for the supported amine adsorbent because of higher uptakes of N_2 on activated carbon in the adsorber. The design of the moving bed adsorption process using activated carbon needs further consideration to obtain a CO_2 product of higher purity. The moving bed cycle considered later in Chapter 8 is specifically suitable for the supported amine adsorbent which will be the main adsorbent considered in the following chapter.

The analysis of a single adsorber (Chapter 6) and the single regenerator, in this chapter, has allowed us to narrow down cases and options to consider for the moving bed cycle incorporating an adsorber and regenerator. The following chapter analyses the performance of the overall cycle and compares it to other post-combustion CO_2 capture technologies.

Chapter 8

Analysis of Adsorption-Desorption Cycles

8.1 Introduction

The most influential parameters for a single adsorber and regenerator were found in sensitivity analyses performed in Chapter 6 and 7. In this chapter, results from simulations of full moving bed CO_2 adsorption cycles are presented. Adsorbents that have been considered in this chapter are the supported amine adsorbent and activated carbon. The moving bed TSA cycle comprises of an adsorber, regenerator as well as an adsorbent heater and cooler.

In this chapter, sensitivity analyses on the following parameters are carried out. Their influence on CO_2 recovery and purity and heat consumption for adsorbent regeneration will be assessed.

- Mass flowrate of adsorbent
- Molar flowrate of gas into the regenerator
- Rate of heat addition to the adsorbent before desorption
- Rate of heat removal from the adsorbent before adsorption
- Mass transfer constants

The benefits of heat integration in the process are assessed and heat exchangers for adsorbents are discussed. The unsuitability of the moving bed TSA cycle using activated carbon is looked at more carefully in this chapter. The performance of moving bed TSA cycles for CO_2 capture with supported amine adsorbent are compared with amine absorption processes and fixed bed CO_2 adsorption processes. Lastly, aspects regarding capital and operating costs for moving bed TSA processes are discussed.

8.2 Moving Bed CO_2 Adsorption Cycle with Supported Amine Adsorbent

8.2.1 Base Case Cycle using the Supported Amine Adsorbent

The diagram of the full moving bed CO_2 capture process using the supported amine adsorbent is given in Figure 8.1. In fact, there would be four parallel processes because the flue gas stream is split into four equal flowrates according to the analogous amine absorption process described by Fisher et al. (2005). The main units in the process include an adsorber, regenerator and heat exchangers (HEX 1 and HEX 2) for cooling and heating the adsorbent respectively.

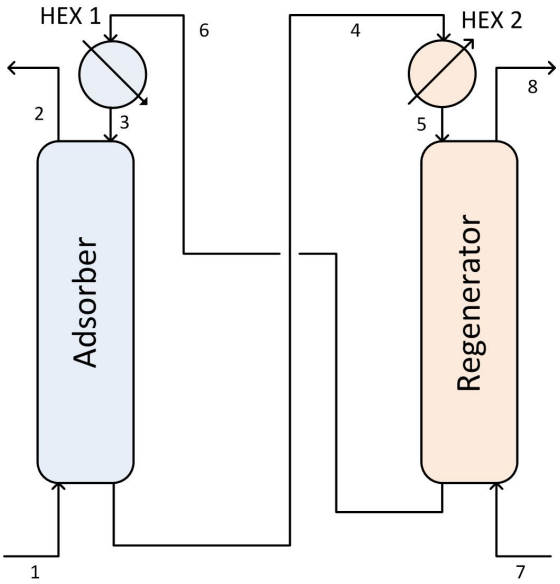

Figure 8.1: Diagram of the base case CO_2 Adsorption Cycle using a counter-current adsorber and regenerator

The parameters used in the units are shown in Table 8.1. The properties of flue gas entering the adsorber are the same for the base case standalone adsorber described in Chapter 6. The gas flowrate into the rengerator has been reduced compared to the base case regenerator (Chapter 7) as the adsorbent is heated to a higher temperature prior to entering the regenerator in HEX 2.

Compared to the mass flowrate of adsorbent used for the single adsorber in Chapter 6, the mass flowrate of adsorbent used in the cycle is higher. This increase is due to the fact that the adsorbent was assumed to enter the single adsorber fully regenerated and therefore it had its highest working capacity. The adsorbent volume fraction, ε_a, is higher for the units in the cycle because of a higher mass flowrate of adsorbent used. ε_a was calculated from Equation 3.49.

The diameter of the adsorbent particle has been chosen to avoid entrainment in the counter-current beds.

The height and diameter of heat exchangers HEX 1 and HEX 2 which are used to cool and heat the adsorbent respectively, have been chosen arbitrarily. They were chosen to have a smaller diameter than the adsorber and regenerator because the gas flowrates in HEX 1 and HEX 2 are assumed to be zero and therefore, they are not subject to fluidisation limits that depend on the gas velocity. However, further work would need to be carried out to determine the correct size of these units. The size of these units will actually depend on the heat transfer area, A_{ext}, required in the heat exchangers. High values of $U_{ext}A_{ext}$ in HEX 1 and HEX 2 were chosen so that the adsorbent enters the adsorber at a sufficiently low temperature, close to the temperature of the coolant in HEX 1, $T_{ext} = 25°C$ and at a temperature close to the temperature of the heat source in HEX 2, $T_{ext} = 120°C$, for the regenerator. In the cyclic process, the molar flowrate of steam used as a regeneration gas is an order of magnitude lower than the flowrate used for the standalone regenerator in Chapter 7 because the adsorbent enters the regenerator at a higher temperature close to 120°C. The impact of the flowrate of steam is assessed in section 8.2.3.

The number of discretisations in the adsorber and regenerator have been halved from the values used for the standalone adsorber and regenerator (Chapters 6 and 7) to reduce the computational times to reach convergence to the solution. For the same, reason, a relatively low number of discretisations have been chosen for HEX 1 and HEX 2. Additionally, the weight factor, α, in the mathematical model has been chosen to be 1 (corresponding to a backwards difference method) to reduce the complexity of the model and convergence times. Other parameter values have been kept the same as for the base case adsorber and regenerator in Chapters 6 and 7.

Table 8.1: Parameters used in the columns and heat exchangers for the base case adsorption cycle

Parameter	**Unit**	**Adsorber**	**HEX 2**	**Regenerator**	**HEX 1**
Adsorbent		Supported amine adsorbent	Supported amine adsorbent	Supported amine adsorbent	Supported amine adsorbent
Gas		Flue gas	-	Regeneration gas	-
L	m	15	1	10	1
D_C	m	10	2	6	2
ε_a	-	0.101	0.861	0.199	0.861
ε_p	-	0.4	0.4	0.4	0.4
D_p	mm	1	1	1	1
P_{in}	Pa	101325	101325	101325	101325
T_g^{in}	°C	40	-	120	-
M_{in}	mol.s^{-1}	5607.5	0	100	0
$\dot{m}_{in}$	kg.s^{-1}	1200	1200	1200	1200
$y_{CO_2}^{in}$	-	0.1233	-	0	-
$y_{H_2O}^{in}$	-	0.07	-	1	-
$y_{N_2}^{in}$	-	0.8067	-	0	-
k_{CO_2}	s^{-1}	10	0	10	0
k_{H_2O}	s^{-1}	10	0	10	0
k_{N_2}	s^{-1}	10	0	10	0
$U_{ext}A_{ext}$	W.K^{-1}	0	10^7	0	10^7
T_{ext}	°C	25	120	120	25
Number of discretisations	-	50	10	50	10
α	-	0.75	1	0.75	1

8.2.1.1 Performance of Base Case Cycle

Stream Table Results

Properties of the gas and solid streams for the base case process are shown in Table 8.2. The streams are shown in Figure 8.1. Adsorbent streams 3, 4, 5 and 6 which enter and exit the adsorber and regenerator are assumed to contain no bulk gas. Similarly, gas streams 1, 2, 7 and 8 are assumed to not contain any solid. Temperatures, flowrates, compositions, component loadings and stream enthalpies are given in Table 8.2.

As the adsorbent is heated prior to entering the regenerator and a very low amount of heat is supplied to the adsorbent by introducing steam into the regenerator, the temperature of the adsorbent decreases as it flows downwards in the regenerator. In addition, other than the introduction of a low flowrate of steam, no external heat has been added to the regenerator. CO_2 and water are desorbed in the regenerator, which consumes heat and also contributes to the drop in adsorbent temperature.

Table 8.2: Properties of streams shown in Figure 8.1

Stream	**1**	**2**	**3**	**4**	**5**	**6**	**7**	**8**
P (Pa)	101325	93405	101325	100325	101325	101325	101325	101139
T_g (°C)	40	26.02	-	-	-	-	120	110.72
T_{ads} (°C)	-	-	25.63	56.79	118.51	98.08	-	-
$\dot{M}$ (mol.s^{-1})	5607.5	4720.58	0	0	0	0	100	986.95
$\dot{m}$ (kg.s^{-1})	-	-	1200	1200	1200	1200	-	-
y_{CO_2} (-)	0.1233	0.011	-	-	-	-	0	0.650
y_{H_2O} (-)	0.07	0.036	-	-	-	-	1	0.328
y_{N_2} (-)	0.8067	0.954	-	-	-	-	0	0.022
q_{CO_2} (mol.kg^{-1})	-	-	1.09	1.62	1.39	1.08	-	-
q_{H_2O} (mol.kg^{-1})	-	-	1.97	2.15	2.13	1.96	-	-
q_{N_2} (mol.kg^{-1})	-	-	0	0	0	0	-	-
$\dot{H}_g$ (MJ.s^{-1})	2.56	0.14	-	-	-	-	0.32	3.14
$\dot{H}_{ads}$ (MJ.s^{-1})	-	-	238.93	241.49	361.64	358.82	-	-

8.2.1.2 Profiles for the Base Case Cycle

Profiles inside the Adsorber

Previously in Chapters 6 and 7, the profiles along the axial position x (distance from gas inlet) in the adsorber and regenerator were analysed for single columns treated independently and for a chosen set of inlet conditions. In this section, profiles inside the adsorber are analysed for the overall CO_2 moving bed adsorption and desorption cycle.

Figure 8.2 shows that the overall trends of the mole fractions of CO_2 and N_2 in the gas are the same for the adsorber in the cycle and for the single adsorber shown in Figure 6.2. However, the final values of mole fractions attained at the outlet differ due to different adsorbent temperatures and loadings at the adsorber inlet. The profile of the mole fraction of water differs from the one found for the single adsorber. In Figure 6.2, there is an overall increase in the mole fraction of water between the gas inlet and outlet. However, this does not occur in the adsorber in the full cycle. Figure 8.2 shows that the level of water in the gas rises as it is desorbed. As more water is adsorbed as the gas leaves the adsorber (cf. Figure 8.3), the mole fraction drops below the inlet mole fraction.

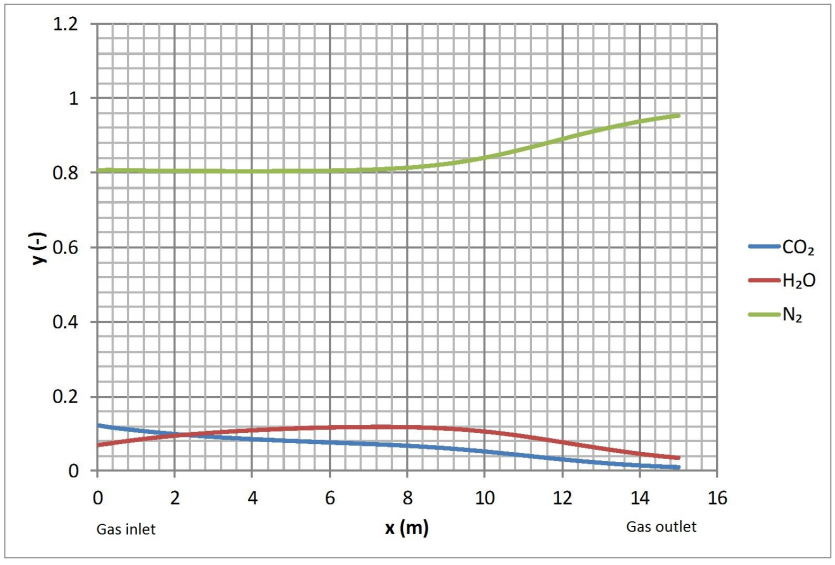

Figure 8.2: Profiles of the component mole fractions in the adsorber in the full CO_2 capture cycle using supported amine adsorbent

Figure 8.3 shows the increase in the CO_2 and water loading in the countercurrent adsorber for the full cycle. A working capacity of CO_2 of 0.53 mol.kg^{-1} is also shown in Figure 8.3. For the single adsorber, a higher working capacity was found (1.8 mol.kg^{-1}) because it was assumed that the adsorbent did not contain CO_2 as it entered the adsorber. The adsorbent pores were also saturated

with water and therefore water was desorbed inside the adsorber. This resulted in a drop in water loading (cf. Figure 6.3). However, for the adsorber in the full capture cycle, there is an increase in the loading of water as the adsorbent does not enter with pores saturated with water.

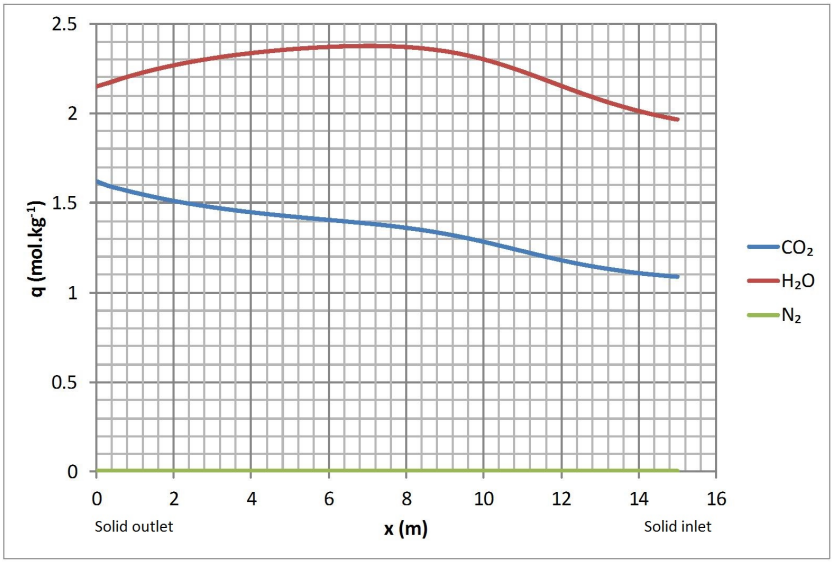

Figure 8.3: Profiles of the component loadings in the adsorber in the full CO_2 capture cycle using supported amine adsorbent

The profiles for mole fractions and loadings, that are shown in Figures 8.2 and 8.3 respectively, use modelled isotherm values which have some error associated with the predicted equilibrium loadings found from the isotherms. At the gas outlet, there is the greatest overestimation of the loading. As shown by the isotherms (Figure 3.10), at the gas outlet where the temperature is lowest, the loadings are overestimated at low CO_2 partial pressures. On the other hand, the CO_2 loadings are underestimated at the gas inlet, where the temperature and CO_2 partial pressure are highest. The CO_2 mole fraction in the gas would therefore be lower than the values shown in Figure 8.2 at the gas inlet and higher than the values shown in Figure 8.2 at the gas outlet. The water loadings are on the whole overestimated by the modelled isotherm at the temperatures in the adsorber therefore the actual H_2O mole fraction in the gas will be higher than shown in Figure 8.2.

The profiles of the total gas flowrate along the adsorber is shown in Figure 8.4. The gas flowrate at the outlet is lower than for the standalone adsorber because water is adsorbed in the adsorber inside the full cycle whereas water was desorbed in the standalone adsorber (cf. Figure 6.5).

The increase in the temperature inside the adsorber in the cycle is shown by the profiles in Figure 8.5. Because the adsorber in the cycle is adiabatic (no heat loss), the temperature rises due to the heat released by the adsorption of

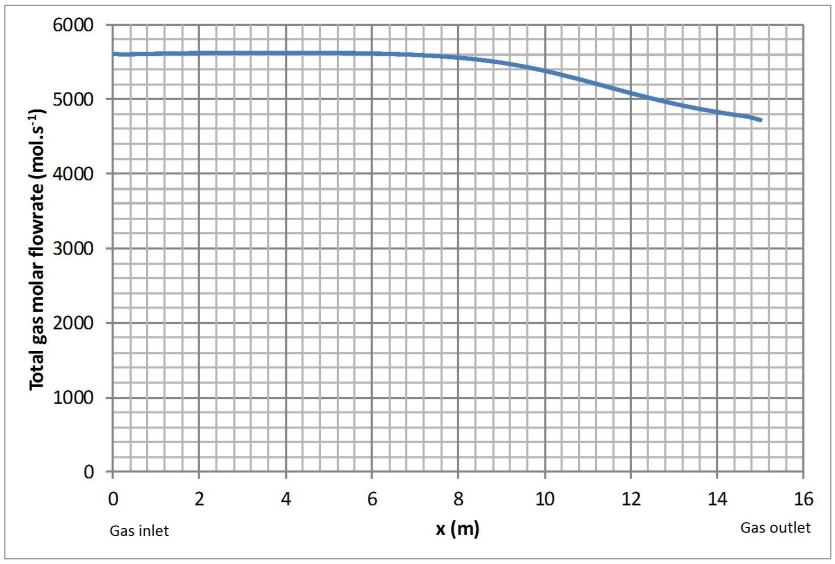

Figure 8.4: Profile of the flue gas molar flowrates in the adsorber in the full CO_2 capture cycle using supported amine adsorbent

CO_2 and water. The temperature in the adsorber drops when the adsorbent leaves the adsorber. Simultaneously, the water loading decreases as shown in Figure 8.3 therefore the heat given off also drops.

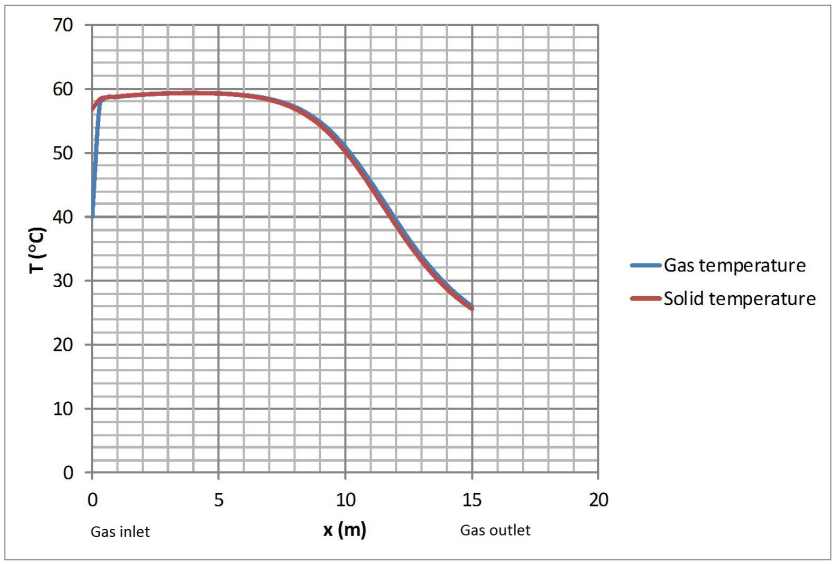

Figure 8.5: Gas and solid temperature profiles in the adsorber in the full CO_2 capture cycle using supported amine adsorbent

The pressure drop inside the counter-current adsorber of the full cycle is shown in Figure 8.6. There is a higher volume fraction of adsorbent in the adsorber inside the full cycle and the pressure drop in the column is higher than for the standalone adsorber.

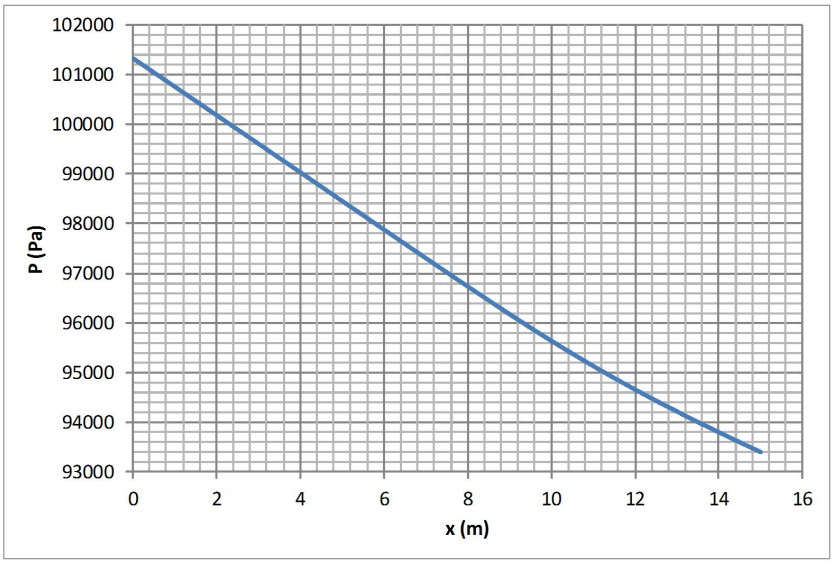

Figure 8.6: Pressure profile in the adsorber in the full CO_2 capture cycle using supported amine adsorbent

Profiles inside the adsorbent heating heat exchanger

Heat Exchanger 2 (HEX 2) is located before the regenerator to increase the temperature of the adsorbent before it reaches the regenerator. For example, the adsorbent can be heated by indirect contact with a heating medium such as steam. Due to the absence of flow of bulk gas on the adsorbent side of the heat exchanger (cf. Table 8.2), the gas components do no leave the pores of the adsorbent and the concentration in the pores is very high. The solid heat exchangers used in the CO_2 capture cycle use the same model as the adsorber but an additional assumption is made for them in the base case: material in the bulk gas is neither adsorbed or desorbed inside the heat exchangers. Therefore, only a change in adsorbent temperature is assumed to occur.

As the temperature of the adsorbent increases (cf. Figure 8.7), the CO_2 loading drops (cf. Figure 8.8) and CO_2 desorbs into the adsorbent pores which causes the concentration of components in the pores to rise. It is only until the adsorbent reaches the regenerator that the material in the pores gets transferred into the bulk gas.

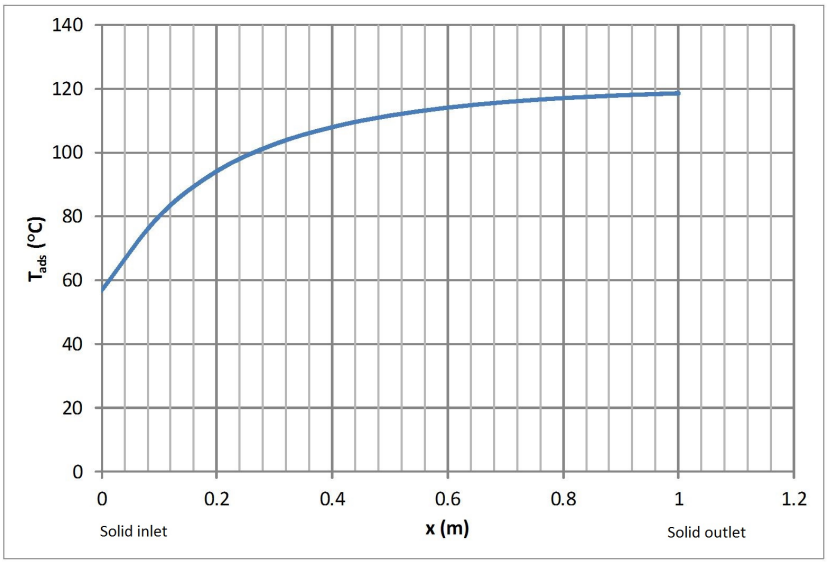

Figure 8.7: Adsorbent temperature profile in HEX 2

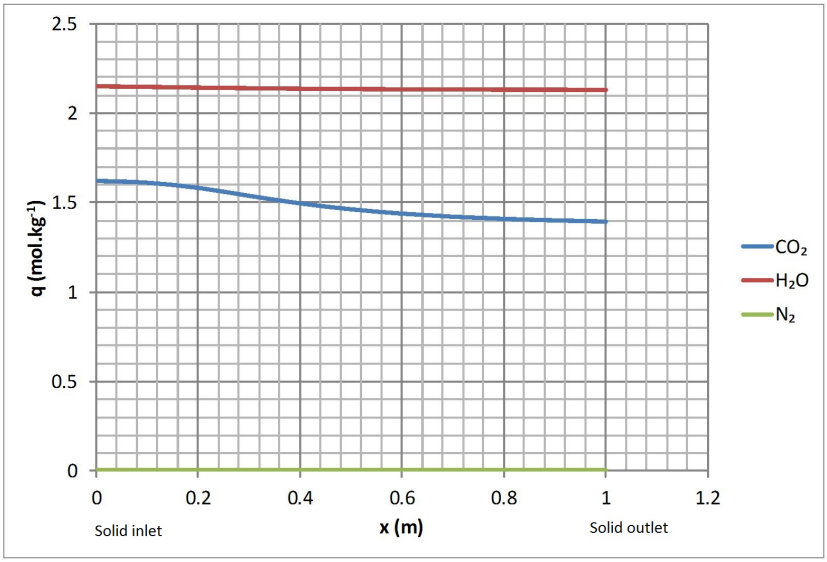

Figure 8.8: Loading profiles of components in HEX 2

Profiles inside the regenerator

The gas used to regenerate the adsorbent in the desorber is steam with a molar flowrate of 100 mol.s^{-1} in the base case. This flowrate is very small. The profiles of the mole fractions of CO_2 and water in the regenerator are given in Figure 8.9. The CO_2 mole fraction increases sharply at the gas inlet but this increase does not coincide with a large drop in CO_2 loading as shown in Figure 8.10. Therefore, at the gas inlet, the rise in the CO_2 mole fraction is because of CO_2 leaving the pores of the adsorbent. The CO_2 mole fraction remains constant in the major part of the regenerator. It increases again at the outlet of the regenerator where the CO_2 loading drops when the adsorbent

enters the regenerator. From Figure 8.9, there is a slight increase in the N_2 mole fraction at the gas outlet of the regenerator. This corresponds to the removal of N_2 stored in the pores of the adsorbent during adsorption. N_2 is therefore transferred from the pores of the adsorbent to the regeneration outlet gas and the CO_2 purity of the gas product leaving the regenerator is reduced due to this increase in N_2 in the gas.

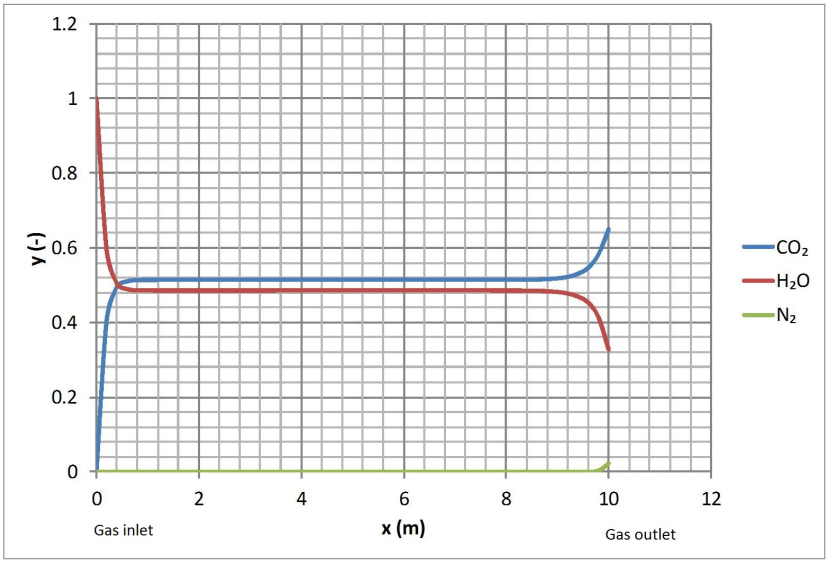

Figure 8.9: Profiles of the component mole fractions in the regenerator in the full CO_2 capture cycle using supported amine adsorbent

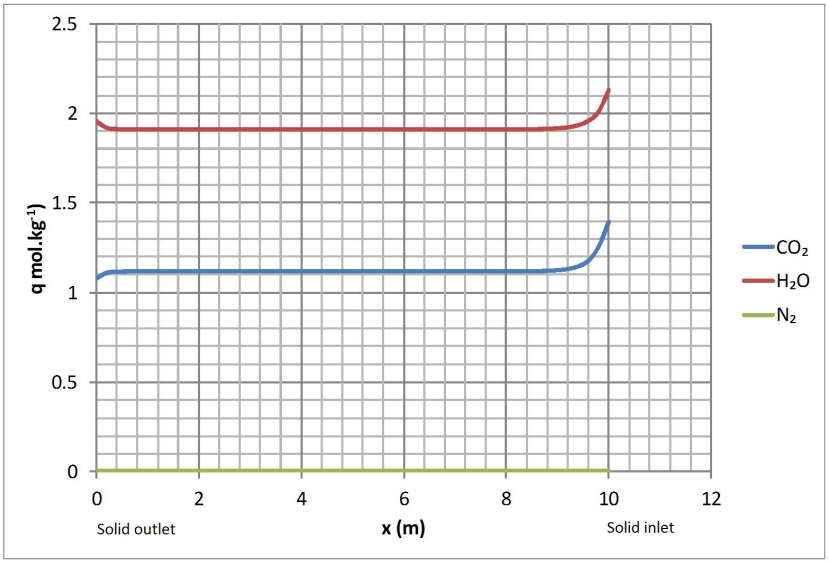

Figure 8.10: Profiles of the component loadings in the regenerator in the full CO_2 capture cycle using supported amine adsorbent

The temperature of the adsorbent exiting the regenerator only increases slightly as it comes into contact with steam (cf. Figure 8.11) which results in

a small drop in CO_2 loading at this point. The largest drop in CO_2 loading is where the adsorbent enters the counter-current regenerator. This is also the location at which the temperature of the adsorbent is greatest.

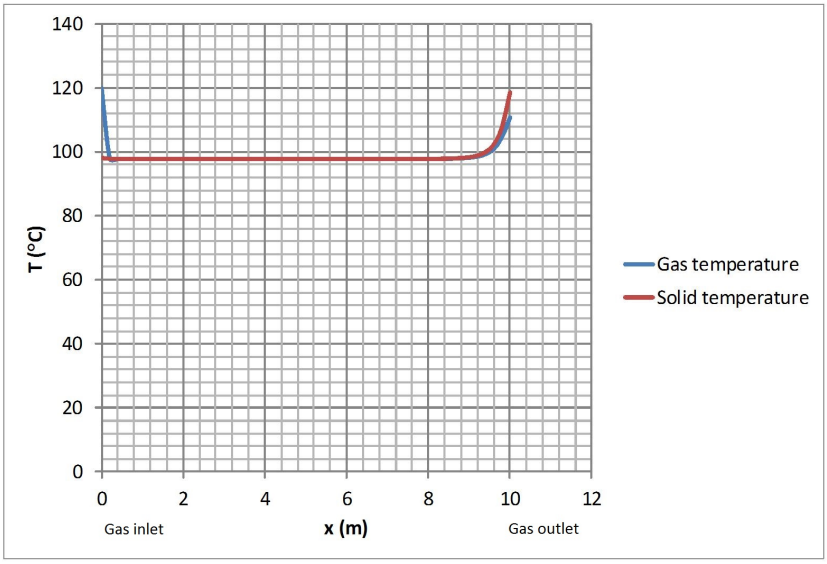

Figure 8.11: Gas and solid temperature profiles in the regenerator in the full CO_2 capture cycle using supported amine adsorbent

The variation in total flowrate of adsorbate and gas in the regenerator is shown in Figure 8.12. It can be seen from this profile, the profiles of mole fractions and loadings (Figures 8.9 and 8.10) that the regenerator is larger than necessary because there is no significant change in the concentrations and loadings in the large part of the regenerator. Most of the desorption of CO_2 occurs near the gas outlet. The regenerator used in the full capture cycle is of the same size as the regenerator considered by Fisher et al. (2005) to regenerate the amine solution. The length of the regenerator could be reduced to only 4 m or 5 m in which mass transfer occurs for the chosen rate constant of $k_{CO_2} = 10\ s^{-1}$. The sharp increase in the total molar flowrate of gas at the adsorbent inlet of the regenerator is not real in practice. It is only obtained here because it has been assumed that no gas was lost in HEX 2. Therefore, as soon as mass transfer is enabled in the regenerator, the molar flowrate of gas immediately rises as desorbed gas contained in the adsorbent pores is released into the bulk gas inside the regenerator.

There is a much greater error between the measured and modelled CO_2 isotherms at temperatures greater than 100°C. Therefore, the loadings shown in Figure 8.10 are higher than the actual values and the performance of the regenerator is underestimated. The CO_2 mole fraction in the gas leaving the adsorber should be greater than shown in Figure 8.9. Consequently, the CO_2

purity of the gas stream exiting the regenerator should be higher than the modelled value.

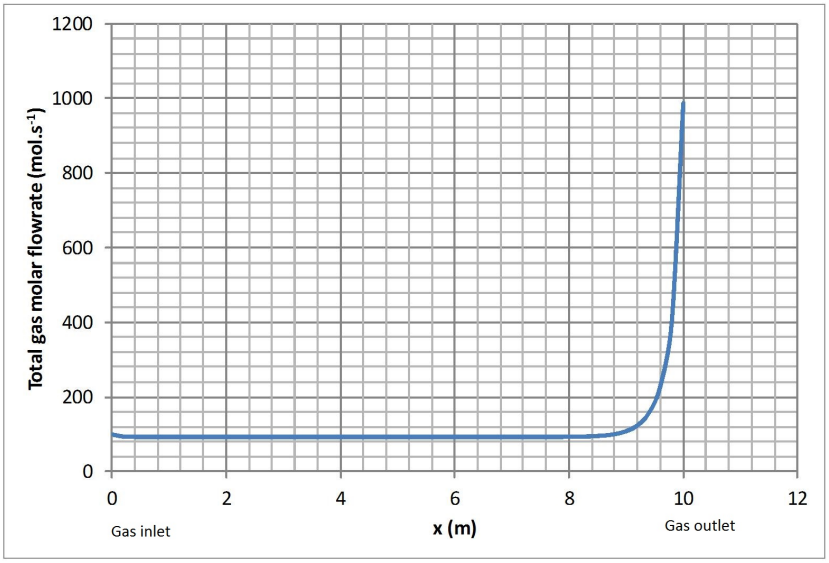

Figure 8.12: Profile of the flue gas molar flowrate in the regenerator in the full CO_2 capture cycle using supported amine adsorbent

As the gas flowrate increases suddenly at the gas outlet where CO_2 and water are predominantly desorbed, the velocity of the gas rises and therefore the pressure drop rises suddenly as shown in Figure 8.13 which is in accordance with Equation 3.86.

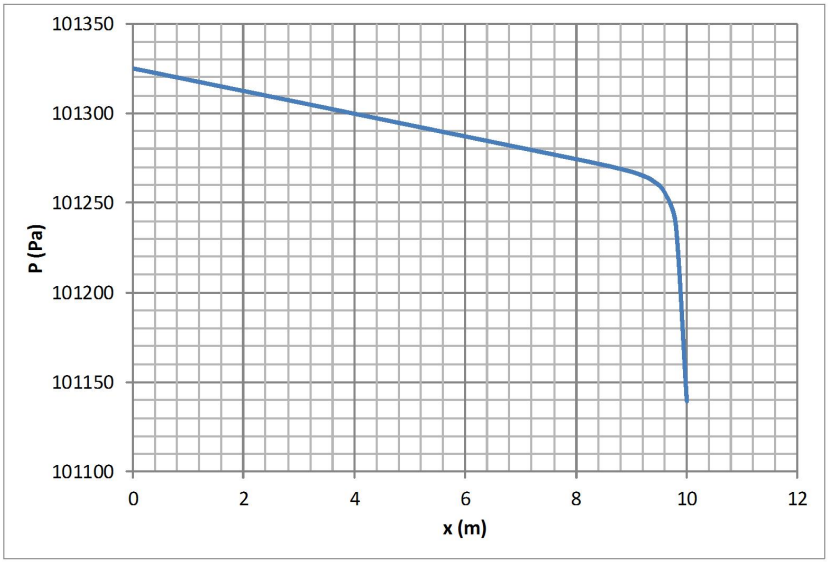

Figure 8.13: Pressure profile in the regenerator in the full CO_2 capture cycle using supported amine adsorbent

Profiles inside the adsorbent cooling heat exchanger

The purpose of Heat Exchanger 1 (HEX 1) is to cool the adsorbent before it enters the adsorber to allow for a higher working capacity. Cooling water could be used to remove heat inside HEX 1.

In HEX 1, as the temperature of the adsorbent drops (cf. Figure 8.14), the concentration of CO_2 and water in the pores of the adsorbent also drop and both components adsorb onto the surface of the adsorbent, which causes the concentration in the pores to drop and the loading of CO_2 and water to rise. Due to the absence of bulk gas, no material is transferred from the bulk gas to the adsorbent pores. The increase in loading of CO_2 and water is only slight as shown in Figure 8.15 because a low amount of gas is contained in the pores of the adsorbent entering HEX 1.

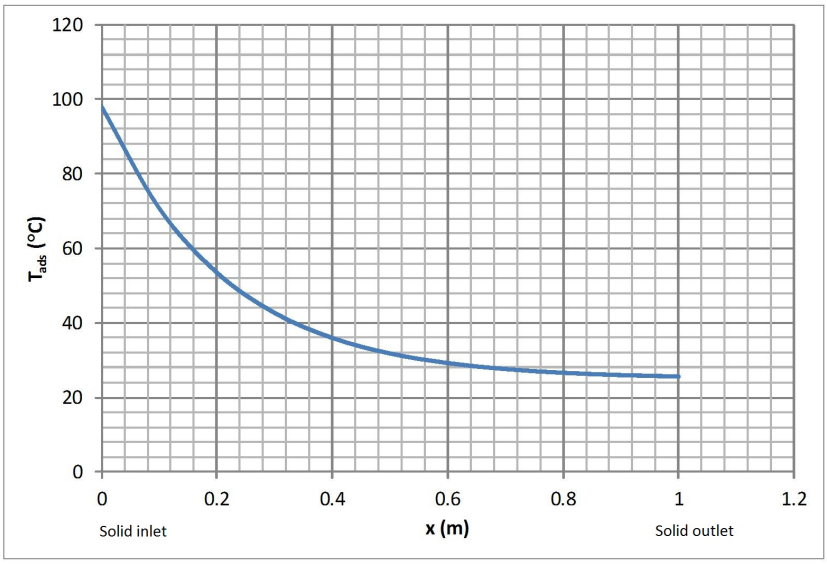

Figure 8.14: Adsorbent temperature profile in HEX 1

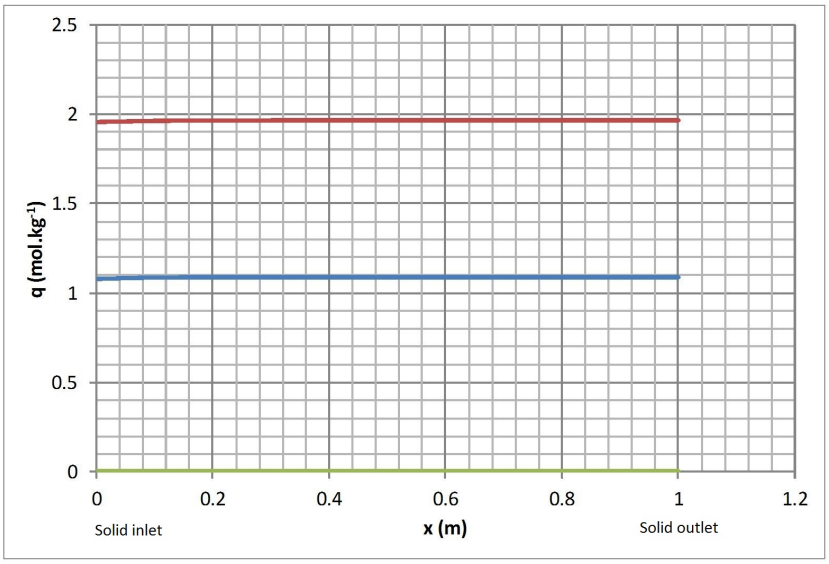

Figure 8.15: Loading profiles of components in HEX 1

8.2.1.3 Results of Adsorber and Regenerator Configurations

Table 8.3 compares CO_2 recoveries, purities and heat consumption for the three types of CO_2 adsorbers in the cycle shown in Figure 8.1 for which the regenerator type is fixed as a counter-current regenerator. The same parameters as given in Table 8.1 are used for the cycle with counter-current, co-current and fluidised bed adsorbers except that for the fluidised bed adsorber, a higher adsorbent void fraction of $\varepsilon_a = 0.4$ is used for the adsorber. The best performance is found for a counter-current adsorber as it allows the highest CO_2 recovery and purity. A cycle with a counter-current adsorber also requires less heat for adsorbent regeneration.

Table 8.3: CO_2 recoveries, purities and regeneration heat duties for CO_2 capture cycles using the supported amine adsorbent

	Counter-current adsorber Counter-current regenerator	Co-current adsorber Counter-current regenerator	Fluidised bed adsorber Counter-current regenerator
CO_2 recovery	92.8%	74.9%	74.6%
CO_2 wet purity	65.0%	66.9%	66.0%
CO_2 dry purity	96.7%	95.6%	95.3%
Steam consumption for regeneration ($kg.s^{-1}$)	55.4	58.5	58.4

The heat consumption for the counter-current adsorber is lower than for the co-current or fluidised bed adsorbers because the adsorbent leaves the counter-current adsorber at a higher temperature than the fluidised bed or the co-

current adsorber as shown in Figure 8.16. Therefore, more heat needs to be supplied to the adsorbent to bring it to the temperature at which regeneration is carried out.

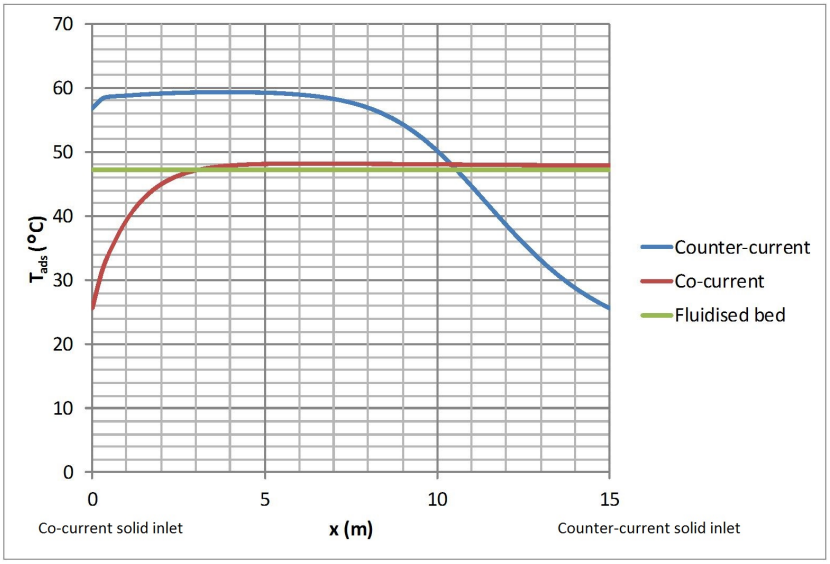

Figure 8.16: Adsorbent temperature profiles for cycles with counter-current, co-current and fluidised bed adsorbers for supported amine adsorbent

The CO_2 recovery is higher for a cycle with a counter-current adsorber because the CO_2 working capacity (difference in CO_2 loading between adsorption and desorption conditions) is higher than for a co-current system as shown in Figures 8.17 and 8.18. During regeneration, there is a CO_2 partial pressure of 0.48 bar for the cycle with a counter-current adsorber (cf. Figure 8.17) and 0.56 bar for the co-current adsorber because water is desorbed therefore it lowers the partial pressure of CO_2.

In the cycle with a co-current adsorber, the equilibrium CO_2 loading needed to achieve a 90% CO_2 capture is lower than the loading of CO_2 at the adsorbent outlet from the regenerator as shown in Figure 8.18.

In order to achieve a 90% CO_2 recovery in the co-current mode, the regenerator must be run such that the CO_2 loading on the adsorbent leaving the regenerator is lower than the CO_2 equilibrium loading at the outlet of the adsorber.

A CO_2 recovery of 90% in co-current mode can't be achieved by increasing the flowrate of adsorbent in the system but it could be obtained by using a much higher flowrate of steam in the regenerator such that the CO_2 partial pressure of gas leaving the regenerator is below 0.3 bar as shown in Figure 8.18.

Krutka and Sjostrom (2011) also failed to achieve a 90% CO_2 recovery for a co-current adsorber and a fluidised bed regenerator. They later modified their process design and used counter-current stages of fluidised beds as the adsorber

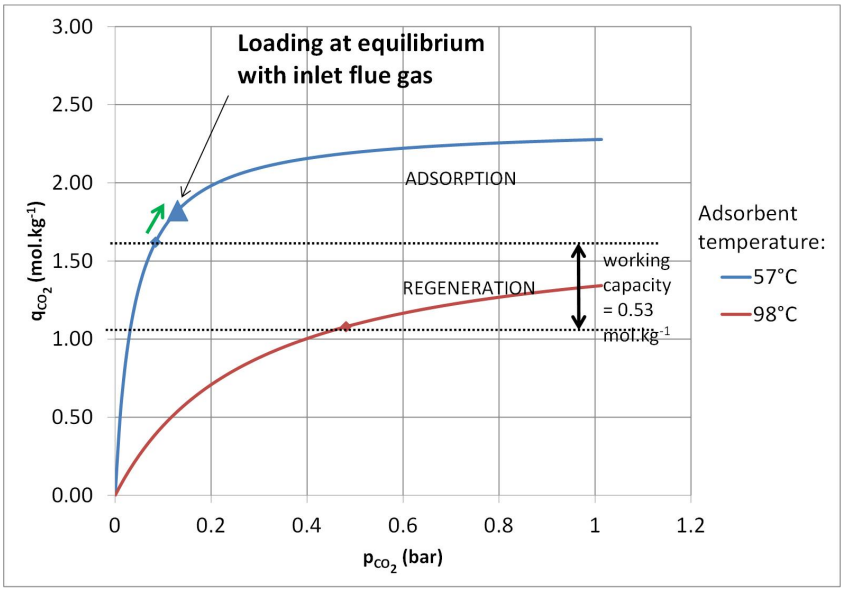

Figure 8.17: Isotherms at adsorption and regeneration for the cycle with a counter-current adsorber for supported amine adsorbent

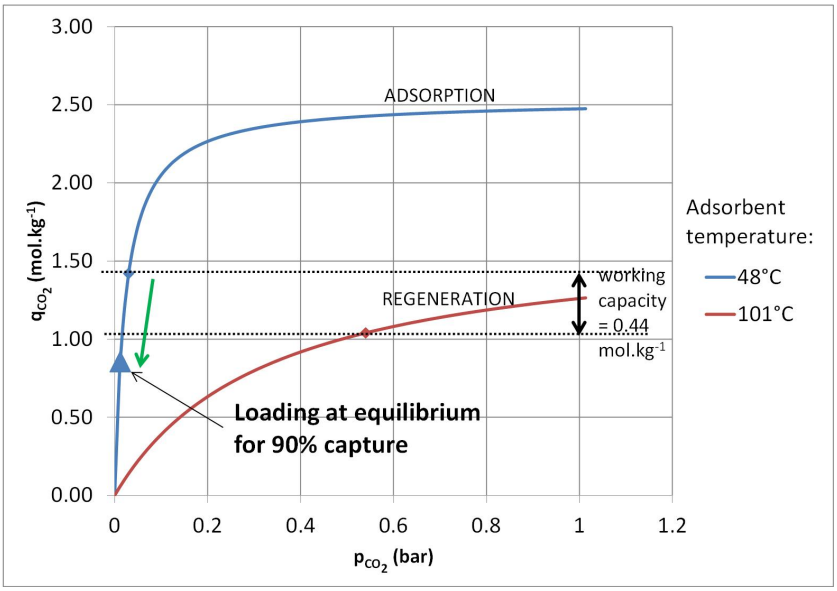

Figure 8.18: Isotherms at adsorption and regeneration for the cycle with a co-current adsorber for supported amine adsorbent

and a single fluidised bed regenerator (Krutka et al. (2013)). Results of this process or any sign of improvement have not yet been published.

8.2.1.4 Heat Consumption in the Base Case

The power consumption to produce the required molar flowrate of steam at 120°C from water assumed to be at 25°C is shown in Figure 8.19. It was calculated from the sensible heat required to elevate the temperature of liquid

water at 25°C to its boiling point, the latent heat of vaporisation and the sensible heat required to elevate the steam temperature from 100°C to 120°C. The total heat rate needed to run the regenerator by external heating and steam purging is therefore:

$$Q_{heat} = Q_{steam} + Q_{ext} \tag{8.1}$$

for which,

$$Q_{steam} = \left(H_{H_2O,gas} + \Delta H_{vap} + H_{H_2O,liq}\right) \dot{M}_{in} \tag{8.2}$$

where:

Q_{heat}: total heat rate provided to the regenerator (W)

Q_{steam}: heat supplied by steam (W)

$H_{H_2O,gas}$: gas enthalpy (J.mol^{-1})

ΔH_{vap}: latent heat of vaporisation (J.mol^{-1})

$H_{H_2O,liq}$: liquid enthalpy (J.mol^{-1})

$\dot{M}_{in}$: molar flowarate of steam (mol.s^{-1})

Q_{ext}: heat rate provided by external heating, $-U_{ext}A_{ext}(T - T_{ext})$ (W)

The gas enthalpy is estimated from Equation 3.37 and with coefficients found from Table 3.1. The liquid enthalpy, $H_{H_2O,liq}$, was found from the same equation as Equation 3.37 but with coefficients given in Table 8.4. Applying Equation 3.37 gives $H_{H_2O,liq}$ in kJ.mol^{-1}. A value of 40706 J.mol^{-1} was used for the latent heat of vaporisation of water as found from Perry et al. (1997).

Table 8.4: Coefficients in for the enthalpy of liquid water (National Institute of Standards and Technology (2014))

	H_2O (liquid)
A	-230.6060
B	1523.290
C	-3196.413
D	2474.455
E	3.855326
F	-256.5478
H_{ref}	-285.8304

In the base case, the heat duty required for one of the four parallel trains is 125.24 MW (500.96 MW in total). Of this heat duty, 120.28 MW (cf. Table

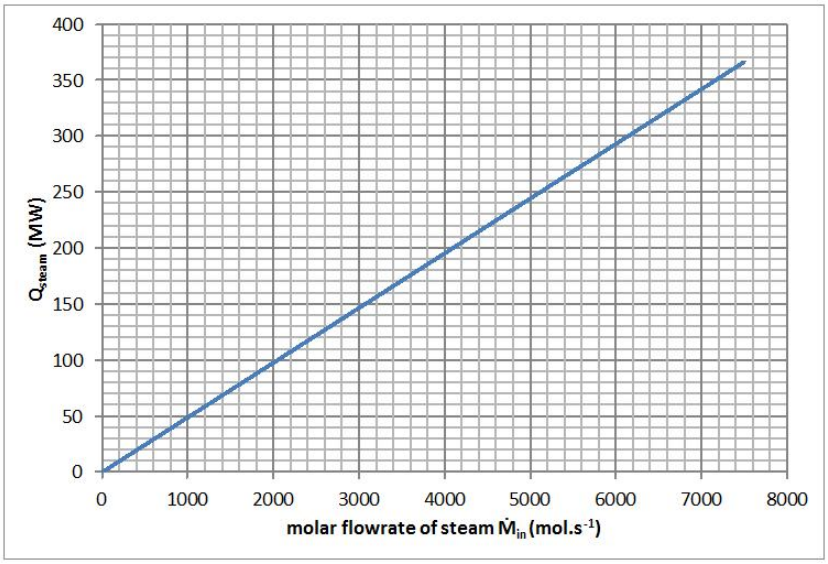

Figure 8.19: Heat supplied to produce steam as a function of steam molar flowrate

8.5) is supplied by HEX 2 whereas 4.96 MW is supplied to make 100 mol.s^{-1} of steam at 120°C into the regenerator.

Table 8.5: Heat requirements of the adsorber, regenerator and heat exchangers

	Adsorber	HEX 2	Regenerator	HEX 1
Heat duty from/to external surroundings (MW)	0	120.28	0	-119.89

The reboiler in the amine absorption process considered by Fisher et al. (2005) supplies roughly the same rate of heat as the base case adsorption system studied here. The heat capacity of the adsorbent (1255 J.kg^{-1}.K^{-1}) is lower than the heat capacity of the 30% by mass MEA solution (3734 J.kg^{-1}.K^{-1}) (Weiland et al. (1997)). The adsorbent mass flowrate (1200 kg.s^{-1}) is greater than the flowrate of the amine-water solution (689 kg.s^{-1}) and therefore there is no benefit achieved as the amine absorption process also requires the same heat duty. The absence of any benefit found by using adsorbents in a moving bed adsorption cycle is also due to this process lacking heat integration to recover heat from the adsorbent which is at high temperature at the outlet of the regenerator. On the other hand, the analogous amine absorption process is equipped with a lean/rich amine heat exchanger to improve energy efficiency. The addition of heat integration to the moving bed adsorption process is also considered and this is discussed in detail later in this chapter in section 8.2.7.

8.2.2 Effect of the Adsorbent Flowrate

Previously in section 6.7, a sensitivity analysis for the supported amine adsorbent, activated carbon and zeolite 13X was carried out in a single countercurrent adsorber for which it was assumed that the adsorbent was fully regenerated as it entered the adsorber. The minimum mass flowrates of the adsorbents required to achieve 90% CO_2 recovery were determined. A similar analysis is carried out in this section for the effect of a variation in mass flowrate of adsorbent in the base case CO_2 moving bed adsorption cycle.

It was also shown previously in Chapter 7, that activated carbon would be less suitable to use in the moving bed process considered and represented by Figure 8.1 because of low CO_2 product purities which is caused by a low CO_2 to N_2 selectivity. Therefore, sensitivity analyses have not been carried out for activated carbon in the full CO_2 capture cycle as it has been assumed that N_2 is not loaded onto the surface of the supported amine adsorbent and a higher selectivity can be reached with this adsorbent. All values shown in Table 8.1 have been used except for the adsorbent mass flowrate which has been varied to test the sensitivity of the base case CO_2 capture system to the adsorbent throughput.

The effect of the mass flowrate of the supported amine adsorbent used is shown in Figure 8.20. It can be seen from this figure that by interpolation, a mass flowrate of at least 1130 $kg.s^{-1}$ must be used to achieve a 90% CO_2 recovery.

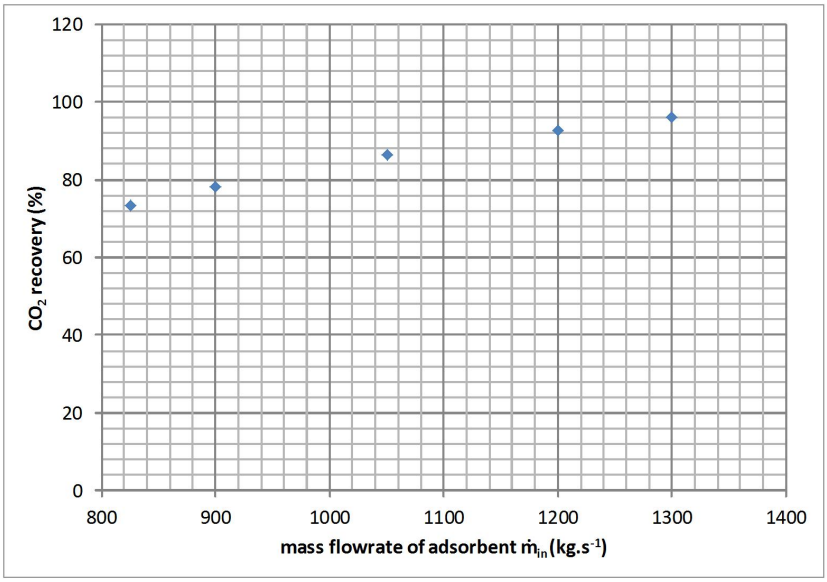

Figure 8.20: Effect of the mass flowrate of adsorbent on CO_2 recovery for the cyclic process using the supported amine adsorbent

The wet CO_2 purity drops with higher mass flowrates of adsorbent (cf.

Figure 8.21) due to higher rates of water being loaded. However, the dry CO_2 purity is not greatly affected by rising adsorbent flowrates as shown in Figure 8.22.

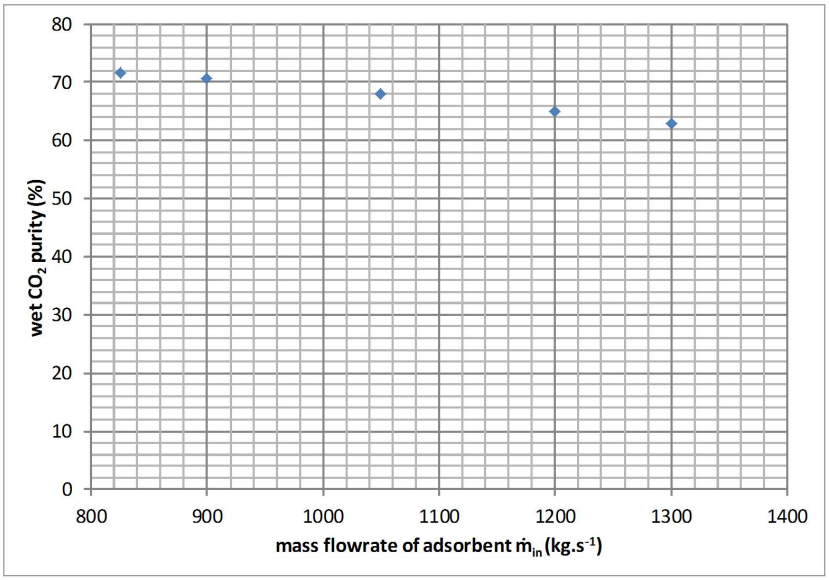

Figure 8.21: Effect of the mass flowrate of adsorbent on the wet CO_2 purity for the cyclic process using the supported amine adsorbent

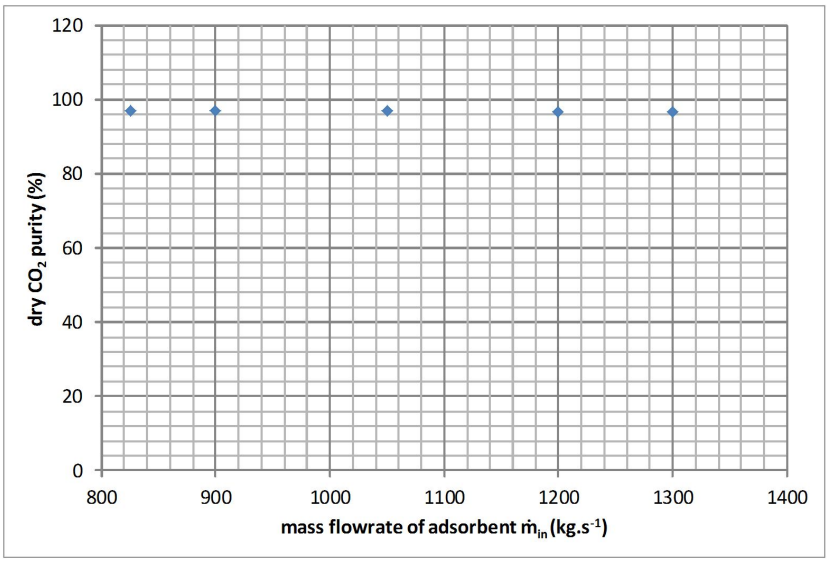

Figure 8.22: Effect of the mass flowrate of adsorbent on the dry CO_2 purity for the cyclic process using the supported amine adsorbent

The heat duty varies linearly with mass flowrate of adsorbent. Thus, lower mass flowrates of the adsorbent reduce the heat duty required to regenerate the adsorbent as shown in Figure 8.23.

For the base case with a flowrate of 1200 kg.s^{-1} through one of the four CO_2 capture trains, the CO_2 recovery found was 92.8% and the heat duty that must

be supplied via HEX 2 and steam used in the regenerator add up to 125.24 MW (500.96 MW in total for four parallel trains). This heat duty is the same heat supplied in the analogous amine absorption process considered by Fisher et al. (2005). Reducing the adsorbent flowrate from 1200 kg.s^{-1} to 1130 kg.s^{-1} would allow the process to still reach a 90% recovery and a dry CO_2 purity of 96% (cf. Figure 8.22). However, the heat duty would be reduced to 118.97 MW for a single train (475.88 MW in total for four trains). Consequently, a saving of 5% in the heat duty would be met if the mass flowrate is reduced.

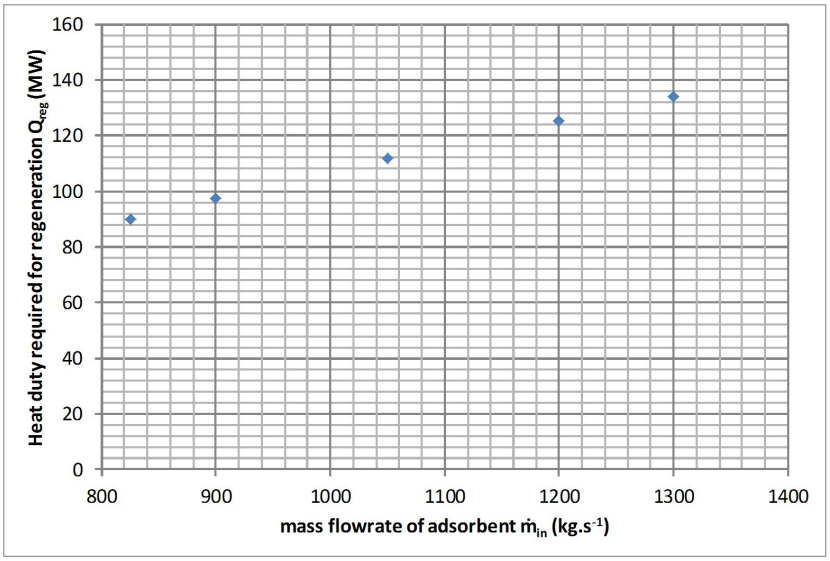

Figure 8.23: Effect of the mass flowrate of adsorbent on the regeneration heat duty for the cyclic process using the supported amine adsorbent

Øi (2007) carried out a sensitivity analysis of the amine solution flowrate in absorption process for CO_2 capture. He also found that as CO_2 recovery increased with higher flowrates, heat consumption increased too. An optimum point for the heat consumption was found for which the amine circulation rate could be minimised.

8.2.3 Effect of the Regeneration Gas Flowrate

Effect of Purging with Steam

In Chapter 7, a lower flowrate of adsorbent was used in the regenerator and a higher flowrate of steam of 1000 mol.s^{-1} as purge gas was used to remove above 90% of adsorbed CO_2. In the cyclic process in this chapter, a higher adsorbent flowrate is used and the adsorbent enters the regenerator at a higher temperature than in Chapter 7.

From Figure 8.24, it can be seen that steam is not necessary to recover above 90% of the CO_2 in the flue gas because the adsorbent is already heated in HEX

2. An additional supply of steam does however improve the CO_2 recovery slightly (cf. Figure 8.24). If steam is not supplied in the regenerator, the CO_2 recovery would be 90.8% and the dry purity of CO_2 would be 96.6%. The heat duty required without steam is 121.14 MW per train (484.56 MW in total) as shown in Figure 8.25. There would be a saving of 3.2% of power consumed in the base case. Yang and Hoffman (2009) suggest that a regeneration gas is necessary in the regenerator to improve heat transfer. If the steam flowrate into the regenerator is increased, the total heat duty required to regenerate the adsorbent increases because of the energy penalty required to produce steam.

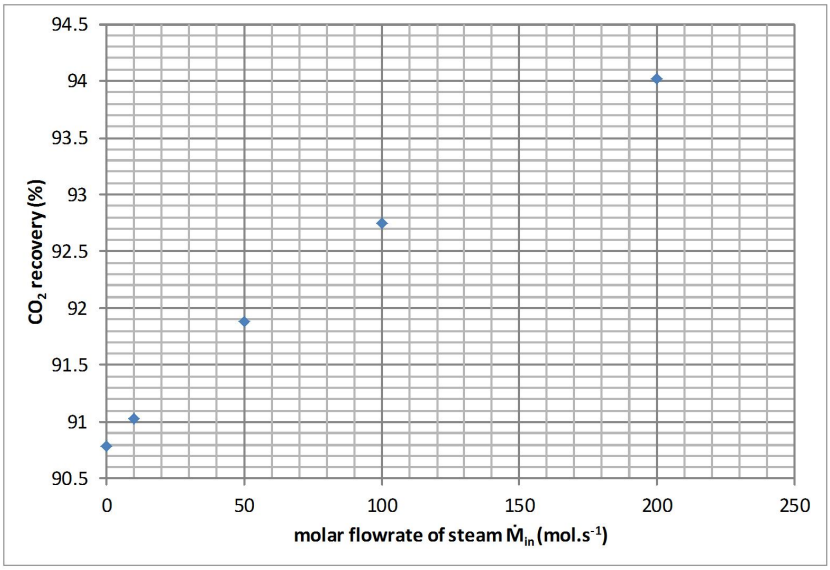

Figure 8.24: Effect of the flowrate of steam used at the inlet to the regenerator on CO_2 recovery for the cyclic process using the supported amine adsorbent

As it can be expected, the wet purity of CO_2 would be higher in the absence of steam as the regeneration gas (cf. Figure 8.26) because the gas leaving the regenerator would contain less water. In large, the dry purity remains unaffected by the use of steam as shown in Figure 8.27.

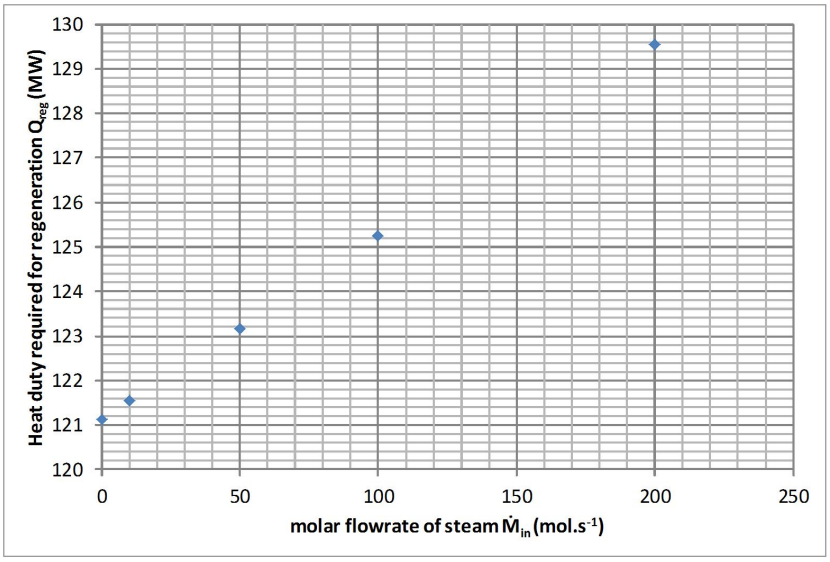

Figure 8.25: Effect of the flowrate of steam used at the inlet to the regenerator on the regeneration heat duty for the cyclic process using the supported amine adsorbent

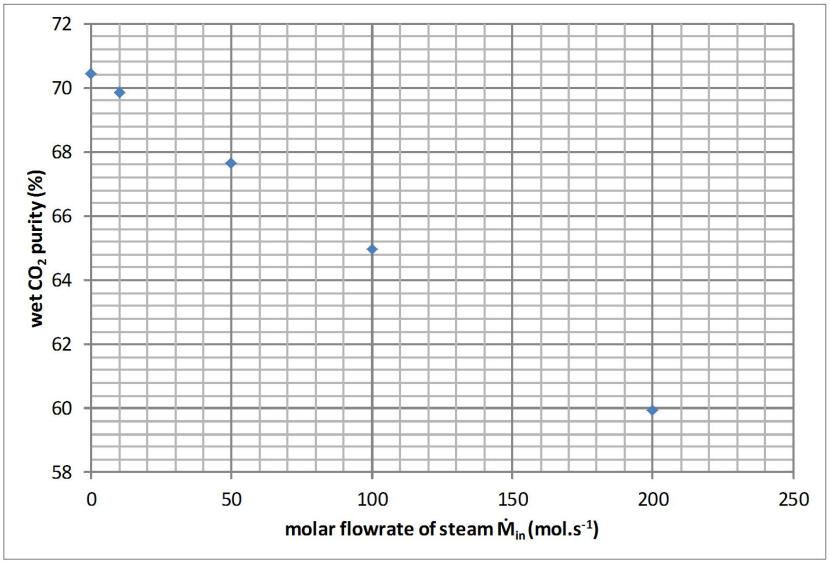

Figure 8.26: Effect of the flowrate of steam used at the inlet to the regenerator on the wet CO_2 purity for the cyclic process using the supported amine adsorbent

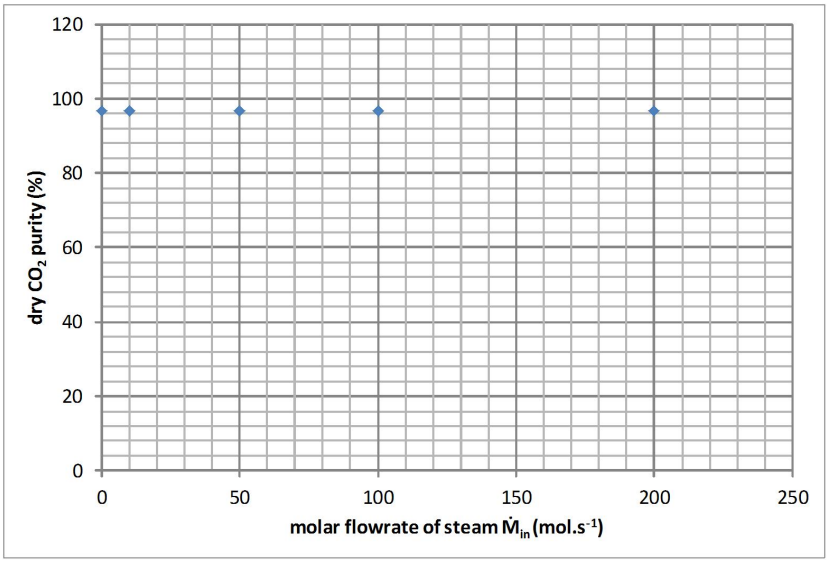

Figure 8.27: Effect of the flowrate of steam used at the inlet to the regenerator on the dry CO_2 purity for the cyclic process using the supported amine adsorbent

Comparison between Supplying Steam as a Purge Gas in the Regenerator or in HEX 2

To regenerate the adsorbent by increasing its temperature, heat can be supplied to HEX 2 and it can be supplied by steam directly supplied into the regenerator which also lowers the partial pressure of CO_2 which increases adsorbent regeneration. In this section, the option that offers the lowest total heat duty for adsorbent regeneration is investigated. It is assumed that the heat supplied to the heat exchanger is supplied by condensing steam.

In Figure 8.28, the flowrate of steam into the regenerator was increased and the mass flowrate of adsorbent was adjusted to maintain a 93% CO_2 recovery. Although there is no a clear advantage for either option, as the curve shown in Figure 8.28 is somewhat flat. However, there is an optimum near 400 mol.s^{-1} of steam into the regenerator which corresponds to a minimum heat duty. If the steam flowrate is reduced, the adsorbent is not well regenerated and a higher flowrate of adsorbent is required which leads to higher heat duties for HEX 2. If the steam flowrate is increased, the heat duty in HEX 2 reduces. The adsorbent is regenerated better and a lower adsorbent flowrate is needed but at the expense of a higher heat duty to produce steam into the regenerator. Based on cost, the optimum case would be to have no flow of steam and remove the regenerator from the process as regeneration can be carried out in HEX 2.

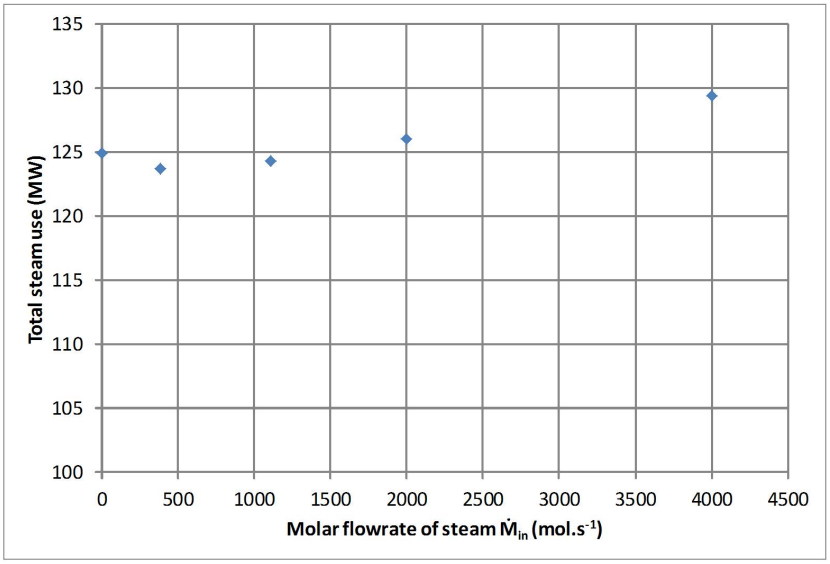

Figure 8.28: Effect of the flowrate of steam used at the inlet to the regenerator on the total energy required for adsorbent regeneration

Effect of Purging with CO_2

It was shown previously in section 7.9 that if pure CO_2 was used to regenerate the adsorbent inside the single regenerator, CO_2 would not be desorbed in the regenerator but instead it would be adsorbed. However, the temperature of the adsorbent at the inlet to the regenerator is higher in the regenerator used inside the full cycle. Additionally at the adsorbent inlet, the concentration in CO_2 of the bulk gas is higher than the pore concentration which caused CO_2 to be adsorbed. The opposite is true for the regenerator in the full cycle and CO_2 can be successfully used to regenerate the supported amine adsorbent but a minimal flowrate of regeneration gas is preferable in order to increase the CO_2 recovery (cf. Figure 8.29). The CO_2 recovery drops because the CO_2 loading at the adsorbent outlet from the regenerator increases for higher flowrates of CO_2 used as the regeneration gas. Therefore, the adsorbent has a lower working capacity which reduces the CO_2 recovery of the process. To achieve higher CO_2 recoveries, it is better to use higher flowrates of steam than CO_2. The heat duty of HEX 2 remains constant for increasing flowrates of CO_2 as regeneration gas because the adsorbent temperature leaving the adsorber remains mostly constant for increasing flowrates of CO_2 (cf. Figure 8.30).

Krutka and Sjostrom (2011), Veneman et al. (2012), Yang and Hoffman (2009) and Zhang et al. (2014) have all attempted or considered to use pure CO_2 at high temperatures above 100°C to regenerate their adsorbent. However, implications of the use of pure CO_2 is not discussed widely in literature. Steam was not considered as a regeneration gas by Krutka and Sjostrom (2011).

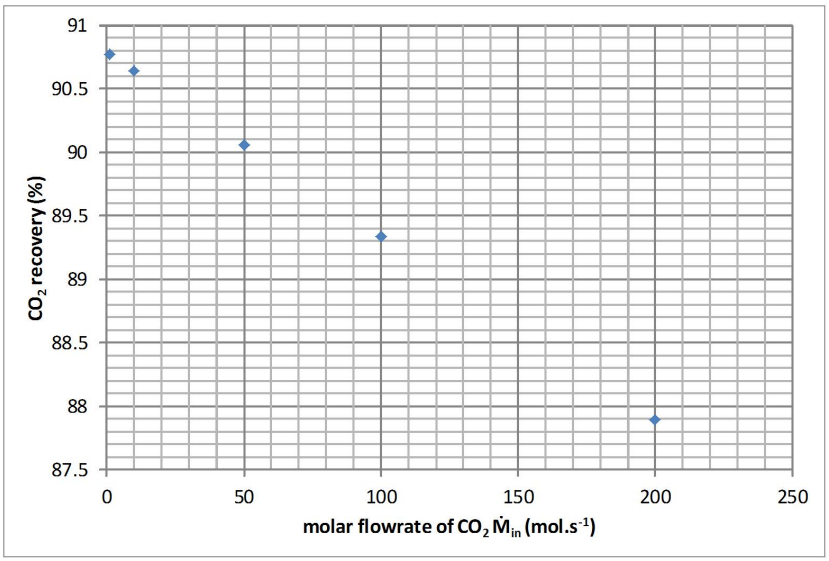

Figure 8.29: Effect of the flowrate of CO_2 used at the inlet to the regenerator on CO_2 recovery for the cyclic process using the supported amine adsorbent

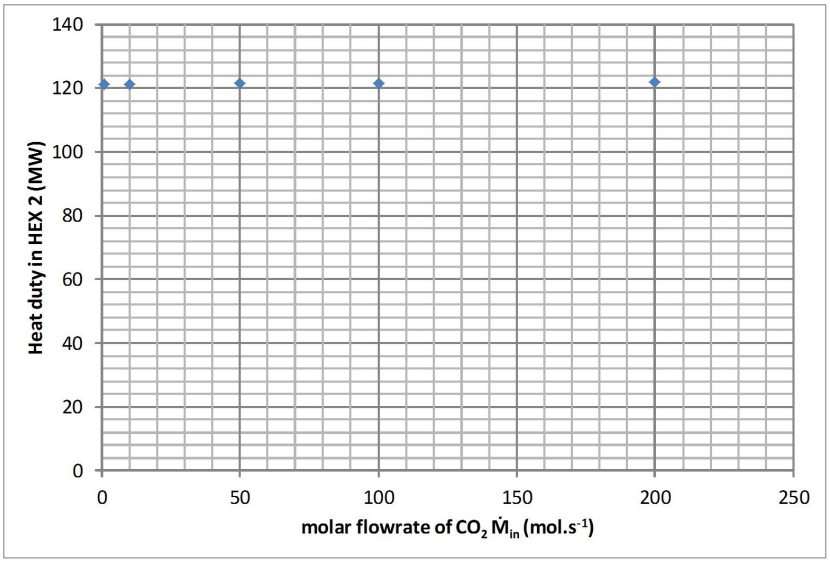

Figure 8.30: Effect of the flowrate of CO_2 used at the inlet to the regenerator on the heat duty in HEX 2 for the cyclic process using the supported amine adsorbent

The wet and dry CO_2 purities for increasing regeneration gas flowrates of CO_2 are shown in Figures 8.31 and 8.32. The wet CO_2 purity increases because the gas at the outlet of the regenerator contains more CO_2. The dry CO_2 purity remains mostly constant although there is also a slight increase in dry CO_2 purity due to higher flowates of CO_2 in the gas leaving the regenerator.

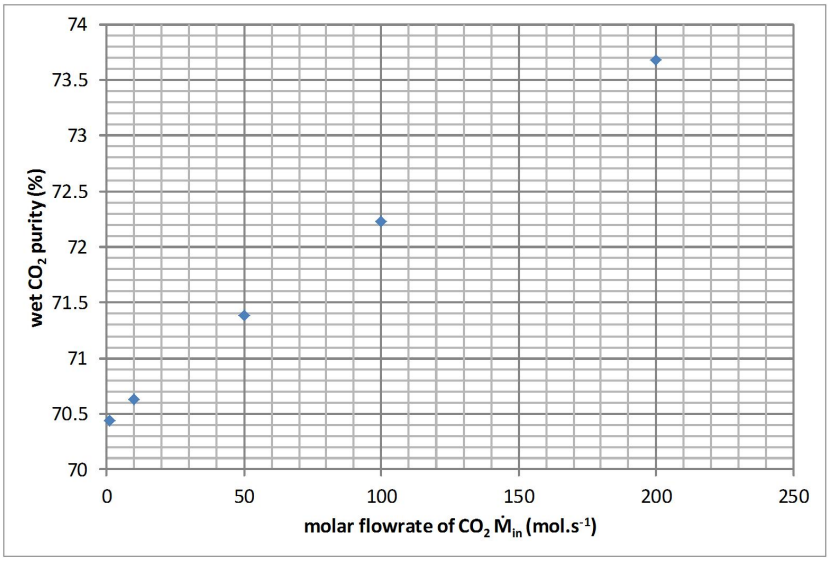

Figure 8.31: Effect of the flowrate of CO_2 used at the inlet to the regenerator on the wet CO_2 purity for the cyclic process using the supported amine adsorbent

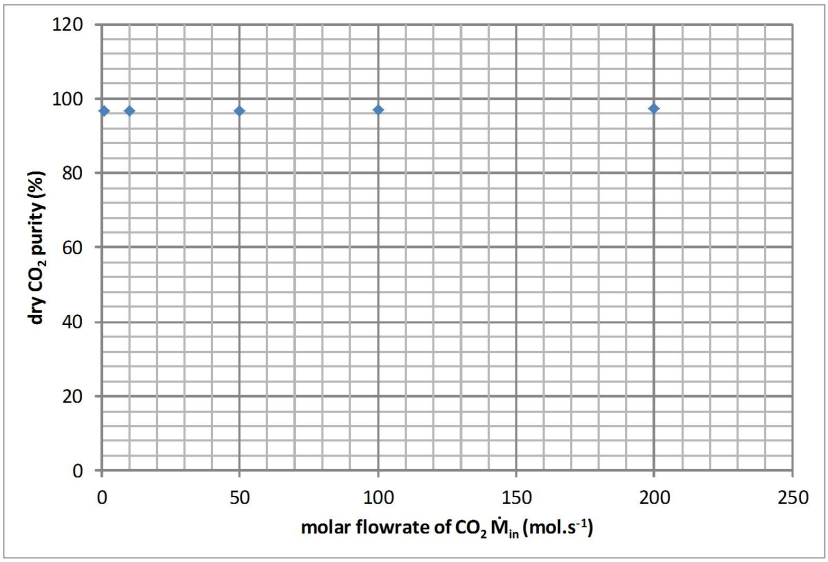

Figure 8.32: Effect of the flowrate of CO_2 used at the inlet to the regenerator on the dry CO_2 purity for the cyclic process using the supported amine adsorbent

In this section it has been seen that the regenerator in the process is unnecessary as it is not doing a great deal of work in regenerating the adsorbent. Only the adsorbent heater (HEX 2) is needed. Either CO_2 or steam can be used as purge gases. Krutka et al. (2013) use a fluidised bed as the regenerator, however, it is effectively an adsorbent heater and there is no real regenerator in their process. They use CO_2 in the heater to keep the bed fluidised.

8.2.4 Effect of the Heat Removal from the CO_2 Lean Adsorbent in HEX 1

It is essential that the adsorbent is sufficiently cool prior to entering the adsorber. This is demonstrated in Figure 8.33 by low CO_2 recoveries for high adsorbent inlet temperatures into the adsorber. The adsorbent should be cooled to at least 28°C for the process to recover 90% of CO_2. If the adsorbent is introduced at a higher temperature, the CO_2 recovery drops greatly because the working capacity of the adsorbent becomes too low.

For example, in Table 8.6, the effect on the adsorbent temperature and working capacity is shown for two cases of adsorbent inlet temperatures into the adsorber. If the adsorbent is only cooled to 86.7°C instead of 25.6°C, the working capacity of the adsorbent is roughly ten times lower.

The wet CO_2 purity passes through a maximum value if the adsorbent enters at a temperature of roughly 50°C as shown in Figure 8.34. The wet CO_2 purity is low if the adsorbent enters the adsorber at a low temperature because more water is adsorbed. When the adsorbent is regenerated, the mole fraction of

Table 8.6: Results of the performance of full CO_2 capture cycles for an outlet adsorbent temperature from HEX 1 at a value higher than the base case and for the base case

Adsorbent temperature at the outlet of HEX 1	**°C**	**86.7**	**25.6**
CO_2 recovery	%	11.03	92.75
Working capacity	$mol.kg^{-1}$	0.06	0.53

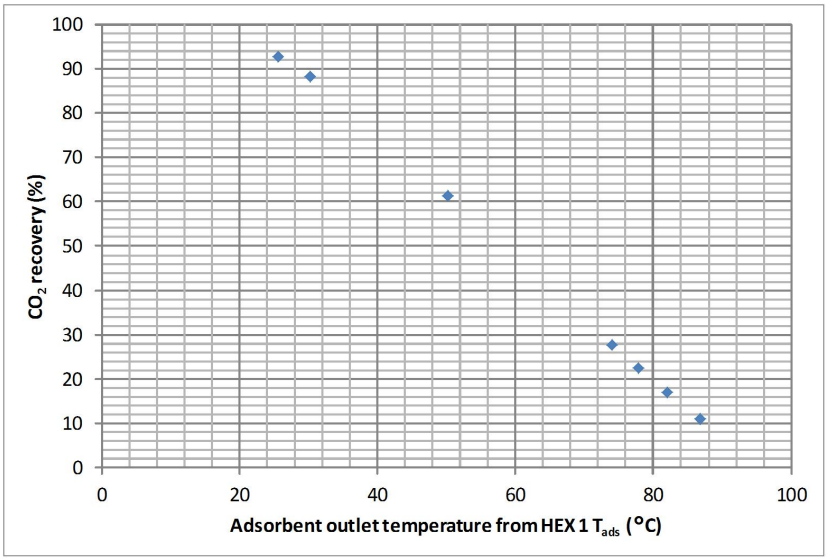

Figure 8.33: Effect of the outlet adsorbent temperature from HEX 1 on CO_2 recovery for the cyclic process using the supported amine adsorbent

water at the outlet of the regenerator would be high and therefore, the wet CO_2 purity drops as shown in Figure 8.34. The dry CO_2 purity is not affected by cooler adsorbent entering the adsorber as it remains close to 97% as shown in Figure 8.35.

If the adsorbent enters the adsorber at higher temperatures, less CO_2 is adsorbed whilst the pores of the adsorbent contains similar levels of N_2 regardless of adsorbent temperature. Consequently, the ratio between the concentration of N_2 and CO_2 at the gas outlet of the regenerator would be higher. Therefore, the wet CO_2 purity drops if the adsorbent is not sufficiently cooled.

If the adsorbent is not cooled enough, the adsorbent leaves the adsorber at a higher temperature, thereby requiring less heat to increase its temperature in HEX 2. Therefore, besides lower capital costs associated with HEX 1 being of smaller size, there is a push to minimise the size of HEX 1. The energy consumption for adsorbent regeneration would be lowered as shown in Figure 8.36. If the adsorbent is introduced into the adsorber at 28°C instead of 25.6°C, 90% of CO_2 is recovered and the heat duty for regeneration is lowered: 122.35

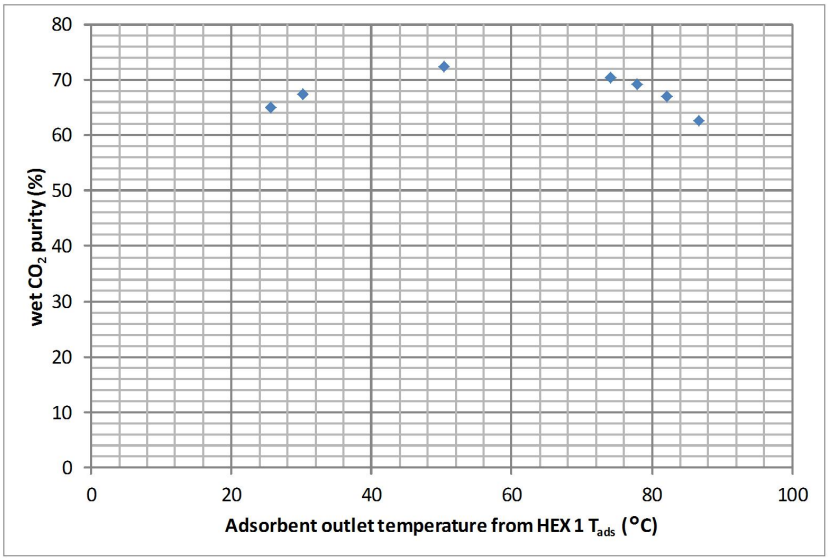

Figure 8.34: Effect of the outlet adsorbent temperature from HEX 1 on the wet CO_2 purity for the cyclic process using the supported amine adsorbent

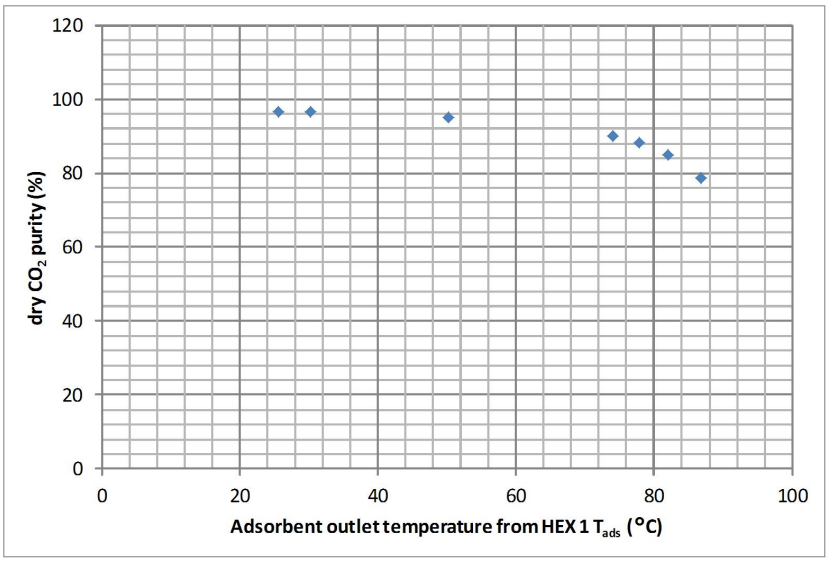

Figure 8.35: Effect of the outlet adsorbent temperature from HEX 1 on the dry CO_2 purity for the cyclic process using the supported amine adsorbent

MW per train (489.4 MW in total). However, the saving in energy is only 2.3% lower than the energy saved by reducing the mass flowrate of the adsorbent or the flowrate of regeneration gas to maintain a 90% CO_2 recovery (cf. sections 8.2.2 and 8.2.3). For a constant CO_2 recovery, if the adsorbent cooler outlet temperature is higher, the CO_2 loading is less and a higher adsorbent flowrate would be required. The heat duty of HEX 2 would therefore increase.

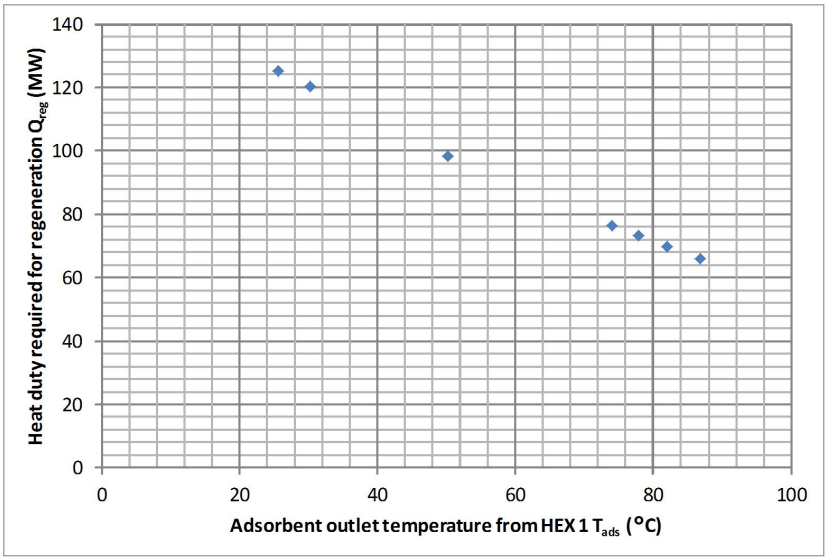

Figure 8.36: Effect of the outlet adsorbent temperature from HEX 1 on the regeneration heat duty for the cyclic process using the supported amine adsorbent

8.2.5 Effect of the Heat Addition to the CO_2 Rich Adsorbent in HEX 2

In this section, the rate of heat transferred to the adsorbent in HEX 2 has been varied whilst all other parameters in Table 8.1 were held constant. If the adsorbent is introduced into the regenerator at a higher temperature, it is expected that more CO_2 would be desorbed, resulting in a higher CO_2 recovery. This is confirmed in Figure 8.37 which shows that the level of CO_2 recovery increases for higher adsorbent temperatures into the regenerator.

Table 8.7 shows the impact of introducing the adsorbent into the regenerator at only 104.8°C instead of 118.5°C. If it is introduced at 104.8°C, 90% CO_2 recovery is not reached because the CO_2 loading at the adsorbent outlet of the regenerator is too high which reduces the working capacity of the adsorbent.

Table 8.7: Results of the performance of full CO_2 capture cycles for an outlet adsorbent temperature from HEX 2 at a value lower than the base case and for the base case

Adsorbent temperature at the outlet of HEX 2	**°C**	**104.8**	**118.5**
CO_2 recovery	%	81.43	92.75
Heat duty	MW	104.74	125.24
CO_2 loading at the outlet of the regenerator	$mol.kg^{-1}$	1.55	1.08

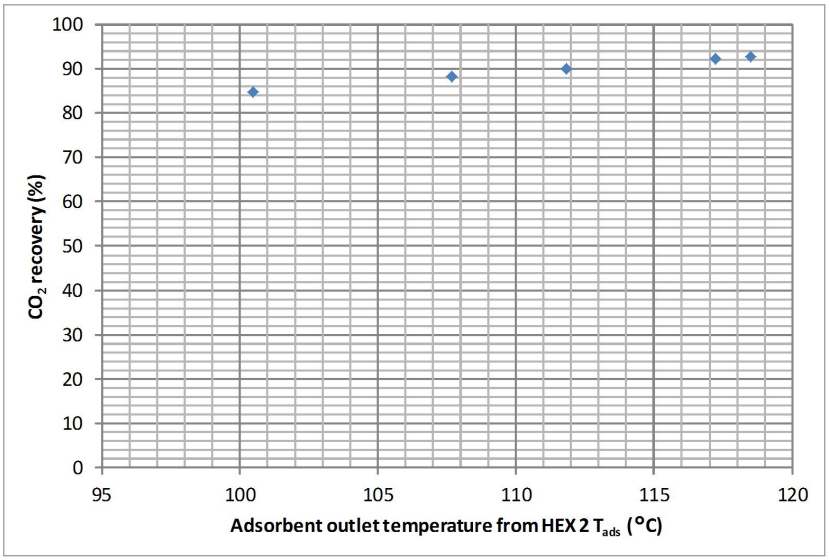

Figure 8.37: Effect of the outlet adsorbent temperature from HEX 2 on CO_2 recovery for the cyclic process using the supported amine adsorbent

Less water is desorbed if the adsorbent inlet temperature into the regenerator is low. Therefore, the wet CO_2 purity drops for increasing adsorbent temperatures into the regenerator because more water would be desorbed in the regenerator (cf. Figure 8.38). The dry CO_2 purity remains constant as shown in Figure 8.39.

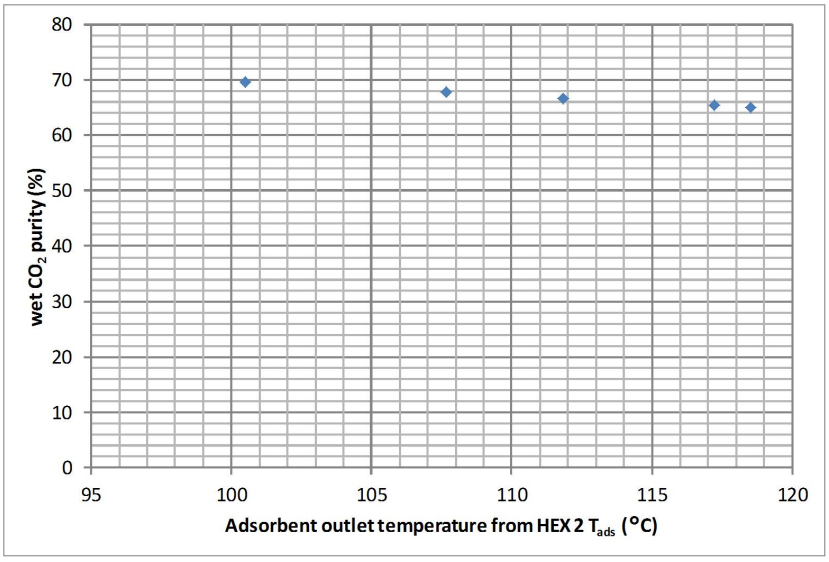

Figure 8.38: Effect of the outlet adsorbent temperature from HEX 2 on the wet CO_2 purity for the cyclic process using the supported amine adsorbent

As Figure 8.37 shows, a minimum CO_2 recovery of 90% can be met only if the adsorbent is introduced into the regenerator at 112°C. The heat duty to regenerate the adsorbent would then be reduced to 119.05 MW per train (476.2

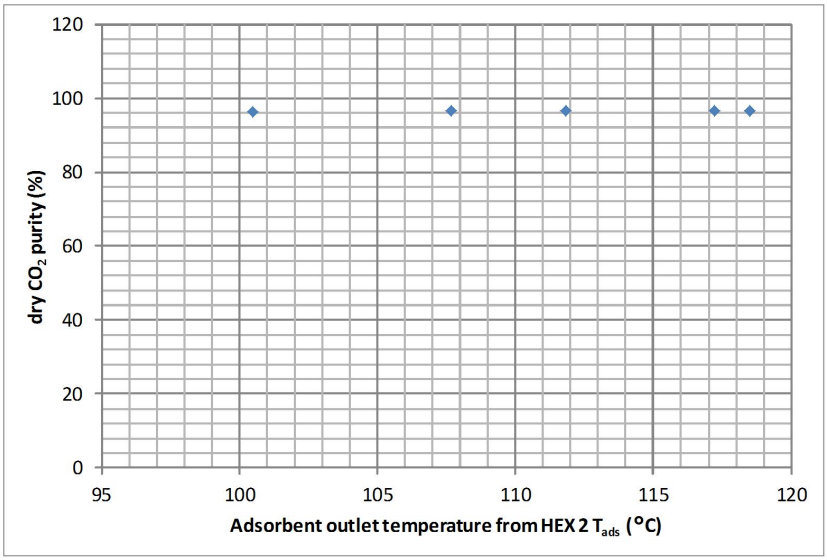

Figure 8.39: Effect of the outlet adsorbent temperature from HEX 2 on the dry CO_2 purity for the cyclic process using the supported amine adsorbent

MW in total) as shown in Figure 8.40, which is equivalent to a 4.9% saving in heat duty over the base case cycle.

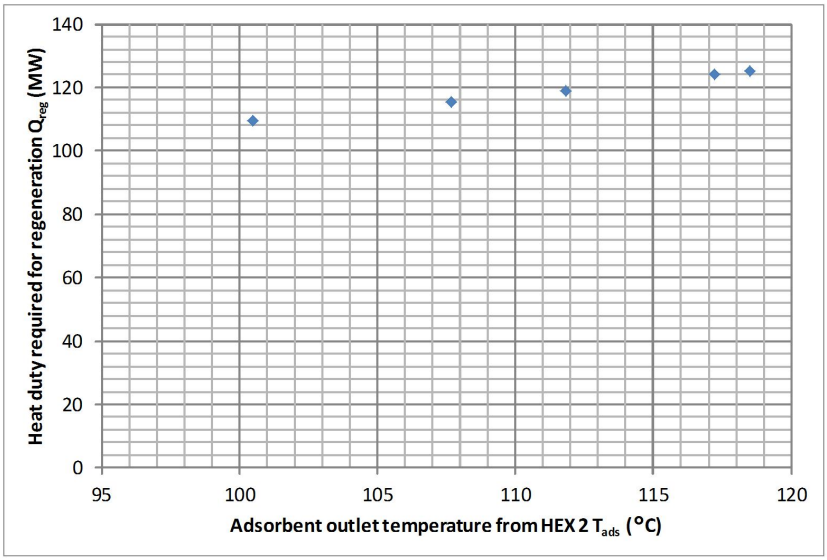

Figure 8.40: Effect of the outlet adsorbent temperature from HEX 2 on the regeneration heat duty for the cyclic process using the supported amine adsorbent

8.2.6 Effect of the Mass Transfer Coefficient

As there is some uncertainty in the mass transfer kinetics for CO_2 adsorption on the supported amine adsorbent, the sensitivity of the mass transfer constant, k_{CO_2} is tested for the base case CO_2 capture process. The mass transfer constant

of water has also been varied, in line with that of CO_2 such that $k_{CO_2} = k_{H_2O}$. The analysis of the impact of these parameters on the performance of the CO_2 capture cycle follows.

The recovery of CO_2 is severely decreased for the process if k_{CO_2} is below 4 s^{-1} (cf. Figure 8.41). It can also be seen from Figure 8.41 that k_{CO_2} should be greater than 4 s^{-1} for the overall process to achieve 90% CO_2 recovery. For the given operating conditions given in Table 8.2, lower values of k_{CO_2} would not allow a sufficient level of CO_2 to be removed from the flue gas. For example, if $k_{CO_2} = k_{H_2O} = 0.5$ s^{-1} (instead of $k_{CO_2} = 10$ s^{-1} used in the base case), the CO_2 recovery is only 33%.

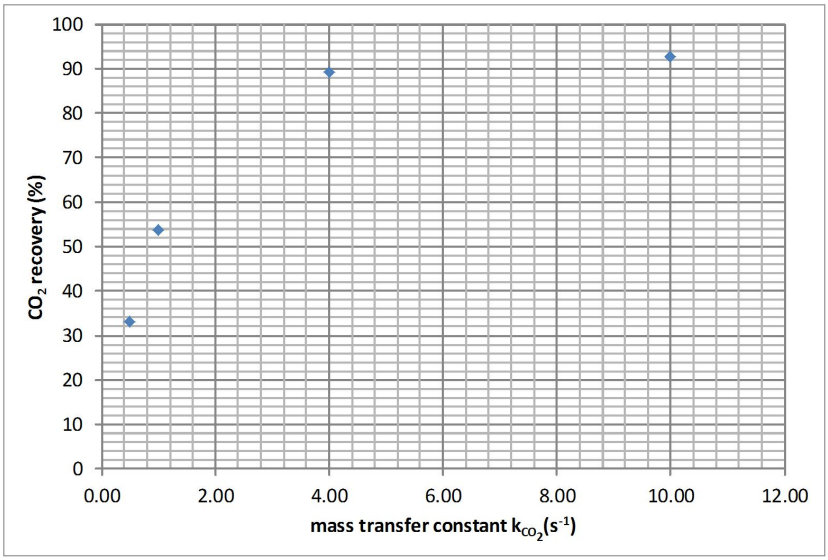

Figure 8.41: Effect of the mass mass transfer constant on CO_2 recovery for the cyclic process using the supported amine adsorbent

For low mass transfer constants, gas and adsorbent require a longer contact time inside the columns or a greater volume of adsorbent needs to be present inside the columns. Alternatively, the mass flowrate of adsorbent must be increased. If the residence time of the adsorbent is increased, the volume of the column would need to be larger however, increasing the size of the columns would also increase capital costs. Increasing the volume fraction of adsorbent in a column, ε_a, would increase the volume of adsorbent inside the column which would compensate for slower rates of adsorption per unit volume of adsorbent present. An increase in ε_a can be achieved by slowing the fall of the adsorbent in a counter-current bed. For example, changing the properties of the structured packing used inside the columns such that the adsorbent is retained for longer inside the packing would increase the residence time of the adsorbent. Using higher mass flowrates of adsorbent to compensate for slow kinetics would make the CO_2 capture process non-viable because a higher heat

duty would be necessary to regenerate the adsorbent. For example, if $k_{CO_2} = 0.5$ s^{-1}, a mass flowrate of 5200 kg.s^{-1} would only allow a 47.7% CO_2 recovery and 77.1% dry purity. The heat duty for the overall process would be 1536 MW which is excessively higher than 501 MW found for the base case process. Therefore, increasing the volume fraction of adsorbent ε_a, in the column is the most effective method to deal with slow rates of adsorption. Therefore, a series of counter-current fluidised beds with higher ε_a values than true counter-current beds would improve performance if adsorption kinetics are slow.

Additionally, low adsorption rates of CO_2 lead to higher N_2 to CO_2 ratios in the gas at the outlet of the regenerator because less CO_2 would have been adsorbed at lower mass transfer rates. But if CO_2 is adsorbed at a higher rate, lower N_2 to CO_2 ratios would be found and consequently, the wet and dry purities of CO_2 increase as shown in Figures 8.42 and 8.43.

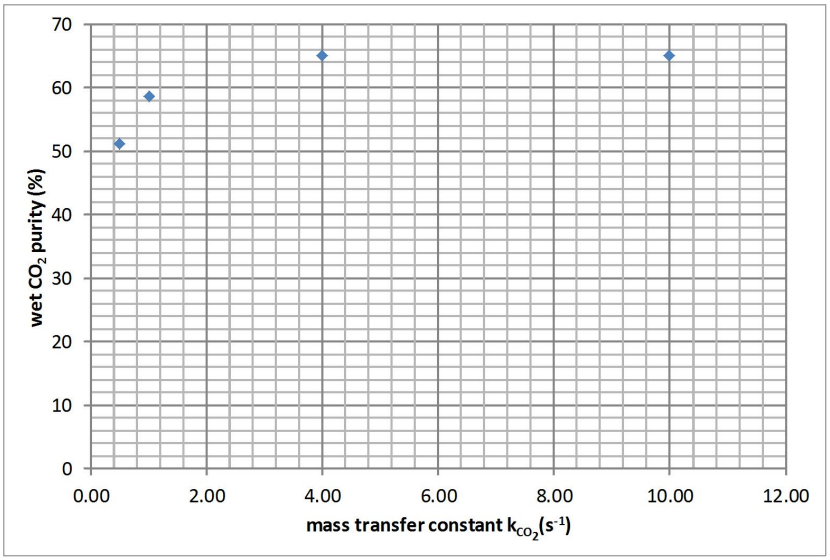

Figure 8.42: Effect of the mass mass transfer constant on the wet CO_2 purity for the cyclic process using the supported amine adsorbent

The power consumption to regenerate the adsorbent drops for increasing values of k_{CO_2} (cf. Figure 8.44) because the adsorbent would leave the adsorber with higher CO_2 and water loadings which means that more heat would be released due to the exothermic heat of adsorption (cf. Equation 3.85). The temperature of the adsorbent at the exit of the adsorber would therefore be higher for higher mass transfer constants. As a result of higher adsorbent temperatures from the adsorber, a lower heat duty needs to be supplied to increase the temperature of the adsorbent to the temperature at which the adsorbent is regenerated (approximately 120°C).

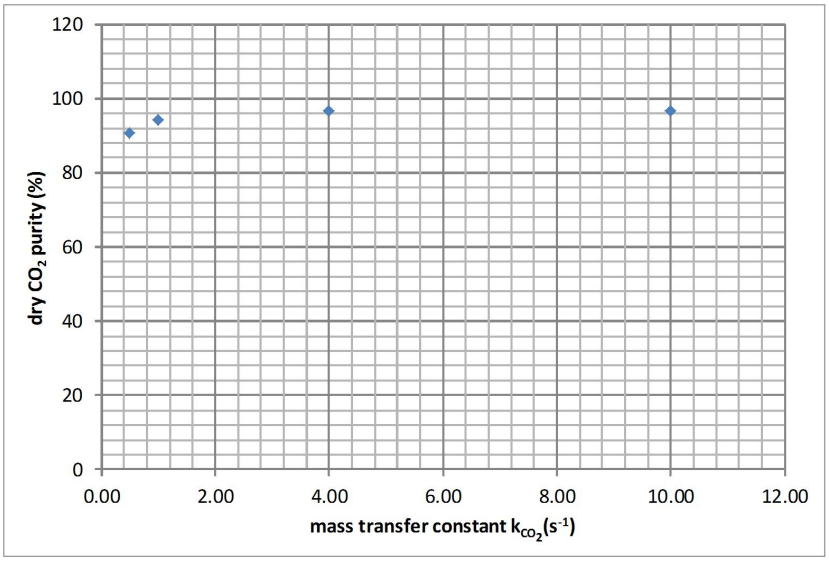

Figure 8.43: Effect of the mass mass transfer constant on the dry CO_2 purity for the cyclic process using the supported amine adsorbent

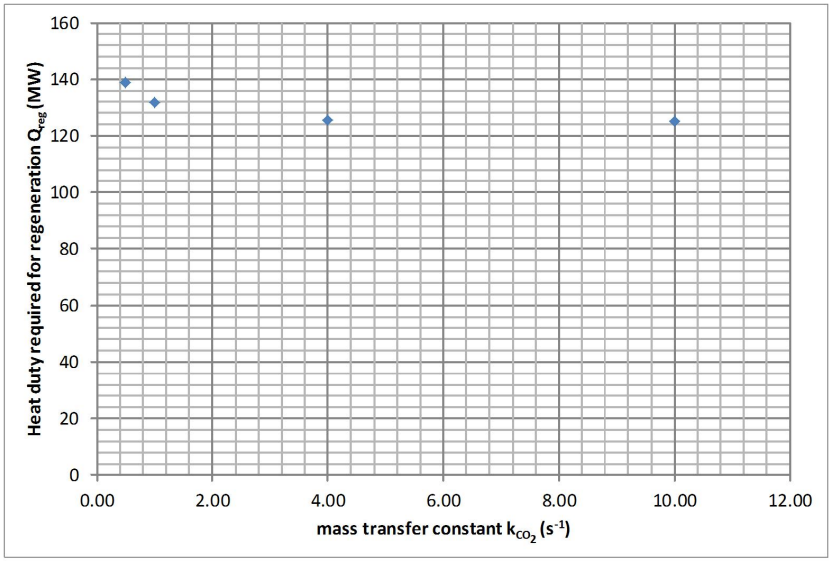

Figure 8.44: Effect of the mass mass transfer constant on the regeneration heat duty for the cyclic process using the supported amine adsorbent

8.2.7 Addition of an Intermediate Heat Exchanger in the Cycle

In amine absorption technologies, heat integration is performed in order to improve the energy efficiency of the overall CO_2 capture process. Heat integration consists of using the heat from a stream (at high temperature) that requires cooling to increase the temperature of a stream (at low temperature) that requires heating.

In this section, the addition of an intermediate heat exchanger in the cycle

is considered and the influence of the surface area of this heat exchanger on the heat duty is evaluated. The intermediate heat exchanger has the purpose of transferring heat from the CO_2 lean adsorbent leaving the regenerator to the CO_2 rich adsorbent leaving the adsorber. The diagram of the modified CO_2 capture process is shown in Figure 8.45.

Results related to the performance of the process with an intermediate solid adsorbent heat exchanger are shown and discussed. The concept of transferring heat between separate adsorbent streams is not common therefore the feasibility of this concept is also discussed later.

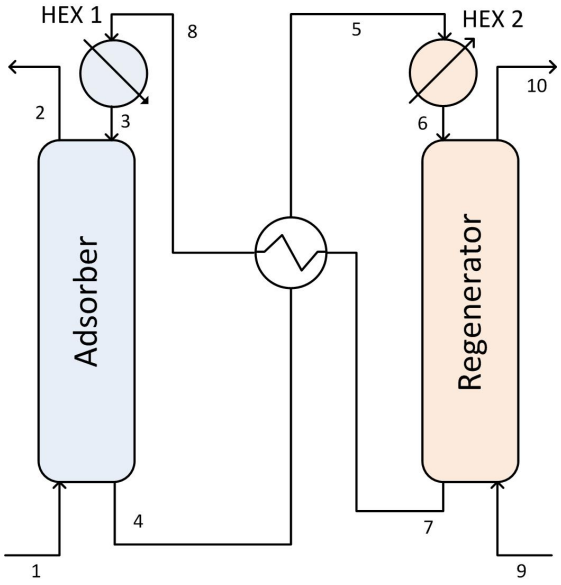

Figure 8.45: Diagram of CO_2 adsorption cycle with heat integration

Parameters and conditions used in the base case with the intermediate heat-exchanger are shown in Table 8.8. The value of $U_{int}A_{int}$ chosen is the same as for the heat recovery heat exchanger in the amine absorption process designed by Fisher et al. (2005). A low number of discretisations has been used for this intermediate heat exchanger to reduce the computational time taken to reach the solution of this moving bed TSA cycle.

Table 8.8: Parameters for the base case intermediate heat exchanger for heat recovery

Parameter	**Unit**	**Intermediate heat exchanger**
Configuration		Counter-current
Adsorbent		Supported amine adsorbent
Gas		-
L	m	1
D	m	2
ε_a	-	0.861
D_p	mm	1
P_{in}	Pa	101325
T_g^{in}	°C	-
M_{in}	mol.s^{-1}	0
$\dot{m}_{in}$	kg.s^{-1}	1200
$y_{in}^{CO_2}$	-	-
$y_{in}^{H_2O}$	-	-
$y_{in}^{N_2}$	-	-
k_{CO_2}	s^{-1}	0
k_{H_2O}	s^{-1}	0
k_{N_2}	s^{-1}	0
$U_{int}A_{int}$	W.K^{-1}	1.2945×10^7
Number of discretisations	-	3
α	-	1

8.2.7.1 Results and Discussion of the Moving Bed Adsorption Cycle with Heat Integration

The CO_2 recovery, wet and dry CO_2 purities of the process do not vary much with or without the intermediate heat exchanger as shown in Figures 8.46, 8.47 and 8.48 respectively.

The major improvement in performance is found by the reduction in heat duty required to regenerate the adsorbent as shown in Figure 8.49. The heat duty drops for higher values of $U_{int}A_{int}$ which can be influenced by higher surface areas of the intermediate heat exchanger.

The $U_{int}A_{int}$ value found for the amine adsorption process for a single train is 1.2945×10^7 W.K^{-1} (Fisher et al. (2005)). If the same value of $U_{int}A_{int}$ is achieveable in the moving bed adsorption process, the total heat duty needed for adsorbent regeneration is only 78.09 MW per train (313.36 MW for the overall capture process). This would be equivalent to a 37.6% saving in energy over the equivalent process without the intermediate heat exchanger (the base case process).

The base case process considered earlier in section 8.2.1 did not offer any great improvement in reaching a lower heat duty than the base case amine

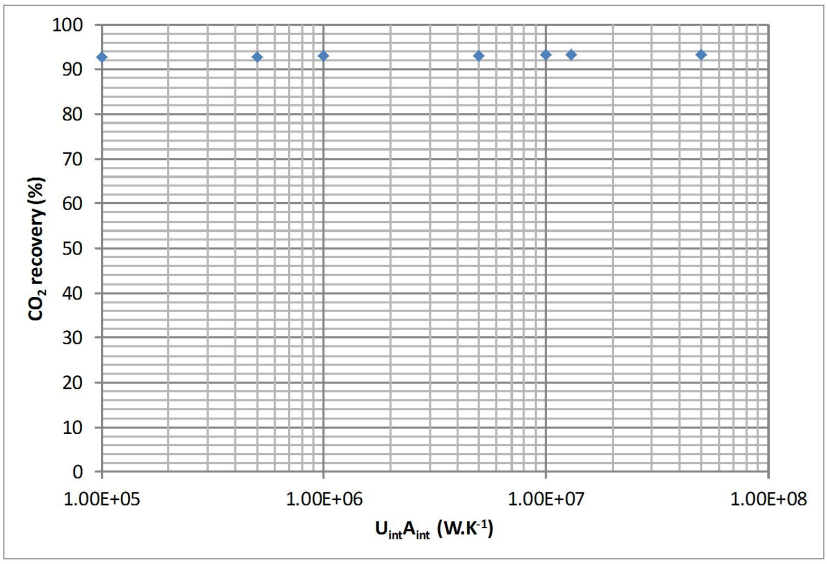

Figure 8.46: Effect of the $U_{int}A_{int}$ value of the lean/rich adsorbent heat exchanger on CO_2 recovery for the cyclic process using the supported amine adsorbent

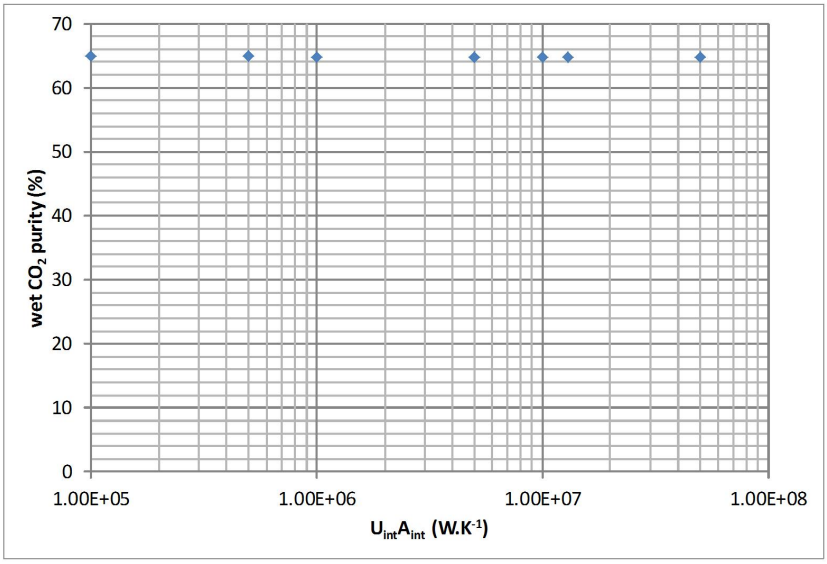

Figure 8.47: Effect of the $U_{int}A_{int}$ value of the lean/rich adsorbent heat exchanger on the wet CO_2 purity for the cyclic process using the supported amine adsorbent

absorption process considered by Fisher et al. (2005), which did include heat integration. If heat integration is carried out in the moving bed adsorption process, there would be a significant improvement over the base case amine absorption system developed by Fisher et al. (2005). The heat duty would also be lower than a modified process of the base case amine absorption process developed by Fisher et al. (2005) with lower heat duty requirements. However this will be discussed further later in section 8.3.

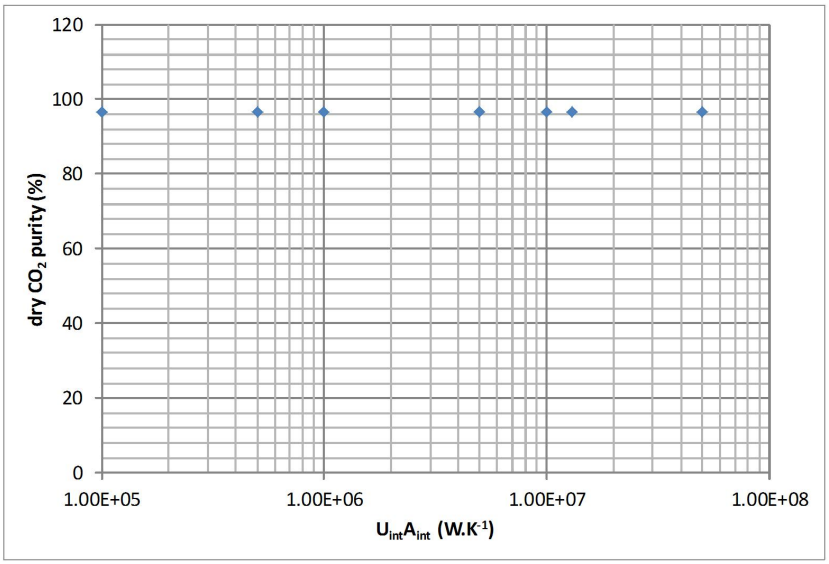

Figure 8.48: Effect of the $U_{int}A_{int}$ value of the lean/rich adsorbent heat exchanger on the dry CO_2 purity for the cyclic process using the supported amine adsorbent

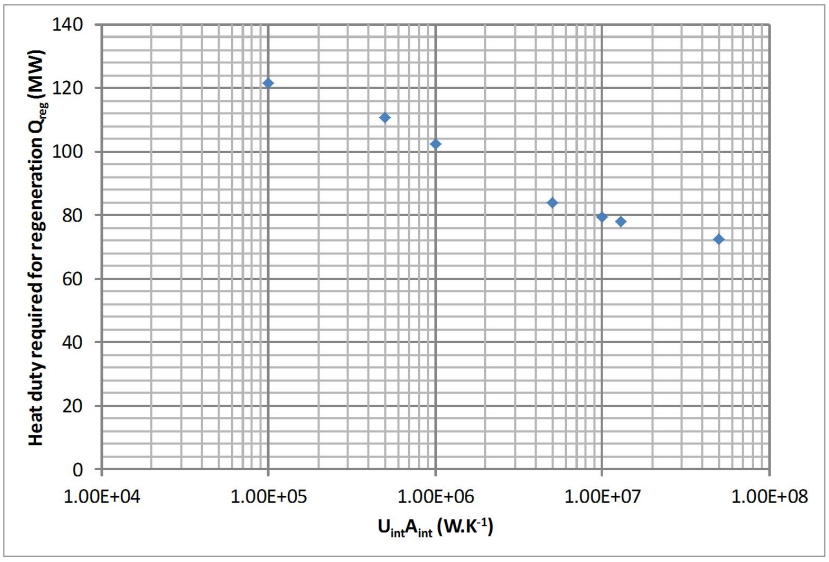

Figure 8.49: Effect of the $U_{int}A_{int}$ value of the lean/rich adsorbent heat exchanger on the regeneration heat duty for the cyclic process using the supported amine adsorbent

The reduction in heat duty of HEX 2 for increasing $U_{int}A_{int}$ values is shown in Figure 8.50. If $U_{int}A_{int}$ is increased, the intermediate heat exchanger transfers more heat, thereby reducing the additional heat that HEX 2 must supply to the adsorbent for it to reach approximately 120°C. The heat duty saved as a percentage of the total heat duty supplied to the adsorbent is shown in Figure 8.51 for increasing values of $U_{int}A_{int}$.

Finally, the effect of $U_{int}A_{int}$ values on adsorbent temperatures in streams 8 and 5 (cf. Figure 8.45) is shown in Figure 8.52. The lowest possible temperature

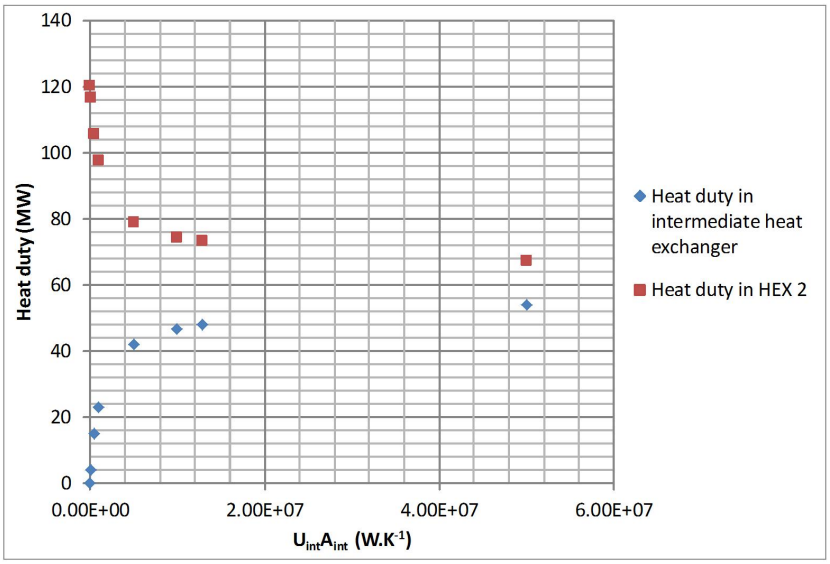

Figure 8.50: Variation in heat duties with increasing values of $U_{int}A_{int}$

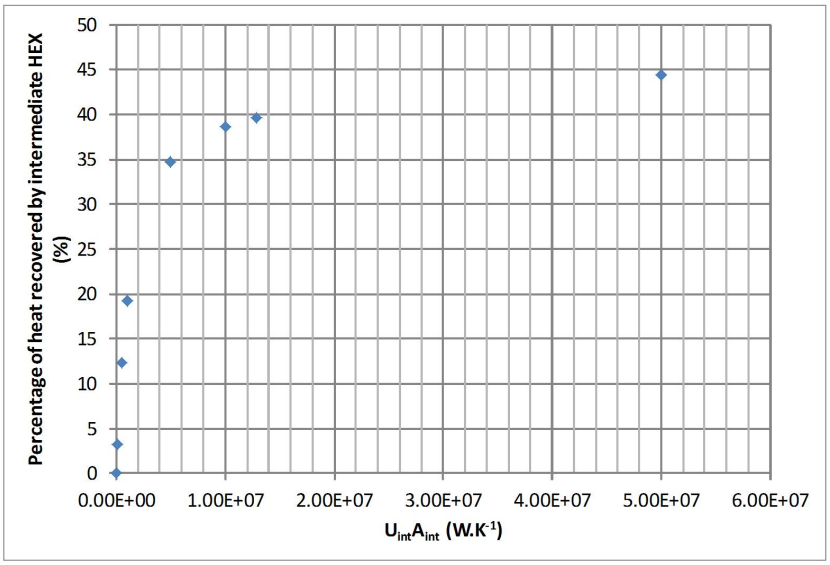

Figure 8.51: Percentage of heat recovered by the intermediate heat exchanger with increasing values of $U_{int}A_{int}$

for stream 8 and the highest possible temperature for stream 5 are desired but the size of the heat exchanger would be extremely large. The energy saved is likely to be offset by the increase in capital expenses due to the large size of the heat exchanger.

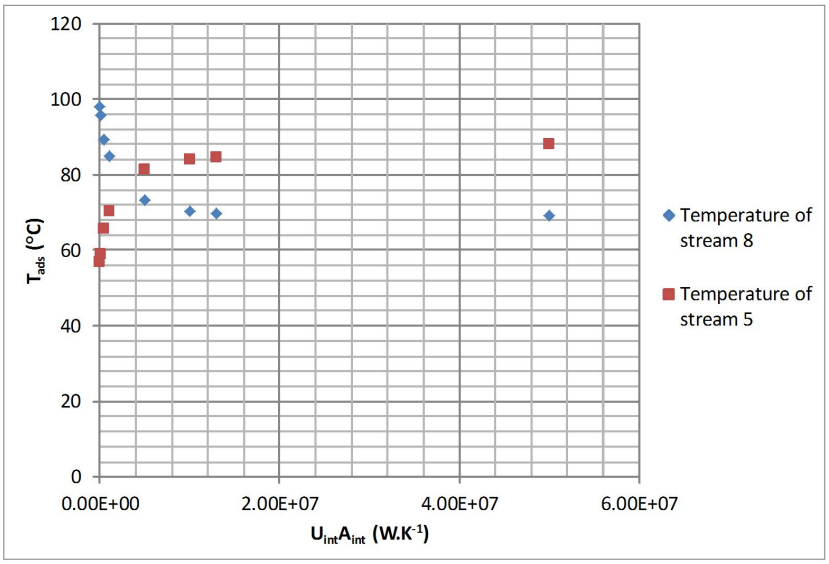

Figure 8.52: Temperatures of the adsorbent streams leaving the intermediate heat exchanger with increasing values of $U_{int}A_{int}$

8.2.7.2 Adsorbent Heat Exchangers

There is a wide variety of types of heat exchangers for fluids (Incropera and DeWitt (1996)). However, transferring heat between solid streams and between solid and fluid streams is not as common as heat transfer between fluid streams.

As with the CO_2 absorption process, moving bed adsorption processes could offer the possibility to use heat integration. Furthermore, it was shown previously in section 8.2.7.1 that heat integration in a moving bed adsorption process would greatly improve its energy efficiency.

Two methods that can be used to transfer heat between adsorbent particles are discussed in this section. Two adsorbent streams at different temperatures can be brought into indirect contact via a heat conductor (such as a plate). Alternatively, a heat transfer fluid could be used as an intermediary to change the temperature of two adsorbent streams.

Parallel Plate Heat Exchanger for Adsorbents

Solid streams at different temperatures can be brought into indirect contact inside a plate heat exchanger (Incropera and DeWitt (1996)). Therefore, heat transfer by conduction would occur through the plates which separate adsorbent streams as shown in Figure 8.53.

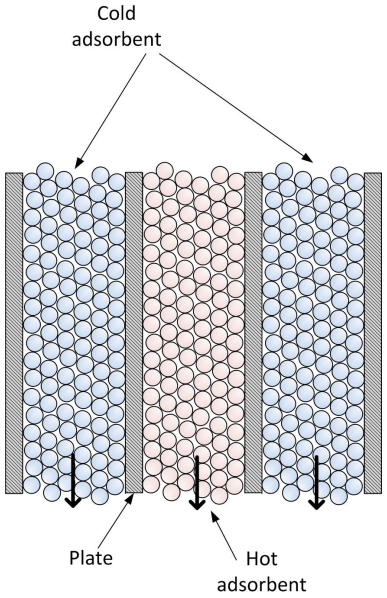

Figure 8.53: Plate heat exchanger for adsorbents with heat transfer by conduction

The configuration of the heat exchanger shown in Figure 8.53 is co-current because both adsorbent streams descend. If the heat exchanger were to be operated counter-currently, a gas stream would be needed to entrain the adsorbent upwards.

Heat Transfer between Solids via a Medium

In contrast to conduction of heat between adsorbent particles, the use of a fluid medium to transfer heat across from one adsorbent stream to another has been considered more commonly in the literature (Kim et al. (2013a), Yang and Hoffman (2009), SRI International et al. (2013) and Krutka et al. (2013)). The diagram of the moving bed TSA using a fluid medium is shown in Figure 8.54.

Kim et al. (2013a) and Yang and Hoffman (2009) have considered parallel plate heat exchangers with cooling or heating fluid flowing between parallel plates as shown in Figure 8.55. However, they have used the heat exchanger as CO_2 adsorbers and regenerators instead of having separate columns. The adsorbent descends between the plates and gas is passed through the adsorbent (cf. Figure 8.55). The particles typically move slowly downwards between the plates which provides long residence times and it minimizes attrition (Yang and Hoffman (2009)). A fluid flowing on the other side of a plate would remove heat in the heat exchanger acting as the adsorber. It would then supply the heat removed from the adsorber to the adsorbent in the heat exchanger which is acting as the regenerator. Yang and Hoffman (2009) used the plate heat

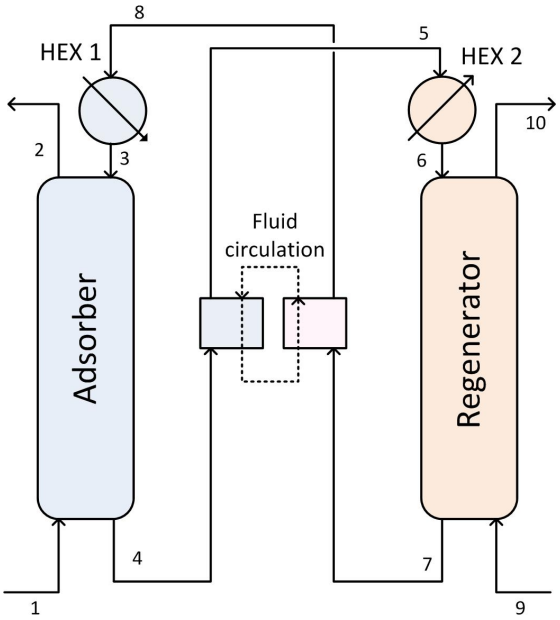

Figure 8.54: Diagram of CO_2 adsorption cycle with heat integration by using a fluid medium

exchanger concept shown in Figure 8.55 for their design of the regenerator but a fluidisation gas (recycled CO_2) was stated to be necessary to improve heat transfer between the fluid on the other side of the plate and the adsorbent.

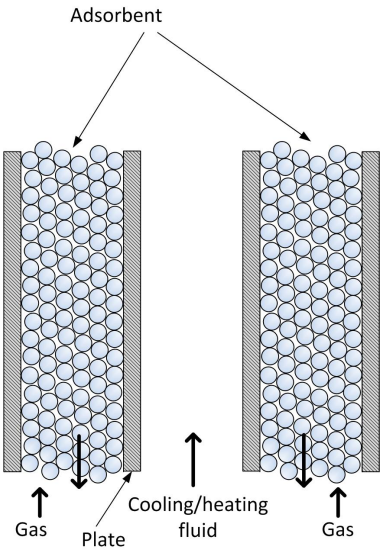

Figure 8.55: Plate heat exchanger transferring heat between adsorbent and heating/cooling fluid (Solex Thermal Science Inc. (2014))

This type of heat exchanger has been commercialised by Solex Thermal Science Inc. (Solex Thermal Science Inc. (2014)) and it has been employed for various solid particles (e.g. grains, fertilisers and catalysts) (Kim et al. (2013a), Yang and Hoffman (2009)).

Another method that has been considered by SRI International et al. (2013) and Krutka et al. (2013) involves the use of heating or cooling fluid flowing through tubes around which adsorbent flows. Kunii and Levenspiel (1991) have also described the application of this method in fluidised beds.

In practice, for a counter-current column, the adsorbent in stream 4 (from Figure 8.54) will need to be moved to the inlet of HEX 2 as it possibly passes through the intermediate heat exchanger. The adsorbent could be lifted by a portion of the CO_2 product gas leaving the regenerator (stream 10). Similarly, adsorbent leaving the regenerator (stream 7) could be moved to HEX 1 by being lifted using a portion of the N_2 rich gas in stream 2.

If the adsorbent were to be heated or cooled directly by the fluid medium, the amount of components adsorbed would change and therefore the CO_2 loading at the inlet to the adsorber may increase and this could affect the working capacity of the adsorbent.

In conclusion, more work would need to be carried out to find out the best option of heat exchangers for adsorbents that would maximise heat transferred and minimise the heat transfer area required. This can be done by determining the overall heat transfer coefficients achievable inside the external heat exchangers (U_{ext}) and independent heat exchangers (U_{int}). The highest overall heat transfer coefficients will reduce the size of the heat exchangers and hence also capital costs.

8.3 Comparisons of the Performance of Absorption and Moving Bed Adsorption Processes

Five cases have been considered for the comparison between absorption and adsorption processes:

- **Case 1**: Amine absorption process - base case (Fisher et al. (2005))

- **Case 2**: Amine absorption process - improved over the base case by multi-pressure stripping (Fisher et al. (2005))

- **Case 3**: This work - base case adsorption process without heat integration

- **Case 4**: This work - adsorption process without heat integration but with the adsorbent leaving HEX 2 at 112°C instead of 118.51°C (base case)

- **Case 5**: This work - base case adsorption process with heat integration

- **Case 6**: This work - adsorption process with heat integration, with the adsorbent leaving HEX 2 at 112°C instead of 118.51°C (base case) and base case steam flowrate into regenerator halved

In each case, similar conditions of the flue gas have been used. Table 8.9 shows important results of the performance of the processes considered for each case.

Table 8.9: Performance of amine absorption and moving bed adsorption systems with supported amine adsorbent

	Case 1	**Case 2**	**Case 3**	**Case 4**	**Case 5**	**Case 6**
CO_2 recovery (%)	90	90	93	90	93	90
Dry CO_2 purity (%)	>99	>99	97	97	97	97
CO_2 working capacity for the sorbent ($mol.kg^{-1}$)	0.90	0.87	0.53	0.52	0.54	0.52
Mass flowrate of sorbent ($kg.s^{-1}$)	2756	2753	4800	4800	4800	4800
Overall heat consumption (MW)	500	391	501	477	312	304
Heat consumption per unit mass of CO_2 removed ($MJ.kg^{-1}$)	4.35	3.40	4.43	4.35	2.75	2.77

The base case amine absorption process (Case 1) considered by Fisher et al. (2005) has a similar heat consumption as the base case moving bed TSA considered in this work (Case 3). However, Case 3 allows a recovery which is 3%

higher than Case 1. Instead, if a 90% CO_2 recovery is chosen for the adsorption process (Case 4), the heat requirement is lower than for the absorption process (Case 1). Both systems would then give similar values of heat consumed per mass of CO_2 removed. At this point, the moving bed adsorption system with supported amine adsorbent offers no advantage over the base case amine absorption system. Although the heat capacity of the solid is lower than the solvent, mass flowrates of adsorbent 1.7 times greater than amine solution flowrates are needed to achieve CO_2 recoveries above 90% in order to compensate for the lower working capacities of the supported amine adsorbent. Gray et al. (2008) outlines the importance of high working capacities and they state that a working capacity greater than 2 mol.kg^{-1} for adsorption technology to allow significant energy savings over absorption processes. Whilst this may possibly be true, this statement was not demonstrated further by Gray et al. (2008).

Improvements in the absorption process have been made by Fisher et al. (2005). This includes multi-pressure stripping of the amine solution in the regenerator as given by Case 2. This modification to their base case process allowed a 20% reduction in heat consumption. The heat consumption per unit mass of CO_2 removed that was found was 3.4 MJ.kg^{-1} CO_2, which is comparable to 3.7 MJ.kg^{-1} CO_2 and 3.63 MJ.kg^{-1} found by Øi (2007) and Ramezan and Skone (2005) respectively.

Newer studies of more complex amine absorption processes (Ahn et al. (2013)) with higher levels of heat integration result in lower heat consumptions but at the expense of higher capital costs. A process involving the addition of multiple units to the amine absorption process (e.g. heat exchangers, flash vessels and compressors) was developed by Ahn et al. (2013). The lowest heat consumption per unit mass of CO_2 captured that was found for the CO_2 capture process (excluding CO_2 compression) was only 2.71 MJ.kg^{-1} CO_2. However, the impact of the additional units on the total capital costs of the process was not assessed.

To offer any benefits, the moving bed adsorption process would need to be more energy efficient than Case 2. For this, heat integration of the adsorbent leaving the regenerator and the adsorber should be carried out. This is shown in the Table 8.9 for Cases 5 and 6. If Case 6 is compared with Cases 1 and 2, the heat consumed per unit mass of CO_2 removed would be lower by 36% and 18% respectively.

In this work, only the heat required for adsorbent regeneration was considered as the main source of the energy penalty in the CO_2 capture system. However, other power requirements in the process include the energy required

to operate pumps (e.g. cooling water circulation) or the flue gas blower. The energy penalty from these is however much lower than for the heat required for adsorbent regeneration (Krutka and Sjostrom (2011)). A calculation of energy required for CO_2 compression for transport and storage would also need to be performed. In amine absorption processes, the solvent is typically regenerated at a pressure of 2 bar instead of at atmospheric pressure (MacDowell et al. (2010)). Therefore, slightly less energy is consumed to compress CO_2 from an amine absorption process than a TSA process operating at atmospheric pressure.

If the power requirement to regenerate the adsorbent is calculated only from the heat required to desorb CO_2, it is underestimated:

$$Q_{heat} = (-\Delta H_{ads,CO_2})(\dot{M}_{in} y^{in}_{CO_2}) \tag{8.3}$$

with:

Q_{heat}: heat rate provided to the regenerator (W)

$\Delta H_{ads,CO_2}$: heat of adsorption of CO_2 ($J.mol^{-1}.K^{-1}$)

$\dot{M}_{in}$: molar flowrate of gas into the adsorber ($mol.s^{-1}$)

$y^{in}_{CO_2}$: CO_2 mole fraction in inlet gas to the adsorber (-)

For the supported amine adsorbent, the overall power requirement calculated from Equation 8.3 is 159.3 MW. This value is significantly lower than 501 MW shown in Table 8.9. Therefore, using Equation 8.3 to calculate power requirements for adsorption processes would not be adequate because it underestimates the power requirement.

If Equation 2.17 is used with values in Table 8.10, the power requirement found would be 519.6 MW which is close to the value of 501 MW in Table 8.9. The value of c_{p,CO_2} is found from National Institute of Standards and Technology (2014) at 120°C. However, the power requirement found from Equation 2.17 is overestimated slightly as it doesn't include the effect of water but it provides a good estimate of energy required for regeneration if no heat integration is carried out. If heat integration is carried out and the effect of components other than CO_2 is to be included, it would be more rigorous to use a model with an energy balance which has been performed in this thesis.

Results for a hypothetical adsorbent with a working capacity of more than double that of the supported amine adsorbent considered in this work are shown in Table 8.11. Other properties of the hypothetical adsorbent are the same as the supported amine adsorbent considered in this work. The heat consumption

Table 8.10: Parameters used to find the power requirement using Equation 2.17

Parameter	**Unit**	**Value**
m_{CO_2}	kg.s^{-1}	85.5
$c_{p,ads}$	J.kg^{-1}.K^{-1}	1255
ΔT	K	80
q_{CO_2}	kg.kg^{-1}	0.07
c_{p,CO_2}	J.kg^{-1}.K^{-1}	931
T_2	K	393.15
T_1	K	313.15
T_{ref}	K	298.15
$\Delta H_{ads,CO_2}$	J.kg^{-1}	-1308945.5

per unit mass of CO_2 captured would be 14% less than for the supported amine adsorbent considered in Case 4.

Table 8.11: Performance for a hypothetical adsorbent in a cycle with a counter-current adsorber and regenerator without heat integration

CO_2 working capacity (mol.kg^{-1})	**1.36**
CO_2 recovery	90%
Wet CO_2 purity	70%
Dry CO_2 purity	99%
Mass flowrate of adsorbent (kg.s^{-1})	1840
Overall heat consumption (MW)	413.1
Heat consumption per unit mass of CO_2 removed (MJ.kg^{-1})	3.76

8.4 Comparisons of the Performance of Moving Bed and Fixed Bed Adsorption Processes

In this section, the results of the performances of the moving bed processes found in this work are compared to results from literature for fixed bed CO_2

adsorption processes. Firstly, moving bed and fixed bed temperature swing adsorption (TSA) processes are compared. A comparison of moving beds and fixed bed pressure swing adsorption (PSA) processes follows.

Grande et al. (2009) studied an electric swing adsorption (ESA) process, which essentially uses TSA but with electric heating, to capture CO_2 from flue gas from a natural gas power station containing 3.5% CO_2. A few assumptions were made. A hypothetical adsorbent was considered with the same CO_2 capacity as zeolite 13X but with higher kinetic rates and with the capability of being regenerated by electric heating. The gas was assumed to be dry. A cyclic process with 5 steps allowed a 79.5% CO_2 recovery, a 79.4% purity and with an electrical energy consumption of 2.04 MJ.kg^{-1} of CO_2 captured. Another case in which 7 steps were used gave a CO_2 recovery of 72%, purity of 89.7% and an electrical energy consumption of 1.9 MJ.kg^{-1}. These energy consumptions corresponded predominantly to heat required to regenerate the adsorbent. Assuming an energy efficiency of 40% to convert thermal energy to electrical energy (Metz et al. (2005)), the corresponding thermal energy needed would be 5.1 MJ.kg^{-1} of CO_2 captured for the 5 step case and 4.75 MJ.kg^{-1} of CO_2 captured for the 7 step case. These values are higher than for the amine absorption process (Fisher et al. (2005)) and moving bed adsorption systems of this work (cf. Table 8.9). However the energy consumption would be higher because Grande et al. (2009) have not included the energy consumption needed to remove water from the flue gas and because a CO_2 recovery of at least 90% was not found.

In another TSA study by Mérel et al. (2006), experimental tests were carried out to capture CO_2 in a single TSA column working as an adsorber and regenerator. A mixture of CO_2 and N_2 gas with 10% CO_2 was separated. Heat was supplied by indirect contact of the bed with steam. A purge gas was not used. A CO_2 recovery of nearly 100% was reported but the thermal energy consumption was considerably high at 7.9 MJ.kg^{-1} of CO_2 captured. If the column was made adiabatic, it would be improved with only 5.9 MJ.kg^{-1} of CO_2 captured of thermal energy. These values are still greater than amine absorption and moving bed systems (cf. Table 8.9).

Data of the performance of PSA systems from literature were also found. Delgado et al. (2011) studied a vacuum swing adsorption (VSA) process which is a type of PSA with desorption carried out under vacuum. Activated carbon was used to separate a mixture of CO_2 and N_2 with 13% CO_2. Recoveries higher than 90% and purities higher than 93% were found. The electrical energy consumption was 0.432 MJ.kg^{-1} of CO_2 captured (1.09 MJ.kg^{-1} of CO_2 captured of thermal energy). This value is considerably less than energies found

in this work for the moving bed systems and the amine absorption processes. However, other groups have found higher energy requirements.

Ishibashi et al. (1996) carried out pilot plant tests for capturing CO_2 at 10% vol. in a vacuum and temperature swing adsorption (VTSA) process in which the gas is desorbed by heating and by lowering the pressure. The addition of the temperature swing to the VSA was reported to reduce energy consumption over the VSA alone. Although CO_2 recoveries and purities were greater than 90% and 99% respectively, 2.02 MJ.kg^{-1} of CO_2 captured of electrical energy was needed. This is equivalent to 5.05 MJ.kg^{-1} of CO_2 captured of thermal energy (assuming 40% efficiency in energy conversion). Therefore, the energy consumption was higher than the amine absorption process (Fisher et al. (2005)) and consequently the moving bed adsorption process of this work.

Finally in another VSA study by Zhang et al. (2008), flue gas from a 12.6% mol CO_2 stream of CO_2 and N_2 was treated in 9 steps in a VSA system. CO_2 recoveries and purities in the range of 60-70% and 90-95% were found respectively. The electrical energy consumed was in the range of 0.52-0.86 MJ.kg^{-1} of CO_2 captured of electrical energy (1.3-2.15 MJ.kg^{-1} of CO_2 captured of thermal energy). A higher range is expected for a 90% CO_2 recovery but there is a large difference in values quoted for energy consumptions in the VSA systems considered by Delgado et al. (2011) and Zhang et al. (2008) on one hand and Ishibashi et al. (1996) on the other. Results from Delgado et al. (2011) suggest that VSA processes would require lower energy consumptions than the amine absorption process (Fisher et al. (2005)) and moving bed temperature swing adsorption processes using the supported amine adsorbent considered for this work.

8.5 Moving Bed CO_2 Adsorption Cycle with Activated Carbon Adsorbent

A simulation of the base case process (cf. Figure 8.1) was carried out by replacing the supported amine adsorbent with activated carbon (properties given in section 2.7.2). The same input parameters as for the supported amine adsorbent process were used (cf. Table 8.1). However, the solid hold up values were changed due to higher particle densities of activated carbon. For the adsorber $\varepsilon_a = 0.0706$, for the regenerator $\varepsilon_a = 0.140$ and for HEX 1 and 2, $\varepsilon_a = 0.604$. Results are shown in Table 8.12.

It can be seen that the performance of the equivalent process using activated carbon (cf. Table 8.12), is inferior to that of the supported amine adsorbent.

Table 8.12: Results of the moving bed process (Figure 8.1) using activated carbon instead of the supported amine adsorbent

CO_2 recovery	48.2%
Wet CO_2 purity	38.77%
Dry CO_2 purity	69.04%
CO_2 working capacity ($mol.kg^{-1}$)	0.28
Overall heat consumption (MW)	524.4
Heat consumption per unit mass of CO_2 removed ($MJ.kg^{-1}$)	3.93

The CO_2 recovery found is well below 90% and the adsorbent flowrate or its residence time would need to be increased. The working capacity of the activated carbon is half of the value found for the supported amine adsorbent and a third of the amine working capacity found by Fisher et al. (2005).

The heat duty for regeneration of the adsorbent is higher than for the other sorbents considered (524.4 MW in total). The heat consumption per mass of CO_2 removed of 3.93 $MJ.kg^{-1}$ suggests that the use of activated carbon in this moving bed cycle would not offer lower heat consumptions over the amine absorption processes (Case 2) (Fisher et al. (2005)). However, improvements will be found with heat integration.

The dry purity of CO_2 found with activated carbon is well below percentages reached with the supported amine adsorbent for which it was assumed that N_2 did not adsorb. For activated carbon, adsorption of N_2 occurs and it results in a higher concentration of N_2 in the pores of the adsorbent entering the regenerator which negatively affects CO_2 purity. Therefore, N_2 contained in the pores must be purged by CO_2 or steam. This could be carried out in an intermediate column before the adsorbent enters the regenerator as carried out by SRI International et al. (2013) who found purities close to 100%. This modified moving bed cycle with a purge stream has not been modelled here due to time constraints but it could be carried out in future work.

8.6 Cost Considerations

Accurate capital cost estimates of the moving bed adsorption processes considered in this work cannot be made at present due to the lack of a complete list of equipment that would be required. In addition, there is uncertainty in the type of technology to be used. For example, the technology required for adsorbent circulation and the type of heat exchanger for solids is yet to be defined.

Fisher et al. (2005) have given capital cost estimations for the amine absorption process that was designed. For columns in the adsorption process of the same size as the for the absorption process, capital costs would be similar. The uncertainty in the kinetics of adsorption and desorption may also affect the size of the vessels. If the rate of adsorption is slow, longer residence times of the adsorbent will be necessary which can be achieved with larger columns. The sizing of the heat exchangers used (CO_2 lean adsorbent heat exchanger (HEX 1), the CO_2 rich adsorbent heat exchanger (HEX 2) and the heat exchanger used for heat recovery) cannot be done until further work is carried out to determine the overall heat transfer coefficient in the heat exchangers.

The adsorbent cost per unit mass of adsorbent has been estimated to be in the range of \$5-15 kg^{-1} (Krutka and Sjostrom (2011)) and the cost of MEA per unit mass is only \$1.2 kg^{-1} (Fisher et al. (2005)). The range of the cost of adsorbent replacement over time is estimated to be \$2-13 per ton of CO_2 removed (Krutka and Sjostrom (2011)). For an average cost of the adsorbent of \$10 kg^{-1}, the loss of adsorbent would be 0.2-1.3 kg of adsorbent per ton of CO_2 captured. Fisher et al. (2005) have stated that the loss of MEA is 1.5 kg of adsorbent per ton of CO_2 captured. Therefore the overall cost of sorbent replacement would be higher for the adsorption process for which it can be up to approximately ten times greater than for amine absorption.

8.7 Conclusions

The performance of a moving bed TSA cycle with a counter-current adsorber and regenerator using a supported amine adsorbent has been assessed in this chapter. It has been shown that without heat integration, the moving bed TSA process does not offer any significant saving in heat consumption for sorbent regeneration over amine absorption. It was also shown why a counter-current adsorber in a moving bed TSA cycle would be the preferred option over co-current and fluidised bed adsorbers.

The main findings from simulations and sensitivity analyses carried out in this chapter are:

- Adsorbent flowrate: the heat consumption increases for higher adsorbent flowrates. To reduce heat consumption during desorption, the adsorbent flowrate should be minimised.

- Regeneration gas flowrate: Higher flowrates of steam improve CO_2 recovery but at the expense of higher energy penalties. If pure CO_2 is used as the regeneration gas, its flowrate should be minimised to maximise CO_2 recovery.

- Adsorbent heating: The heat consumption of the process can be minimised by reducing the heat duty of the adsorbent heater before regeneration. For the low flowrate of steam chosen as the regeneration gas into the regenerator, the adsorbent must be added into the regenerator at a high enough temperature to allow a CO_2 recovery of 90%.

- A regenerator is not required in the process if an adsorbent heater is used.

- CO_2 mass transfer constant: the moving bed TSA cycle requires relatively high mass transfer rates to achieve a CO_2 recovery of 90%. If the adsorbent kinetics are slow, a greater volume of adsorbent must be used in the adsorber and regenerator.

- Steam can be supplied as a regeneration gas into the regenerator or it can be supplied indirectly to heat the adsorbent before it enters the regenerator. Either option results in a similar level of overall heat consumption to regenerate the adsorbent.

- High levels of heat integration and the use of adsorbents with higher CO_2 working capacities would offer significantly lower heat consumptions for moving bed adsorption processes than amine absorption processes.

- Finally, due to a lower CO_2 working capacity of activated carbon, the performance of the process considered in this work with activated carbon was worse than for the same process using the supported amine adsorbent. Additionally, the design of the process would need to be changed if activated carbon were to be used because of the low CO_2 product purity found.

Chapter 9

General Conclusions and Future Work

Simulations based on a numerical model for moving bed TSA processes for post-combustion CO_2 capture have been carried out to find out if these processes can offer significant reductions in energy consumption compared to other technology.

9.1 Adsorbent Suitability

The application of adsorbents to CO_2 capture from wet flue gas restricts the choice of suitable adsorbents available. The choice of the adsorbent used is also limited by the regeneration gases considered which are CO_2 and steam. For example, zeolite 13X would not be regenerated with steam and regenerating in pure CO_2 would not provide a high enough CO_2 working capacity.

Although activated carbon is tolerant to water, its low CO_2/N_2 selectivity causes a low CO_2 product purity for the moving bed TSA considered. Additionally, it does not have a high enough CO_2 working capacity.

A supported amine adsorbent gave the best performance from the adsorbents considered in this work. It offers a higher CO_2 working capacity than activated carbon and a higher CO_2/N_2 selectivity which improves substantially the CO_2 product purity. Furthermore, it is tolerant to water.

9.2 Adsorber Configuration

In a counter-current adsorber, the solid flows in the opposite direction to the gas. Due to higher CO_2 loadings reached at the adsorbent outlet (which is also the gas inlet), the counter-current configuration offers a better performance

than co-current or fluidised bed configurations. For a given CO_2 recovery, adsorbent mass flowrates and the heat duty for adsorbent regeneration are lower.

9.3 Fluidisation Considerations

Fluidisation limits of adsorbent particles need to be carefully considered when considering adsorption systems and in particular, moving bed adsorption systems. For a given column diameter, the adsorbent particle diameter must be larger for counter-current and fluidised beds than co-current beds to prevent the adsorbent being entrained by the gas. Higher adsorbent densities would also benefit counter-current adsorption systems.

9.4 Performance of Moving Bed TSA Cycles

In this work, it was found that the moving bed TSA cycle with supported amine adsorbent and without heat integration would not offer any important reductions in heat consumption to regenerate the adsorbent. For a CO_2 recovery of 90%, the heat consumption per unit mass of CO_2 removed from the flue gas was the same as for a similar amine absorption process, which is the current benchmark for post-combustion CO_2 capture. Compared to amine solutions, adsorbents tend to have lower heat capacities, which make them a relatively attractive option. But they also tend to have lower CO_2 working capacities than amine solutions which means that higher sorbent flowrates are needed. Amine absorption processes offer certain advantages such as higher CO_2 purities than the moving bed TSA processes. Most importantly though, heat recovery is performed in amine absorption processes but it was not performed in the base case moving bed TSA studied in this work.

However, to improve moving bed TSA cycles, it was also found that for similar levels of heat integration as in an amine absorption process with a basic level of heat integration, the heat consumption would be lowered by approximately 40%. If the CO_2 working capacity of the adsorbent could be approximately doubled, the heat consumption can be lowered by approximately 15%.

9.5 Future Work

The work presented in this thesis can be considered as a first step towards the prediction of the performance of post-combustion CO_2 moving bed TSA

processes using existing adsorbents. However, work on this subject could be extended in the following areas:

- Components: Whilst the main components in the flue gas (CO_2, water, N_2) were included in this work, the effect of minor components such as O_2 and SO_x were neglected because of limited information in the literature about the adsorption of these components on the adsorbents considered. Depending on the adsorbent used, these components could hinder the performance of the overall process. This study could therefore be extended to include the effect of minor components on the process.

- Multicomponent adsorption: The loadings of CO_2 and water have been considered to be independent of each other. However, it would be more accurate to take into account the competition between these components to adsorb. Therefore, more accurate multicomponent isotherm data would be required.

- Adsorbents: The adsorbents considered were a supported amine adsorbent, activated carbon and zeolite 13X (for dry flue gas). Other possible adsorbents such as alkali-metal adsorbents (e.g. sodium or potassium carbonates) or more novel adsorbents could have been considered.

- Kinetics: A major uncertainty in this study is the kinetic rate of mass transfer of the components within the adsorbent. Experimental data for the mass transfer constants would need to be obtained for more accurate predictions.

- Practical issues: Some practical difficulties that may be encountered in full scale systems are adsorbent loss, conveying and good distribution of the adsorbent but also heat exchange for solid adsorbents. These problems have not been considered to much extent in this thesis. However, for moving bed CO_2 adsorption systems to be developed further, they need to be looked into further. For example, the behaviour of adsorbent particles within structured packing may need to be studied if counter-current adsorbers are to be used. In addition, assumptions about the volume fraction occupied by the solid have been made and these would need to be verified.

- Fluidisation limits: Fluidisation limits in the counter-current, co-current and fluidised beds were considered in this thesis but for a single adsorbent particle only. The effect on the adsorbent of other particles and external equipment were not taken into account. For example, the presence of

structured packing on fluidisation limits in a counter-current bed was not investigated. The prediction of fluidisation limits in moving bed adsorbers therefore needs further consideration.

- Mathematical model: The model that has been developed here relied on making many assumptions for simplification and to reduce the number of unknown parameters in the model. A more complex model with fewer assumptions could be constructed in future work.

- Cycle designs: Only a single and basic cycle design was considered in this work but improvements could be found for more complex cycles. For example, to improve the CO_2 purity with activated carbon, a modification of the cycle would be necessary to allow the purge out of adsorbed N_2.

- Experimental validation: The findings in this thesis may not be achieved in practice but the results found here represent outcomes that can be expected in theory. Results found in this work would need to be validated experimentally.

Bibliography

Abanades, J. C., Anthony, E. J., Wang, J., and Oakey, J. E. (2005). Fluidized bed combustion systems integrating CO_2 capture with CaO. *Environmental Science & Technology*, 39(8):2861–2866.

Ahn, H., Luberti, M., Liu, Z., and Brandani, S. (2013). Process configuration studies of the amine capture process for coal-fired power plants. *International Journal of Greenhouse Gas Control*, 16(0):29 – 40.

Aronu, U. E., Ghondal, S., Hessen, E. T., Haug-Warberg, T., Hartono, A., Hoff, K. A., and Svendsen, H. F. (2011). Equilibrium in the H_2O-MEA-CO_2 system: new data and modeling. *Energy Procedia*, 0(0):1 –3.

Bacsik, Z., Ahlsten, N., Ziadi, A., Zhao, G., Garcia-Bennett, A. E., Martin-Matute, B., and Hedin, N. (2011). Mechanisms and kinetics for sorption of CO_2 on bicontinuous mesoporous silica modified with n-propylamine. *Langmuir*, 27(17):11118–11128.

Belmabkhout, Y. and Sayari, A. (2010). Isothermal versus non-isothermal adsorption-desorption cycling of triamine-grafted pore-expanded MCM-41 mesoporous silica for CO_2 capture from flue gas. *Energy & Fuels*, 24(9):5273–5280.

Bezerra, D., Oliveira, R., Vieira, R., Cavalcante, Clio., J., and Azevedo, D. (2011). Adsorption of CO_2 on nitrogen-enriched activated carbon and zeolite 13X. *Adsorption*, 17(1):235–246.

Bollini, P., Brunelli, N. A., Didas, S. A., and Jones, C. W. (2012). Dynamics of CO_2 adsorption on amine adsorbents. 1. Impact of heat effects. *Industrial & Engineering Chemistry Research*, 51(46):15145–15152.

Broadhurst, T. E. and Becker, H. A. (1975). Onset of fluidization and slugging in beds of uniform particles. *AIChE Journal*, 21(2):238–247.

Campbell, R. J. (2013). *Increasing the Efficiency of Existing Coal-Fired Power Plants*. Congressional Research Service.

Cavenati, S., Grande, C. A., and Rodrigues, A. E. (2004). Adsorption equilibrium of methane, carbon dioxide, and nitrogen on zeolite 13X at high pressures. *Journal of Chemical & Engineering Data*, 49(4):1095–1101.

Chan, K., Chao, C., and Bahrami, M. (2012). Heat and mass transfer characteristics of zeolite 13X/$CaCl_2$ composite adsorbent in adsorption cooling systems. *Proceedings of the ASME 2012 6th International Conference on Energy Sustainability & 10th Fuel Cell Science, Engineering and Technology Conference*, pages 1–10.

Chue, K. T., Kim, J. N., Yoo, Y. J., Cho, S. H., and Yang, R. T. (1995). Comparison of activated carbon and zeolite 13X for CO_2 recovery from flue gas by pressure swing adsorption. *Ind. Eng. Chem. Res.*, 34(2):591–598.

Cinke, M., Li, J., Jr., C. W. B., Ricca, A., and Meyyappan, M. (2003). CO_2 adsorption in single-walled carbon nanotubes. *Chemical Physics Letters*, 376(56):761 – 766.

Crittenden, B. and Thomas, W. (1998). *Adsorption Technology & Design*. Elsevier Science.

Davidson, R. (2009). Post-combustion carbon capture - solid sorbents and membranes. *IEA Clean Coal Centre*.

Delgado, J. A., Uguina, M. A., Sotelo, J. L., Águeda, V. I., Sanz, A., and Gmez, P. (2011). Numerical analysis of CO_2 concentration and recovery from flue gas by a novel vacuum swing adsorption cycle. *Computers & Chemical Engineering*, 35(6):1010 – 1019.

Department of Energy and Climate Change (2012). *CCS Roadmap - Supporting deployment of Carbon Capture and Storage in the UK*. DECC.

Didas, S. A., Kulkarni, A. R., Sholl, D. S., and Jones, C. W. (2012). Role of amine structure on carbon dioxide adsorption from ultradilute gas streams such as ambient air. *ChemSusChem*, 5:2058 – 2064.

Drage, T. C., Snape, C. E., Stevens, L. A., Wood, J., Wang, J., Cooper, A. I., Dawson, R., Guo, X., Satterley, C., and Irons, R. (2012). Materials challenges for the development of solid sorbents for post-combustion carbon capture. *J. Mater. Chem.*, 22:2815–2823.

Duan, L., Zhao, M., and Yang, Y. (2012). Integration and optimization study on the coal-fired power plant with CO_2 capture using MEA. *Energy*, 45(1):107 – 116.

Fang, F., Li, Z.-s., and Cai, N.-s. (2009). CO_2 capture from flue gases using a fluidized bed reactor with limestone. *Korean Journal of Chemical Engineering*, 26(5):1414–1421.

Fennell, P. S., Davidson, J. F., Dennis, J. S., and Hayhurst, A. N. (2007). Regeneration of sintered limestone sorbents for the sequestration of CO_2 from combustion and other systems. *Journal of the Energy Institute*, 80(2):116–119.

Figueroa, J. D., Fout, T., Plasynski, S., McIlvried, H., and Srivastava, R. D. (2008). Advances in CO_2 capture technology-the US department of energy's carbon sequestration program. *International Journal of Greenhouse Gas Control*, 2(1):9 – 20.

Finlayson, B. (2014). *Introduction to Chemical Engineering Computing*. Wiley.

Fisher, K., Beitler, C., Rueter, C., and Searcy, K. (2005). *Integrating MEA Regeneration with CO_2 Compression and Peaking to Reduce CO_2 Capture Costs*. DOE/NETL.

Gao, H., Zhou, L., Liang, Z., Idem, R. O., Fu, K., Sema, T., and Tontiwachwuthikul, P. (2014). Comparative studies of heat duty and total equivalent work of a new heat pump distillation with split flow process, conventional split flow process, and conventional baseline process for CO_2 capture using monoethanolamine. *International Journal of Greenhouse Gas Control*, 24(0):87 – 97.

Global CCS Institute 2013 (2013). *The Global Status of CCS: 2013*. Melbourne. Australia.

Grande, C. A., Ribeiro, R. P., Oliveira, E. L., and Rodrigues, A. E. (2009). Electric swing adsorption as emerging CO_2 capture technique. *Energy Procedia*, 1(1):1219 – 1225. Greenhouse Gas Control Technologies 9 Proceedings of the 9th International Conference on Greenhouse Gas Control Technologies (GHGT-9), 1620 November 2008, Washington DC, USA.

Gray, M., Champagne, K., Fauth, D., Baltrus, J., and Pennline, H. (2008). Performance of immobilized tertiary amine solid sorbents for the capture of carbon dioxide. *International Journal of Greenhouse Gas Control*, 2(1):3 – 8.

Gunasekaran, P., Veawab, A., and Aroonwilas, A. (2013). Corrosivity of single and blended amines in CO_2 capture process. *Energy Procedia*, 37(0):2094 – 2099. GHGT-11.

Guo, B., Chang, L., and Xie, K. (2006). Adsorption of carbon dioxide on activated carbon. *Journal of Natural Gas Chemistry*, 15(3):223 – 229.

Haider, A. and Levenspiel, O. (1989). Drag coefficient and terminal velocity of spherical and nonspherical particles. *Powder Technology*, 58(1):63 – 70.

Harkin, T., Hoadley, A., and Hooper, B. (2012). Using multi-objective optimisation in the design of CO_2 capture systems for retrofit to coal power stations. *Energy*, 41(1):228 – 235.

Harlick, P. J. and Tezel, F. H. (2004). An experimental adsorbent screening study for CO_2 removal from N_2. *Microporous and Mesoporous Materials*, 76(13):71 – 79.

Hefti, M., Marx, D., Joss, L., and Mazzotti, M. (2013). Experimental and theoretical investigation of binary CO_2 and H_2O adsorption. In *FOA11: 11th International Symposium on the Fundamentals of Adsorption, 2013 in Baltimore, MD*.

Herzog, H., Golomb, D., and Zemba, S. (1991). Feasibility, modeling and economics of sequestering power plant CO_2 emissions in the deep ocean. *Environmental Progress*, 10(1):64–74.

Hoffman, J., Richards, G., Pennline, H., Fischer, D., and Keller, G. (2008). Factors in reactor design for carbon dioxide capture with solid, regenerable sorbents. In *33rd International Technical Conference on Coal Utilization & Fuel Systems, Clearwater, FL, June 1-5, 2008*.

Incropera, F. and DeWitt, D. (1996). *Fundamentals of Heat and Mass Transfer*. John Wiley & Sons, Inc., 4th edition.

Intergovernmental Panel on Climate Change (2013). *Climate Change 2013 - The Physical Science Basis*. Cambridge University Press.

International Energy Agency (2008). *IEA Energy Policies Review - The European Union 2008*. Paris. France.

International Energy Agency (2009). *Technology Roadmap - Carbon capture and storage*. IEA Publications.

International Energy Agency (2012). *IEA Statistics - Electricity Information*. Paris. France.

International Energy Agency (2013a). *IEA Statistics - CO_2 Emissions From Fuel Combustion*. Paris. France.

International Energy Agency (2013b). *Redrawing the Energy-Climate Map - Executive Summary*. Paris. France.

Ishibashi, M., Ota, H., Akutsu, N., Umeda, S., Tajika, M., Izumi, J., Yasutake, A., Kabata, T., and Kageyama, Y. (1996). Technology for removing carbon dioxide from power plant flue gas by the physical adsorption method. *Energy Conversion and Management*, 37(6-8):929 – 933.

Jadhav, P. D., Chatti, R. V., Biniwale, R. B., Labhsetwar, N. K., Devotta, S., and Rayalu, S. S. (2007). Monoethanol amine modified zeolite 13X for CO_2 adsorption at different temperatures. *Energy & Fuels*, 21(6):3555–3559.

Kelley, C. (2003). *Solving Nonlinear Equations with Newton's Method*. Fundamentals of Algorithms. Society for Industrial and Applied Mathematics.

Kikkinides, E. S., Yang, R. T., and Cho, S. (1993). Concentration and recovery adsorption CO_2 from flue gas by pressure swing adsorption. *Ind. Eng. Chem. Res.*, 32(11):2714–2720.

Kim, K., Son, Y., Lee, W. B., and Lee, K. S. (2013a). Moving bed adsorption process with internal heat integration for carbon dioxide capture. *International Journal of Greenhouse Gas Control*, 17(0):13 – 24.

Kim, Y. E., Lim, J. A., Jeong, S. K., Yoon, Y. I., Bae, S. T., and Nam, S. C. (2013b). Comparison of carbon dioxide absorption in aqueous MEA, DEA, TEA, and AMP solutions. *Bulletin of the Korean Chemical Society*, 34(3):783 –787.

Krutka, H. and Sjostrom, S. (2011). *Evaluation of Solid Sorbents As a Retrofit Technology for CO_2 Capture from Coal-fired Power Plants - Final Technical Report*. ADA-Environmental Solutions.

Krutka, H., Sjostrom, S., Starns, T., Dillon, M., and Silverman, R. (2013). Post-combustion CO_2 capture using solid sorbents: 1 MWe pilot evaluation. *Energy Procedia*, 37(0):73 – 88. GHGT-11.

Kunii, D. and Levenspiel, O. (1991). *Fluidization Engineering*. Butterworth-Heinemann Series in Chemical Engieering.

Lee, J. B., Eom, T. H., Oh, B. S., Baek, J.-I., Ryu, J., Jeon, W. S., Wi, Y. H., and Ryu, C. K. (2011). CO_2 capture from flue gas using potassium-based dry regenerable sorbents. *Energy Procedia*, 4(0):1494 – 1499. 10th International Conference on Greenhouse Gas Control Technologies.

Lee, K. B. and Sircar, S. (2008). Removal and recovery of compressed CO_2 from flue gas by a novel thermal swing chemisorption process. *AIChE Journal*, 54(9):2293–2302.

Lee, S.-S., Yoo, J.-S., Moon, G.-H., Park, S.-W., Park, D.-W., and Oh, K.-J. (2004). CO_2 adsorption with attrition of dry sorbents in a fluidized bed. *Prepr. Pap.*, 49(1):314–315. Div. Fuel Chem.

Li, L., Li, Y., Wen, X., Wang, F., Zhao, N., Xiao, F., Wei, W., and Sun, Y. (2011). CO_2 capture over $K_2CO_3/MgO/Al_2O_3$ dry sorbent in a fluidized bed. *Energy & Fuels*, 25(8):3835–3842.

Liang, Y., Harrison, D. P., Gupta, R. P., Green, D. A., and McMichael, W. J. (2004). Carbon dioxide capture using dry sodium-based sorbents. *Energy & Fuels*, 18(2):569–575.

Liebenthal, U., Pinto, D. D. D., Monteiro, J. G. M.-S., Svendsen, H. F., and Kather, A. (2013). Overall process analysis and optimisation for CO_2 capture from coal fired power plants based on phase change solvents forming two liquid phases. *Energy Procedia*, 37(0):1844 – 1854. GHGT-11.

Liu, Y., Ye, Q., Shen, M., Shi, J., Chen, J., Pan, H., and Shi, Y. (2011). Carbon dioxide capture by functionalized solid amine sorbents with simulated flue gas conditions. *Environmental Science & Technology*, 45(13):5710–5716.

MacDowell, N., Florin, N., Buchard, A., Hallett, J., Galindo, A., Jackson, G., Adjiman, C. S., Williams, C. K., Shah, N., and Fennell, P. (2010). An overview of co2 capture technologies. *Energy Environ. Sci.*, 3:1645–1669.

Mahle, J. J. (2002). An adsorption equilibrium model for type 5 isotherms. *Carbon*, 40:2753–2759.

Mangalapally, H. P., Notz, R., Asprion, N., Sieder, G., Garcia, H., and Hasse, H. (2012). Pilot plant study of four new solvents for post-combustion carbon dioxide capture by reactive absorption and comparison to MEA. *International Journal of Greenhouse Gas Control*, 8(0):205 – 216.

Mérel, J., Clausse, M., and Meunier, F. (2006). Carbon dioxide capture by indirect thermal swing adsorption using 13x zeolite. *Environmental Progress*, 25(4):327–333.

Metz, B., Davidson, O., de Coninck, H., Loos, M., and Meyer, L. (2005). *IPCC Special Report on Carbon Dioxide Capture and Storage*. Cambridge University Press for the Intergovernmental Panel on Climate Change.

Mulgundmath, V. P., Tezel, F. H., Saatcioglu, T., and Golden, T. C. (2012). Adsorption and separation of CO_2/N_2 and CO_2/CH_4 by 13X zeolite. *The Canadian Journal of Chemical Engineering*, 90(3):730–738.

National Institute of Standards and Technology (2011 (accessed May 5, 2014)). *NIST Chemistry WebBook, NIST Standard Reference Database Number 69*. `http://webbook.nist.gov/chemistry/`.

Nelson, T. O., Green, D. A., Box, P., Gupta, R. P., Henningsen, G., and Turk, B. S. (2009). *Carbon Dioxide Capture from Flue Gas Using Dry Regenerable Sorbents - Final Report*. RTI International. Research Triangle Park.

Øi, L. E. (2007). Aspen HYSYS simulation of CO_2 removal by amine absorption from a gas based power plant. *SIMS2007 Conference, Gøteborg*, pages 73 – 81.

Park, Y. C., Jo, S.-H., Park, K.-W., Park, Y. S., and Yi, C.-K. (2009a). Effect of bed height on the carbon dioxide capture by carbonation/regeneration cyclic operations using dry potassium-based sorbents. *Korean Journal of Chemical Engineering*, 26(3):874–878.

Park, Y. C., Jo, S.-H., Ryu, C. K., and Yi, C.-K. (2009b). Long-term operation of carbon dioxide capture system from a real coal-fired flue gas using dry regenerable potassium-based sorbents. *Energy Procedia*, 1(1):1235 – 1239. Greenhouse Gas Control Technologies 9 Proceedings of the 9th International Conference on Greenhouse Gas Control Technologies (GHGT-9), 1620 November 2008, Washington DC, USA.

Park, Y. C., Jo, S.-H., Ryu, C. K., and Yi, C.-K. (2011). Demonstration of pilot scale carbon dioxide capture system using dry regenerable sorbents to the real coal-fired power plant in korea. *Energy Procedia*, 4(0):1508 – 1512. 10th International Conference on Greenhouse Gas Control Technologies.

Pearson, P., Hollenkamp, A. F., and Meuleman, E. (2013). Electrochemical investigation of corrosion in CO_2 capture plantsinfluence of amines. *Electrochimica Acta*, 110(0):511 – 516.

Peleg, M. (1993). Assessment of a semi-empirical four parameter general model for sigmoid moisture sorption isotherms. *Journal of Food Process Engineering*, 16(1):21–37.

Perry, R., Green, D., and Maloney, J. (1997). *Perry's Chemical Engineers' Handbook*. Chemical Engineering Series. McGraw-Hill Professional Publishing, 7th edition.

Pirngruber, G. D., Carlier, V., and le Cocq, D. L. (2013a). Post-combustion CO_2 capture by vacuum swing adsorption using zeolites - a feasibility study. *Oil & Gas Science and Technology Rev. IFP Energies nouvelles*, pages 1 – 15.

Pirngruber, G. D., Guillou, F., Gomez, A., and Clausse, M. (2013b). A theoretical analysis of the energy consumption of post-combustion CO_2 capture processes by temperature swing adsorption using solid sorbents. *International Journal of Greenhouse Gas Control*, 14(0):74 – 83.

Qi, S., Hay, K. J., Rood, M. J., and Cal, M. P. (2000). Equilibrium and heat of adsorption for water vapour and activated carbon. *Journal of Environmental Engineering*, 126(3):267–271.

Ramezan, M. and Skone, T. J. (2005). *Carbon Dioxide Capture from Existing Coal-Fired Power Plants*. DOE/NETL.

Ribeiro, R. P., Sauer, T. P., Lopes, F. V., Moreira, R. F., Grande, C. A., and Rodrigues, A. E. (2008). Adsorption of CO_2, CH_4, and N_2 in activated carbon honeycomb monolith. *Journal of Chemical & Engineering Data*, 53(10):2311–2317.

Ruthven, D. (1984). *Principles of Adsorption and Adsorption Processes*. Wiley-Interscience Publication. Wiley.

Samanta, A., Zhao, A., Shimizu, G. K. H., Sarkar, P., and Gupta, R. (2012). Post-combustion CO_2 capture using solid sorbents: A review. *Industrial & Engineering Chemistry Research*, 51(4):1438–1463.

Sayari, A., Belmabkhout, Y., and Serna-Guerrero, R. (2011). Flue gas treatment via CO_2 adsorption. *Chemical Engineering Journal*, 171(3):760 – 774. Special Section: Symposium on Post-Combustion Carbon Dioxide Capture.

Shen, C., Grande, C. A., Li, P., Yu, J., and Rodrigues, A. E. (2010). Adsorption equilibria and kinetics of CO_2 and N_2 on activated carbon beads. *Chemical Engineering Journal*, 160(2):398 – 407.

Shigemoto, N., Yanagihara, T., Sugiyama, S., and Hayashi, H. (2006). Material balance and energy consumption for CO_2 recovery from moist flue gas employing K_2CO_3-on-activated carbon and its evaluation for practical adaptation. *Energy & Fuels*, 20(2):721–726.

Sjostrom, S. and Krutka, H. (2010). Evaluation of solid sorbents as a retrofit technology for CO_2 capture. *Fuel*, 89(6):1298 – 1306. Advanced Fossil Energy Utilization.

Sluijs, J. V. D., Hendriks, C., and Blok, K. (1992). Feasibility of polymer membranes for carbon dioxide recovery from flue gases. *Energy Conversion and Management*, 33(58):429 – 436. Proceedings of the First International Conference on Carbon Dioxide Removal.

Smith, L. (2011). *Carbon capture and storage: additional background - Standard note*. House of Commons Library: Science and Environment Section.

Solex Thermal Science Inc. (2014 (accessed September 5, 2014)). *Solex Thermal Science*. `http://www.solexthermal.com/products`.

SRI International, ATMI Inc., and DOE National Energy Technology Center (2011). Development novel carbon sorbents for carbon dioxide capture. In *2011 NETL CO_2 Capture Technology Meeting August 22-26, 2011 in Pittsburgh, PA*.

SRI International, ATMI Inc., National Carbon Capture Center, University of Toledo, and DOE National Energy Technology Center (2013). Development novel carbon sorbents for carbon dioxide capture. In *2013 NETL CO_2 Capture Technology Meeting July 8-11, 2013 in Pittsburgh, PA*.

SRI International, ATMI Inc., University of Toledo, and DOE National Energy Technology Center (2012). Development novel carbon sorbents for carbon dioxide capture. In *2012 NETL CO_2 Capture Technology Meeting July 9-12, 2012 in Pittsburgh, PA*.

SRI International, ATMI Inc., D. (2010). Development novel carbon sorbents for carbon dioxide capture. In *2010 NETL CO_2 Capture Technology Meeting September 13-17, 2010 in Pittsburgh, PA*.

Stichlmair, J., Bravo, J., and Fair, J. (1989). General model for prediction of pressure drop and capacity of countercurrent gas/liquid packed columns. *Gas Separation & Purification*, 3(1):19 – 28.

Su, F., Lu, C., Cnen, W., Bai, H., and Hwang, J. F. (2009). Capture of CO_2 from flue gas via multiwalled carbon nanotubes. *Science of The Total Environment*, 407(8):3017 – 3023.

Tien, C. (1984). *Adsorption Calculations and Modelling*. Chemical Engineering Series. Butterworth-Heinemann.

United Nations Framework Convention on Climate Change (2009). *Draft-Decision - Copenhagen Accord*. United Nations.

Vargas, D. P., Giraldo, L., Silvestre-Albero, J., and Moreno-Pirajn, J. C. (2011). CO_2 adsorption on binderless activated carbon monoliths. *Adsorption*, 17(3):497–504.

Veneman, R., Li, Z., Hogendoorn, J., Kersten, S., and Brilman, D. (2012). Continuous CO_2 capture in a circulating fluidized bed using supported amine sorbents. *Chemical Engineering Journal*, 207208(0):18 – 26. 22nd International Symposium on Chemical Reaction Engineering (ISCRE 22).

Wang, D., Sentorun-Shalaby, C., Ma, X., and Song, C. (2011a). High-capacity and low-cost carbon-based molecular basket sorbent for CO_2 capture from flue gas. *Energy & Fuels*, 25(1):456–458.

Wang, Q., Luo, J., Zhong, Z., and Borgna, A. (2011b). CO_2 capture by solid adsorbents and their applications: current status and new trends. *Energy Environ. Sci.*, 4:42–55.

Wang, T. and Jens, K.-J. (2014). Oxidative degradation of aqueous PZ solution and AMP/PZ blends for post-combustion carbon dioxide capture. *International Journal of Greenhouse Gas Control*, 24(0):98 – 105.

Wappel, D., Gronald, G., Kalb, R., and Draxler, J. (2010). Ionic liquids for post-combustion CO_2 absorption. *International Journal of Greenhouse Gas Control*, 4(3):486 – 494.

Weiland, R. H., Dingman, J. C., and Cronin, D. B. (1997). Heat capacity of aqueous monoethanolamine, diethanolamine, n-methyldiethanolamine, and n-methyldiethanolamine-based blends with carbon dioxide. *Journal of Chemical & Engineering Data*, 42(5):1004–1006.

Wu, Y., Chen, X., Dong, W., Zhao, C., Zhang, Z., Liu, D., and Liang, C. (2013). K_2CO_3/Al_2O_3 for capturing CO_2 in flue gas from power plants. Part 5: Carbonation and failure behavior of K_2CO_3/Al_2O_3 in the continuous CO_2 sorptiondesorption system. *Energy & Fuels*, 27(8):4804–4809.

Xu, D., Zhang, J., Li, G., Xiao, P., Webley, P., and chun Zhai, Y. (2011). Effect of water vapor from power station flue gas on CO_2 capture by vacuum swing adsorption with activated carbon. *Journal of Fuel Chemistry and Technology*, 39(3):169–174.

Xu, X., Song, C., Andresen, J. M., Miller, B. G., and Scaroni, A. W. (2002). Novel polyethylenimine-modified mesoporous molecular sieve of MCM-41 type as high-capacity adsorbent for CO_2 capture. *Energy & Fuels*, 16(6):1463–1469.

Xu, X., Song, C., Miller, B. G., and Scaroni, A. W. (2005). Influence of moisture on CO_2 separation from gas mixture by a nanoporous adsorbent based on polyethylenimine-modified molecular sieve MCM-41. *Industrial & Engineering Chemistry Research*, 44(21):8113–8119.

Yang, R. (1987). *Gas Separation by Adsorption Processes*. Butterworths Series in Chemical Engineering. Butterworths.

Yang, W.-C. and Hoffman, J. (2009). Exploratory design study on reactor configurations for carbon dioxide capture from conventional power plants employing regenerable solid sorbents. *Industrial & Engineering Chemistry Research*, 48(1):341–351.

Yi, C.-K., Jo, S.-H., Seo, Y., Lee, J.-B., and Ryu, C.-K. (2007). Continuous operation of the potassium-based dry sorbent CO_2 capture process with two fluidized-bed reactors. *International Journal of Greenhouse Gas Control*, 1(1):31 – 36. 8th International Conference on Greenhouse Gas Control Technologies GHGT-8.

Zhang, J., Webley, P. A., and Xiao, P. (2008). Effect of process parameters on power requirements of vacuum swing adsorption technology for CO_2 capture from flue gas. *Energy Conversion and Management*, 49(2):346 – 356.

Zhang, W., Liu, H., Sun, C., Drage, T. C., and Snape, C. E. (2014). Capturing CO_2 from ambient air using a polyethyleneiminesilica adsorbent in fluidized beds. *Chemical Engineering Science*, 116(0):306 – 316.

Zhang, Z., Zhang, W., Chen, X., Xia, Q., and Li, Z. (2010). Adsorption of CO_2 on zeolite 13X and activated carbon with higher surface area. *Separation Science and Technology*, 45(5):710–719.

Zhao, C., Chen, X., and Zhao, C. (2012a). K_2CO_3/Al_2O_3 for capturing CO_2 in flue gas from power plants. Part 1: Carbonation behaviors of K_2CO_3/Al_2O_3. *Energy & Fuels*, 26(2):1401–1405.

Zhao, C., Chen, X., and Zhao, C. (2012b). K_2CO_3/Al_2O_3 for capturing CO_2 in flue gas from power plants. Part 2: Regeneration behaviors of K_2CO_3/Al_2O_3. *Energy & Fuels*, 26(2):1406–1411.

Zhao, C., Chen, X., and Zhao, C. (2012c). K_2CO_3/Al_2O_3 for capturing CO_2 in flue gas from power plants. Part 4: Abrasion characteristics of the K_2CO_3/Al_2O_3 sorbent. *Energy & Fuels*, 26(2):1395–1400.

Zhao, C., Chen, X., Zhao, C., Wu, Y., and Dong, W. (2012d). K_2CO_3/Al_2O_3 for capturing CO_2 in flue gas from power plants. Part 3: CO_2 capture behaviors of K_2CO_3/Al_2O_3 in a bubbling fluidized-bed reactor. *Energy & Fuels*, 26(5):3062–3068.

Zhicheng, X., Shujuan, W., Bo, Z., and Changhe, C. (2013). Study on potential biphasic solvents: Absorption capacity, CO_2 loading and reaction rate. *Energy Procedia*, 37(0):494 – 498. GHGT-11.